The Chemical Vapour Deposition of Tetraethoxysilane on Zeolite ZSM-5

By

Dipl.-Ing. Heiko Manstein

Submitted to the University of Cape Town
in fulfillment of the requirements
for the degree of
Doctor of Philosophy

Department of Chemical Engineering
University of Cape Town
Rondebosch
Cape Town, September 2001

Acknowledgements

This thesis could not exist without Prof. Hans Schulz, Karlsruhe, and Prof. Cyril O'Connor, Cape Town, who both founded a very fruitful friendship and collaboration across the continents.

My gratitude belongs to my supervisors. Thank you, Dr. Klaus Möller, for infinite patience, enormous passion, stimulating discussions, hard work, friendship and the always open office door throughout the years. Thank you, Prof. Cyril O'Connor, for the motivation, encouragement, reassurance, support and the open ear whenever it was needed.

Words cannot express the respect for the family which put up with the lifetime student named son, brother, nephew, and grand-son for so many years.

I am greatly indebted to my friend from school days, Peter Schwan, who passionately convinced me, that Cape Town would offer more experiences than Biberrach. Thanks, for restoring the believe whenever I lost it and that piercing analytical mind whenever the view got hazy.

Thanks, to my good friend Uwe Wilkenhöner, for the more difficult surname and many mind-broadening and mind-blowing experiences. Carry on, whatever blows your hair back.

Thank you, Nikki, for reminding me that there is so much more.

Where would I be without the students from the department of chemical engineering?

Thank you, Natascha, for the good neighbourhood and being a friend with emotions. And to Brigitte and David, Nick, Warwick, Giles and Mike for surfing the same wave at the right moment. A big hand to Frank, Rein, Ashley and the other old legion, for being accepting and trusting. And to Gillian, not only for XRD and TPDs.

I also want to express my appreciation to the entire staff for adding the spices to these days and making them enjoyable. Jack, Walter, Eric, Dee, Dave, Martin, Peter, Joe. What a thought provoking concoction.

And of course to the old friends back home. For not forgetting, despite the distance, and for accepting my offer to help themselves to a beer out of my fridge.

And what about the unnamed ones; there are so many deserving mentioning and none of them is forgotten.

The past four years have been so much more than only science; it was the greatest experience with all of you "Menschen".

Synopsis

This thesis reports on the investigation of a cyclic chemical vapour deposition (CVD) method eliminating unwanted surface reactions and enhancing shape selective properties by depositing inert silica onto the external surface of zeolite ZSM-5.

A CVD treatment consists out of a deposition, flushing and heating step followed by calcination in flowing air.

Modifications are carried out in up to 33 cycles on one and the same sample employing tetraethoxysilane (TEOS) as silica precursor at deposition temperatures ranging from 50 to 400°C.

After each CVD treatment the catalyst is tested with appropriate test reactions in order to quantify the extent of modification.

The gradual inertisation of the external surface is followed with the catalytic cracking of 1,3,5-triisopropylbenzene (1,3,5-TiPB) which is too bulky to enter the micro-pore structure of ZSM-5. The disproportionation of toluene (TDP) is employed to monitor changes of the internal activity and alterations in the shape selective properties of the catalyst.

The analysis of reactor effluent during the deposition, flushing and heating step of the modification cycle allows investigating the reaction pathway. The deposition reaction proceeds with the reaction of the alkoxy groups of TEOS with the terminal hydroxyls of the zeolite under the formation of ethanol.

The saturation of the dissociative adsorption of TEOS on the surface leads to the formation of alkoxy species which are unreactive to the modifier agent. Thus, the defined deposition of the equivalent of one TEOS monolayer per modification treatment is possible.

Brønsted acidity of the fresh catalyst and deposition temperatures higher than 200°C lead to increased in-situ water formation from ethanol dehydration. Water propagates the decomposition of alkoxy to silanol species and additional ethanol. This autocatalytic step facilitates the enhanced and uncontrolled deposition of silica on the external surface. As result, pore openings are rapidly blocked and the catalyst is severely deactivated.

Reduction of the external surface activity requires at least two to three deposition treatments, de-

pending on the modification temperature. The lower the deposition temperature is chosen, the more cycles have to be applied which is due to inhibited in-situ water generation.

Shape selective improvements towards higher para-xylene (p-xylene) contents in the product of up to 90 % p-xylene selectivity during TDP are observed at all investigated deposition temperature. The most rapid changes occur at the highest deposition temperatures.

The improvements in shape selectivity are accompanied by significant losses in overall activity of the catalyst. While it is desired to decrease and eliminate the contribution of the external surface, additional reduction in activity is observed. This is attributed to the deactivation of catalyst particles due to the uncontrolled and non-uniform deposition of silica. The higher the deposition temperature, the more severe the deactivation progresses, as silica deposition increases.

Because of the accelerated catalyst deactivation at high temperatures, desirably high p-xylene yields, 2.5 times that of the unmodified catalyst, can only be obtained at deposition temperatures below 150°C and after many time consuming CVD cycles.

From TEOS breakthrough curves, the deposited amount per cycle is determined allowing the establishment of a correlation between deposited mass and observed inertisation, deactivation and diffusional effects.

It is shown that the deactivation of the external activity for the 1,3,5-TiPB-cracking, external TDP and xylene isomerisation decreases exponentially with the deposited amount of silica while the extent of pore blocking increases exponentially. The restricted access to the micro-pores results in the decreasing effective diffusivity and hence, effectiveness factor of the catalytic system.

The changes of effectiveness factor are responsible for the separation of the xylene isomers, due to the different intrinsic diffusion properties, as the severity of pore blockage increases. Reduction of the secondary isomerisation reaction of xylenes on the external surface contributes only marginally to alterations of shape selectivity. The intrinsic composition of xylenes is close to the thermodynamic equilibrium, as they diffuse out of the crystal.

Changes in shape selective properties and both, external and internal deactivation behaviour are simulated with a kinetic reaction model, assuming irreversible first order reaction rates for disproportionation and isomerisation of toluene and the xylene isomers as well as a paring mechanism (dealkylation) for higher alkylated aromatics.

The model shows reasonable reproduction of the experimental data thus supporting the assumptions.

Furthermore, the experimental data can be fitted with remarkable precision which allows the prediction of both, kinetic and diffusional parameters.

Contents

Contents iii

List of Figures ix

List of Tables xv

1 Introduction 1

1.1 Zeolites . . . 2

1.1.1 Activity and acidity of zeolites . . . 2

1.1.2 ZSM-5 . . . 2

1.1.3 Shape selectivity . . . 3

1.1.4 The contribution of external active sites on the catalytic behaviour . . . 5

1.1.5 Application of ZSM-5 . . . 6

1.2 Modification of the external surface . . . 6

1.2.1 Chemical vapour deposition (CVD) . . . 6

1.2.2 Silica Precursors . . . 7

1.2.3 Alkoxysilanes . . . 7

1.2.4 Reaction mechanism for alkoxysilanes with zeolites . . . 7

1.2.5 Methods of deposition . . . 8

1.2.6 Pre/Post CVD treatment . . . 8

1.2.7 Parameters which influence the modification procedure . . . 9

1.3 Characterisation of silanised zeolites . . . 11

1.3.1 Conservation of crystal interior . . . 11

1.3.2 Acidity of the zeolite . . . 11

1.3.3 Morphology of deposited layer . . . 11

1.3.4 Modification of the pore mouth . . . 12

1.3.5 Blocking of the pore openings . . . 13

1.3.6 Catalytic testing . . . 14

1.4 Modification and characterisation . . . 17

1.4.1 CVD method of choice . . . 17
1.4.2 Test reactions to monitor the effects of CVD . . . 17
1.5 Objective of this study . . . 21

2 Experimental **23**
2.1 Materials . . . 23
2.1.1 Chemicals . . . 23
2.1.2 Catalyst . . . 24
2.2 Experimental apparatus . . . 25
2.2.1 Apparatus . . . 25
2.2.2 Reactor . . . 25
2.2.3 Saturator . . . 26
2.2.4 GC-online analysis . . . 26
2.2.5 GC-Analysis of unretained compounds and light hydrocarbon samples . . . 26
2.3 Experimental procedure . . . 26
2.3.1 Preparation of powder . . . 26
2.3.2 Preparation of catalyst pellets . . . 26
2.3.3 Loading of the reactor . . . 27
2.3.4 Run preparation and setting of reactor conditions . . . 27
2.3.5 Setting to test reaction temperature . . . 27
2.3.6 Setting to CVD reaction temperature . . . 27
2.3.7 CVD-step . . . 28
2.3.8 Cyclic CVD-reaction-sequence . . . 28
2.3.9 Effect of reaction temperature on TDP over powder . . . 29
2.3.10 Long time TDP studies over pellets . . . 29
2.3.11 Variation of WHSV during TDP over pellets . . . 29
2.3.12 Isomerisation of para-xylene over silica gel . . . 30
2.4 Evaluation of catalytic reaction data . . . 30
2.4.1 Molar flow rates . . . 30
2.4.2 Concentrations . . . 30
2.4.3 Conversion . . . 30
2.4.4 Carbon balance . . . 31
2.4.5 p-Xylene selectivity (benzene free) . . . 31
2.4.6 Selectivity . . . 31
2.4.7 p-Xylene yield . . . 31
2.4.8 Integral TEOS conversion for CVD treatment . . . 32

2.4.9 Silica loading on the external surface . . . 32
2.4.10 Silicon density from the TEOS monolayer . . . 32
2.4.11 Integral carbon balance for CVD treatment . . . 33
2.4.12 First order rate constant . . . 33
2.4.13 Normalised first order rate constant . . . 33
2.4.14 Reaction rates . . . 33
2.4.15 Error in conversion data . . . 34
2.4.16 Weight hourly space velocity . . . 34
2.4.17 Time on stream . . . 34
2.4.18 Modified space time . . . 34
2.4.19 Linear velocity . . . 34
2.4.20 Film diffusion . . . 35
2.4.21 Plug flow . . . 35
2.4.22 Reactor dead time . . . 35

3 Results **37**

3.1 Product Analysis during TEOS deposition . . . 37
3.1.1 TEOS breakthrough . . . 37
3.1.2 Ethene and ethanol . . . 38
3.2 Integral TEOS conversion . . . 39
3.3 Amount of deposited Silica on external surface . . . 41
3.4 Activity of the external surface - Cracking of 1,3,5-TiPB . . . 42
3.5 Disproportionation of toluene . . . 46
3.5.1 Unmodified catalyst . . . 46
3.5.2 Effect of WHSV on selectivity . . . 47
3.5.3 Improvements in shape selectivity . . . 47
3.5.4 Benzene to Xylene Ratio . . . 50
3.5.5 Toluene conversion . . . 51
3.5.6 Effect of space velocity on para-selectivity during TDP . . . 54
3.6 Long time runs . . . 57
3.6.1 1,3,5-TiPB-cracking . . . 57
3.6.2 Disproportionation of toluene . . . 57
3.7 Reproducibility . . . 59
3.7.1 TEOS deposition . . . 59
3.7.2 1,3,5-TiPB-cracking . . . 59
3.7.3 Disproportionation of toluene . . . 59

3.8 Repeatability . . . 60
3.8.1 CVD of TEOS . . . 60
3.8.2 1,3,5-TiPB-cracking and TDP . . . 60

4 Discussion **61**
4.1 Deposition of silica . . . 61
4.1.1 Breakthrough curve analysis . . . 61
4.1.2 Integral conversion . . . 62
4.1.3 Reaction scheme . . . 63
4.1.4 Development of a reaction pathway for TEOS conversion . . . 67
4.1.5 Closing remarks on TEOS deposition . . . 70
4.2 Deactivation . . . 72
4.2.1 External surface: 1,3,5-TiPB-cracking . . . 72
4.2.2 Overall: TDP . . . 75
4.3 Quantification of deactivation behaviour . . . 80
4.3.1 External . . . 80
4.3.2 Deactivation of effective internal crystal activity . . . 84
4.4 Shape selectivity during TDP . . . 85
4.4.1 Improvement of para-selectivity on a benzene free basis . . . 85
4.4.2 The sequence of the xylene selectivity variation with CVD . . . 85
4.4.3 Pore blocking and reduced isomerisation . . . 85
4.4.4 Effect of WHSV on para-selectivity . . . 91
4.4.5 Diffusional constraints . . . 92
4.5 Catalyst performance: P-xylene Yield . . . 93
4.5.1 Para-xylene yield versus toluene conversion plot . . . 93
4.5.2 Loss of xylenes . . . 96
4.6 Modelling effects of CVD on TDP . . . 97
4.6.1 Reaction pathway . . . 97
4.6.2 Assumed rate expressions . . . 99
4.6.3 The effect of CVD on the reaction rate of external reactions . . . 100
4.6.4 The effect of CVD on diffusion properties . . . 100
4.6.5 Reactor and catalyst mass balance . . . 102
4.6.6 Boundary conditions . . . 102
4.6.7 Application of collocation . . . 103
4.6.8 Typical simulation results . . . 105
4.6.9 Typical fitting of model data using GREG . . . 109

5 Conclusions 117

A BET, TPD and XRD analysis 125

B Concentration and breakthrough curves 129

C Sketches 135

D Gas Chromatography 137

E Additional Figures 145

F Methods 147

F.1 Reactor dead time 147

F.2 Isomerisation of para-xylene 147

F.3 Correction for internal activity during TDP 148

F.4 CVD on sand 148

F.5 Sample calculation for silica loading 149

G Tables 151

H Literature Overview 173

List of Figures

1.1 The channel network of ZSM-5 (Kokotailo et al., 1978). 3

1.2 Shape selectivity in zeolites: a) reactant-, b) product-, c) restricted transition state shape selectivity (Csicsery, 1979). 4

1.3 Dependence of the extent of pore mouth narrowing on the Si/Al ratio (Hibino et al., 1993). 13

1.4 Effect of pore blocking on effective diffusivity and effectiveness factor (Theodorou and Wei, 1983). 14

1.5 Mechanism of toluene disproportionation over zeolites (Uguina et al., 1993). 18

1.6 Model for selective toluene disproportionation (Olson and Haag, 1984). 19

2.1 SEM micrograph of ZSM-5 24

2.2 Flowsheet of reaction apparatus. 25

2.3 Illustration of the calculation of the integral TEOS conversion from a breakthrough curve. 32

3.1 TEOS breakthrough curves on powder at T_{CVD}=50 and 400°C (last CVD treatments of the series, cycle 12 and 20, respectively). 38

3.2 Illustration of the calculation of the integral TEOS conversion from a breakthrough curve at T_{CVD}=50°C (20th CVD treatment). 39

3.3 Integral TEOS conversions on powder. 40

3.4 Integral TEOS conversions on pellets. 40

3.5 Cumulative amount of deposited silica on powder. 41

3.6 Cumulative amount of deposited silica on pellets. 42

3.7 Cracking of 1,3,5-TiPB over the parent sample of the 50°C-powder series (X_{TiPB}(average between 25 and 65 min)=70.4%, σ=0.79, carbon-balance=98%, σ=0.79, reaction conditions given in Table 2.3). 43

3.8 Inhibition of 1,3,5-TiPB-cracking over powder with increased silica deposition (common trend line shown for the 50, 100, 150, 200 and 300°C-series). 44

3.9 Inhibition of 1,3,5-TiPB-cracking over pellets with increased silica deposition (common trend line for the 100 and 200°C-series). 44

3.10 Number of CVD cycles to inhibit cracking of 1,3,5-TiPB at various deposition temperatures. 45

3.11 Effect of reaction temperature (450, 500 and 550°C), time on stream and WHSV on conversion and para-selectivity during toluene disproportionation over unmodified powder (reaction conditions and data given in Table G.13). 46

3.12 Effect of time on stream and WHSV on conversion and para-selectivity during toluene disproportionation over unmodified pellets at 450° (reaction conditions and data given in Table G.14). 47

3.13 Disproportionation of toluene over the unmodified sample of the 50°C-powder series ($X_{Toluene}$(average between 25 and 65 min)=8.26%, σ= 0.36, carbon-balance= 100.71%, σ=2.59, reaction conditions given in Table 2.3). 48

3.14 Changes in p-xylene selectivity with increasing silica deposition on powder. 49

3.15 Changes in p-xylene selectivity with increasing silica deposition on pellets. 49

3.16 Benzene/xylene ratios of the products of TDP over powder (reaction conditions given in Table 2.3). 50

3.17 Benzene/xylene ratios of the products of TDP over pelletised samples (reaction conditions given in Table 2.4). 51

3.18 Decrease in relative conversion during TDP with increasing silica deposition on powder. Data which was badly effected by experimental error (encircled), was not used for further calculation and discussion. 52

3.19 Decrease in relative conversion during TDP with increasing silica deposition on pellets. Data which was badly effected by experimental error (encircled), was not used for further calculation and discussion. 52

3.20 Changes in para-selectivity during TDP at 550°C by changing WHSV over unmodified and modified (15 cycles at 150°C) powder (reaction conditions given in Table G.13). . 53

3.21 Changes in para-selectivity during TDP at 450°C by changing WHSV over unmodified and modified (20 cycles at 100°C) pellets (reaction conditions given in Table G.13). . . 54

3.22 Effect of reaction temperature (450, 500 and 550°C and WHSV on conversion and para-selectivity during toluene disproportionation over modified powder (15 CVD cycles at 150°C; reaction conditions given in Table G.13). 55

3.23 Effect of time on stream and WHSV on conversion and para-selectivity during toluene disproportionation over modified pellets (20 CVD cycles at 100°C, reaction conditions and data given in Table G.14). 56

3.24 Long time behaviour and reproducibility of 1,3,5-TiPB-cracking over unmodified pellets at 210°C. (Reaction conditions given in Table 2.4.) 57

3.25 Long time run and reproducibility of the disproportionation of toluene over unmodified pellets at 450°C (Reaction conditions are given in Table G.14). 58

3.26 CVD on sand 59

3.27 Repeatability of CVD on ZSM-5. 60

4.1 Scheme of reactions of TEOS and products during the deposition and heating step. . . 68

4.1 **(continued)** Side reactions during the deposition of TEOS. 69

4.2 Reaction scheme in the investigated temperature range during the deposition of TEOS. 70

4.3 Activity for the cracking of 1,3,5-TiPB (first order reaction rate constants of the modified samples are normalised by the constant of the unmodified samples). 73

4.4 Activity for TDP (first order reaction rate constants of the modified samples are normalised by the constant of the unmodified samples). 76

4.5 Changes in the first order rate constants for cracking of 1,3,5-TiPB and external disproportionation of toluene with increasing Si/nm^2 (assuming internal activity of 50% at 50°C, 50% at 100°C, 30% at 150°C and 80% for Pe100°C. For the deposition temperatures of 200, 300 and 400°C the internal activity cannot be determined.) 79

4.6 Fitting of ln(first order rate constants) for the cracking of 1,3,5-TiPB. 82

4.6 **(continued)** Fitting of ln(first order rate constants) for the cracking of 1,3,5-TiPB. . 83

4.7 Changes in xylene-selectivities with increasing number of CVD treatments for powder samples. 87

4.8 Changes in xylene-selectivities with increasing number of CVD treatments for pelletised samples. 88

4.9 Effect of the linear increase of pore blockage with silica loading on relative diffusivity and effectiveness factor. 88

4.10 Effect of the exponential increase of pore blockage with silica loading on relative diffusivity and effectiveness factor. 89

4.11 Selectivity plots for TDP over CVD modified powder and pellet samples. Data obtained over the unmodified samples are encircled. 94

4.11 **(continued)** Selectivity plots for TDP over CVD modified powder and pellet samples. Data obtained over the unmodified samples are encircled. 95

4.12 Model of TDP over ZSM-5 in a fixed bed reactor. 99

4.13 Comparison of the effect of linear and exponential increase of pore blocking (α=0.7, n_b=40). 101

4.14 Flow chart of simulation and fitting procedure to obtain simulation parameters p_1 - p_6. 104

4.15 Typical simulation: selectivity versus conversion during TDP with changing amount of deposited silica without paring reaction. 108

4.16 Typical simulation: selectivity versus conversion during TDP with changing amount of deposited silica including the paring reaction of xylene isomers. 108

4.17 Typical fit to simulated experiments without paring reaction: uniqueness of fitted parameters. 110

4.18 Typical fit to simulated experiments with paring reaction: uniqueness of fitted parameters. 110

4.19 Typical fit to simulated experiments with 5 % random error without paring reaction: quality of fitting. 111

4.20 Typical fit to simulated experiments with 5 % random error with paring reaction: quality of fitting. 111

4.21 Typical fit to actual experiments without paring reaction. 113

4.22 Typical fit to actual experiments with paring reaction. 113

A.1 Nitrogen BET isotherm of MFI-90 powder. 126

A.2 Nitrogen BET isotherm of MFI-90 pellets. 126

A.3 NH_3-TDP-spectrum of MFI-90 powder. 127

A.4 XRD-spectrum of MFI-90 powder (K-α radiation source; wave length: 1.54056 Å). . . 128

B.1 TEOS concentration curves for all deposition cycles on powder at all deposition temperatures. 130

B.2 Ethene concentration curves for all deposition cycles on powder at all deposition temperatures. 131

B.3 Ethanol concentration curves for all deposition cycles on powder at all deposition temperatures. 132

B.4 Normalised TEOS breakthrough curves for powder samples at all temperatures. 133

B.5 Normalised TEOS breakthrough curves for pelletised samples at 100 and 200°C. . . . 134

C.1 Sketch of reactor. 136

C.2 Sketch of saturator. 136

D.1 GC-trace of full CVD deposition. 139

D.2 GC-trace of full 1,3,5-TiPB-cracking run. 140

D.3 GC-trace of full TDP run. 141

D.4 GC-trace of analysis of unretained compounds during TEOS deposition at 200°C. . . . 142

D.4 **(continued)** GC-trace of analysis of unretained compounds during the heating step (reactor temperature approximately 250°C) of a TEOS deposition at 200°C. 143

D.5 GC-trace of analysis of light hydrocarbons during TDP at 550°C. 144

E.1 Changes in first order rate constants for cracking of 1,3,5-TiPB and disproportionation of toluene with increasing Si/nm^2. 146

F.1 Isomerisation of p-xylene over CVD treated silica gel. 148

List of Tables

2.1 List of Chemicals 23
2.2 Catalyst specifications 24
2.3 Reaction conditions for powder samples (catalyst mass: 0.5 g; carrier gas: nitrogen; see G.15 for detailed list of linear velocities and WHSV for kinetic studies of TDP). . 28
2.4 Reaction conditions for pelletised samples (catalyst mass: 1.5 g; carrier gas: nitrogen; see G.15 for detailed list of linear velocities and WHSV for kinetic studies of TDP). . 29

3.1 Numbers of cycles required to inhibit 1,3,5-TiPB-cracking 43

4.1 Deactivation constants α for the respective temperature series for 1,3,5-TiPB-cracking. 83
4.2 Base and estimation parameters. 106
4.3 Estimated model parameter from simulation data (values given as $p_i \pm \sigma$). 112
4.4 Estimated model parameter from experimental data (all parameters as in Table 4.3). . 114
4.5 Estimated reaction rate constants. 115

D.1 Specification of gas-chromatography 138
D.2 Operation conditions for gas-chromatography 138
D.3 Specification of gas-chromatography for the analysis of the light gas fraction during CVD and TDP. 138

F.1 Intrinsic activity plateaux 148
F.2 CVD on sand 149

G.1 Reactor temperature in $°C$ during heating ramp. 152
G.2 Reaction conditions: Powder modified at 50°C. 153
G.3 Reaction conditions: Powder modified at 100°C. 154
G.4 Reaction conditions: Powder modified at 100°C (aborted series). 155
G.5 Reaction conditions: Powder modified at150°C. 156
G.6 Reaction conditions: Powder modified at 200°C. 157
G.7 Reaction conditions: Powder modified at 300°C. 158

G.8 Reaction conditions: Powder modified at 400°C. 159
G.9 Reaction conditions: Pellets modified at 100°C. 160
G.10 Reaction conditions: Pellets modified at 200°C. 161
G.11 Reaction conditions: Pellets modified at 200°C (reproducibility run). 162
G.12 Reaction data of 1,3,5-TiPB-cracking over unmodified pellet samples (reaction temperature = 210°C). 163
G.13 Reaction data of kinetic studies of toluene disproportionation over powder samples (toluene partial pressure = 13.4 kPa). 164
G.14 Reaction data of toluene disproportionation over pellet samples (toluene partial pressure = 13.4 kPa, reaction temperature = 450°C). 168
G.15 Linear velocities for empty reactor at reaction temperature 170
G.16 Analysis of p-xylene isomerisation over CVD modified silica gel (mass of silica gel: 0.9020 g; surface area: 675 m^2/g; 35-70 mesh; pore diameter:40 Å: CVD: 5 cycles (1h) at 200°C; reaction temperature: 550°C; partial pressure of p-xylene 2.7 kPa; saturator pressure: 120 kPa; reactor head pressure: 110 kPa; carrier gas: nitrogen; flow rate: 15 ml/min). 171
G.17 Repeatability of catalytic reaction work on powder and pellets. 172

H.1 Glossary for Tables H.2 and H.3 174
H.2 Overview of literature related to CVD of alkoxy-precursors on zeolitic and similar material. 175
H.3 Overview of catalytic studies on ZSM-5 employing CVD of alkoxysilanes (TEOS and TMOS). 178

Nomenclature

BET	Brunauer Emmet Teller
ck	Cracking
d_p	Crystal size
d_{kin}	Kinetic diameter
D	Diffusion constant (cm^2/s)
Da	Dammköhler number
DP	Disproportionation
EXAFS	Extended X-ray adsorption fine structure
F	Volumetric flow rate (ml/min)
IR	Infra Red
ISO	Isomerisation
k	First order reaction rate constant (s^{-1})
L	Diffusion path way
n	Number of moles (mol); Silica loading (Si/nm^2)
mS	Meta-xylene selectivity
MTO	Methanol to olefin synthesis
oS	Ortho-xylene selectivity
Pe100°C	Pellets, modified at 100°C
Pe200°C	Pellets, modified at 200°C
pS	Para-xylene selectivity
R	Particle radius
R^2	Correlation coefficient
pY-X-plot	Plot of p-xylene Yield versus toluene conversion
S	Selectivity
SIMS	Secondary ion mass spectroscopy
SOCONY	Standard Oil Company of New York
TDP	Toluene disproportionation
TPD	Temperature programmed desorption
TEM	Transmission electron microscopy
V	(Reactor) volume (m^3)
XPS	X-ray photoelectron spectroscopy
XRD	X-ray diffraction
ZSM	Zeolite SOCONY Mobil
x	Fraction
[i]	Concentration of species i (mol/m^3)
Greek letters	
α	Constant for deactivation of external reactions

β	Constant for deactivation of overall activity
η	Effectiveness factor
σ	Standard deviation
Indices:	
b	Blockage
p	para
m	meta
o	ortho
CVD	Chemical vapour deposition
DP	Disproportionation
ISO	Isomerisation
TiPB	1,3,5-TiPB-cracking
o	Intrinsic property
Chemicals	
mX	Meta-xylene
oX	Ortho-xylene
pX	Para-xylene
T	Toluene
B	Benzene
TMB	Trimethylbenzene
TeMB	Tetramethylbenzene
TiPB	Triisopropylbenzene

Chapter 1

Introduction

Zeolites show great versatility for catalytic reaction and have found widespread use in the chemical industry. Particularly, the occurrence of Brønsted acidity paired with geometric properties have made acid zeolites successful catalysts for a wide range of reactions. The unique structural dimensions of zeolite ZSM-5 facilitate simple aromatic compounds to undergo cracking, disproportionation, transalkylation and isomerisation reactions. The preferential formation of spatially unconstrained products has been termed shape-selectivity and is attributed to two mechanisms: (i) selective diffusion of the participating molecules and (ii) steric constraints in the transition-state of the catalytic transformation. In contrast to the shape-selective influence of the channel geometry inside the zeolite, non-shape-selective reactions occur on the spatially unconstrained activity centers on the external surface.

The chemical vapour deposition is one of many modification methods which have been reported in literature to successfully deactivate the external surface activity and improve the shape selective performance of zeolites. Using suitable alkoxysilanes as precursors, it is possible to selectively deposit silica on only the external surface while retaining the intrinsic pore-structure of the zeolite. The effect of the deposited silica has been investigated using a large variety of catalytic test reactions which preferably have simple reaction pathways. Deactivation of the external surface as well as improved shape-selectivity has been observed. While deactivation of the external surface is easily understood, the cause for the alterations of the shape selectivity remain under debate. Explanations include the elimination of the non-shape-selective contribution of the external surface to selective screening of product molecules which struggle to diffuse through narrowed pore openings. However, too much silica leads to the deactivation of the catalyst due to severe pore mouth blockage.

Röger et al. (1998a) succeeded in monitoring the gradual improvement of shape-selectivity during the disproportionation of toluene when ZSM-5 was modified in successive cycles. Tetraethoxysilane (TEOS) was used as silica source and applied at low modification temperature, viz. 100°C, in up to 16 cycles. Unfortunately, the mass of silica which was deposited onto the external surface was not

determined.

Obviously, the time consuming modification using a cyclic low temperature method is not a desirable process for larger scale application. Since the deposition of TEOS onto the zeolite is a chemical reaction, variation of the modification temperature would appear to be the key parameter in an attempt to understand and control the deposition process.

1.1 Zeolites

Zeolites are crystalline aluminosilcates, consisting of an infinitely extended three-dimensional network of SiO_4 and AlO_4^--tetrahedra. By sharing the oxygen atoms, the primary building units join together into rings which are the secondary building units and determine the internal dimensions of the crystal structure. A well defined channel structure with uniformly sized pore openings is formed. Classification of zeolites proceeds via the number of tetrahedra (T atoms) in the secondary building unit and the dimensionality of the channels (Meier et al., 1996).

1.1.1 Activity and acidity of zeolites

Because of the negative charge that is introduced with each AlO_4^--tetrahedra, the crystal structure has to be counter charged with charge balancing cations. In the case where the compensation occurs with protons, the zeolite exhibits hydroxyl groups which act as Brønsted acid sites. It has to be differentiated between bridging hydroxyls inside the channels and terminal hydroxyls which complete the surface of the three-dimensional structure. The nature, strength and location of the Brønsted acid sites and hydroxyl-acidity is still a matter of debate (Trombetta et al., 2000).

Furthermore, electronically unsaturated species occurring from extra-framework cations, displaced aluminium, defect sites and dehydroxylation at elevated temperature, introduce Lewis acidity into the zeolite (Dyer, 1988; Martens et al., 1997). The contribution of Lewis acidity to the catalytic activity of zeolites remains an unclarified issue (Guisnet et al., 2000).

1.1.2 ZSM-5

Synthesis of ZSM-5 was first reported by Mobil researchers (Argauer and Landolt, 1972). The linking of five membered secondary building units leads to the formation of chains of elliptical shape and a three-dimensional channel structure is constructed (Figure 1.1). The structure consists out of sinusoidal and straight channels which exhibit pore openings of 5.3×5.6Å and 5.2×5.7Å, respectively (Meier et al., 1996).

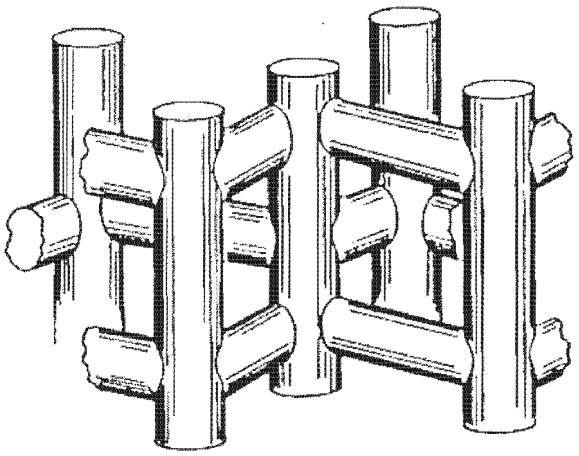

Figure 1.1: The channel network of ZSM-5 (Kokotailo et al., 1978).

1.1.3 Shape selectivity

The reason for shape selectivity lies in the major fraction of active sites being located inside the zeolite channel. Three types of shape selectivity have been distinguished by Csicsery (1979): (a) reactant, (b) product and (c) restricted transition state shape selectivity (Figure 1.2). Reactant selectivity allows only those molecules to react inside the zeolite, which are small enough to diffuse into the structure. In contrast to that, product selectivity occurs, when some of the products are too bulky to diffuse out. In the third type, steric constraints exerted by the zeolite, prevent the transformation of molecules via bulky transition states of a reaction. Reactant and products diffuse and less spatially demanding transition states proceed unhindered.

The two underlying working principles are based either in the steric constraints and/or in the differences in diffusivity of the participating molecules.

In the case of mass transport limitations on the products, the classical diffusion reaction inhibition relationship applies (Chen et al., 1994). Mass transport limitations are described by the Thiele modulus, $\Phi = R\sqrt{k/D}$, with the crystal size R, diffusivity D and intrinsic rate constant k (Thiele, 1939). Introducing the intrinsic selectivity $S = k_A/k_B$, the observed selectivity for two parallel reactions becomes:

$$S_{obs} = \frac{k_A \eta_A}{k_B \eta_B} = S\frac{\eta_A}{\eta_B} \tag{1.1}$$

The selectivity thus can be directed by choosing the appropriate catalyst parameters, viz. particle size and catalytic activity. Under severe diffusion limitations the effectiveness factor $\eta = 1/\Phi$ and thus:

$$S_{obs} = \frac{k_A \Phi_A}{k_B \Phi_B} = \sqrt{\frac{k_A D_A}{k_B D_B}} \tag{1.2}$$

The degree of selectivity in this case is determined by the ratio of the individual diffusivities inside a specific zeolite.

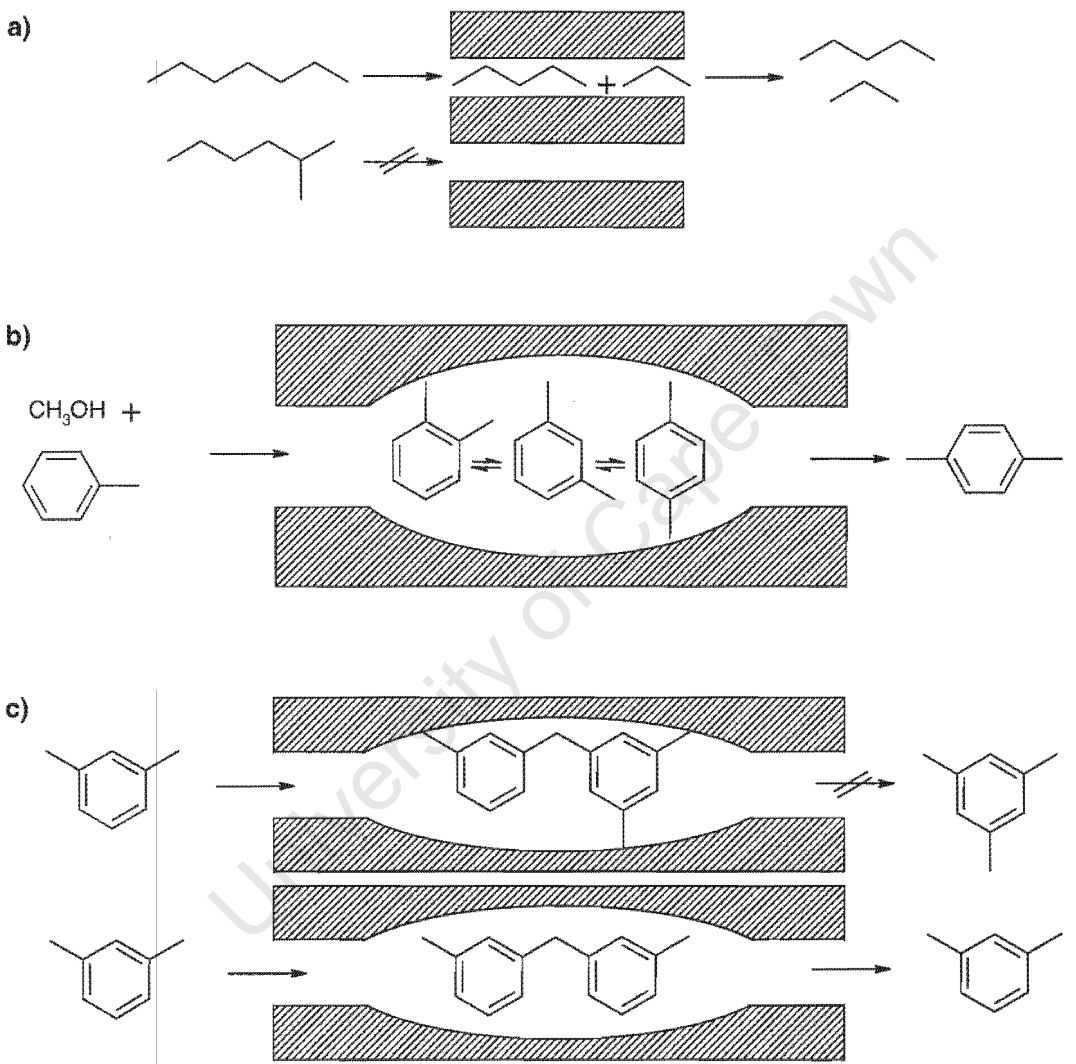

Figure 1.2: Shape selectivity in zeolites: a) reactant-, b) product-, c) restricted transition state shape selectivity (Csicsery, 1979).

1.1.4 The contribution of external active sites on the catalytic behaviour

The catalytic effect of the external surface does not contribute significantly, when the rate of reactions which are catalysed by the external active sites are small in comparison to the reactions which occur inside the zeolite. Also, adsorption and diffusion effects as well as the fraction of external surface of the total area play significant roles.

Effect on activity

Farcasiu and Degnan (1988) presented a general kinetic expression to describe both contributions of internal and external to the overall activity:

$$k_{obs} = (1 - f)\eta k_{int} + f k_s \tag{1.3}$$

where f is the fraction of active sites on the external surface and k_{int} and k_s are the intrinsic rate constants for the internal and external reaction, respectively. The accessability of the internal sites is considered by the effectiveness factor, η. It becomes obvious, that a large fraction of external area and severe diffusional constraints both favor the contribution of the external activity. So would a large difference in the intrinsic rate constants; however, it is unlikely that this is the case over unmodified catalyst.

Effect on shape selectivity

Chandawar et al. (1982) proposed for the alkylation of benzene with ethanol to predominately form the spatially least constrained product inside the zeolite. In the alkylation of toluene with ethanol over ZSM-5, para-ethyltoluene is the main product which isomerises in a secondary step on the external surface and produces the expected ortho- and meta-isomers (Paparatto et al., 1987). In the case of the disproportionation of toluene over ZSM-5, where the rate constant of the xylene isomerisation is reported to be 7000-times larger than the main reaction (Olson and Haag, 1984), the reaction rates would become comparable. The contribution of the external surface would reduce the intrinsic shape selective product spectrum. Recent results by Kim et al. (1998) and Kunieda et al. (1999) in the methylation of toluene and the disproportionation of toluene indicate that the shape selectivity is governed by both diffusional effects and the secondary reaction on the external surface.

Proportion of the external surface

The proportion of the external surface has an important bearing on the catalytic contribution of the external active sites. Since zeolite samples are often far from perfectly spherical and thus exhibit mesopores (Harvey et al., 1995), the external surface is expected to be larger than the ideal geometric

areas. Remy and Poncelet (1995) and Melson and Schüth (1997) reported that around 50% of the total active sites were located on the external surface for small ZSM-5 crystals ($d_p < 0.1\mu m$).

Thus, the contribution of the external surface to the overall reaction must not be underestimated; especially when catalytic systems are investigated where secondary reactions of differing rates and effectiveness factors might interfere.

1.1.5 Application of ZSM-5

ZSM-5 is considered the most useful out of the family of the 10-membered zeolites. High activity, high tolerance to coking, and high hydrothermal stability have made ZSM-5 a widely used catalyst in the petrochemical industry for isomerisation, oligomerisation, disproportionation, cyclisation, aromatisation, esterifications, cracking, hydro-cracking and many other reactions (Corma, 1992; Chen et al., 1994, 1996).

1.2 Modification of the external surface

The modification of the external surface of zeolites has been achieved with several methods which involve the exchange of cations, poisoning of acid sites with organic base molecules, selective coking and the continuation/coating of the structure with the "inert" building component, i.e. silica (Vansant, 1988; Choplin, 1994; Chen et al., 1994).

Several methods for coating with silica have been reported which range from growing aluminium-free silica-shells on the zeolite (Rollmann, 1980) over the liquid phase (Bergna et al., 1989) to the vapour phase deposition (Niwa et al., 1982; Wang et al., 1988). Suitable precursors allow silica deposition of the external surface only. Weber et al. (1996); Weber (1998) compared the above mentioned coating procedures and concluded, that silica deposition from the vapour phase was the preferred method. It achieved the elimination of the external surface without significantly changing the acidic properties of the zeolite.

1.2.1 Chemical vapour deposition (CVD)

The chemical vapour deposition (CVD) of various silica precursors and methods has been reviewed frequently (Vansant, 1988; Chu et al., 1989; Murakami, 1989; Niwa and Murakami, 1989; Choplin, 1994; Iwasawa, 1997; Weber, 1998; Röger, 1998; Kühl, 1999; Impens et al., 1999). The advantages of CVD can be summarised as: (i) high purity of the gaseous reagents, (ii) easy and precise control of the modification conditions and thus on the progress of the reaction and (iii) the possibility to accurately determine intermediates and degree of deposition with conventional techniques (Niwa and

Murakami, 1989). The difficulty in the scaling-up and the involvement of expensive and sometimes hazardous materials are disadvantageous for industrial application.

1.2.2 Silica Precursors

A large variety of silicon containing compounds has been studied for their applicability of silica deposition. References for the use of silanes are found from the early 70's by Kerr (1972) and the selection of suitable compounds has been extended ever since. With the growing number of precursors, the variety of designations for the modification process expanded and is usually referred to as silylation (von Ballmoos and Kerr, 1985; Impens et al., 1999), silynation (Shaikh et al., 1999), silanation (Niwa et al., 1982), disilanation (Yan et al., 1989) or silanisation (Weber et al., 2000).

In summary it can be said that the above mentioned expressions ultimately describe the deposition of silica onto/into a support material, however, involving different reaction mechanisms.

1.2.3 Alkoxysilanes

Particularly suitable silica precursors where found in the class of alkoxysilanes. Niwa et al. (1982) reported on the use of an alkoxysilane: tetramethoxysilane (TMOS) which was larger than the pore size of zeolite mordenite and thus would not affect the acid properties (Niwa et al., 1984a). The larger molecular dimensions of tetraethoxysilane (TEOS) and the lower reactivity (Niwa and Murakami, 1989) as well as lower toxicity (Röger, 1998) make TEOS a promising reagent for a broader range of zeolite types. Tetraalkoxysilanes are known to readily undergo hydrolysis (Bradley, 1989).

1.2.4 Reaction mechanism for alkoxysilanes with zeolites

It is generally accepted that the hydroxyl groups are the reaction points for the alkoxysilanes (Niwa et al., 1984a, 1986b, 1988; Hibino et al., 1993; Tynjälä and Pakkanen, 1997; Shaikh et al., 1999).

A reaction mechanism for TMOS and the surface mordenite was first reported by Niwa et al. (1984a) and clarified in following studies (Niwa et al., 1988). The reaction can be classified as dissociative adsorption. TMOS adsorbs on the surface and yields adsorbed trimethoxy species and methanol. Because the adsorbed trialkoxy species can also undergo condensation reaction with neighbouring adsorbed species, siloxane bonds can be formed. A subsequent hydrolysis step and/or thermal treatment transforms the alkoxy groups into hydroxyls which become susceptible for further deposition. Thus, the formation of silica layers on the external surface is achieved. Niwa et al. (1988) reported that a temperatures lower than 100°C and in the absence of water the adsorbed alkoxy species would not react further, thus favoring the formation of mono-atomic silica fragments. Chun et al. (1994) applied this reaction mechanism to the surface reaction of TEOS on zeolite β.

1.2.5 Methods of deposition

The number of reported CVD methods employing alkoxysilanes is enormous. Table H.2 provides an overview of CVD methods for the deposition of alkoxysilanes on zeolites and related materials. The techniques can be classified depending on whether the modification is carried out under (i) static or (ii) flow conditions. When the modification is carried out on static balance systems (Niwa et al., 1984a), the mass gain due to deposition can be conveniently determined. However, Niwa et al. (1986b) and Weber et al. (1998, 2000) pointed out, that the presence of gaseous deposition products interferes with the primary deposition reaction. In contrast to that, flow systems ensure (Wang et al., 1988), that gaseous decomposition products are continuously removed from the catalyst bed. The degree of deposition can however only be determined indirectly, employing chromatographic techniques.

To ensure uniform deposition across the catalyst bed, the appropriate operation conditions have to be chosen, facilitating low concentration gradients and differential conversion (Röger, 1998). This stipulation aggravates the comparison of modifications which were carried out under static and flow conditions (Weber et al., 2000).

The degree of deposition can be varied by choosing the appropriate contact time of the catalyst with the modifier. Because of the (apparent) self-limiting nature of the deposition reaction at low reaction temperatures, higher amounts of silica can be deposited by the cyclic repetition of modification procedure (Hibino et al., 1988, 1991).

Modification of zeolites in industrial size processes has also been stated. By making use of the ideal mixing behaviour of fluidised beds, Chihara et al. (1996) demonstrated that zeolite Na-A could be successfully modified for mass production. Chang and Rodewald (1996) reported the modification ("trim selectivation") during the initial stage of toluene disproportionation by co-feeding the silicon precursor into the feed stream .

1.2.6 Pre/Post CVD treatment

Modification in static vacuum systems is usually preceded by evacuation and/or calcination of the sample while a calcination step removes impurities in flow systems. Subsequent hydrolysis, evacuation and calcination in air generally follows as the final step of the modification in the respective systems. It has been confirmed that the deposited silicon compound are completely oxidised and stabilised on the external surface (Niwa et al., 1984a).

1.2.7 Parameters which influence the modification procedure

Zeolite type

Hibino et al. (1993) reported that more silica layers were needed for the inertisation of ZSM-5 than for mordenite. Similarly, Weber et al. (2000) found that it was possible to inertise mordenite and β in one CVD cycle, while surface activity of ZSM-5 remained. They concluded, that the deposition occurred more rapidly over the aluminium-rich mordenite and β.

Si to Al ratio

The catalytic properties of zeolites are strongly related to the acidity and in turn to their composition. The CVD enhancing effect of the presence of structural acidity in various materials, such as ZSM-5, silica-alumina, alumina and kieselguhr, was shown by Wang et al. (1988). It must be assumed that the composition of the zeolite strongly affects the CVD (Weber et al., 2000). In contrast to that Hibino et al. (1993) reported that the Si/Al-ratio of mordenite did not affect the deactivation of the external surface with CVD. They furthermore concluded that the CVD proceeded without being influenced by the cation type.

Crystal morphology

A study reported by Bhat et al. (1996c) showed that the crystal size and shape affected the degree of deposition. More silica was required to achieve para-selectivity in the ethylation of toluene when smaller crystals were used. Also, the interference of extra-framework aluminium, requiring higher amounts silica for successful modification, was reported (Hibino et al., 1993).

Extrusion and pelletisation

For practical reasons, zeolite powder is often pressed to pellets, granules or extrudate. Particularly ZSM-5, custom tailored by means of pre-coking and silica modification, is widely used for T-DP (Tsai et al., 1999). Wang et al. (1988) showed that typical binder materials, such as silica and alumina, were reactive to TEOS. However, the use of pellets may influence the effectiveness factor for a catalytic reaction. Thus, an effect of binder on the CVD is conceivable. From a practical point of view the handling of catalyst pellets might be preferred (Weber et al., 2000).

Co-feeds

The modification method of Wang et al. (1988) employed toluene and methanol as co-feeds. It can only be speculated that toluene acts as a unreactive diluent below 200°C (Tsai and Wang, 1991) to retard the deposition rate and allow control over the deposited amount of silica. Wang et al. (1988) claimed that the co-feeding of methanol which subsequently undergoes dehydration, led to water formation which facilitated a more uniform deposition. This conclusion might be misleading since the presence of water also facilitates the formation of the closed silica network (Katada et al., 1994) resulting in the blocking of pores and the deactivation of the catalyst. Ethers might be co-fed to control the amount of water formation when alcohols are present.

Deposition temperature

CVD has been carried out from 25 to 400°C (Table H.2). Niwa et al. (1988) and Hibino et al. (1988) observed the "saturation effect" of the product inhibited deposition reaction at room temperature and at 320°C. This showed that TMOS was more reactive to the hydroxyl groups on the fresh surface than to the adsorbed species on the surface after reaction.

Studies, which in particular focused on the deposition temperature, were reported by (Niwa et al., 1984a, 1986a; Hibino et al., 1988; Wang et al., 1988, 1989; Tsai and Wang, 1991; Chun et al., 1994; Fei et al., 1995). Their aim was to establish the reaction conditions which ensure (i) a desired degree of deposition and (ii) the uniform modification of the catalyst bed by controlling the deposition rate. The effects of the modification was then tested with the adsorption of probe molecules and with catalytic test reactions. Niwa et al. (1984a) showed with temperature programmed desorption (TPD) of NH_3 that the amount of acidity was not significantly changed, when the deposition temperature was varied between 220 and 320°C.

Apart from controlling the deposition rate, the reaction temperature determines the extent of side reactions of the involved reactants and products. Especially the dehydration of alcohols, occurring over acid zeolites, must be considered.

The role of water

The presence of water requires careful attention and cannot be decoupled from the deposition temperature. In-situ generated water catalyses the deposition process (Niwa et al., 1988), thus propagating the deposition reaction. This could provoke the closure of the interlinked silica network on the surface (Katada et al., 1994) detrimentally affecting the accessibility to the zeolite. Thus, water in the reaction and it's autocatalytic function might significantly influence the quality of the deposited silica layer.

It appears that the effects of reaction temperature and the generation of water assume key roles in the deposition process. Conclusions regarding the influence of these parameters on CVD were not found in the literature.

1.3 Characterisation of silanised zeolites

The effects of CVD on zeolites have been studied extensively. Table H.3 serves as an overview of the reported studies.

1.3.1 Conservation of crystal interior

Several adsorption studies, employing small, fast diffusing probe molecules (Niwa et al., 1986b), established that the internal pore space remains unaffected by CVD of TMOS and TEOS. X-ray photoelectron spectroscopy (XPS) measurements by Niwa et al. (1984a) and secondary ion mass spectroscopy studies by Fetting and Dingerdissen (1990) showed that silica is exclusively deposited on the external surface of the zeolite.

When probe molecules of similar size to the channel dimensions, such as para-, ortho-xylene and pyridine, were used, large differences in diffusivities in the zeolite became apparent. While no significant alterations in uptake rates and adsorption capacity for molecules like n-hexane and para-xylene (p-xylene) were observed, bulky molecules, such as o-xylene and trimethylbenzene, were strongly affected. This provoked conclusions to be made about alterations of the pore openings.

Comparing uptake rates of small and fast-diffusing molecules to the rates of bulky and slow-diffusing molecules does, however, not allow deducing changes of the pore geometry.

1.3.2 Acidity of the zeolite

The TPD of NH_3 showed that the CVD of TMOS did neither change the number nor the strength of acid sites of mordenite (Niwa et al., 1984a) and ZSM-5 (Niwa et al., 1986b) when the catalyst was modified in a static system. Pyridine adsorption by Weber et al. (1998) on TEOS modified ZSM-5 confirmed the above observations in both static and flow systems. Inconsistencies at high degree of modification were explained by reduced access of the probe molecules to the internal acid sites due to pore blockage

1.3.3 Morphology of deposited layer

The thickness and the growth orientation of the deposited layer are therefore key variables to explain the effects of CVD. Because of the four functional groups of the TMOS and TEOS, growth could

proceed vertically and horizontally. It would be desirable to continue the zeolite structure with a crystalline layer, rather than depositing amorphous, debris like material. Hibino et al. (1989b,a) studied the deposition of germanium-methoxide, using EXAFS, XPS and TEM. They concluded that the deposited phase resembled amorphous or thinly layered GeO_2. This was taken as indication that the final stabilised deposit would consist of interlinked tetrahedral units. It was also shown that the deposited layer deteriorated under humid conditions which resulted in bulky particles on the surface. Weber et al. (2000) discussed the relative crystallinity of zeolite mordenite, β and ZSM-5 and concluded that the deposited material was amorphous in nature.

Applying the above findings to silica, the CVD should lead to the formation of a thin layered interlinked siloxane network. Because of the low reactivity of the adsorbed alkoxy species it seems likely that growth proceeds horizontally first. The presence of water could facilitate the growth in the vertical direction.

The lack of reactivity of the adsorbed alkoxy species at low temperatures ("saturation-effect") prevents the deposition of sufficient silica, which is needed to cover all potential attachment sites on the external surface (Niwa et al., 1984a, 1986b, 1988). Thus, either higher deposition temperatures or cyclic deposition is necessary to obtain the required silica loading.

The thickness of ca. 3 Å was estimated for a monolayer of SiO_2 (Niwa et al., 1984a). Relating the deposited mass to the assumed attachment site density allows calculation of the thickness. Niwa et al. (1988) showed that one to two layers of silica were obtained, when the deposition reached saturation over mordenite between 0 and 100°C. Saturation over a modified sample resulted in the formation of half a silica layer. Surface analysis with XPS measurements was in good agreement with the calculations (Murakami, 1989).

It can be assumed, that CVD of tetra-alkoxysilanes leads to the formation of thin layers on the external surface. It remains questionable if the structure of the deposited phase can undoubtedly be classified as either crystalline or amorphous.

1.3.4 Modification of the pore mouth

The pronounced differences in uptake rates and equilibrium amounts for the adsorption of p-, o-xylene, n-hexane and water was first reported by Niwa et al. (1984a). CVD resulted in the sequential exclusion of o-xylene, p-xylene and n-hexane from mordenite. Because of the decreasing kinetic diameters of these molecules, it was concluded that CVD allows controlling the size of the pore openings in a uniform manner.

In contrast to the deposition of silica on the external surface, Hibino et al. (1993) found the alterations of the pore opening to depend strongly on the Si/Al ratio. Highly siliceous mordenite required more silica layers to show the molecule sieving effect. It was proposed that the differences in bond length

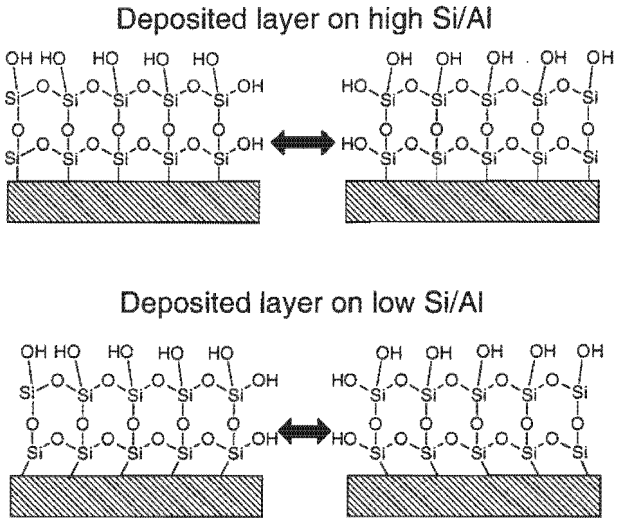

Figure 1.3: Dependence of the extent of pore mouth narrowing on the Si/Al ratio (Hibino et al., 1993).

between Si-O-Al of the zeolite and Si-O-Si of the deposited layer caused the protrusion of silica into the pore opening. This would effectively narrow the pore opening and higher aluminium content would increase the distorting effect (Figure 1.3.4).

After all it must born in mind that the molecular dimensions have a pronounced effect on the diffusivities of the sorption molecules in the zeolite (Wei, 1982). When comparing the uptake rates of molecules of largely differing diffusivities ($D_{p-X}/D_{o-X} \approx 1000$) appropriate measures must be undertaken to determine the equilibrium amounts of the adsorbed species, especially in large crystals (Chen et al., 1994). Consideration must be also given to the dimensionality of the modified zeolite. Modifications of a three-dimensional zeolite (e.g. ZSM-5, β, Y) will not affect the adsorption capacity, unless all pore openings are blocked. When however, the entrances of the same channel in one- and two dimensional systems (e.g. mordenite) are blocked, adsorption capacity will become reduced proportionally to the channel volume.

1.3.5 Blocking of the pore openings

The blocking of pore-openings on the external surface of a 3-dimensional catalyst was mathematically described by Theodorou and Wei (1983). They simplified the 3-dimensional structure to a 2-dimensional, 21 × 21-interconnected-cell-network. Monte-Carlo simulations on a 11 × 11-grid reflected the intra-crystalline reaction and diffusion situation for a monomolecular equilibrium reaction ($A \rightleftharpoons B$) at constant temperature and pressure but at varying degrees of structural modifications. They showed that, as the extent of pore blockage increases, the effective diffusivity and consequently, the effectiveness factor η (i.e. effective reaction rate) decreases (see Figure 1.4). In other words, pore blocking decreases the diffusivity of reacting molecules more effectively than pore narrowing or the introduction of intra-pore restrictions.

Pore blocking is thus another method to achieve selectivity and deactivation. This effect is due to the

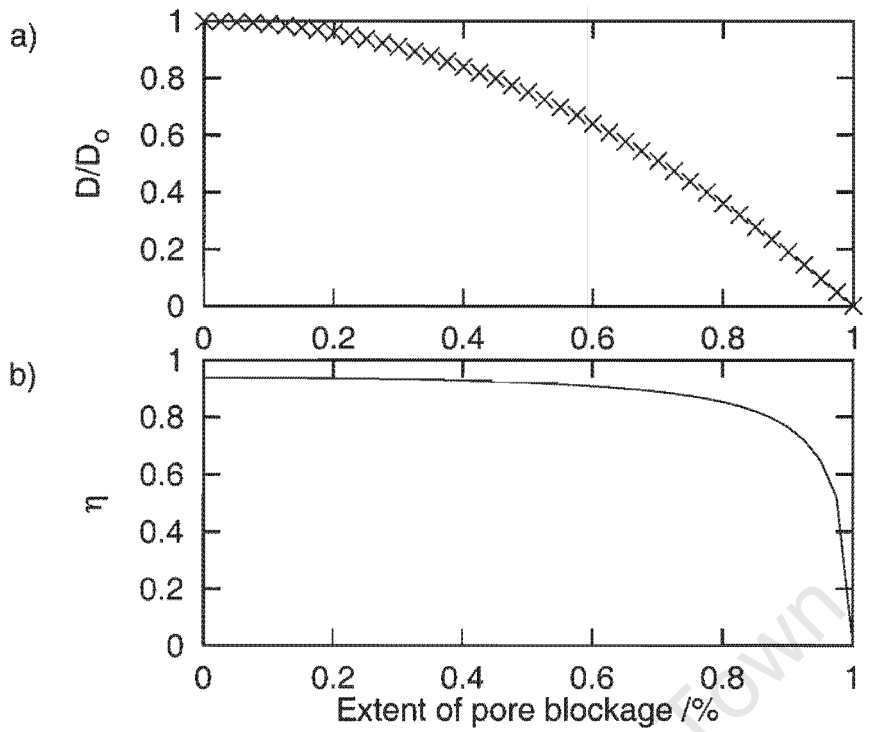

Figure 1.4: Effect of pore blocking on effective diffusivity and effectiveness factor (Theodorou and Wei, 1983).

increased path length that molecules have to traverse in order lo leave a partially blocked catalyst. Most of the selectivity changes occur in the small range of $3 > \Phi > 30$, i.e. the switch between the not diffusion limited range to the strongly diffusion limited regime.

In conclusion, it becomes obvious that regardless, whether the CVD leads to the narrowing or the blocking of the pore openings, differences in mobility and molecular size are both considered in the diffusivity of the molecules. In particular the adsorption of benzene and the three xylene isomers is known to have produced inconsistent results (Chen et al., 1994).

1.3.6 Catalytic testing

The changes of the physio-chemical properties on the external surface are closely related to changes in activity and selectivity of the zeolite for the conversion of hydrocarbons. A catalytic conversion is considered as the "most sensitive" response to modification of the catalyst (Kva et al., 1989). Suitable "test reactions" (Table H.3) provide insight into the key aspects of the catalytic behaviour of the modified zeolites.

Activity of the modified zeolite

Modification via CVD is expected to affect the zeolite's activity in two ways: (i) to eliminate the contribution of the external surface and (ii) to reduce the contribution of the interior by imposing

diffusional constraints on the reaction system.

1,3,5-triisopropylbenzene (1,3,5-TiPB, d_{kin}=8.5Å) is too bulky to enter the channels of mordenite and ZSM-5 (Hibino et al., 1993). Thus, the cracking or isomerisation of this molecule is limited to the external surface only; i.e. to the spatially unconstrained active sites that are located either on the external surface or in the pore entrances. Several authors have applied the cracking of 1,3,5-TiPB on mordenite and ZSM-5 and reported on the inertisation of the external surface (Hibino et al., 1991, 1993; Kim et al., 1996; Röger, 1998; Röger et al., 1998a, 2000; Weber, 1998; Weber et al., 2000). The applicability of the transformation of 1,2,4-trimethylbenzene as a test reaction to monitor the effects of CVD was investigated by Röger (1998); Röger et al. (1998a). It proved to be equivalent to the cracking of 1,3,5-TiPB in probing the external surface activity.

For reactions that make use of shape selective interior of zeolites, clear differentiation between the contributions of the external surface and the catalyst's interior is not readily possible. However, it is frequently reported that CVD resulted in the activity loss for alkylation, disproportionation, aromatisation and cracking reactions (Table H.3). The loss of activity was ascribed to both the inertisation of the external surface as well as increased diffusional constraints which decrease the effectiveness factor of the respective reaction. However, the relationship between the two activity contributions has not yet been quantified (Röger, 1998).

Selectivity

The generation of shape selectivity in zeolites has been extensively studied. Particularly the formation of the valuable para-dialkylbenzenes is of both academic and industrial interest. Since the early work by Kaeding et al. (1981b,a) and Young et al. (1982), the differences in diffusivities of the xylene isomers was invoked to explain the increased para-selectivity of modified ZSM-5. A mathematical model was derived by Wei (1982) which correlated the observed selectivities to the Thiele modulus, $\Phi = R\sqrt{k/D}$. Subsequent models were extended to also incorporate adsorption effects in the zeolite (Klemm et al., 1997). Additionally, Paparatto et al. (1987) proposed that restricted transition shape selectivity favored the formation of the para-isomer inside the crystal but that a secondary isomerisation step on the external active sites yielded an isomer composition in the thermodynamic equilibrium. This suggestion was confirmed for the ethylation of toluene when the external surface was poisoned with β-naphtoquinoline (Wang et al., 1989).

It has been shown for the disproportionation of toluene over ZSM-5 that the para-selectivity improved gradually with increased silica deposition (Hibino et al., 1991). The subtle increase in para-selectivity was monitored by Röger et al. (1998a) by increasing the number of successive CVD cycles of TEOS at 100°C on one and the same sample. Unfortunately, the degree of deposition could not be established.

The difficulty arises in separating both influencing parameters, diffusion and external surface. Kim et al. (1999) and Kunieda et al. (1999) studied the methylation and disproportionation of toluene,

respectively, over 20 kinds of ZSM-5. While the diffusion property of the zeolite was the predominant factor for para-selectivity in the methylation, no such clear conclusion could be drawn for the disproportionation. Thus, CVD that increases diffusional constraints and deactivates the external sites would enhance para-selectivity.

Lifetime

Niwa et al. (1986b) and Sawa et al. (1990) reported on the deactivation behaviour of modified ZSM-5 and dealuminated mordenite, respectively, for the methanol to olefin synthesis (MTO). The modified ZSM-5 showed similar deactivation rates to the parent sample while severe deactivation was observed for the modified mordenite when the degree of deposition was increased.

It is well known that heavy aromatics act as precursor for coke formation inside the zeolite. This leads to the deactivation of the catalyst with extended reaction times. Restricted diffusion retards bulky molecules inside the crystal which undergo further reaction (Guisnet et al., 2000). Recent results by Röger et al. (2000) show that paring of alkyl branches from poly-alkylbenzenes occurs as result of increased diffusional constraints after the CVD on ZSM-5.

If coking also occurs on the external surface, increased pore blocking could influence the rate of deactivation (Suzuki et al., 1983). This will strongly depend on the dimensionality of the zeolite. However, the elimination of external activity should suppress coke formation and hence, increase the life time of the catalyst. Röger (1998) concluded that the interplay of the catalytic system, reaction temperature and amount of deposited silica together determine the effect of deactivation.

1.4 Modification and characterisation

It is apparent that the CVD of tetraalkoxysilanes has gained an important position as post-synthesis technique to improve the shape selectivity of various zeolites. Despite the wide application of this method, several key questions remain unresolved; (i) generation of shape selectivity and (ii) deactivation with increase silica loading. The complete understanding of the effects of CVD is indispensable in order to achieve most successful modification of zeolites.

1.4.1 CVD method of choice

Röger (1998) has monitored the smallest incremental step changes in para-selectivity, due to increased silica deposition, which have been reported in literature so far. ZSM-5 was modified by the CVD of TEOS at 100°C in a flow type system. By repeating the CVD with up to 16 cycles, it was possible to monitor the improving para-selectivity for the disproportionation of toluene over ZSM-5. The p-isomer in the xylene fraction reached a maximum of 98%. Because of catalyst deactivation, the space velocity had to be decreased to maintain a constant toluene conversion of approximately 2.5%. Cracking of n-hexane showed that the interior of the catalyst remained unaffected by the CVD process. The inertisation of the external surface was confirmed by the cracking of 1,3,5-TiPB.

Röger (1998) also applied the transformation of 1,2,4-trimethylbenzene (1,2,4-TMB) as a test reaction, serving to monitor the effects of CVD. The reaction pathway for the rather complex reaction system was elucidated (Röger et al., 1998b).

Röger (1998) concluded that the isomerisation of 1,2,4-TMB on the external surface showed equivalent results to the cracking of 1,3,5-TiPB. The disproportionation reaction inside the crystal however, was very sensitive to increased diffusional constraints as result of CVD. This reaction was thus not desirable as a test reaction for the internal surface.

Thus, the cyclic CVD of TEOS at 100°C provided complete control over the effects of silica deposition with respect to inertisation, retained activity of the interior and improved shape selectivity. However, the mass of the deposited silica could not be determined.

1.4.2 Test reactions to monitor the effects of CVD

Cracking of 1,3,5-triisopropylbenzene (1,3,5-TiPB)

The cracking rate of 1,3,5-TiPB was suggested by Namba et al. (1986) to serve as a measure for the external activity and acidity . The conversion of the bulky molecule, which cannot enter the pore openings of ZSM-5, should be due to dealkylation and isomerisation reactions.

Disproportionation of toluene

The disproportionation of toluene over ZSM-5 is a well established process in the production of p-xylene and highly selective catalysts are desired (Tsai et al., 1999; Kunieda et al., 1999). The primary disproportionation products are benzene and the three xylene isomers. Thermodynamic equilibrium calculations show that the formation of tri- and tetra-methylbenzenes are also possible (Olson and Haag, 1984). However, in the reaction over ZSM-5, these compounds are usually found in negligible amounts only (Kaeding et al., 1981a; Meshram et al., 1983; Chen et al., 1996). Furthermore, Röger et al. (2000) showed that the polymethylbenzenes undergo the paring reaction mechanism at high temperatures yielding light hydrocarbons and benzene.

Three different reaction mechanisms (Figure 1.5) for the acid catalysed disproportionation have been suggested (Uguina et al., 1993): (a) the intermolecular transfer of a methyl group, (b) the dissociative mechanism of dealkylation and subsequent alkylation and (c) the bimolecular mechanism, involving a diphenylmethyl intermediate.

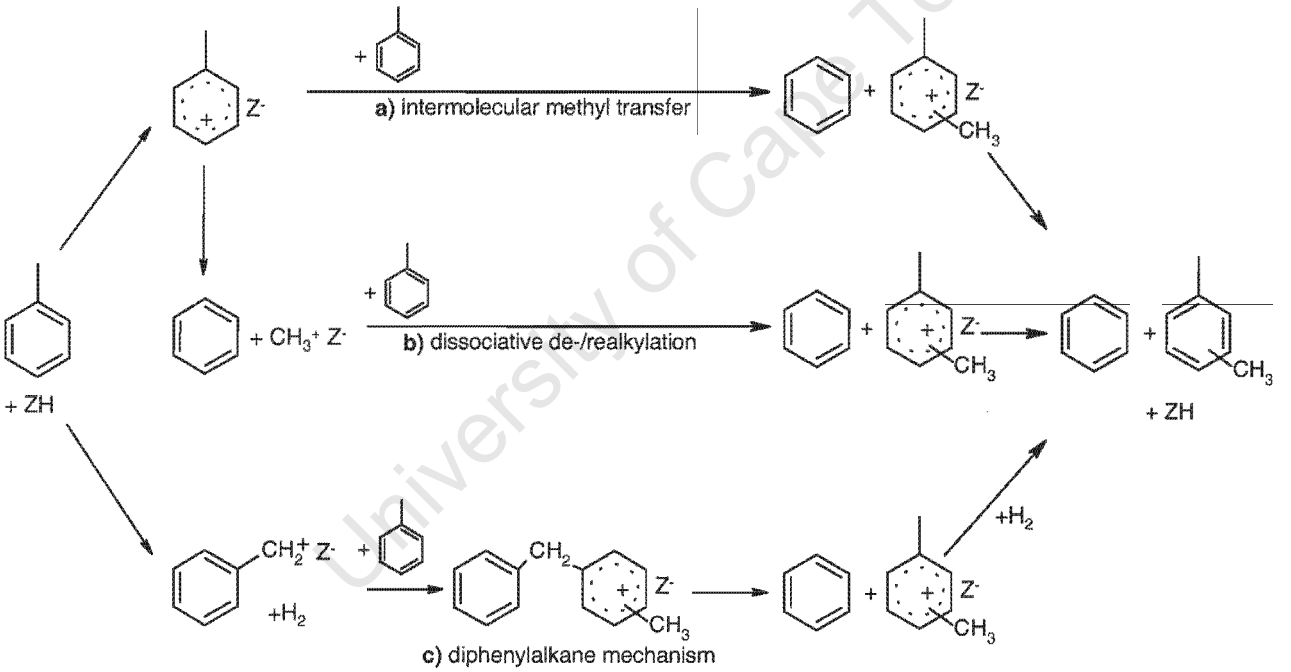

Figure 1.5: Mechanism of toluene disproportionation over zeolites (Uguina et al., 1993).

Isotopic labelling of toluene with deuterium indicated that the first step of the disproportionation inside the ZSM-5 crystal proceeds via the bimolecular transition state (Xiong et al., 1995). The proposed transition state would be snugly accommodated in the straight channels. Not only the reaction mechanism remains a matter of discussion but also the precise kinetics over unmodified ZSM-5 are still under debate (Uguina et al., 1993). However, pseudo-homogeneous first and second order rate laws have been successfully applied (Bhaskar and Do, 1990; Dooley et al., 1990).

TDP is known to produce thermodynamic xylene isomer compositions over a wide range of conversion and reaction temperatures (Kaeding et al., 1981a). The maximum conversion is limited by

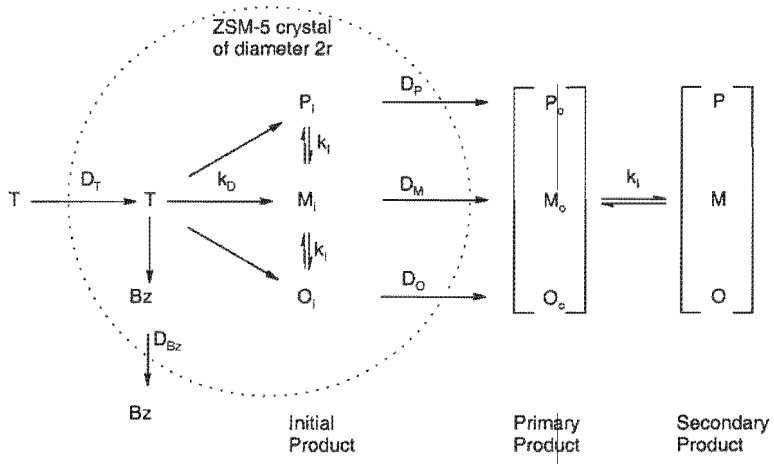

Figure 1.6: Model for selective toluene disproportionation (Olson and Haag, 1984).

thermodynamic equilibrium to 50% (Wei, 1982).

Hibino et al. (1991) showed that para-selectivity of unmodified ZSM-5 increased when the toluene conversion decreased below 1%.

Higher para-selectivities could be achieved by methods constricting the channel dimensions (Kaeding et al., 1981a) and by CVD of tetraalkoxysilanes (Wang et al., 1988, 1989; Hibino et al., 1991; Das et al., 1994; Röger et al., 1998a). Processes that employ the silica deposition and the pre-coking for the para-selectivation of ZSM-5 are reported in literature (Tsai et al., 1999).

The CVD of TMOS (Hibino et al., 1991) and TEOS (Röger et al., 1998a) showed only modest deactivating effects of the modified catalyst for TDP. However, this was only reported for conversion levels of below 2.5%.

Kaeding et al. (1981a) reported that higher para-selectivity over boron-modified ZSM-5 was obtained when the reaction temperature was increased from 500 to 700°C. Similar results over unmodified ZSM-5 were explained with the dependencies of the Thiele modulus, resulting in increased diffusional constraints at higher reaction temperatures (Olson and Haag, 1984). The relationship between xylene-selectivity and structural effects of the zeolite are illustrated in Figure 1.6.

Modification of the channel dimensions affect the diffusional properties. Increased diffusional constraints favor the fast diffusing species and p-xylene concentration outside the crystal becomes enriched. Olson and Haag (1984) explained the detrimental effects of longer space times on the high para-selectivity with the subsequent isomerisation when the para-isomer reenters the structure, yielding all xylene-isomers.

In contrast to that it has been suggested that the transition state restrictions and product selectivity in ZSM-5 limit the mass transport of xylenes to the para-isomer only. Secondary isomerisation on the external surface is held responsible for non-shape selective conversion (Derouane, 1980; Nayak

and Riekert, 1986; Fraenkel, 1990).

Reaction mechanism of xylene isomerisations

The isomerisation of xylenes follows two possible reaction mechanisms (Guisnet et al., 2000). In absence of diffusional limitations, the isomerisation proceeds via the (i) intramolecular mechanism which involves the 1,2-shift of a methyl group in the adsorbed and protonated xylene molecule. This isomerisation is strictly sequential (p-X $\leftrightarrow$ m-X $\leftrightarrow$ o-X) and the direct isomerisation of p- to o-xylene is not possible. In contrast, the predominant mechanism under diffusional constraints is the (ii) intermolecular mechanism. This mechanism requires the disproportionation of two xylene molecules to form a trimethylbenzene and a toluene molecule as the first and rate limiting step. The secondary transalkylation step transfers a methyl group from the trimethylbenzene to either a toluene or more likely to a reactant xylene, allowing the direct p- to o-xylene transformation. The spatial constraints within the ZSM-5 crystal however, impede the formation of bulky bimolecular transition states, so that the isomerisation proceeds mainly via the intramolecular mechanism.

In conclusion it is clear that the observed para-selectivity during TDP over ZSM-5 depends on: (i) the primary product distribution and (ii) the mass transport inside the crystal and on (iii) non-shape selective reactions on the external surface.

1.5 Objective of this study

The review of the present literature showed:

1. CVD of TEOS is an important technique to improve the para- selectivity of ZSM-5.
2. The cyclic CVD method developed by (Röger et al., 1998a) provides excellent control over the degree of modification.
3. Cracking of 1,3,5-TiPB allows quantification of the external activity.
4. Disproportionation of toluene reflects changes in shape-selectivity due to modification of the external surface.

The above stated modification technique and test reactions provide tools to (i) determine the extent and (ii) elucidate the effects of silica deposition.

The objectives are:

1. To develop a broader understanding of the reaction steps that are involved in the modification.
2. To elucidate the amount of deposited silica which causes the change in the catalytic properties of the catalyst.
3. To investigate the effect of the deposition temperature on the quality of the deposited layer with special regards to deactivation with increasing silica loading.
4. To separate the contribution of the external activity from the activity of the interior.
5. To understand the influence of diffusion effect on the reaction pathways.

Chapter 2

Experimental

2.1 Materials

2.1.1 Chemicals

Analytical grade reactants (see Table 2.1) were used without further purification. They were fed into the reactor by means of saturators. Acid washed sea sand, used for the dilution of the catalyst, was boiled three times in distilled water and calcined in air at 950°C for 12 hours. Nitrogen was used as a carrier gas in all experiments. The reactor was operated at 150 kPa absolute pressure. Synthetic air was used in all calcinations and regenerations.

Table 2.1: List of Chemicals

Chemical	Producer	Purity	B. P.	ρ at 25°C	Molar mass	Description
		%	$°C$	g/cm^3	g/mol	
Tetra-ethoxysilane	Fluka	> 98.0	163-167	0.933	208.33	Cat.-#86580
Toluene	Saarchem	> 99.8	119-112	0.867	92.14	Cat.-#608 1040; batch 1010013
1,3,5-tri-iso-propyl-benzene	Aldrich	> 97	232-236	0.845	204.36	
p-xylene	Saarchem	> 99	138	0.860	106.17	
sea sand	Aldrich			2.5-2.8		Cat.-#27.473-9; quartz, white -50 +70 mesh, Lot 20084-107
Silica Gel	Aldrich					Cat.-#24.217-9; 675 m^2/g; 35-70 mesh; 40Å
Nitrogen	Messer Fedgas	4.5				
Air (synthetic)	Messer Fedgas					

2.1.2 Catalyst

MFI catalyst powder, supplied by Südchemie AG in the hydrogen exchanged form, was used throughout all experiments. The silicon to aluminum ratio was 44. The scanning electron micrograph in Figure 2.1 shows that the catalyst particles had a narrow diameter distribution of around 150 nm. Nitrogen adsorption was carried out using a Micromeretics ASAP 2000 analyser. The external surface areas were calculated using the BJH algorithm (Webb and Orr, 1997). The BET isotherm of the catalyst are shown in Figures A.1 and A.2 and the NH_3-TPD spectrum in Figure A.3. The total acidity of 0.74 mmol NH_3/g was determined for the catalyst.

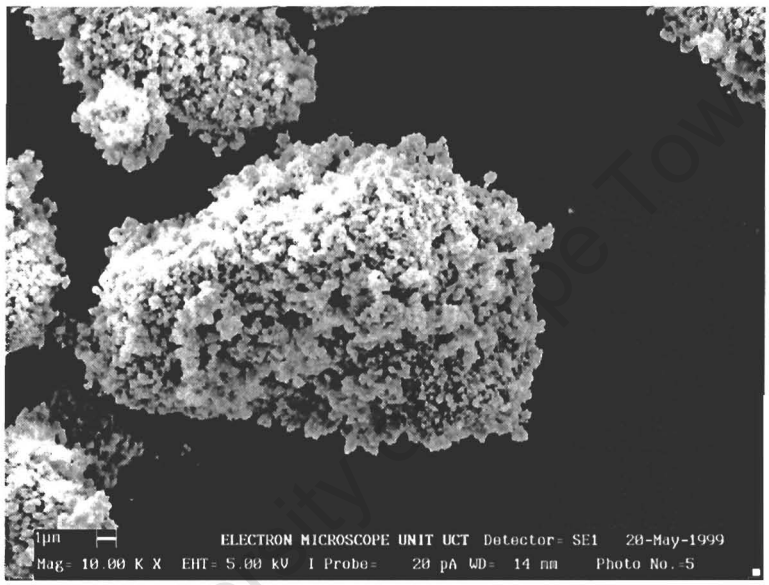

Figure 2.1: SEM micrograph of ZSM-5

Table 2.2: Catalyst specifications

Catalyst type	MFI	
Producer	Südchemie AG	MFI-90
Si/Al	44	
powder		
total BET surface area (m^2/g)	425.1	(N_2)
external surface area (m^2/g)	128.4	(N_2)
Acidity (mmol/g)	0.74	NH_3-TPD
pellets		
total BET surface area (m^2/g)	406.4	(N_2)
external surface area (m^2/g)	132.0	(N_2)

2.2 Experimental apparatus

2.2.1 Apparatus

All reactions, CVD and test reactions, were carried out in the apparatus shown in Figure 2.2. All flow rates were regulated by Unit mass flow controllers. Thermostated glass saturators were attached to the apparatus via neoprene tube connections. The saturator could be bypassed. The total pressure in the saturator which was monitored with a pressure sensor, could be adjusted by a needle valve (N1). The reactor bypass line was equipped with a needle valve (N2) with which equal pressure differentials of bypass and reactor bed could be achieved. Thus, the feed stream in the bypass line and in the reactor head were of the same composition. The reactor head pressure was controlled with a back pressure regulator in the product line and was monitored with a pressure sensor located at the reactor inlet. The reactor was housed in a custom made tubular furnace which showed good isothermal behavior over the length of the catalyst packing. The temperature of the catalyst packing was measured by a thermocouple placed in the center of the reactor (see Figure C.1). Feed and product lines of the apparatus were heated to 120°C.

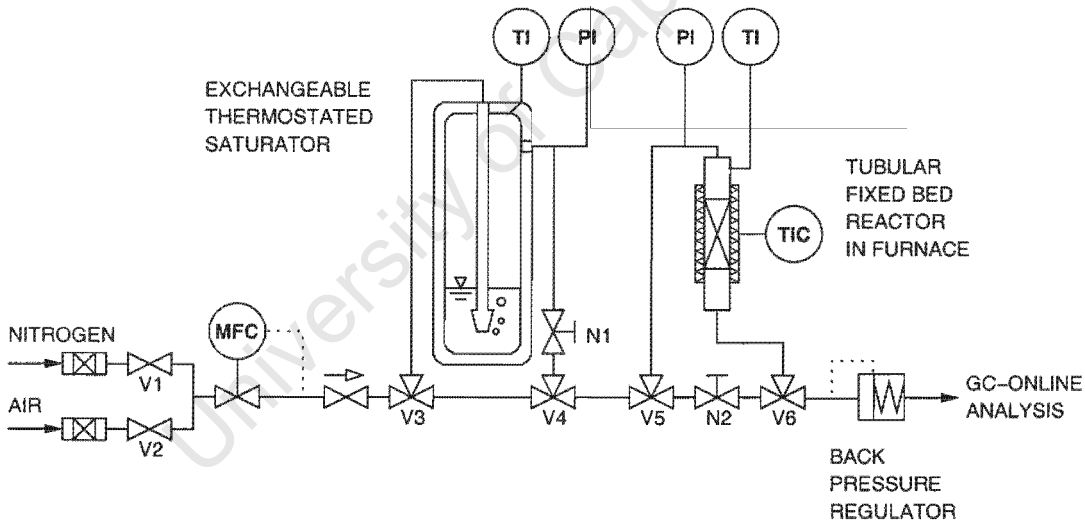

Figure 2.2: Flowsheet of reaction apparatus.

2.2.2 Reactor

A stainless steel tube with 10 mm internal diameter and 80 mm length was used as reactor (approximately 7 cm^3 volume). To measure the temperature in the center of the catalyst packing, a thermowell with an outer diameter of 3.1 mm was fitted to the reactor head. The reactor could be connected to the reaction rig via VCR-vacuum-fittings which were welded on both the inlet and outlet of the tube. A sketch of the reactor is shown in Figure C.1 (Appendix C).

2.2.3 Saturator

Reactants were fed using single stage bubble saturators which were made from glass. Full saturation of the gas stream was a priori confirmed by monitoring the constant liquid level in the reservoir of a second saturator in-line. The carrier gas was dispersed by a frit as fine bubbles and percolated through the liquid reservoir. The jacket around the saturater contained water which was supplied by a thermostated bath. The fine dispersion of the carrier gas into the liquid ensured full saturation of the gas over a wide range of flow rates. A sketch of the saturator can be found in Figure C.2 (Appendix C).

2.2.4 GC-online analysis

Reactor effluents were analysed using online GC. A fixed volume (500 μl) sample loop was used to inject the gas samples into the separation column. Conditions of the operation of the GC are given in Table D.1 (Appendix D).

2.2.5 GC-Analysis of unretained compounds and light hydrocarbon samples

For additional analysis of the gaseous products leaving the reactor samples could be taken with a gas-syringe. An access port was located before the sample valve. Gas samples could then be transported for further analysis to a cryogenic GC. Condensation of the light hydrocarbons in the gas-syringe at room temperature did not occur. Details of the GC specifications and conditions for the analysis are given in Table D.3 (Appendix D).

2.3 Experimental procedure

2.3.1 Preparation of powder

The H-MFI powder was attached to sand in order to maintain isothermal conditions throughout the reactor bed, to avoid channelling effects and to enhance plug flow. 0.5 g Catalyst powder was mixed with 4.5 g catalytically inert sand, wetted with distilled water and intensely stirred. The catalyst sand mixture was dried at 50°C.

2.3.2 Preparation of catalyst pellets

Catalyst powder was compressed to wafers (1 mm thickness) by applying pressure of 40 kN with a hydraulic press (34 mm diameter). The wafers were crushed and sieved to obtain the particle size

fraction of 300-500 μm. 1.5 g pellets mixed with 4 g sand were used for the modification and test reactions.

2.3.3 Loading of the reactor

The catalyst, 0.5 g powder (attached to 4.5 g sand) or 1,5 g pellets (mixed with 4 g sand), were placed inside the tubular reactor. The depth of the catalyst bed was approximately 4 to 5 cm. Sand packing of 3 g each up- and down-stream ensured isothermal conditions and a well developed flow pattern. After loading, the reactor was attached to the reaction rig (down-flow mode) and a leak test was performed.

2.3.4 Run preparation and setting of reactor conditions

In preparation for each run (CVD or reaction) the catalyst was calcined (pretreatment and regeneration) in a stream of flowing air at 550°C for at least 3 hours. An overview of the reaction conditions for the experiments on powder and pelletised samples are given in Tables 2.3 and 2.4, respectively.

2.3.5 Setting to test reaction temperature

After calcination the stream of air was replaced by nitrogen and the desired reaction temperature set (see Tables 2.3 and 2.4). Once this temperature was reached and the pressure readings were taken, the reactor was switched to bypass mode and the bypass line pressure could be adjusted to the correct value. The thermostated feed saturator was attached, the desired head pressure adjusted and the flow was allowed to stabilise for 1 h while bypassing the reactor. The moment the reactor was switched on-line is defined as zero time on stream for the test reaction run.

2.3.6 Setting to CVD reaction temperature

After the calcination prior to a deposition treatment, the reactor was sealed off and allowed to cool down to the desired deposition temperature. Then, the reactor was opened to the nitrogen flow in order to establish the pressure for a maximum period of 5 min. Thereafter the reactor was switched to bypass again and the bypass needle valve was adjusted to obtain the desired pressure in the bypass. Then, the TEOS saturator was attached and stabilised for 1h, bypassing the reactor. The moment the reactor was switched on line is defined as zero time on stream.

2.3.7 CVD-step

For CVD treatment, the nitrogen carrier stream was saturated with TEOS vapour and passed over the catalyst bed for 1 h. After the deposition the TEOS saturator was disconnected and the pure nitrogen carrier gas was flushed through the reactor for 10 min. Only then, the reactor was heated at a rate of 10°C/min to the final calcination temperature of 550°C. Once this temperature was reached, the nitrogen carrier stream was replaced by air.

2.3.8 Cyclic CVD-reaction-sequence

CVD treatment and test reactions were carried out in the same apparatus. After the fresh catalyst's initial calcination, cracking of 1,3,5-triisopropylbenzene (1,3,5-TiPB-cracking) and disproportionation of toluene (TDP) were used to determine the catalytic performance of the parent catalyst. The partial pressures of the probe compounds were derived from standard literature on physical properties of liquid and gases (Reid et al., 1987). An overview of the reaction conditions is given in Tables 2.3 and 2.4. After the reaction time the 1,3,5-TiPB saturator was disconnected, the nitrogen carrier gas replaced by air and the reactor ramped to the final calcination temperature of 550°C. A heating ramp of 10°C/min was employed. After each TDP run, the saturator was detached and the reactor was allowed to cool down to 300°C, before the gas stream was switched from nitrogen to air. Only then the reactor was ramped to the final calcination temperature. The cooling step was introduced to avoid alterations in the catalyst bed due to thermal shock resulting from temperature spikes after the sudden combustion of coke at 550°C when introducing air into the reactor. Bypass samples and samples of the reactor effluent were taken by means of GC-online analysis (see Tables D.1, D.3 and D.2). The catalyst was not exchanged throughout the number of CVD treatments and test reactions during the investigation of a temperature series.

Table 2.3: Reaction conditions for powder samples (catalyst mass: 0.5 g; carrier gas: nitrogen; see G.15 for detailed list of linear velocities and WHSV for kinetic studies of TDP).

	CVD	TiPB	TDP	Calcination
feed	TEOS	TiPB	Toluene	
partial pressure of feed (kPa)	0.88	0.17	12.31	
flow rate carrier gas (ml/min)	100	92	50	100
reaction temperature (°C)	various	270	550	550
reactor head pressure (kPa)	150	150	150	
linear velocity in empty reactor at reaction conditions (cm/s)	various	2.63	2.34	3.81
WHSV ($g_{feed}/(g_{catalyst}h)$)	0.51	0.10	1.72	
time on stream (min)	60	65	65	180

Table 2.4: Reaction conditions for pelletised samples (catalyst mass: 1.5 g; carrier gas: nitrogen; see G.15 for detailed list of linear velocities and WHSV for kinetic studies of TDP).

	CVD	TiPB	TDP	Calcination
feed	TEOS	TiPB	Toluene	
partial pressure of feed (kPa)	0.88	0.17	12.31	
flow rate carrier gas (ml/min)	300	100	10	300
reaction temperature (°C)	various	210	450	550
reactor head pressure (kPa)	160	160	120	
linear velocity in empty reactor at reaction conditions (cm/s)	various	2.54	0.62	10.81
WHSV ($g_{feed}/(g_{catalyst}h)$)	0.55	0.04	0.11	
time on stream (min)	60	65	65	180

2.3.9 Effect of reaction temperature on TDP over powder

In order to study the effect of the reaction temperature on TDP, both flow rate of the carrier gas and reactor temperature were varied. The carrier gas flow was adjusted to the minimal possible rate (around 10-15 ml/min) at which constant flow was ensured. The maximum flow rate of around 130 ml/min was given by the limitations of the mass flow controller as well as the high pressure limit with which the glass saturator could be operated. The reactor temperature was set to 450, 500 and 550°C. When the reactor had reached the desired temperature, the carrier gas flow was allowed to stabilise and 3 samples were taken at 10 min intervals before the flow rate was adjusted. The results are displayed in Figure 3.11. Deactivation of the catalyst was not observed (see Table G.13).

2.3.10 Long time TDP studies over pellets

In order to monitor loss of activity with increased time on stream the unmodified (parent) and modified pellet samples were submitted to TDP up to 265 min. Samples were taken every 10 min and the results are shown in Figures 3.12 and 3.23.

2.3.11 Variation of WHSV during TDP over pellets

After 20 CVD cycles at 100°C the modified pellet sample was used to investigate the effect of toluene conversion of p-xylene-selectivity. The conversion was altered by changing the flow rate of the carrier gas to 10, 20 and 40 ml/min. When the flow through the reactor and the pressure readings for the saturator and the reactor head were stable, 4 samples were taken at 10 min intervals. The results are shown in Figures 3.12 and 3.23.

2.3.12 Isomerisation of para-xylene over silica gel

Para-xylene (p-xylene) was reacted over silica gel in order to estimate the extent of the isomerisation reaction at 450°C. 0.90 g silica gel (adsorption surface 675 m^2/g), diluted with 4 g sand, was subjected to 5 CVD treatments at 200°C with the above described procedure for pellets. P-xylene was feed via a saturator at a partial pressure of 2.67 kPa. The flow rate of the carrier gas was set to 10 ml/min. Bypass samples were taken at 10 min intervals. The reactor was switched online and the first sample was taken after 5 min on stream. The total time on stream was 35 min.

2.4 Evaluation of catalytic reaction data

2.4.1 Molar flow rates

The molar flow rate of the carrier gas was controlled by the volumetric flow rate, $\dot{v}_{cg}$, at standard pressure and temperature assuming ideal gas behavior:

$$\dot{n}_{cg} = \frac{p^{\circ}\dot{v}_{cg}}{RT^{\circ}} \tag{2.1}$$

The molar flow rate of the feed was determined by the partial pressure, p_i, the total pressure in the saturator, p_{sat}, and the molar flow rate of the carrier gas, $\dot{n}_{cg}$:

$$\dot{n}_{feed} = \frac{p_i}{p_{sat} - p_i}\,\dot{n}_{cg} \tag{2.2}$$

The total molar flow rate of feed and carrier gas stream was calculated according to:

$$\dot{n}_{total} = \frac{p^{\circ}\dot{v}_{cg}}{RT^{\circ}}\left(1 + \frac{p_i}{p_{sat} - p_i}\right) \tag{2.3}$$

2.4.2 Concentrations

The concentration of the feed species at reactor conditions was calculated applying the ideal gas law:

$$c_{feed} = \frac{\dot{n}_{feed}\, p_{reactor}}{\dot{n}_{total} R T_{reactor}} \tag{2.4}$$

2.4.3 Conversion

The conversion of the reactants is defined as:

$$X_{feed} = (1 - \frac{\dot{n}_{feed,\ out}}{\dot{n}_{feed,\ in}}) \times 100\% \tag{2.5}$$

2.4.4 Carbon balance

From the GC spectra carbon mass balances were obtained, using the ratios of the total peak area for a sample at the time = t and the peak area of the bypass samples.

$$C - balance = \frac{\sum_i Peak\ area_{i,\ out}}{Peak\ area_{feed}} \times 100\% \tag{2.6}$$

Coke formation in the reactor reduces the precision of the carbon balance. However, it does not effect the calculation of the conversions.

2.4.5 p-Xylene selectivity (benzene free)

P-xylene selectivity during the TDP is calculated as concentration of p-xylene divided by the sum of the concentrations of all xylene isomers in the product, i.e. on a benzene-free basis.

$$pS = \frac{[p-xylene]}{[p-xylene] + [m-xylene] + [o-xylene]} \tag{2.7}$$

2.4.6 Selectivity

The selectivity of the desired product i of a reaction is defined as:

$$S = \frac{[product_{\ desired}]}{\sum_i [product]} \tag{2.8}$$

2.4.7 p-Xylene yield

The p-xylene yields are calculated as the product of the conversion of toluene, X, and the selectivity for p-xylene, S, i.e. on a benzene free basis and in mol-%.

$$Y = S \times X \tag{2.9}$$

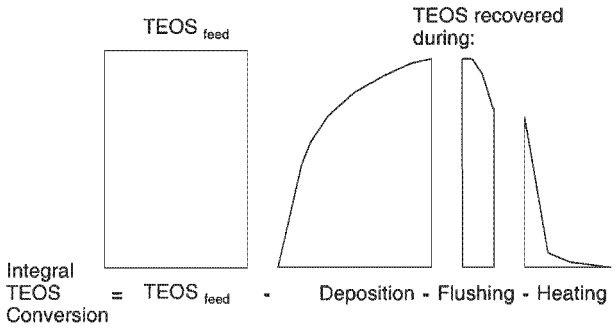

Figure 2.3: Illustration of the calculation of the integral TEOS conversion from a breakthrough curve.

2.4.8 Integral TEOS conversion for CVD treatment

The concentration of TEOS in the carrier gas stream was confirmed by analysing bypass samples before the deposition step. The saturated TEOS vapour was fed into the reactor for 60 min. TEOS was recovered during the deposition, flushing and heating step. Samples were taken every 5 min. The amount of recovered TEOS was determined by integrating the area below the breakthrough curve. With the known concentration of TEOS in the feed and the amount of recovered TEOS, the integral TEOS conversion for CVD treatment was calculated. The calculation of the integral TEOS conversion from a breakthrough curve is illustrated in Figure 3.27.

$$X_{TEOS,\ integral} = (1 - \frac{n_{TEOS\ recovered}}{\dot{n}_{TEOS\ bypass} \times 60\,min}) \times 100\% \tag{2.10}$$

2.4.9 Silica loading on the external surface

The degree of deposition can be expressed as silicon-oxide- or silicon-density on the external surface (Niwa et al., 1984a), assuming that each converted TEOS molecule is deposited as SiO_2. The external surface area was measured by nitrogen-BET-adsorption area. A sample calculation can be found in section F.5.

$$Si/nm^2 = \frac{amount\ of\ converted\ TEOS}{external\ surface\ area\ of\ catalyst} \tag{2.11}$$

2.4.10 Silicon density from the TEOS monolayer

The molecular diameter of TEOS was assumed to be 0.96 nm (Yue et al., 1997). Thus the number of TEOS molecules adsorbed on a monolayer on the external surface of the catalyst is:

$$n_{TEOS\ on\ monolayer} = \frac{external\ surface\ area\ of\ catalyst}{\pi \frac{d^2_{TEOS}}{4}} \tag{2.12}$$

Furthermore, each adsorbed TEOS molecule deposits as SiO_2 on the surface. Thus, the silicon density upon adsorption of a TEOS monolayer is:

$$Si/nm^2{}_{from\ TEOS\ monolayer} = \frac{n_{TEOS\ in\ monolayer}}{external\ surface\ area\ of\ catalyst} \tag{2.13}$$

2.4.11 Integral carbon balance for CVD treatment

Integration of the total peak areas of the samples taken during a CVD treatment produced the mass of carbon leaving the reactor. The ratio of the carbon mass leaving to the carbon mass feed, represents the integral carbon balance for a CVD treatment.

$$C - balance_{\ integral} = \frac{C_{\ recovered}}{\dot{C}_{\ bypass} \times 60\,min} \times 100\% \tag{2.14}$$

2.4.12 First order rate constant

Apparent first order rate constants at reaction temperature and pressure in a plug flow reactor were determined, assuming the reactions to occur in a constant density system and reactants obey the ideal gas law.

$$k = -\frac{\dot{n}_{total}\,RT}{m_{cat}\,p}\ln(1-X) \tag{2.15}$$

2.4.13 Normalised first order rate constant

In order to highlight the changes in the first order rate constant and to compare the individual modification series, the actual first order rate constants after the modification were normalised by the first order rate constant of the respective parent sample. Thus, the normalised first order rate constant was obtained:

$$k_{\ normalised} = \frac{k_{\ modified}}{k_{\ unmodified}} \tag{2.16}$$

2.4.14 Reaction rates

First order reaction rates, r, were calculated using the first order reaction rate constant k and the concentration of the feed at reactor conditions, C.

$$r = k\,C \tag{2.17}$$

2.4.15 Error in conversion data

For the calculation of the fractional conversions from the reaction data, samples taken between 25 min and 65 min time on stream were averaged. The standard deviation over the average, $\bar{x}$, of the number of samples, n, is taken as the error in measurement:

$$\sigma = \sqrt{\frac{1}{n-1}\sum_{i=1}^{n}(x_i - \bar{x})^2} \tag{2.18}$$

It indicates the expected deviation from the mean value in the confidence interval of 68.3%.

2.4.16 Weight hourly space velocity

The mass flow of feed per mass of catalyst and hour is defined as weight hourly space velocity:

$$WHSV = \frac{\dot{m}_{feed}}{m_{cat}} \tag{2.19}$$

2.4.17 Time on stream

The moment, when the reactor was switched in line, is defined as zero time on stream, thus including the dead time. Reaction data for the cracking of 1,3,5-TiPB and TDP were evaluated when the system reached pseudo steady state (after 25 min). Thus, the dead time of the reactor does not affect the data.

2.4.18 Modified space time

The modified space time is defined as:

$$\tau = \frac{1}{WHSV} \tag{2.20}$$

2.4.19 Linear velocity

The gas velocity at reaction conditions in an empty reactor is defined as the linear velocity:

$$u = \frac{\dot{n}_{total} R T}{p_{reactor}\,\pi(d^2_{reactor} - d^2_{thermowell})} \tag{2.21}$$

2.4.20 Film diffusion

Mass transfer through the stagnant film around a catalyst particle can become the reaction limiting step at low linear velocities and high reaction rates. For the same experimental apparatus and similar particle sizes, Röger (Röger, 1998; Röger et al., 1998b) has shown that film diffusion limitation was negligible for the transformation of 1,2,4-trimethylbenzene (TMB) over ZSM-5 at 450°C. The minimal linear gas velocity and the maximal reaction rate of TMB was 0.2 cm/s and 2.95×10^{-3} mol/(kg s), respectively.

Since in this kinetic study at 550°C the minimal linear velocity was higher (0.71 cm/s) and the reaction rate for TDP was lower (3.79×10^{-4} mol/(kg s)), film diffusion limitations will not occur.

2.4.21 Plug flow

Röger (Röger, 1998) has shown that for linear velocities between 0.2 and 3.6 cm/s both criteria for plug flow

$$\frac{d_p}{ID_{reactor}} > 15 \tag{2.22}$$

(Chu and Ng, 1989) and axial dispersion

$$\frac{L}{d_p} > \frac{20n}{Pe_p} ln\frac{1}{1-X} \tag{2.23}$$

(Moulijn et al., 1991) up to X=0.9 are fulfilled.

In this study the linear velocities varied between 0.71 and 10 cm/s and the conversions were generally below 0.9. It can be thus concluded that the experiments were carried out at plug flow conditions.

2.4.22 Reactor dead time

The lowest linear flow rate of 10 ml/min was used in the reaction temperature study of TDP over pelletised samples. The maximum residence time at standard (1 bar, 25°C) and reaction conditions (1,5 bar, 550°C) is thus 42 and 1.3 s, respectively. Sampling was thus not affected by the reactor dead time.

Chapter 3

Results

3.1 Product Analysis during TEOS deposition

The Deposition of TEOS was monitored by following the breakthrough of TEOS and its decomposition products, ethanol and ethene, in the reactor effluent using GC analysis. Figure D.1 shows the complete GC trace of a modification step at 200°C.

Ethanol and ethene are the main decomposition products of TEOS in the investigated temperature range. Compounds which were not retained in the 25 m BP20-column were analysed separately in a cryogenic GC equipped with a 50 m PONA-1 column. GC operation conditions and GC-traces of gas samples, taken during deposition and heating step, are both given in Table D.3 and Figure D.4. Ethene was the biggest contributor to the peak area of unretained compounds during the deposition at 200°C. During the heating step (at approximately 250°C) methane, ethane, diethylether, dimethylether and short hydrocarbons were observed. However, the quantities of these compounds were small compared to the ethene peak area. Thus, only ethene was considered in further quantitative analysis and the peaks of the unretained compounds are referred to as ethene.

3.1.1 TEOS breakthrough

Figure 3.1 shows representative breakthrough curves of TEOS during the deposition, flushing and heating step of a modification treatment at 50°C and 400°C. The breakthrough curves for all other temperature series are given in Figure B.1.

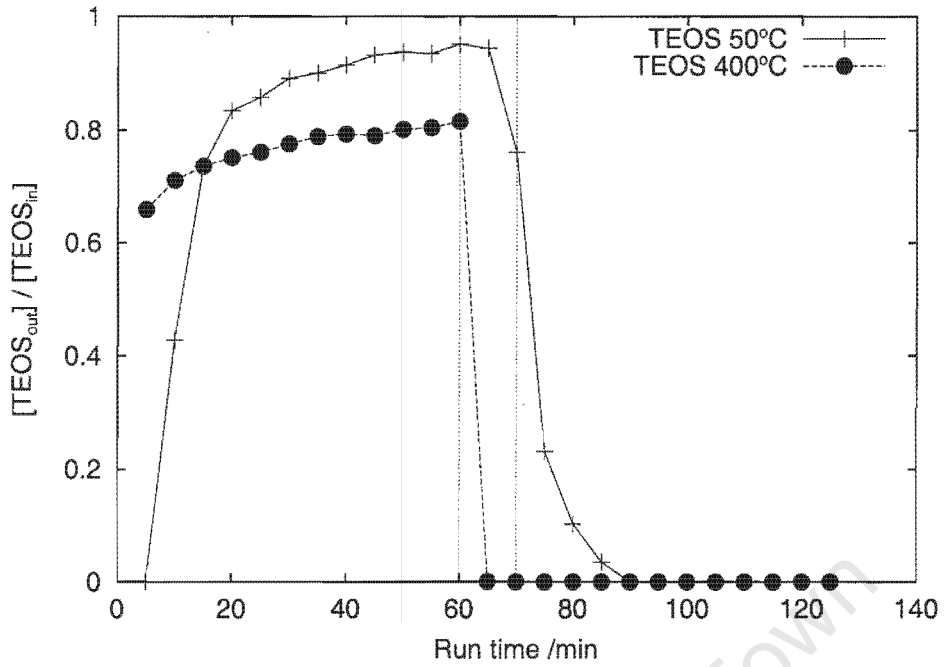

Figure 3.1: TEOS breakthrough curves on powder at T_{CVD}=50 and 400°C (last CVD treatments of the series, cycle 12 and 20, respectively).

3.1.2 Ethene and ethanol

Ethene

The CVD treatment can be subdivided into two distinct sections. The first part is the actual deposition of TEOS at constant temperature and lasted 60 min. During the second part, no TEOS is fed and pure carrier gas flows through the reactor, viz. the flushing and heating step. The concentrations of the ethene and ethanol which were detected during these two steps varied with changing deposition temperature.

Figure B.2 shows the ethene concentration curve during the modification between 50 and 400°C. No ethene is observed during the deposition and flushing step at low modification temperatures. High ethene concentrations are observed during the heating of the reactor to the final calcination temperature. At high modification temperatures, ethene is observed from the beginning of the deposition. The subsequent flushing and heating step shows only small amounts of ethene. The maximum concentration was found during the heating step, when the reactor was ramped to approximately 250°C (95 min). A second, lower maximum was seen at the reactor temperature of approximately 400°C (110 min).

Ethanol

The reverse behavior as for ethene, was observed for the formation of ethanol and is shown in Figure B.3. Modification at low temperatures leads to an increased ethanol concentration in the beginning of the deposition. Large amounts of ethanol are observed during the temperature ramp. The deposition at high temperatures results in the continuous formation of ethanol. Comparably less ethanol is found in the reactor effluent during flushing and heating steps. The maximum concentration was found during the temperature ramp when the reactor reached 200°C (90 min).

3.2 Integral TEOS conversion

The area below the concentration curve was integrated and the amount of recovered TEOS was determined, as shown in Figure 3.2. The difference of feed and recovered amount of TEOS was assumed to be deposited onto the zeolite and the reactor packing (see also Appendix F.4). With the known concentration of TEOS in the feed stream and the recovered fraction the integral TEOS conversion for the entire deposition, flushing and heating sequence was calculated.

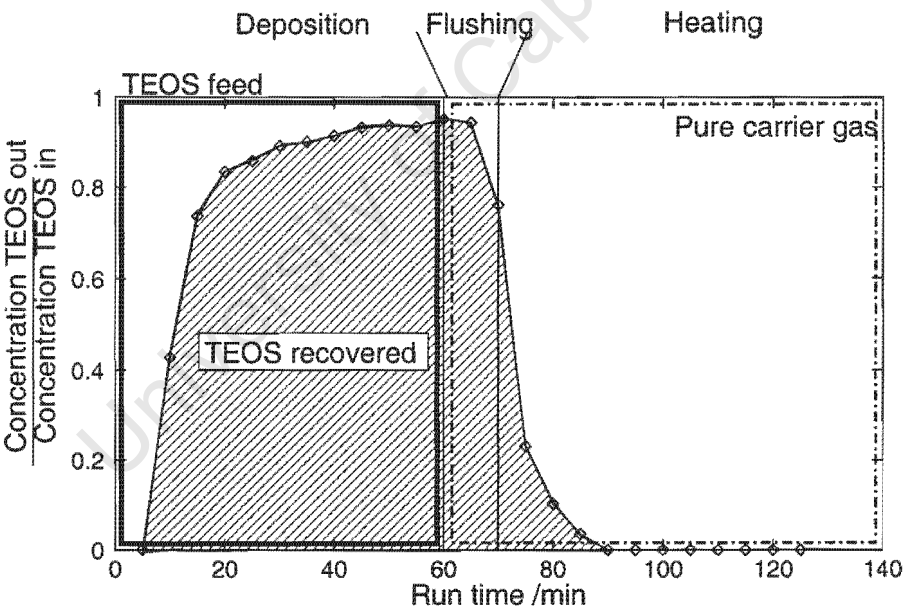

Figure 3.2: Illustration of the calculation of the integral TEOS conversion from a breakthrough curve at T_{CVD}=50°C (20th CVD treatment).

Figures 3.3 and 3.4 show the integral TEOS conversion per modification cycle at the various modification temperatures for the catalyst in powder and pellet form, respectively. During the modification at low temperatures, viz. 50, 100, 150 and 200°C, similar quantities are deposited for each cycle. Increasing the deposition temperature to 300 and 400°C results in larger amounts of TEOS being deposited on the catalyst. For the 300°C series, the amount of deposited TEOS decreases with repeated modification and levels out at a similar plateau as it was observed for the low temperature modifications. Deposition at 400°C results in the complete conversion of TEOS during the first

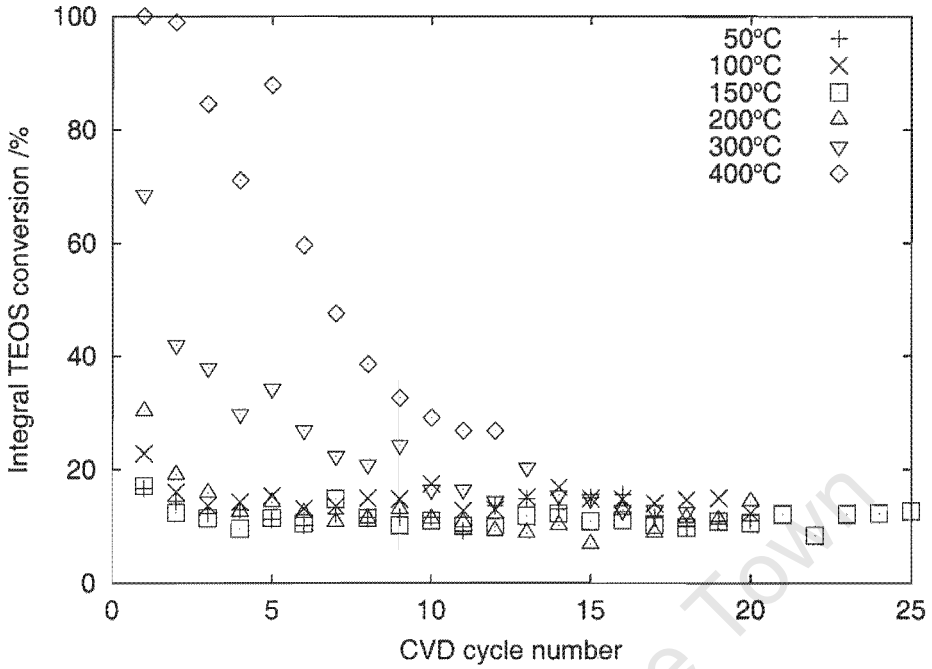

Figure 3.3: Integral TEOS conversions on powder.

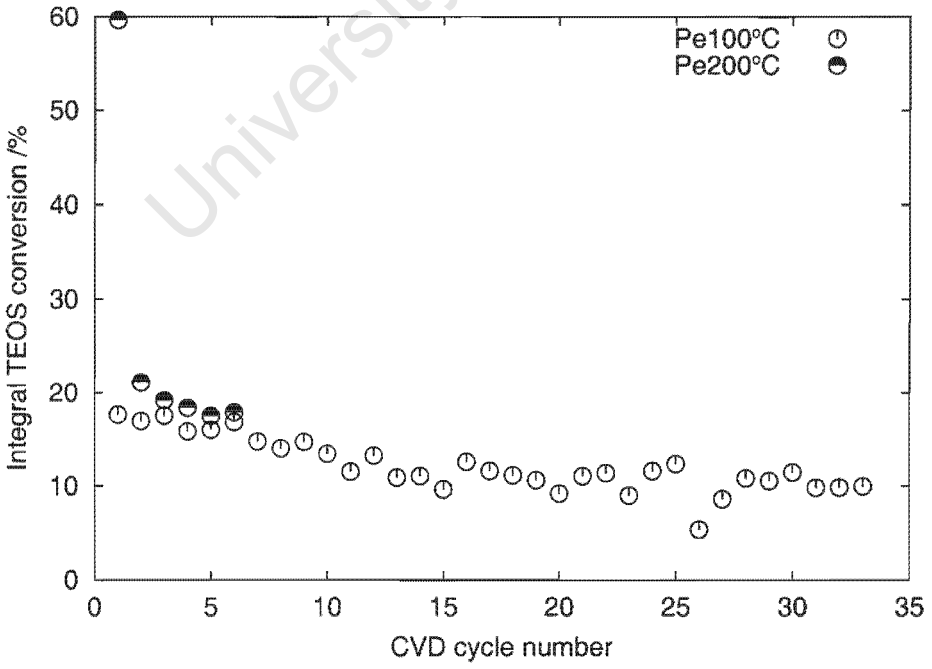

Figure 3.4: Integral TEOS conversions on pellets.

two cycles. Thereafter the conversion decreases, tending to a steady value. The higher value for the steady state conversion implies that in addition to the surface reaction, homogeneous gas phase reaction of TEOS occurred at 400°C.

The modification of pellets at 100 and 200°C followed the same trends as for powder. As will be shown in section 4.2.2, the deposition at 200°C resulted in a severe loss of activity for TDP and was thus terminated after 6 modification cycles.

3.3 Amount of deposited Silica on external surface

Equation 2.11 was used to calculate the deposited silicon concentration on the external surface. Figures 3.5 and 3.6 show that summation of the deposited amounts per modification treatment increases steadily with increasing number of cycles.

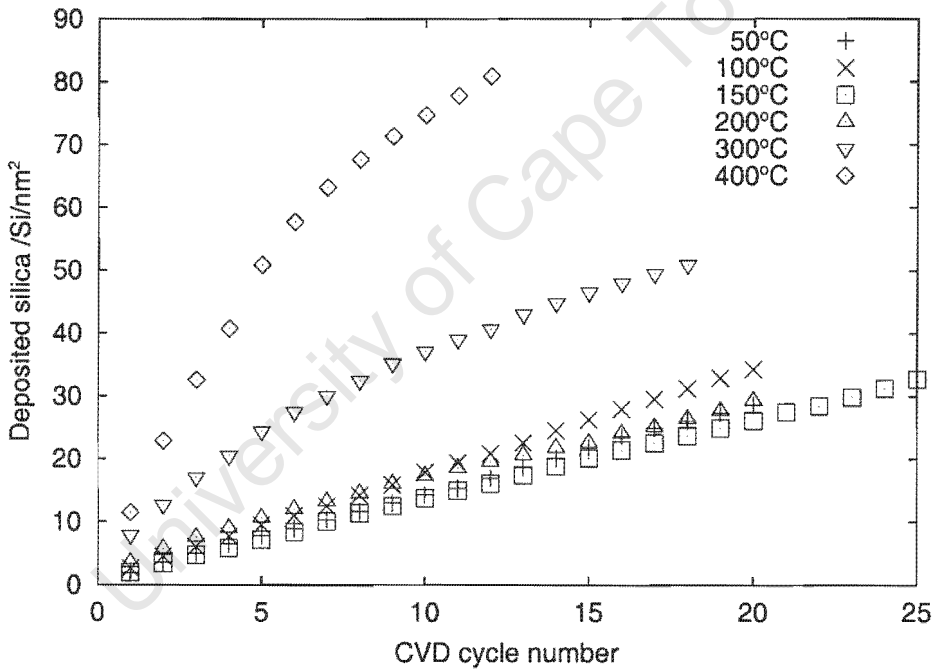

Figure 3.5: Cumulative amount of deposited silica on powder.

An almost linear relationship is seen for modification temperatures below and at 200°C. At higher temperatures, a steep increase of deposited silica is observed for the initial cycles. However, the slope decreases after 5-10 cycles, but still remains steeper than that at the lower temperature with an approximately linear relationship. Figure 3.6 shows that the modification of pellets at 100°C resulted in the same increase of deposited silica as for powder. For pellets which were modified at 200°C, higher amounts of deposited silica were obtained.

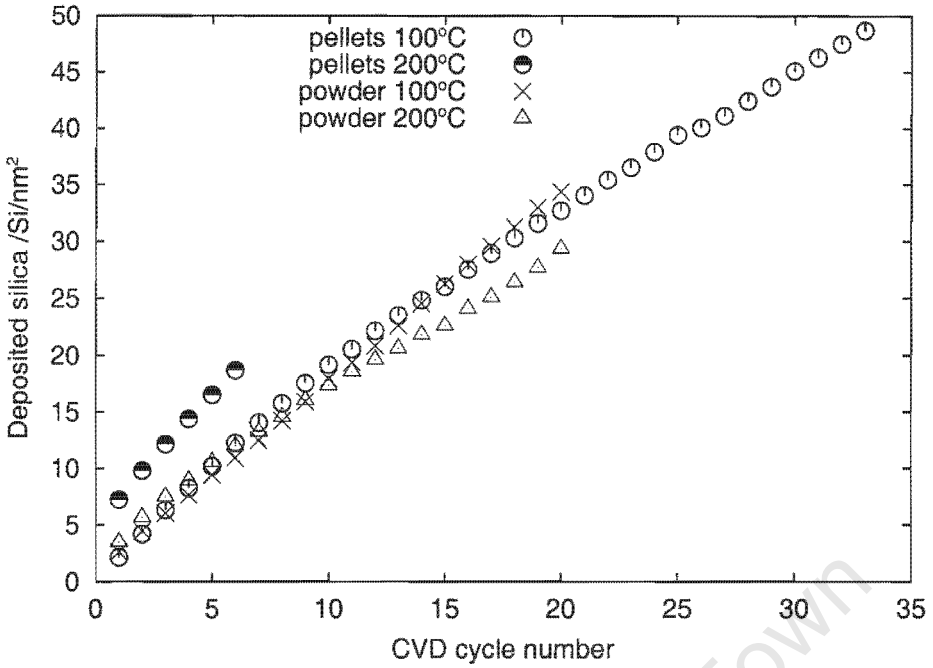

Figure 3.6: Cumulative amount of deposited silica on pellets.

3.4 Activity of the external surface - Cracking of 1,3,5-TiPB

The effect of silica deposition on the catalytic activity of the external surface was monitored by the cracking of 1,3,5-triisopropylbenzene (1,3,5-TiPB).

Figure 3.7 shows the results of a representative 1,3,5-TiPB-cracking run which lasted 65 min. The conversion levelled off after 25 min. The conversions of the samples taken between 25 and 65 min are averaged and given as the steady state activity of the external surface. The standard deviation is used as a measure of the error in the data. Carbon balances, determined for the powder samples, were usually between 95 and 105%. A representative GC-trace for a complete 1,3,5-TiPB-cracking run can be found in Figure D.2 in the Appendix.

The number of CVD cycles which were required for the inertisation of the external surface of the catalyst, are summarised in Table 3.1.

Figures 3.8 and 3.9 show the decrease in cracking conversion with increasing silica deposition. The modification at temperatures below 400°C lead to the similar results. The relative conversion over the catalyst drops to below 10% of the parent sample after approximately 10 to 15 Si/nm^2 were deposited on the external surface. For the powder sample which was modified at 400°C, around 30 to 40 Si/nm^2 had to be deposited before the conversion is reduced by 90%.

Less cycles are needed with increasing CVD temperature to achieve the same degree of deposition, viz. Si/nm^2, and surface inertisation, as is shown in Figure 3.10.

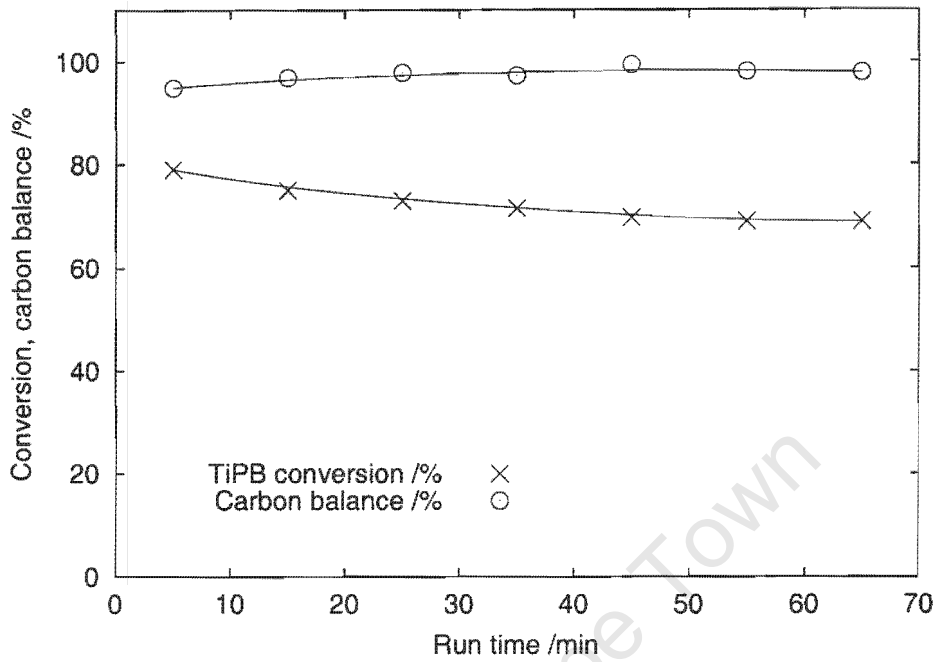

Figure 3.7: Cracking of 1,3,5-TiPB over the parent sample of the 50°C-powder series (X_{TiPB}(average between 25 and 65 min)=70.4%, σ=0.79, carbon-balance=98%, σ=0.79, reaction conditions given in Table 2.3).

Table 3.1: Numbers of cycles required to inhibit 1,3,5-TiPB-cracking

Series (T_{TEOS})	number of cycles	1,3,5-TiPB conversion	deposited silica	number of silica layers
$°C$		%	Si/nm^2	
		powder		
50	6	< 7	8.9	1
100	7	< 7	12.5	1.4
150	3	< 6	4.7	0.5
200	2	< 4	5.7	0.6
300	2	< 6	12.7	1.4
400	3	< 5	32.6	3.7
		pellets		
Pe100	7	< 6	14.0	1.6
Pe200	2	< 3	9.8	1.1

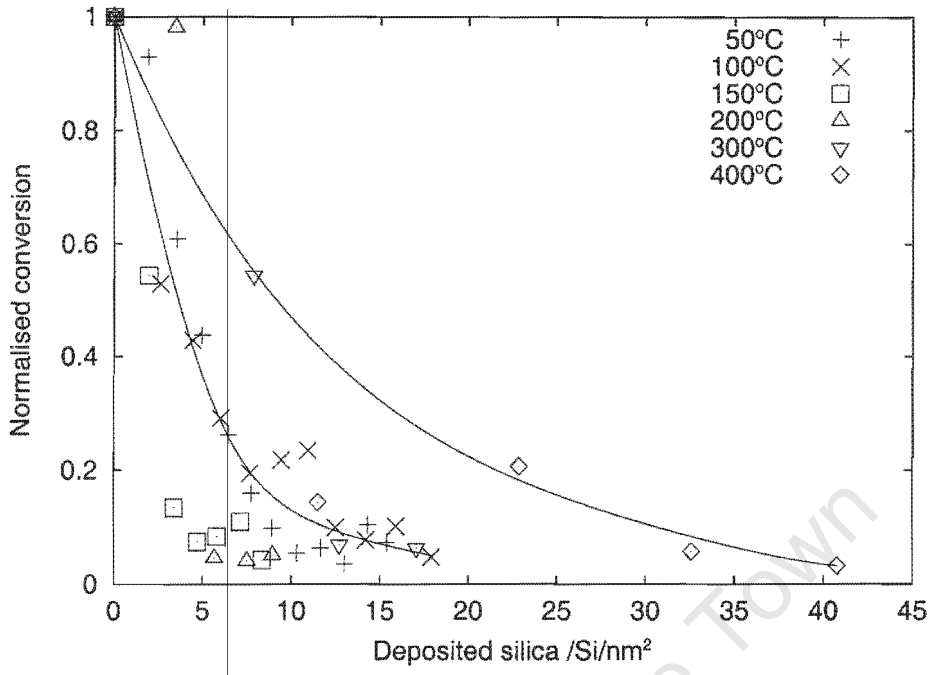

Figure 3.8: Inhibition of 1,3,5-TiPB-cracking over powder with increased silica deposition (common trend line shown for the 50, 100, 150, 200 and 300°C-series).

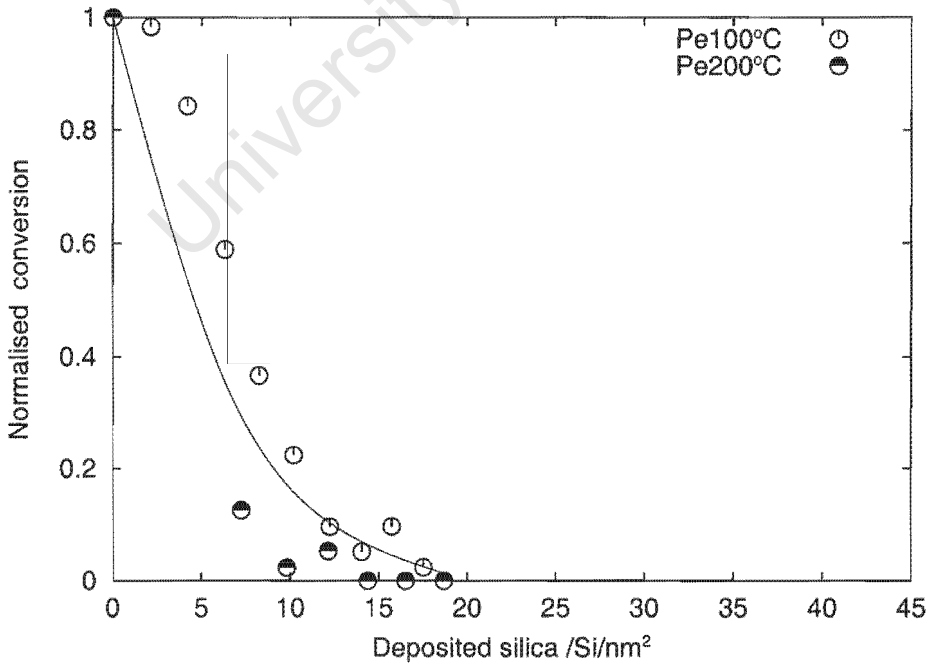

Figure 3.9: Inhibition of 1,3,5-TiPB-cracking over pellets with increased silica deposition (common trend line for the 100 and 200°C-series).

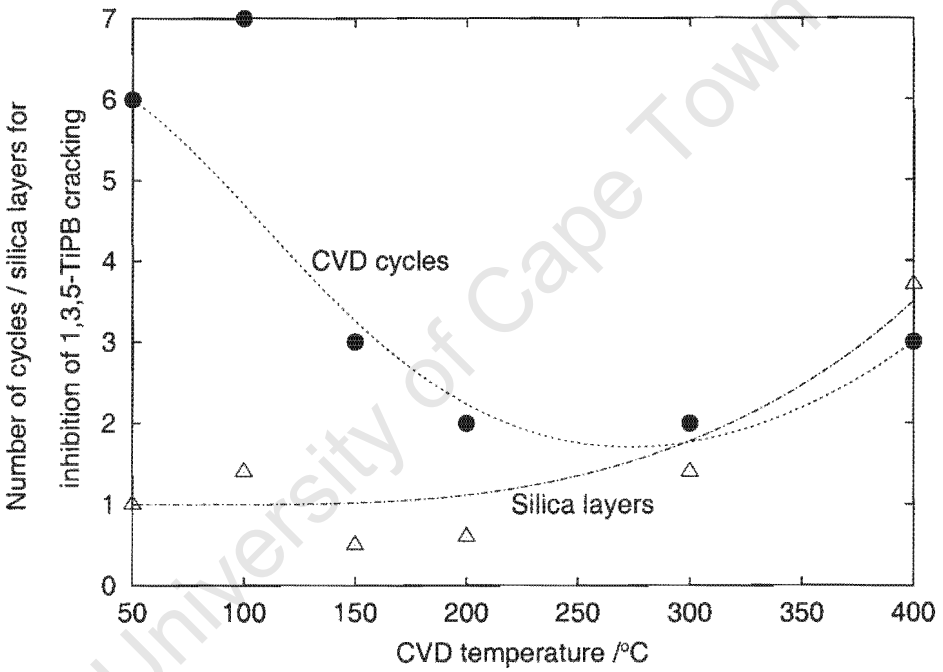

Figure 3.10: Number of CVD cycles to inhibit cracking of 1,3,5-TiPB at various deposition temperatures.

3.5 Disproportionation of toluene

3.5.1 Unmodified catalyst

For both powder and pellets the parent samples were tested for the catalytic performance.

Conversion versus time

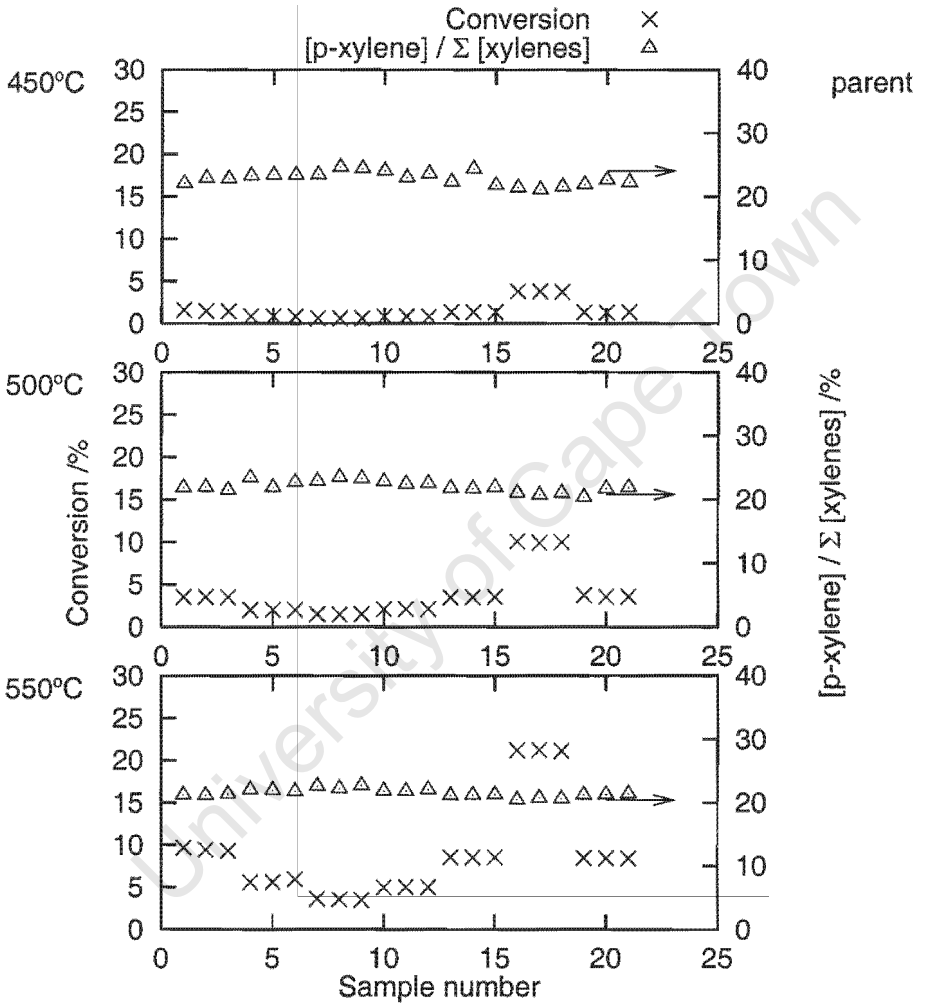

Figure 3.11: Effect of reaction temperature (450, 500 and 550°C), time on stream and WHSV on conversion and para-selectivity during toluene disproportionation over unmodified powder (reaction conditions and data given in Table G.13).

In order to elucidate the time on stream behaviour of the powder and pellets, the disproportionation of toluene was carried out for 200 and 185 min, respectively (see Figures 3.11 and 3.12). The catalyst did not show signs of significant deactivation during the period on stream.

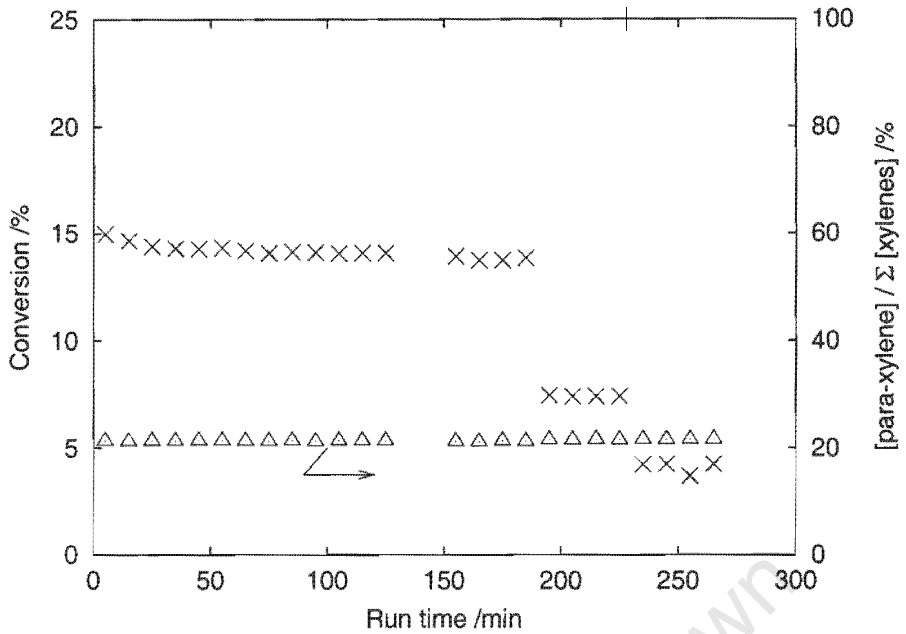

Figure 3.12: Effect of time on stream and WHSV on conversion and para-selectivity during toluene disproportionation over unmodified pellets at 450° (reaction conditions and data given in Table G.14).

3.5.2 Effect of WHSV on selectivity

The effect of the conversion level on the shape selectivity was examined by altering the WHSV during the reaction. Figures 3.11 and 3.12 show that the thermodynamic equilibrium composition was obtained at all conversion levels over the unmodified powder and pellet samples.

3.5.3 Improvements in shape selectivity

Improvements in shape selective performance of the catalyst was observed during the disproportionation of toluene (TDP). A representative TDP run is shown in Figure 3.13. The run lasted 65 min and the conversion reached steady state after 25 to 35 min. Light hydrocarbons, benzene, diehtylbenzene and xylene-isomers were the main product of the disproportionation reaction. Trimethylbenzenes were found only in trace amounts and were thus neglected in further quantitative analysis. A sample GC-chromatogram of a complete TDP run can be found in Figure D.3. Detailed analysis revealed that the fraction of the light hydrocarbons consisted of methane, ethene, ethane, propene and propane (see Figure D.5). Ethane however, was the main product within the light hydrocarbons.

The carbon balances were stable and showed no significant loss of carbonaceous material due to coking. Thus, the conversion was calculated from the concentrations of the reactor effluents only, assuming 100% carbon balance. The steady state activity of the catalyst is given as the average conversion of the samples taken between 25 and 65 min. It should be noted that the p-xylene selectivity is calculated on a benzene-free basis.

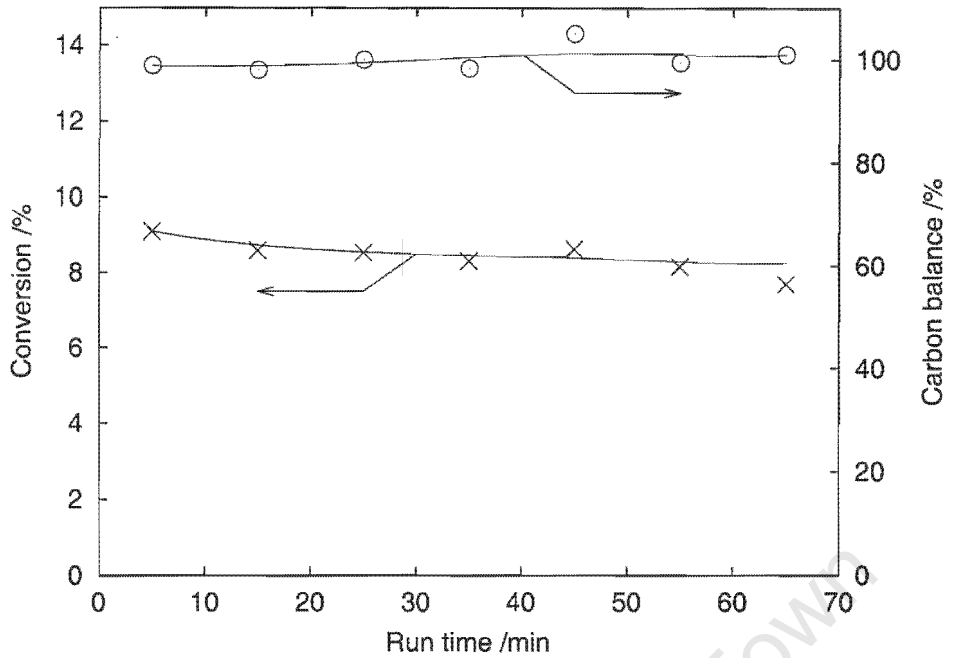

Figure 3.13: Disproportionation of toluene over the unmodified sample of the 50°C-powder series ($X_{Toluene}$(average between 25 and 65 min)=8.26%, σ= 0.36, carbon-balance= 100.71%, σ=2.59, reaction conditions given in Table 2.3).

The changes in xylene selectivity for powder and pellets are depicted in Figures 4.7 and 4.8, respectively. Modification of the powder samples at increased temperatures resulted in faster and steeper changes of the p-xylene selectivity with number of cycles. For the modification of pellets only the at 100°C modified series shows improved para-selectivity. As pointed out earlier, the deposition at 200°C imposed a severe loss of activity for TDP on the catalyst and the series was terminated before changes in shape selectivity were observed.

Figures 3.14 and 3.15 present the p-xylene selectivities as a function of the deposited silica. The curves for the at 50, 100, 150, 200 and 300°C modified powders are almost identical. 10 Si/nm^2 had to be deposited in order to notice changes in shape selective behaviour for the powder samples.

In the case of the 400°C modified series, high para-selectivity was achieved at very high silica loadings. Also, this curve rises more slowly than the other series.

The increase in the para-selectivity for the 100°C-pellet series occurs after 20 Si/nm^2 is deposited onto the external surface. However, shape and maximum of this curve compares well with the powder samples modified below and at 300°C. No improvements of para-selectivity were found during the six modification treatments of the 200°C-pellet series, because the catalyst was already completely deactivated in contrast to the 100°C series.

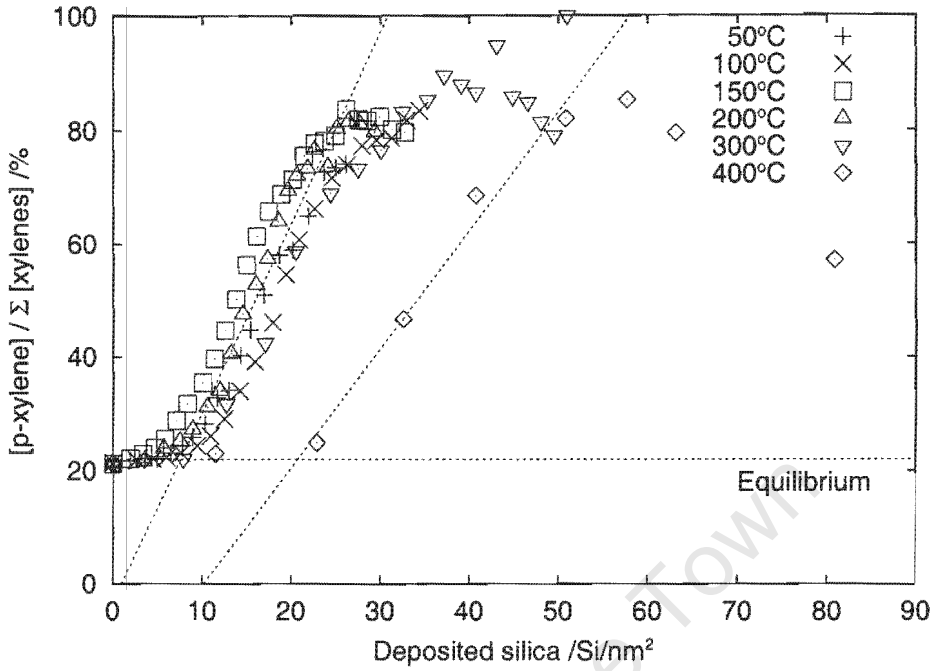

Figure 3.14: Changes in p-xylene selectivity with increasing silica deposition on powder.

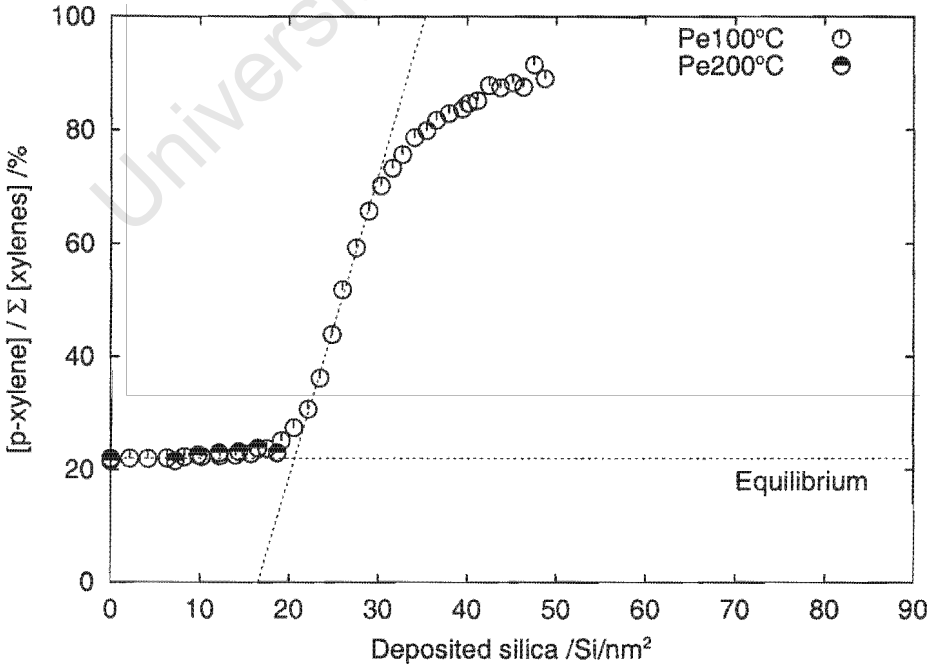

Figure 3.15: Changes in p-xylene selectivity with increasing silica deposition on pellets.

3.5.4 Benzene to Xylene Ratio

The benzene/xylene ratios for the respective TDP runs were calculated and are depicted in Figures 3.16 and 3.17. This ratio serves as a measure to quantify possible dealkylation side reactions which result in an increased amount of benzene which is likely to occur at elevated temperatures (Bhaskar and Do, 1990; Uguina et al., 1991, 1993). A ratio of unity is expected since two toluene molecules disproportionate to form one benzene and one xylene molecule. These results show that a rapid increase in the benzene/xylene ratio occurs in the low CVD temperature data at high silica loadings. In contrast, for the high CVD temperature data the ratio remains closer to unity.

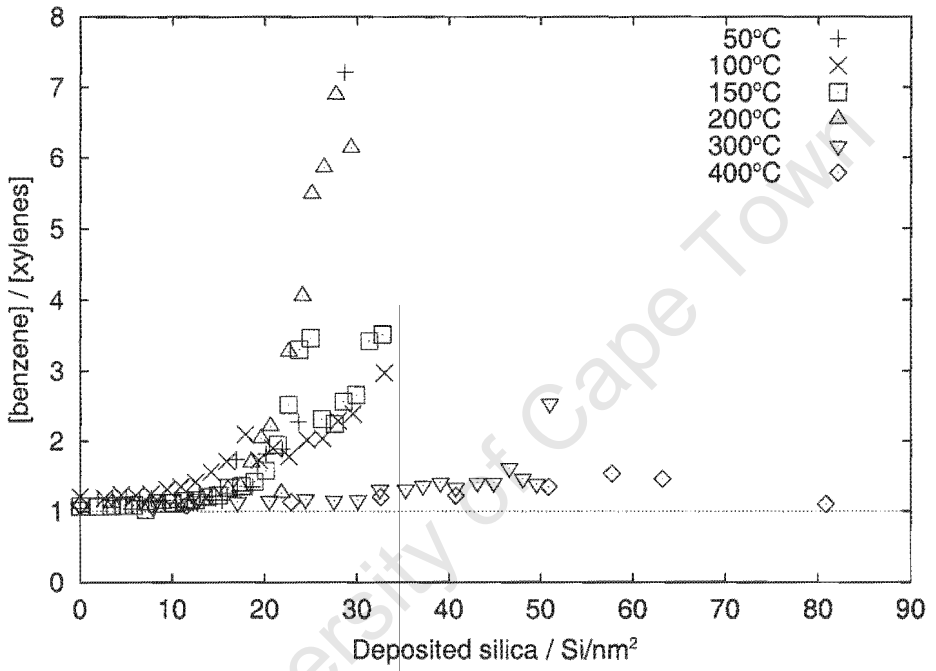

Figure 3.16: Benzene/xylene ratios of the products of TDP over powder (reaction conditions given in Table 2.3).

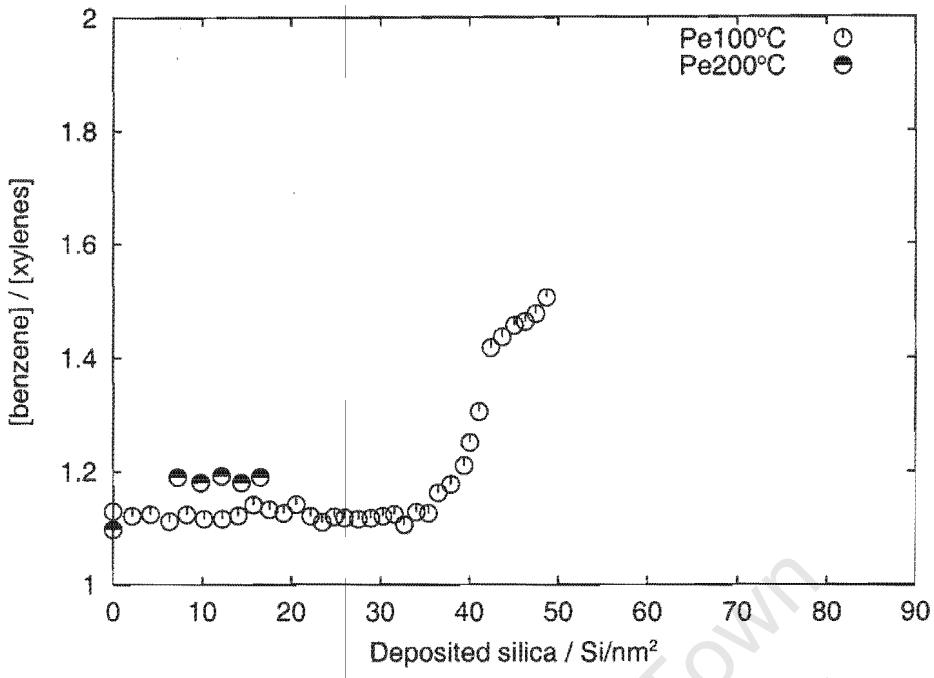

Figure 3.17: Benzene/xylene ratios of the products of TDP over pelletised samples (reaction conditions given in Table 2.4).

3.5.5 Toluene conversion

Disproportionation of toluene occurs on both the external and internal surface of the catalyst. Thus, as long the external surface is not fully deactivated, TDP serves as a test reaction for the overall catalyst activity. Once the external surface is passivated, as shown by the inhibition of the 1,3,5-TiPB-cracking reaction, only the internal activity contributes to the conversion of toluene.

Figures 3.18 and 3.19 show the changes in the relative conversion of toluene for powder and pellets, respectively. The toluene conversions are normalised against the respective conversion over the unmodified parent sample of each series. It should be noted that the WHSV and the reaction temperature for the powder and pellets sample differed from 1.72 to 0.15 g_{HC}/h g_{cat} and 550°C to 450°C, respectively.

Data points which were badly affected by experimental error due to leakages in the reactor system were not considered for further analysis.

The experimental data for TDP are given in Tables G.2 to G.10.

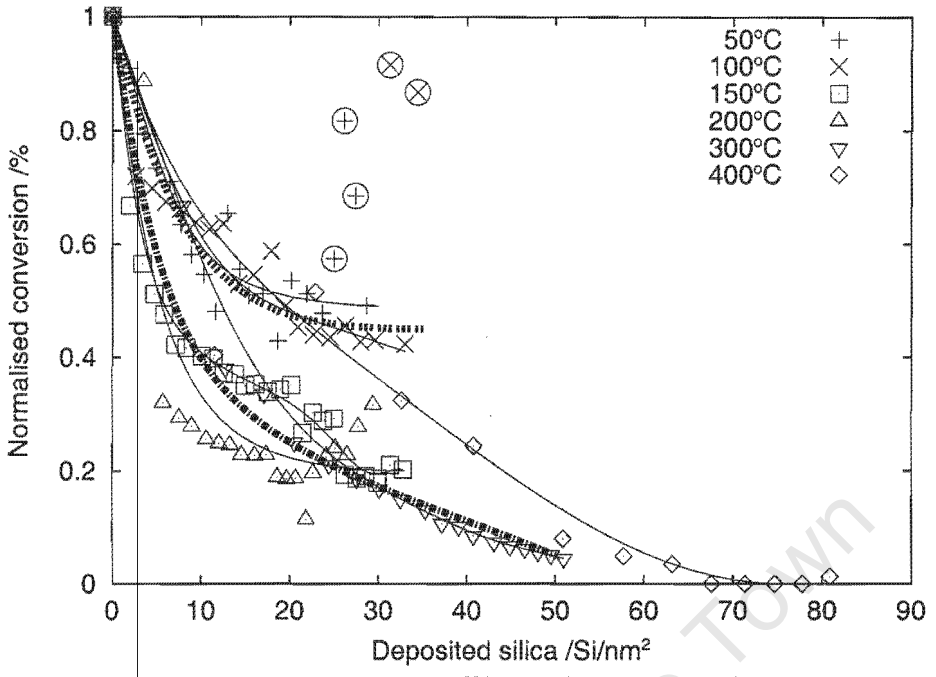

Figure 3.18: Decrease in relative conversion during TDP with increasing silica deposition on powder. Data which was badly effected by experimental error (encircled), was not used for further calculation and discussion.

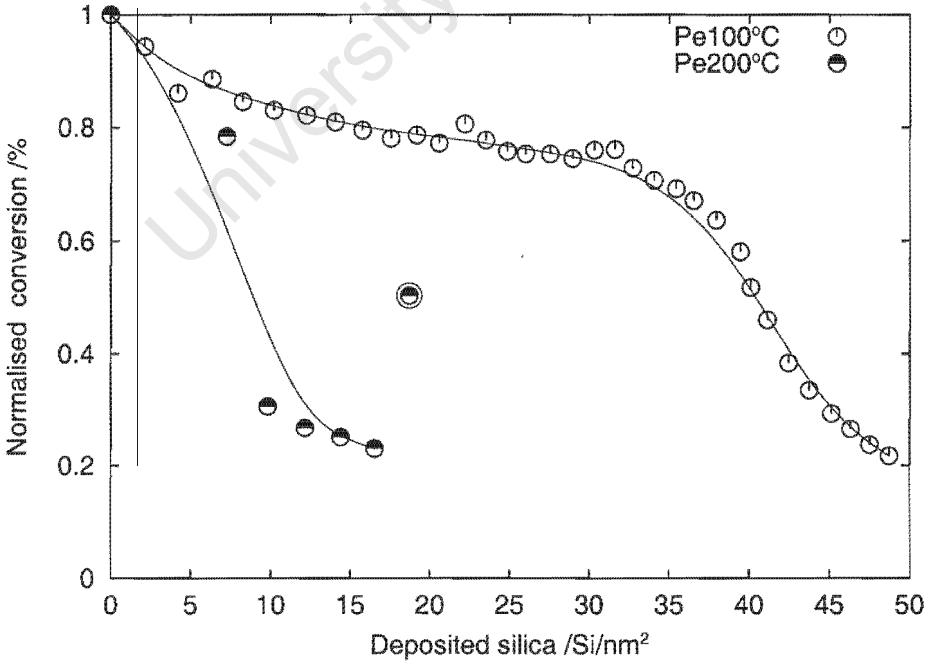

Figure 3.19: Decrease in relative conversion during TDP with increasing silica deposition on pellets. Data which was badly effected by experimental error (encircled), was not used for further calculation and discussion.

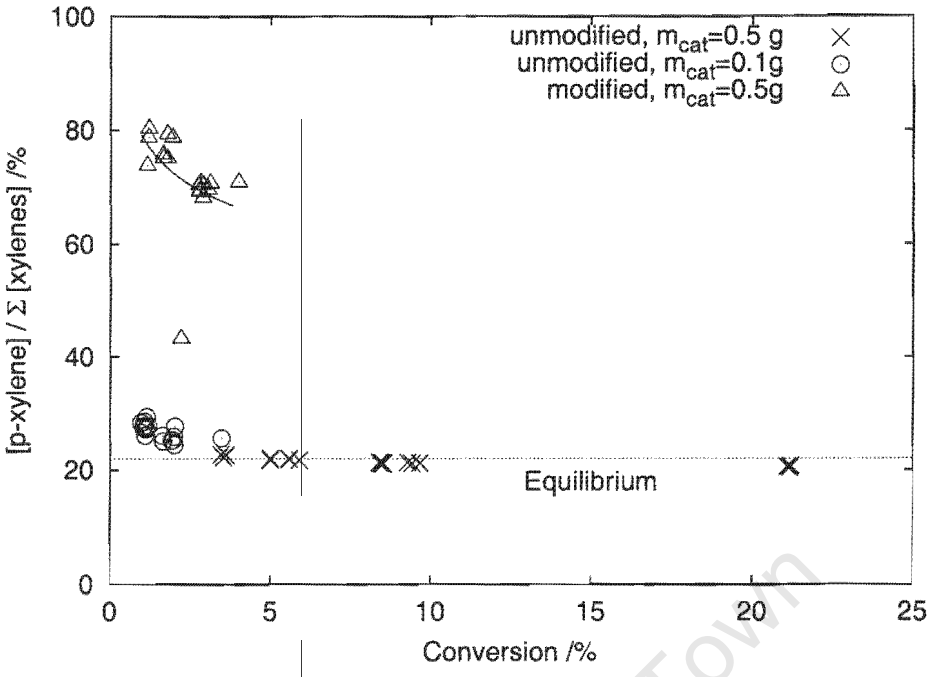

Figure 3.20: Changes in para-selectivity during TDP at 550°C by changing WHSV over unmodified and modified (15 cycles at 150°C) powder (reaction conditions given in Table G.13).

Powder

It can be seen that modification at 50 and 100°C resulted in the loss of around 50% of the conversion after which a plateaux is obtained. Increasing the deposition temperature leads to increased reduction in conversion. The formation of a steady conversion level at around 20% of the unmodified sample can be seen for the 150 and 200°C series. After repeated modification at 300 and 400°C no steady conversion level is achieved and continuous decrease in conversion leading to total deactivation of the catalyst can be observed.

Pellets

Silica deposition at 100°C on the pellet sample leads to an initial loss of conversion of around 20%. A slow decline to the conversion level of around 75% is observed when the deposition of silica is increased from 20 to 30 Si/nm^2. Further deposition causes a rapid decay of the conversion to around 20% of the parent sample. After reaching this low conversion level, investigation of this temperature series was terminated. The modification of pellets at 200°C almost duplicates the decrease in conversion of the powder samples, treated at the same CVD temperature.

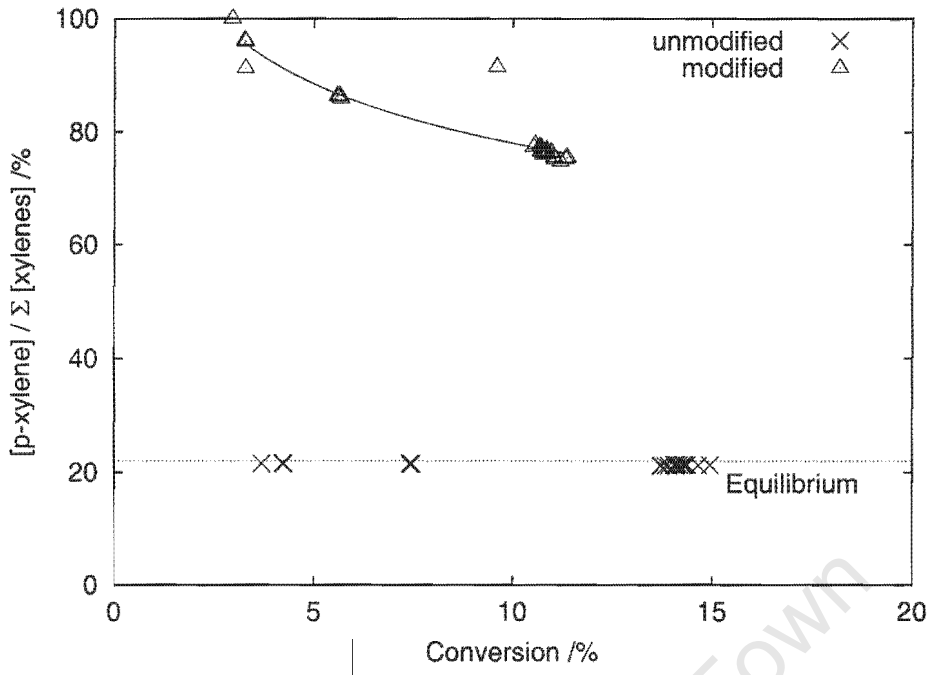

Figure 3.21: Changes in para-selectivity during TDP at 450°C by changing WHSV over unmodified and modified (20 cycles at 100°C) pellets (reaction conditions given in Table G.13).

3.5.6 Effect of space velocity on para-selectivity during TDP

Figures 3.20 and 3.21 show the effects of variation of the WHSV on the para-selective performance during TDP over unmodified and modified powder and pellets, respectively.

In order to alter the WHSV, the linear flow rate and the catalyst mass was varied for TDP at 550°C over the powder samples. The linear flow rate was varied between 14 and 127 ml/min. The catalyst mass of the unmodified samples was reduced from 0.5 to 0.1 g. The reaction conditions are given in G.13 and the results for the unmodified and modified samples are shown in Figures 3.11 and 3.22, respectively.

For TDP at 450°C over the pelletised samples, the WHSV was altered by changing the linear flow rate only. The results for the pelletised sample are shown in Figure 3.23 and the reaction conditions are given in Table G.13. These figures show that the unmodified sample is not influenced by changing WHSV and the products remain close to the equilibrium composition. In contrast, the CVD modified samples show a significant increase in selectivity with decreasing conversion.

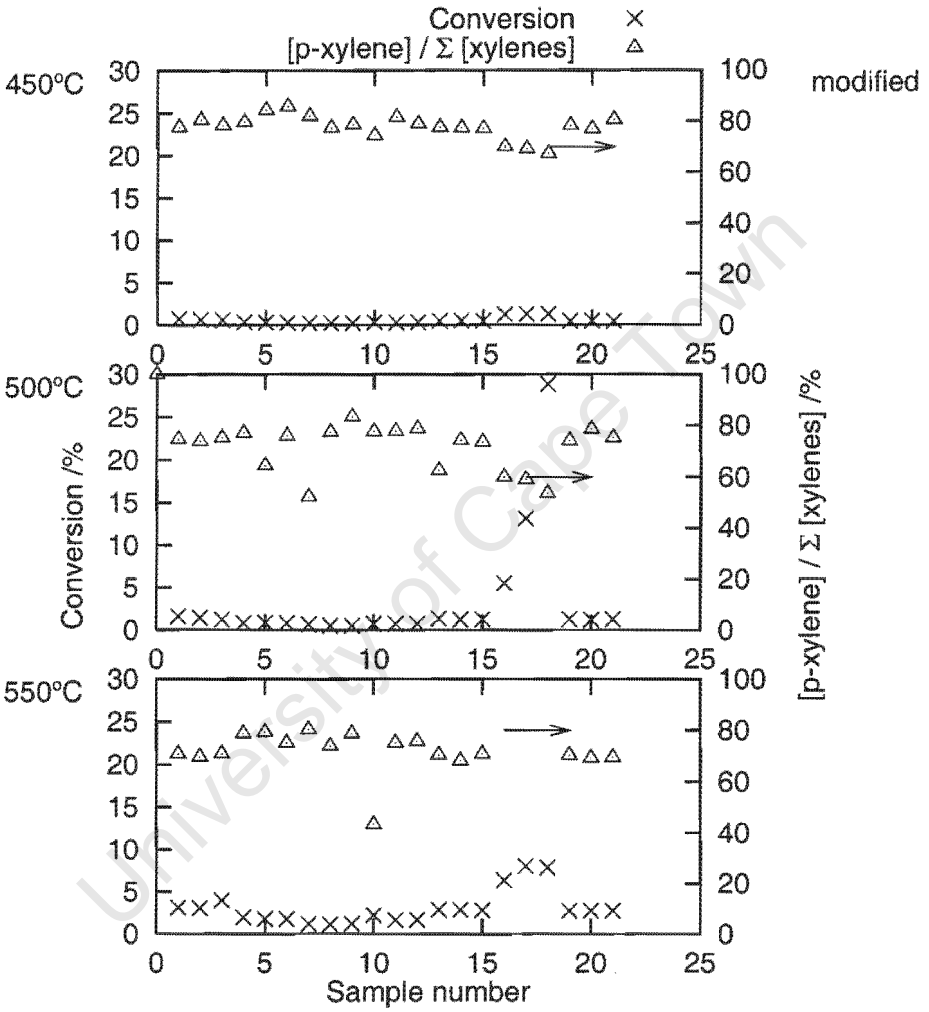

Figure 3.22: Effect of reaction temperature (450, 500 and 550°C and WHSV on conversion and para-selectivity during toluene disproportionation over modified powder (15 CVD cycles at 150°C; reaction conditions given in Table G.13).

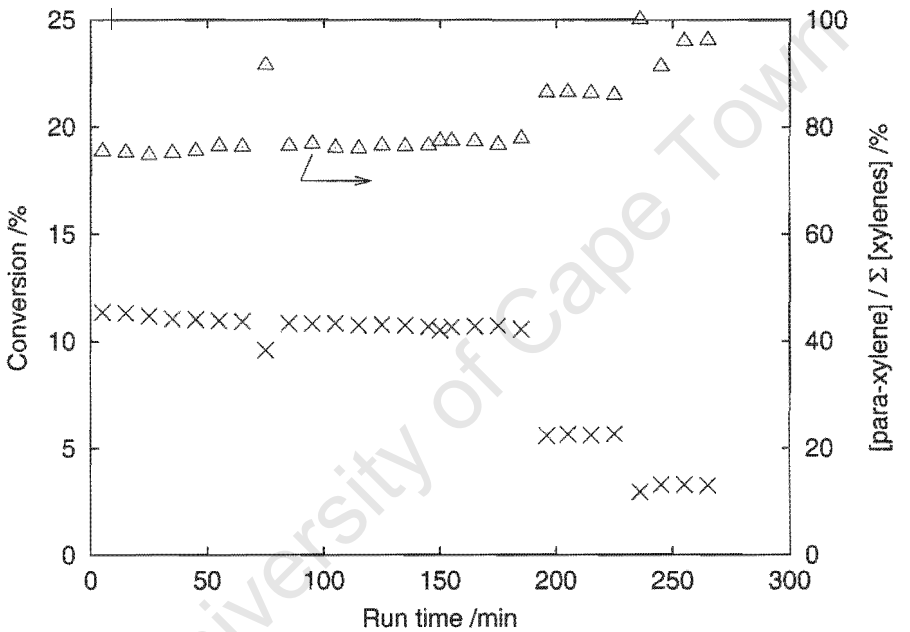

Figure 3.23: Effect of time on stream and WHSV on conversion and para-selectivity during toluene disproportionation over modified pellets (20 CVD cycles at 100°C, reaction conditions and data given in Table G.14).

3.6 Long time runs

3.6.1 1,3,5-TiPB-cracking

The cracking of 1,3,5-TiPB over unmodified pellets was carried out for 305 min at 210°C. Figure 3.24 shows that the carbon balance and conversion reach approximately 95 % and 96 % after 300 min, respectively. The relative deviation of the conversion during the period of 25 to 65 min time on stream is below 1.5 %, while the carbon balance improves by approximately 2 % (Table G.12). The average conversion data in this period is taken as steady state value and deactivation of the catalyst was not further considered.

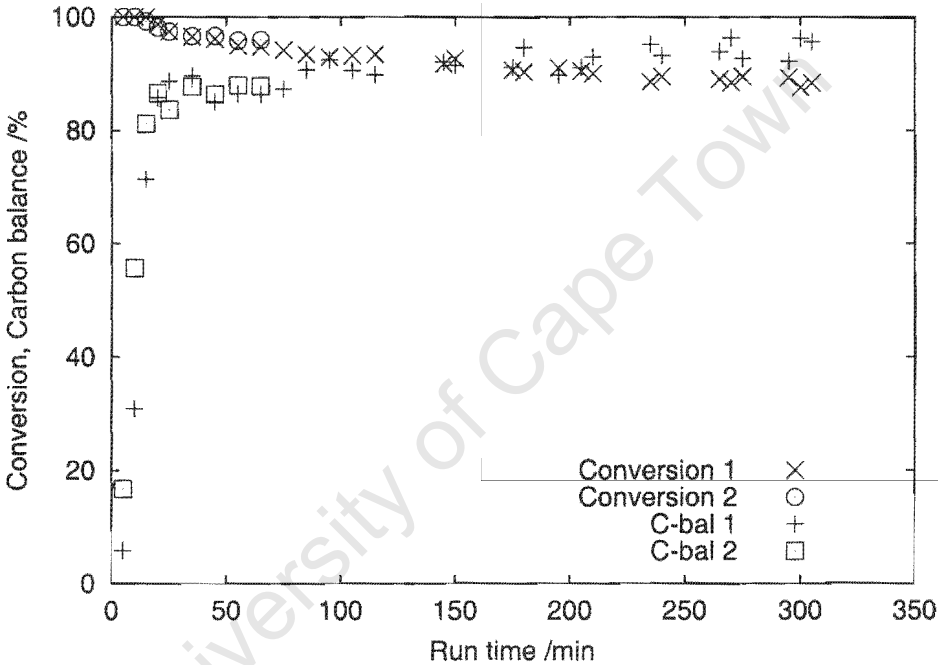

Figure 3.24: Long time behaviour and reproducibility of 1,3,5-TiPB-cracking over unmodified pellets at 210°C. (Reaction conditions given in Table 2.4.)

3.6.2 Disproportionation of toluene

The loss of conversion that was measured during the first run remains below 2.5 % over the period from 5 to 185 min. The average deviation of the para-selectivity during both runs is below 1%. Deactivation of the catalyst for TDP is thus considered insignificant.

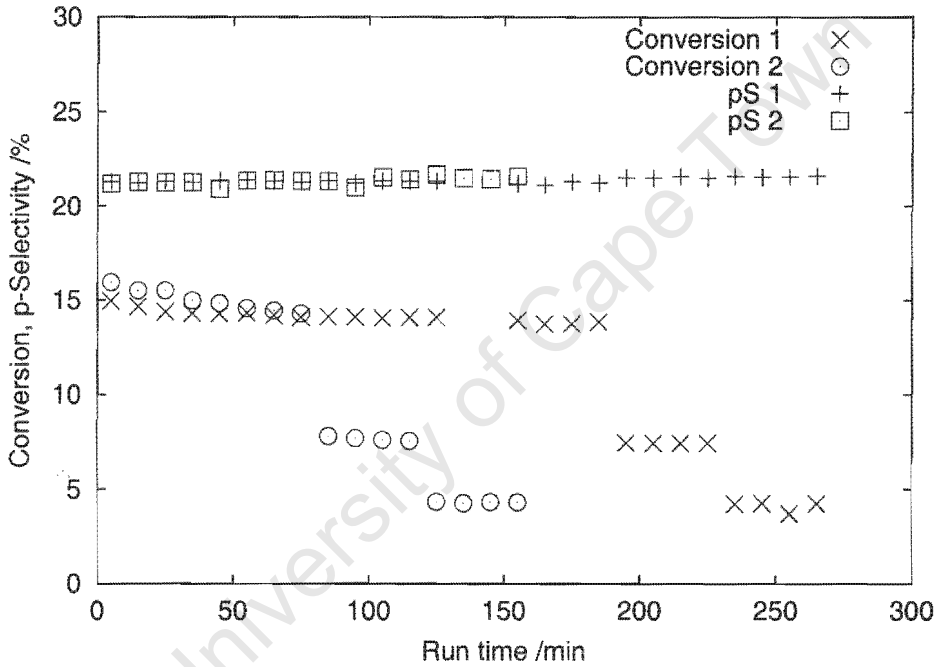

Figure 3.25: Long time run and reproducibility of the disproportionation of toluene over unmodified pellets at 450°C (Reaction conditions are given in Table G.14).

3.7 Reproducibility

3.7.1 TEOS deposition

The deposition of TEOS on sand was carried in two and three subsequent cycles at 50 and 400°C, respectively. The corresponding concentration curves are shown in Figure 3.26. The standard deviation are 0.2 and 0.6 respectively which results to an relative error of below 5 and 8%, respectively (see Table F.2).

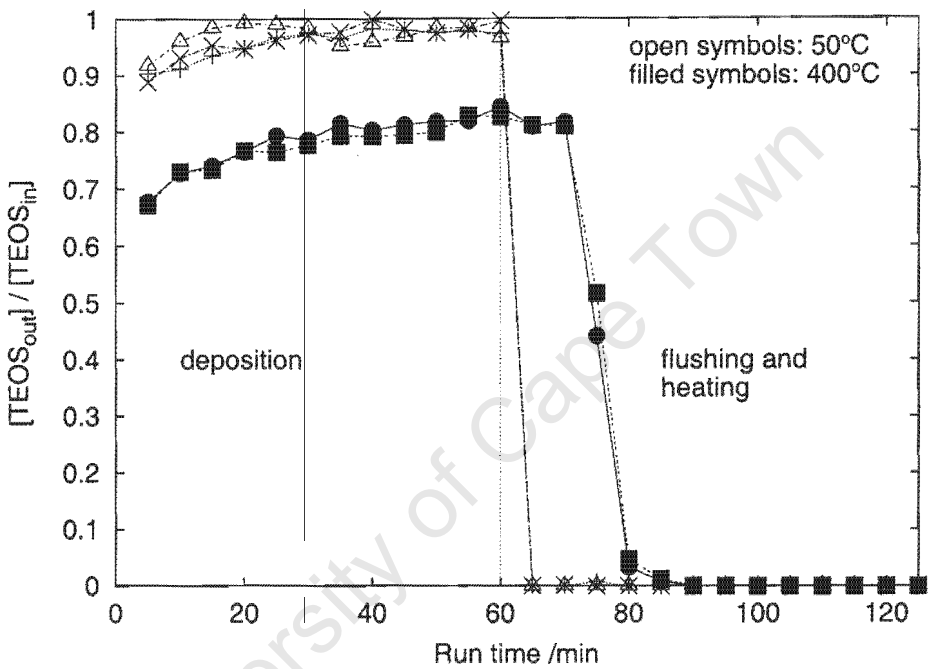

Figure 3.26: CVD on sand

3.7.2 1,3,5-TiPB-cracking

The repetition of the cracking of 1,3,5-TiPB over unmodified pellets is shown in Figure 3.24. The relative deviation of the conversion data and the carbon balance is smaller than 5 % (Table G.12) and shows good reproducibility.

3.7.3 Disproportionation of toluene

The disproportionation of toluene was repeated over the unmodified pellet sample at 450°C and is shown in Figure 3.25. The reaction data is given in Table G.14. The conversion data of the two runs shows a maximum relative deviation of below 6% between 5 and 75 min on stream.

3.8 Repeatability

3.8.1 CVD of TEOS

The 100°C-powder and 200°C-pellet series were repeated with 6 and 4 cycles, respectively. The respective data is given in Tables G.3 and G.4 for the powder and in Tables G.10 and G.11 for the pellets (Appendix G). Figure 3.27 shows that the curves for both series exhibit identical trends and only deviate slightly in the amounts of deposited silica. This error is attributed to the difficulties in identically repacking the reactor due to the particle size distribution of the powder and pellets which were loaded into the reactor.

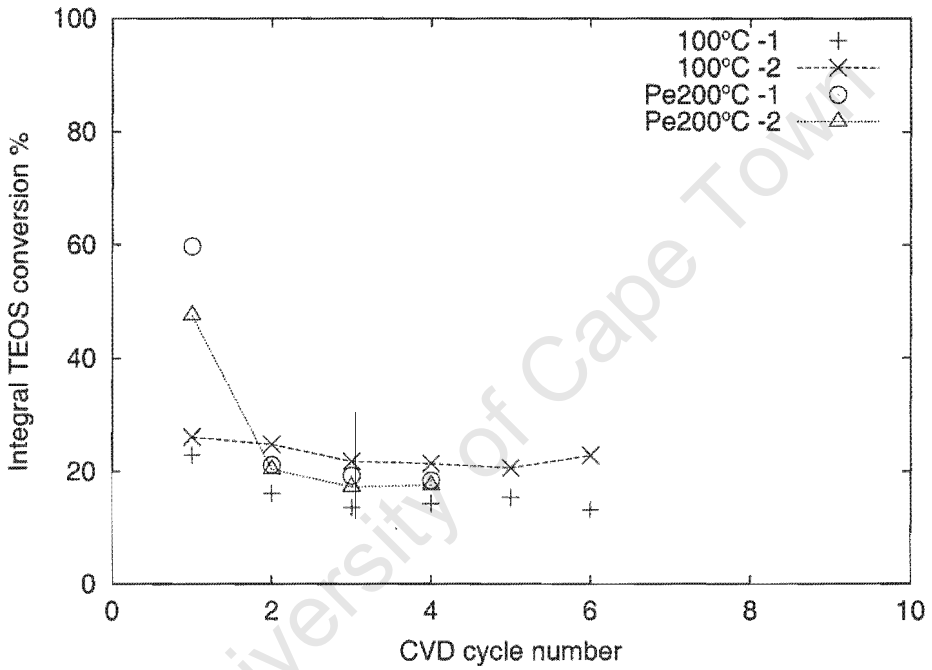

Figure 3.27: Repeatability of CVD on ZSM-5.

3.8.2 1,3,5-TiPB-cracking and TDP

In order to establish the repeatability of the catalytic reaction work over the powder and pellet samples, the 1,3,5-TiPB-cracking and TDP data over the unmodified samples is compared. Table G.17 in Appendix G shows that the conversion data could be repeated with less than 9 % relative difference.

Chapter 4

Discussion

4.1 Deposition of silica

4.1.1 Breakthrough curve analysis

The TEOS breakthrough curves in Figures B.1 and B.4 differ greatly with changing CVD temperature and number of cycles. The reaction during the deposition step reaches "saturation" at 50, 100, 150 and 200°C after 1-2 cycles, as at this point no conversion of TEOS takes place. At higher temperatures, a steady conversion of TEOS is achieved as a function of time, particularly during the initial cycles.

Low temperature

The curves at 50-150°C in Figure B.4 show that breakthrough of TEOS occurs earlier as the deposition temperature is increased; indicating that the adsorption capacity of the zeolite is reduced. At 200°C, high TEOS concentrations during the deposition continue to be observed after 10-15 min, with the exception of the first cycle. Furthermore, desorption of TEOS does not occur during the flushing and heating step. This suggests that physisorption of TEOS at temperatures higher than 200°C does not contribute to the deposition of silica.

High temperature

At 300 and 400°C, conversion during TEOS deposition is seen to decrease with increasing number of CVD cycles, indicating that the surface is being deactivated and/or the deposition is non-uniform, leaving less active zeolite after each cycle. This observation was also reported by Hibino et al. (1988), Weber et al. (1998) and Shaikh et al. (1999).

TEOS conversion

The absence of desorption of TEOS in the flushing and heating step at high CVD temperatures implies that TEOS is continuously converted during the deposition step. This clear distinction cannot be made for the lower CVD temperatures, viz. 50-150°C. If only adsorption occurred at low temperature, the heating step is of crucial importance to facilitate the surface reaction of TEOS. Therefore, at low temperatures the surface becomes uniformly saturated, leading to a uniform deposition of silica upon heating.

4.1.2 Integral conversion

Low temperature

The integral TEOS conversion (equation 2.10) was constant at 15% for low temperature CVD between 50-150°C (Figures 3.3 and 3.4). This implies that the same amount of TEOS reacted on the catalyst, regardless of changing adsorption capacities and activities with temperature between 50 and 150°C. This suggests that the reaction of TEOS is limited by the surface properties of the catalyst. The reaction occurring during the deposition step becomes inhibited by the "adsorption" of products. Removal of the adsorbed products and regeneration of the surface, i.e. calcination, is a necessary step to facilitate deposition. However, slightly higher amounts of TEOS were converted on the fresh catalyst, viz. during the first cycle of each series. The occurrence of a "saturation effect" at low temperature was frequently reported in literature for both, the breakthrough of the modifier and the weight gain during deposition (Niwa et al., 1984a; Wang et al., 1988; Hibino et al., 1988; Chun et al., 1994; Fei et al., 1995; Weber et al., 1998).

High temperature

Higher integral conversions for deposition at 200, 300 and 400°C depend on the number of CVD cycles. The highest conversions are obtained on the fresh catalyst. The integral conversion for the 200- and 300°C series approach the same steady value, found for the low CVD temperatures.

On the contrary, the integral conversion at T_{CVD}=400°C remained at 25% after 11 cycles. In this case only 12 CVD cycles were carried out, due to rapid catalyst deactivation, and no clear indication of the final conversion was possible. Wang et al. (1988) and Weber et al. (1998) reported that TEOS was converted on Kieselguhr and silica at 320 and 400°C, respectively. Nevertheless, TEOS undergoes not only surface reaction at this temperature but is also converted by homogeneous gas phase reactions like decomposition, condensation/polymerisation (Niwa et al., 1988; Bhat and Halgeri, 1993; Herzler et al., 1997; Jurgens-Kowal and Rogers, 1998). Thus, the levelling off at higher conversions is expected and also suggested by the data.

Reactivity of silica for TEOS deposition

A complete silica coating is expected after extended modification. The existence of a steady integral conversion after 15 cycles at all CVD temperatures below 400°C shows that TEOS deposited on silica. However, the desorption of TEOS ceased at 150°C and reaction at lower CVD temperatures might have occurred only during the heating step.

Integral conversion and TEOS monolayer

If only one TEOS monolayer is adsorbed on the external surface, the integral conversion of 12 and 11.5% (at the WHSV used in this study) would be observed for powder and pellets, respectively . It has to be noted, that these limiting values do not depend on the concentration of TEOS in the feed stream but on the total amount which is fed through the reactor.

The number of exposed T-atoms per area that have a charge imbalance, and are thus potential attachment sites on the idealised ZSM-5 crystal, is 8.9 Si/nm^2 (Niwa et al., 1986b)). The adsorption of one TEOS monolayer is equivalent to the silicon concentration of 1.39 Si/nm^2 (see section 2.4.10). Thus, the successive adsorption and decomposition of 6-7 TEOS monolayers achieves the silicon density of 8.9 Si/nm^2 and one theoretical monolayer of silica is formed. In other words, the coverage of all possible attachment sites is completed in 6-7 cycles. The integral conversion of around 15% (which marks the steady plateau for the CVD treatments below 400°C) implies that the equivalent amount of one TEOS monolayer has reacted per CVD cycle.

4.1.3 Reaction scheme

In this section a reaction pathway for TEOS conversion on ZSM-5 a both high and low deposition temperature is developed.

The higher integral TEOS conversions on the fresh catalyst shows that acid sites influence the surface reaction. The dependence of the amount of deposited silica on the acidity of the catalyst has also been documented by Wang et al. (1988), Chu et al. (1989) and Weber et al. (1998).

This section will firstly discuss deposition on a SiO_2 surface, followed by the influence of the acid sites.

Reaction of TEOS with ZSM-5

Deposition at 50°C

For CVD at 50°C no ethanol and ethene is detected during the deposition step and a large desorption of TEOS was observed during the heating step. Large amounts of ethanol, formed during the heating step around 200°C, implies that the surface reaction only occurs during the heating of the reactor. Thus, it is concluded that TEOS does not easily react with the surface at 50°C.

Chun et al. (1994) reported that TEOS did not readily react with zeolite H-β at room temperature. Weber et al. (1998) however reported that longtime exposure (40 h) to TEOS at 50°C and the subsequent calcination at 500°C lead to the increased pore blockage of ZSM-5 (as measured by n-hexane adsorption) which implies that the surface reaction had taken place, although at an extremely slow rate.

Surface reaction between 50 and 100°C

No significant desorption of TEOS was observed above 100°C during the heating and/or flushing steps. The integral conversion indicates that surface reaction of TEOS must have taken place. This is also shown by the presence of ethanol. It has been shown that the first reaction step of TEOS with the surface involves the formation of tri- or diethoxy species on the surface and the generation of ethanol (Crowell et al., 1990; Spitzmüller et al., 1998).

Product inhibition

The reaction of one TEOS monolayer approximately represents the formation of tri- or diethoxy species on the surface. This implies that these species are unreactive for further TEOS deposition. The reaction with the surface thus becomes product inhibited and ceases after all "adsorption" sites have reacted, i.e. $\equiv Si - O - Z \equiv$ or $= Si -(-O - Z \equiv)_2$ species are formed on the surface.

Ethoxy-decomposition and ethanol-dehydration

The largest formation of ethanol and ethene was observed during the heating step, when the reactor reached around 200 and 250°C, respectively. Since TEOS desorption was not observed during the heating step of the 150°C series, the large ethanol and ethene formation cannot be attributed to TEOS reaction with the surface. Hence, it must have originated from the decomposition of the surface-ethoxy species. Ethene is expected as the product of ethanol-dehydration (Aronson et al., 1986; Li-Feng et al., 1989; Weber et al., 1998; Lin and Ko, 2000) and indicates in-situ generation of water. Water is known to decompose TEOS via hydrolysis (Bradley, 1989). Thus, ethoxy species are

converted ("regenerated") to silanol groups which are susceptible to TEOS adsorption and reaction. The presence of water catalyses the deposition reaction of TEOS (Niwa et al., 1988). Since all un-reacted TEOS desorbs during the flushing step, the amount of deposition was limited by the monolayer of surface-reacted TEOS, as indicated by the integral conversion of 15%.

Regeneration during deposition

At a CVD temperature of 300°C, the deposition, dehydration and regeneration reaction occurred predominately during the deposition step, as the formation of ethanol and ethene is observed during the deposition part. The approach to a limited integral conversion suggests that the acidity of the CVD-derived surface is not sufficient to sustain the formation of water and thus the autocatalytic deposition-regeneration reaction. It might be speculated that ethene which is found during the heating step at around 450°C, is attributed to the decomposition of isolated ethoxy species which were not regenerated or to the removal of carbonaceous products. At a CVD temperature of 400°C, all reactions occur during the deposition step and ethene and ethanol are produced in high concentrations. Weber et al. (1998) observed that ethene and water were formed in the initial period and thereafter ethanol was the product when TEOS was deposited on SiO_2. The rapid reaction of TEOS with the surface together with the gas phase reactions which are catalysed by the production of water, could not have proceeded in a controlled manner. Weber et al. (1998) reported that CVD at 400°C resulted in the non-uniform deposition of silica.

Surface reaction over fresh catalyst

Decreasing integral TEOS conversion was observed at high temperatures and for the first cycle at low CVD temperatures. This decrease is attributed to removal of easily accessible acid sites of the catalyst. At low temperatures, TEOS reacts selectively with the easily accessible acid sites and physisorbs to the remaining surface. Thus, some ethanol might be formed which is adsorbed by the catalyst. Ethanol dehydration over strong acid sites occurs readily above 170°C (Aronson et al., 1986). Thus, the in-situ formation of water at very slow rates could be possible already at room temperature. This water hydrolyses ethoxy species and facilitates further deposition during the first cycle. Reaction of physisorbed TEOS with the surface occurs during the heating step, as shown by the high ethanol and ethene concentrations. The removal of the easily accessible acid sites becomes evident during the second deposition cycle, when lower integral conversions are observed, and by the cracking of TiPB. The spatial requirements of TEOS are high and interaction with the surface at low temperature is restricted to physisorption. Thus, the deposition of silica becomes limited to the equivalent of one adsorbed TEOS monolayer and constant integral TEOS conversions are obtained. Some ethanol and ethene is detected during the deposition at 50 and 100°C, however only in trace amounts. It might be speculated that ethanol, diffusing into the crystal would either adsorb or dehydrate over the strong acid sites in the channels. The in-situ generated water would in turn

adsorb in the channels or diffuse into the bulk gas phase. When diffusing out, hydrolysis of adsorbed ethoxy species on the external surface can occur. Thus, ethanol dehydration in the interior would become a key reaction in controlling the degree of deposition by either long contact times or increased reaction temperature.

At higher deposition temperatures, TEOS chemisorbs on the surface and larger amounts of ethanol are formed during the deposition step. As the dehydration of ethanol proceeds more readily, higher concentrations of water are generated in-situ and larger quantities desorb when the deposition temperature increases. This results in enhanced deposition and higher integral TEOS conversions.

In the event of pore blocking, access to acid sites inside the crystal becomes restricted and the dehydration reaction slows down as the number of CVD cycles increases. As the formation of water decreases, the probability of in-situ regeneration of ethoxy groups diminishes and the possibility of further TEOS deposition during the same cycles is reduced. Thus, when all strong and easily accessible acid sites are blocked, TEOS reaction only occurs to the extent of the adsorbed monolayer and the steady integral TEOS conversion is observed.

The cracking of 1,3,5-TiPB (Figure 4.3) showed that each CVD cycle and successive treatment has a deactivating effect on the active sites on the surface. The silica layer either shields the particular active site or prevents access to it. As result, the "weakening" of the acidity of the surface becomes apparent in reduced 1,3,5-TiPB-cracking rates. With increasing number of silica layers the shielding effect increases and the acidity "becomes weaker". Tsai and Wang (1991) concluded that as the number of deposition layers on zeolite H-β increased, the acidity of the skin layer became weaker, resulting in decreasing deposition between 140-250°C. Hibino et al. (1988) reported that acidity of ZSM-5 diminishes after 4 layers of silica from TMOS were formed on the external surface. The weakest acidity is reached when essentially pure silica is present at the surface.

However, in the absence of accessible acid sites, the deposited amount per cycle is limited to the reaction of the adsorbed monolayer and the integral conversion converges to a steady value. Furthermore, the fast and random deposition of silica in the first cycle may cause non-uniform deposition and rapid pore blockage. The extent, to which chemisorption of TEOS and ethanol dehydration are influenced when the acidity of the surface is altered by structural changes, remains unanswered.

Non-uniform deposition at 400°C

Complete TEOS conversion was observed during the first two cycles at a CVD temperature of 400°C. High temperature and the autocatalytic acceleration of the TEOS deposition by water lead to extremely high reaction rates and rapid deposition. The deposition proceeds from the beginning of the reactor bed, achieving 100% TEOS conversion before the exit of the bed is reached. Therefore, the downstream section remains untreated in the first few cycles. As the initial section of the bed deactivates, more TEOS can move through the bed and react over the active surface of the

bed further downstream. Only during subsequent cycles is the acidity and hence, reactivity of the complete reactor bed, reduced. Thus, the integral TEOS conversion decreases with number of cycles.

4.1.4 Development of a reaction pathway for TEOS conversion

This section will present the reaction pathway of TEOS over ZSM-5, based on the component analysis of the deposition data and the above considerations.

The primary reactions of TEOS

The CVD of alkoxysilanes on zeolites has been focus in many studies. In particular Niwa et al. (1988) have clarified the reaction mechanism of tetramethoxysilane (TMOS) with mordenite. Since then, several authors have proposed (Chun et al., 1994) and extended possible reaction mechanisms for the surface deposition of TEOS on acid zeolites (Röger, 1998). It is generally accepted that hydroxyl groups are the attachment sites for the deposition of alkoxysilanes on acid zeolites (Niwa and Murakami, 1989). The reaction of TEOS with the hydroxyls on the zeolite's external surface leads to the formation of tri- and diethoxy species and the liberation of ethanol (see scheme 4.1.1) and 2)). The ethoxy species which are unreactive to TEOS can be thermally decomposed during a calcination step and diethylether and ethene are produced. As a result, silanol groups appear (see scheme 4.1.3) and 4)). Regeneration of the surface is also possible via treatment with water vapour; hydrolysis of ethoxy groups yields ethanol and simultaneously produces silanol groups (see scheme 4.1.5)). However, a final calcination step needs to be performed to remove the adsorbed decomposition products (Hibino et al., 1988). Exposure to higher temperatures leads to the dehydroxylation of silanol and yields Si=O groups (see scheme 4.1.9)). Weber et al. (1998) reported that thermal cracking of TEOS was not observed at 500°C. From pyrolysis studies of TEOS however it is reported that decomposition begins at around 450°C (Ivanov et al., 1985; Chu et al., 1991).

Side reactions

Several side reactions of the deposition byproducts in the presence of acidic ZSM-5 have to be considered. Ethanol can dehydrate over the acid sites at temperatures below 180°C and the formation of ethene, diethylether and water is observed (Aronson et al., 1986; Li-Feng et al., 1989; Weber et al., 1998; Lin and Ko, 2000)(see scheme 4.1.10), 11), 12)). Also, ethene is reported to oligomerise over ZSM-5 to yield higher hydrocarbons at room temperature (van den Berg et al., 1983; Bessel and Seddon, 1987) (see scheme 4.1.13)).

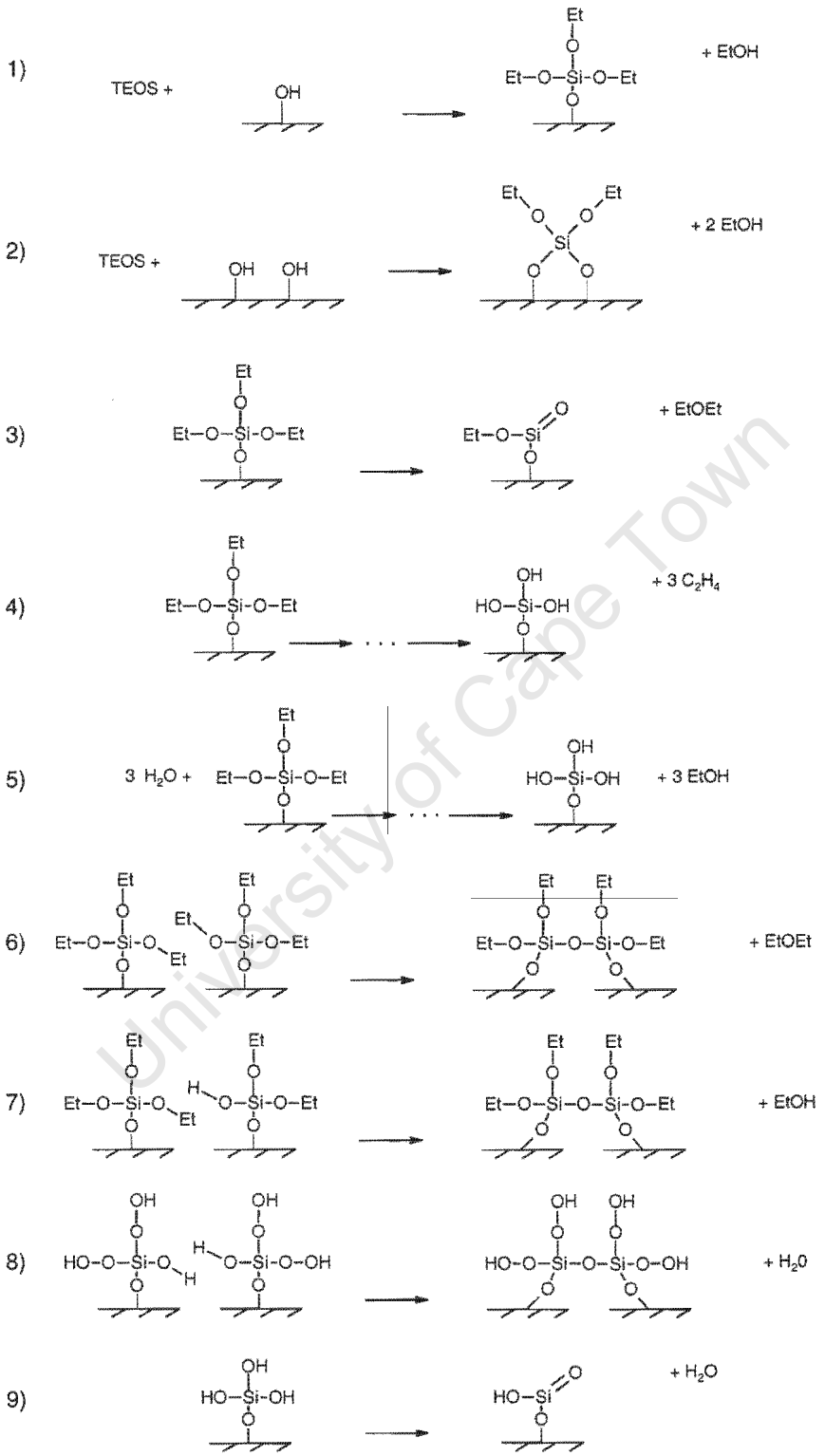

Figure 4.1: Scheme of reactions of TEOS and products during the deposition and heating step.

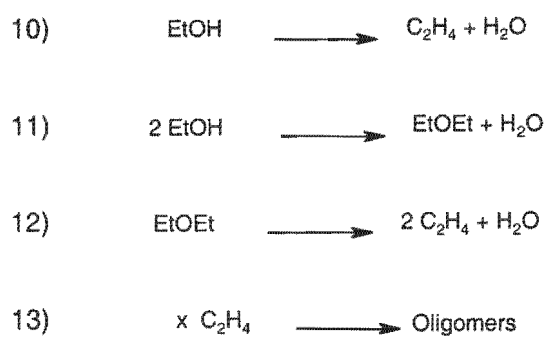

Figure 4.1: (continued) Side reactions during the deposition of TEOS.

Reaction pathway based on component analysis

Based on the analysis of the compounds in the reactor effluent at the different CVD temperatures, the following reaction steps can be distinguished for the deposition of TEOS on ZSM-5. TEOS surface reaction takes place between 50 and 100°C. Decomposition of ethoxy species leads to the formation of ethanol around 200°C. Dehydration of ethanol occurs around 250°C and results in the in-situ generation of water and ethene. It may be speculated that isolated monoethoxysiloxane species decompose thermally around 450°C. The sequence of the reactions with increased temperature is illustrated in Figure 4.2. The analogy to the reaction mechanism of TMOS on zeolites, as proposed by Niwa et al. (1988), becomes apparent and is confirmed by the results in this study.

The degree of silica deposition at temperatures below 200°C and in absence of accessible acid sites is limited to the reaction of the TEOS monolayer. The amount of accumulated silica in the initial cycles, particularly at higher deposition temperatures, can be controlled by adjusting the contact time with the modifying reagent when the conversion is differential, as reported by Wang et al. (1988).

Critical reflection of component analysis during deposition

The analysis of the deposition products proved to be inaccurate in determining absolute amounts of the unretained compounds, in particular ethene and diethylether. Hence, detailed analysis of the carbon product in the reactor effluent was not possible. Also, water cannot be detected with a FID, thus valuable information about reaction which are associated/accompanied by the formation of water, is not available. Water can be detected with a thermal conductivity detector (TCD), however unconverted TEOS from the deposition step could have deposited on the sensitive filaments of the detector which would have resulted in the irreversible loss in sensitivity and the final destruction of the instrument. Analysis of the reactor effluent with a TCD was thus not further considered.

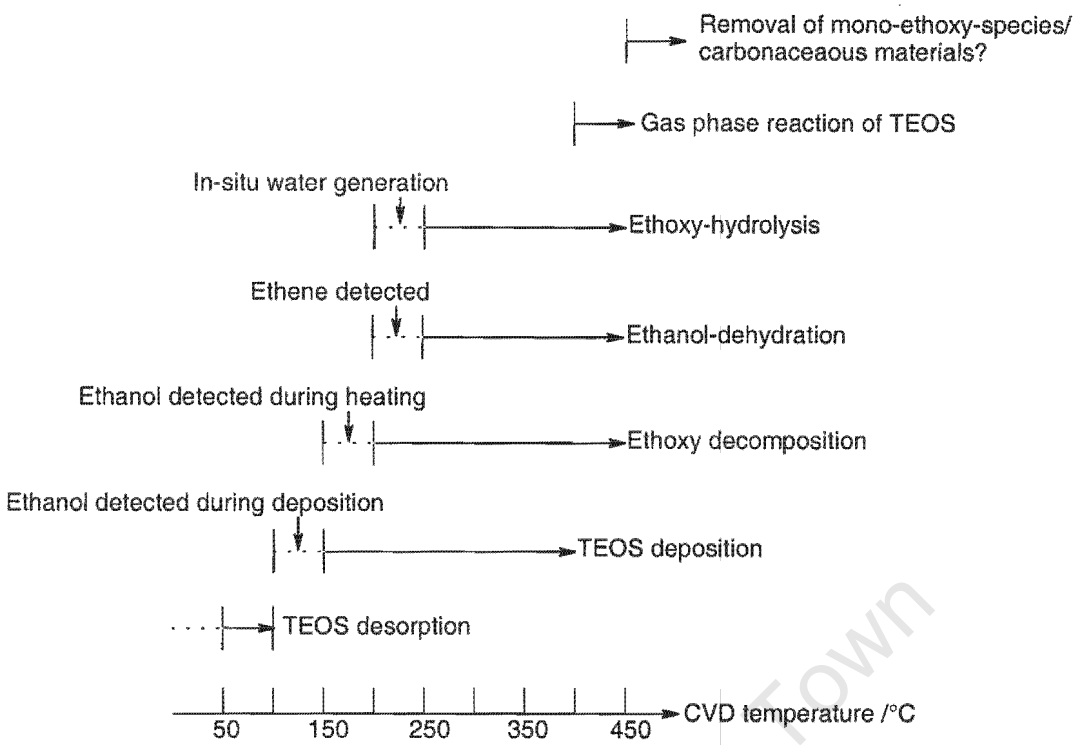

Figure 4.2: Reaction scheme in the investigated temperature range during the deposition of TEOS.

4.1.5 Closing remarks on TEOS deposition

The role of acidity

It is evident that the extent of deposition strongly depends on the acidity of the catalyst before and during a deposition step. The strong and accessible acidity of the fresh catalyst is responsible for higher amounts of deposition in the first cycle of each series. The interplay of weak remaining acidity and low reactivity of TEOS at 50-200°C allows the deposition of equal amounts of TEOS per cycle. With increasing temperature, side reactions of TEOS deposition become more likely. However, in absence of accessible acid sites, viz. over a CVD derived surface, high temperature CVD obtains similar conversions as at low temperature. The findings by Weber et al. (1998) suggest that the deposition reaction at 50°C occurs at very slow rates and leads to blockage of pores when the catalyst is exposed to the modifier for long times, viz. 40 h.

Thus, it can be concluded that strong acidity and high temperatures are required for ethanol dehydration and the in-situ generation of water. This and perhaps long contact times would facilitate the deposition of larger amounts of TEOS on the surface. The deposition at low temperature occurs at slow rates and with reactant inhibition, allowing to deposit silica selectively onto the external surface and avoiding excessive blocking of pores when relatively short contact times are chosen.

The role of water

The role of water in the deposition process cannot be decoupled from the acidity of the catalyst. Strong acidity of the catalyst is responsible for in-situ water formation. Katada et al. (1994) have suggested that contamination water is responsible for the closure of silanol-links and thus, for the formation of a siloxane-network (see scheme 4.1). Additionally Jurgens and J.W. Rogers (1995) reported that the formation of the silica-network on TiO_2 using TEOS did not occur uniformly on the surface. The closure of siloxane bridges across the pore reduces the accessibility of the zeolite. Hibino et al. (1988) concluded that association of water vapour with the alkoxide TMOS is an effective means to obtain a higher amount of deposited silica. It must however be speculated that the presence of water would lead to the closure of the silica network and thus blocking of the pores. The goal of CVD modification is to eliminate undesired acidity on the external surface, while retaining high internal catalyst activity. Closed pore entrances mean the introduction of diffusional constraints into the system, by extending the diffusion pathway for both reactant and product molecules.

The formation of in-situ generated water is hence the key parameter for the extent of pore blockage that occurs during a CVD cycle.

Comparison of powder and pellets

The CVD of TEOS on pelletised samples lead to the same degree of deposition, as expressed in Si/nm^2 (see Figure 3.6). Slightly more silica was deposited during the first cycle on the pelletised sample at 200°C than on the powder. While powder and pellets behaved similarly during the TEOS deposition, the catalytic reactions showed significant differences. This will be shown in Sections 4.2 and 4.4.

4.2 Deactivation

The response of 1,3,5-TiPB-cracking and TDP to surface modification was investigated at constant reaction conditions. Therefore, the changes in conversion, activity and selectivity are related to changes of the catalytic properties of the catalyst.

A reliable measure of the degree of modification

The cyclic CVD treatment results in the deposition of "inert" silica on the "active" zeolite surface. Using the number of deposition cycles as a measure of the degree of modification can only be successful, when each cycle deposits the same amount of silica on the external surface. This is however not true, as seen in section 4.1. Thus, a more reliable measure of the degree of modification can be obtained by using the amount of deposited silica, expressed as Si/nm^2 (see section 2.4.9).

Inertisation of the externally accessible acid sites

The 1,3,5-TiPB molecule is too bulky (molecular diameter 8.5 Å(Hibino et al., 1993)) to enter the channel structure of the zeolite and thus, cracking can only occur on the external surface of the catalyst. The exact location of the external acid sites - on the external surface or in the secondary layer of the pore opening - is still a controversial issue in present literature. Because the surface of ZSM-5 is far from uniform (Weber et al., 2000) and not ideally smooth, 1,3,5-TiPB-cracking must be considered as a probe reaction for the spatially unconstrained active sites. Once all external surface activity is reduced to a minimum, the catalyst is regarded to be inertised.

4.2.1 External surface: 1,3,5-TiPB-cracking

Deposition at T_{CVD} = 50 to 200°C

The change of conversion with CVD can be related to the external surface acidity by the ratio of the first order rate constants of the modified and the fresh sample, as shown in Figure 4.3. It can be seen that CVD severely reduces the activity. However, the activity is not completely removed, with about 5% residual activity remaining. It has been observed that "inert" silica exhibits sufficient activity to dehydrate tert-butylalcohols and isomerise 1-butene (Niwa et al., 1990), low cracking activity for 1,3,5-TiPB (Röger et al., 1998a) and the reaction of trimethylaluminum (Bartram et al., 1991). The higher the chosen deposition temperature, the faster the inhibition of 1,3,5-TiPB-cracking (see Table 3.1). However, the amount of silica that was required for inertisation, ranged between 5 and 15 Si/nm^2 for both powder and pellets. This is 1-2 fold the amount of silica, needed to cover the potential attachment sites on ZSM-5, as described in section 4.1.2. The value of one to two completed

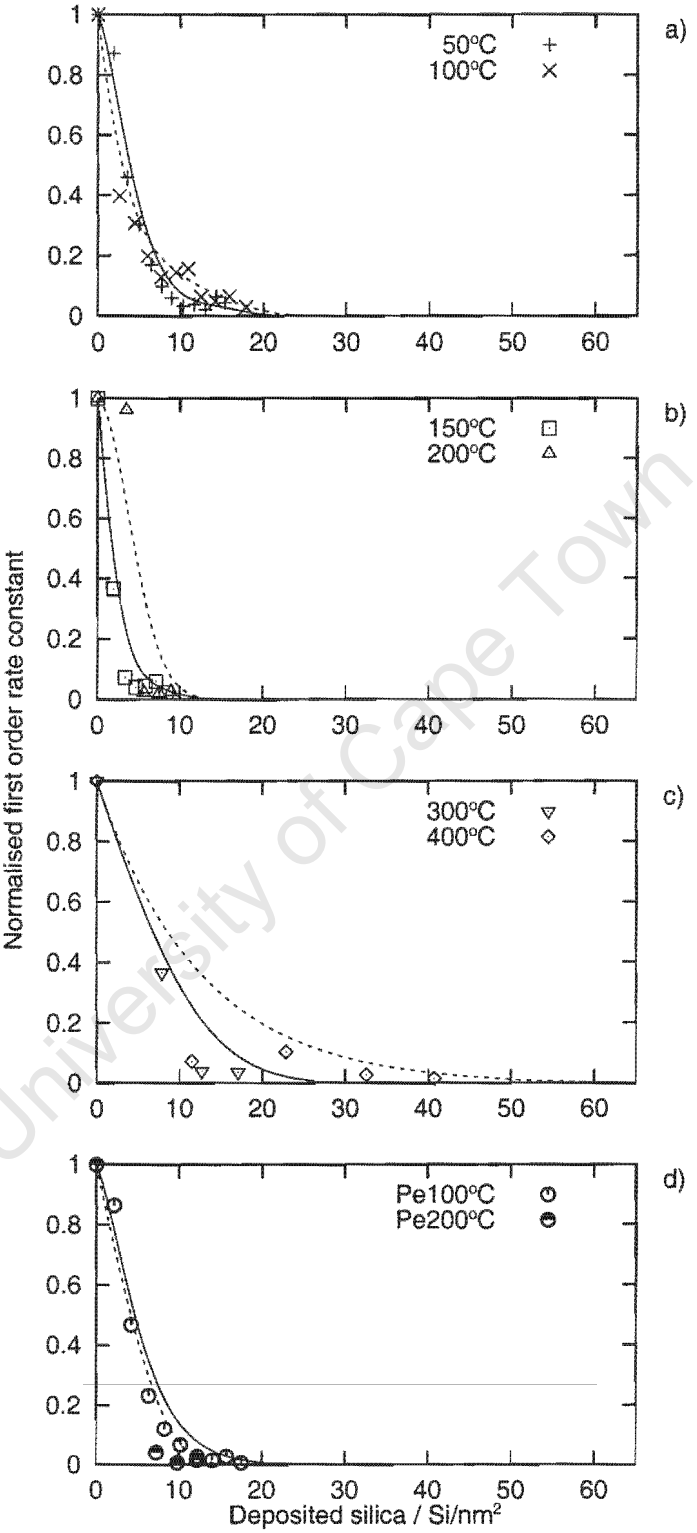

Figure 4.3: Activity for the cracking of 1,3,5-TiPB (first order reaction rate constants of the modified samples are normalised by the constant of the unmodified samples).

silica layers is in good agreement with the value reported by Hibino et al. (1988) for H-Mordenite, modified with tetramethoxysilane (TMOS) at 320°C in a static system. It must be noted that the same authors pointed out that for the deactivation of ZSM-5, more silica was required than for mordenite (Hibino et al., 1993).

Deposition at T_{CVD}= 300 and 400°C

More cycles were needed and more silica had to be deposited in order to depress the activity at 300 and 400°C (around 40 Si/nm^2 were required to achieve inertisation at 400°C). This is approximately four times the amount of silica which is needed to cover the potential attachment sites for TEOS. The high silica loading required, is an indication that the reactor bed is only partially deactivated. It also implies that the deposition of the silica is non-selective and does not only occur on the external surface acid sites. The non-homogeneous deposition of TEOS across the reactor bed is attributed to the too high CVD temperature at which the rapid reaction, catalysed by water, consumes all the TEOS before it can exit the reactor bed. Evidence for the non-uniform deposition of tetramethoxygermanium (TMOGe) on mordenite at a high deposition temperature was reported by Niwa et al. (1986a). Röger (1998) observed a higher degree of deactivation of the external surface when the CVD temperature was increased form 50 to 450°C. He attributed his findings to either a higher amount of deposited silica or to more uniform coating of the external surface at higher modification temperatures.

Selectivity of CVD at 50 to 200°C

In section 4.1 it was shown that 6-7 CVD cycles at low temperature are required to cover all potential attachment sites on the external surface. The activity for the cracking of 1,3,5-TiPB was completely reduced to residual activity after 6-7 cycles. Thus, the calculations are consistent with the experimental data. Similarly, Röger (1998) had to apply 5 CVD cycles with TEOS at 100°C in order to reduce the cracking activity of ZSM-5 by 98%.

Selectivity of CVD at 300 and 400°C

At high temperatures, more Si is needed to inertise the external surface, suggesting that either the deposition was not selective to acid sites or there was a gradient across the bed. Therefore, the deposition was non-uniform across the bed; consistent with the complete conversion observed in the initial CVD cycles.

Hibino et al. (1993) reported that the external surface of ZSM-5 was inertised after four to five complete layers of silica were deposited using TMOS at 320°C. This number corresponds to a silicon density of 36-45 Si/nm^2 which is similar to the one that was required to inertise the powder at 400°C in this present study (see Figure 3.8). It must be noted that the 400°C-powder series showed severe

deactivation for TDP (see Figure 3.18). Furthermore, the severe deactivation suggests, that the deposited layer was not selective to the acid sites and formed silica-networks on the surface causing pore blockage. This non-uniform deposition was also reported by Weber et al. (1998).

4.2.2 Overall: TDP

In contrast to 1,3,5-TiPB-cracking, TDP occurs on the external and internal surface and is thus a sensitive test reaction for the deactivation of the entire catalytic system. In the case of the small crystals used in this study, the contribution of the external surface is large. Hence, lower toluene conversions due to both loss of external surface activity and accessibility to the pore system are expected over the CVD modified samples, as compared to the fresh catalyst. The decay in relative conversion during TDP as a function of silica loading, can be seen in Figures 3.18 and 3.19. Similar results for TDP have been reported (Wang et al., 1989; Hibino et al., 1991; Das et al., 1994).

Relative activity at low CVD temperatures

Changes in relative activity for TDP are shown in Figure 4.4. From the 100°C-pellet series, it becomes apparent that three distinct steps can be distinguished, describing the deactivation due to site-selective CVD.

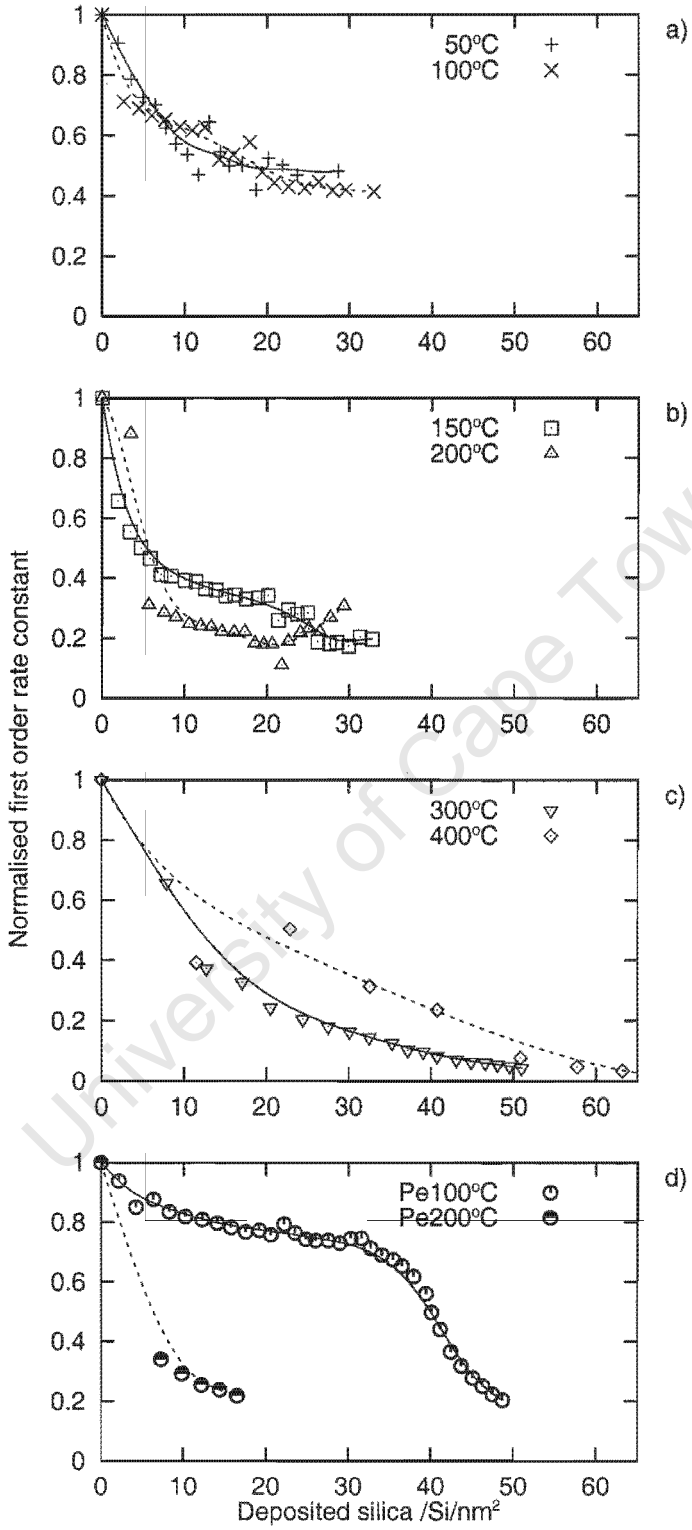

Figure 4.4: Activity for TDP (first order reaction rate constants of the modified samples are normalised by the constant of the unmodified samples).

(i) Initial loss of activity: external

There is a steep initial decline in the activity for samples modified at 50-200°C which is attributed to the inertisation of the external surface. The findings correlate well with the results of 1,3,5-TiPB-cracking, i.e 6-7 cycles are needed to eliminate external activity (Figure 4.5). The decreases in activity for the 50-150°C-powder and 100°C-pellet series are in good agreement with BET-analysis in which approximately 30% of the total surface area was attributed to external surface (see Table 2.2). Deposition at 200°C caused the activity to decrease to ca. 30% which indicates a change of deposition mechanism similar to that found for 1,3,5-TiPB-cracking (section 4.2.1).

(ii) Formation of activity plateau: intrinsic activity of the micro-pores

Deposition between 10-35 Si/nm^2 does not change the activity significantly and the formation of an activity plateau can be seen in Figure 4.4. This plateau is attributed as the intrinsic activity of the catalyst. This is particularly true for the 100°C-pellet series. At this point the extent of CVD has eliminated the external acidity and has not limited the accessibility of the toluene into the pores. Thus, the rate of reaction remains unaffected, provided the primary reaction steps are irreversible or in this case, at low conversion. The impact on selectivity will be addressed in subsequent sections.

(iii) Total deactivation: restricted toluene accessibility to the micro-pores

Silica deposition exceeding 35 Si/nm^2, resulted in the reduction of the observed internal activity. As TEOS cannot modify the internal surface (Niwa et al., 1986b; Hibino et al., 1991; Kim et al., 1996; Suzuki et al., 1998; Weber et al., 1998), the loss of activity must arise from the restricted access of the reactant from the catalyst pores. Excessive deposition would lead to complete blocking of all available pores, hence reducing activity.

Relative activity at high CVD temperatures

Severe deactivation without an activity plateau is observed with samples which have been treated with CVD at 300 and 400°C. Changes in activity arise from reduced accessibility of toluene into the catalyst pores. The TEOS deposition mechanism undergoes a change at high temperatures, leading to pore blockage and non-uniform deposition. The 200°C series appears intermediate and marks the turning point between blockage and selective external surface modification.

The 200°C-pellet series provides an interesting contrast to the powder sample. The powder sample still shows good activity while the pellet sample is deactivated. This seems to suggest that the deposition of TEOS has occurred at a different location in the pellet samples. It is possible that the rapid deposition in the pellet sample would lead to the formation of a shell around the pellet and

not the individual crystals. This would lead to complete and rapid blockage of the pellet and the activity of many crystals would be eliminated with each cycle. This suggests that rapid deposition of TEOS on pellets is diffusion limited in the macro-pores and occurs only on the outer shell. At low deposition temperature, the reaction is slow enough not to be diffusion limited and hence, uniform deposition is achieved on the crystal.

Effect of pore blocking on diffusivity and reaction rates (Theodorou and Wei, 1983)

As TEOS only deposits on the external surface, the model of pore blockage developed by Theodorou and Wei (1983) (see Section 1.3.5) provides a qualitative description of the modification process that is occurring, i.e. rapid direct deactivation of the external surface simultaneously with the slower deactivation of the internal pore space via blocking.

In all cases the internal pore space is never modified. The change in accessibility to the pore space may be viewed as a change in the effective diffusion coefficient of all species.

Conclusion

The observed decay in activity for TDP is attributed to the contribution of two simultaneously occurring effects. Firstly, the elimination of the external activity. Both 1,3,5-TiPB-cracking and TDP provide direct evidence for the deactivation of the external surface which occurs rapidly. This process is complete after the deposition of one silica monolayer. Secondly, pore blocking, which initially occurs much more slowly, becomes significant after excessive silica deposition, leading to catalyst deactivation via a reduction of the effective diffusivity (i.e. accessibility to the pore space).

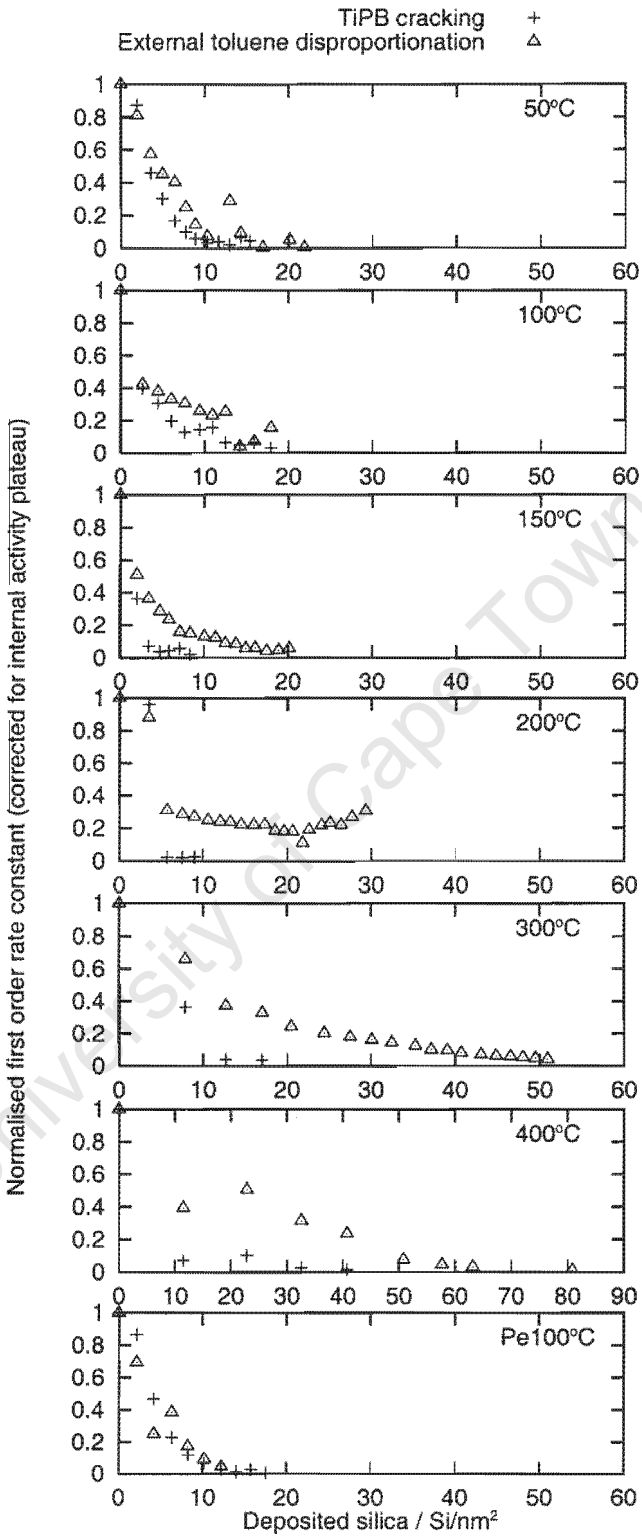

Figure 4.5: Changes in the first order rate constants for cracking of 1,3,5-TiPB and external disproportionation of toluene with increasing Si/nm^2 (assuming internal activity of 50% at 50°C, 50% at 100°C, 30% at 150°C and 80% for Pe100°C. For the deposition temperatures of 200, 300 and 400°C the internal activity cannot be determined.)

4.3 Quantification of deactivation behaviour

The changes in activity for TDP in section 4.2.2 revealed that two processes have to be considered when describing the deactivation behaviour of the entire catalyst. Firstly, deactivation of the external surface and secondly, decreased accessibility to the micro-pores due to pore blocking.

4.3.1 External

On examining the changes of the relative first order rate constants for 1,3,5-TiPB-cracking in Figure E.1, a logarithmic decay with increasing silica loading becomes apparent. This observation should also apply to all other reactions on the external surface, viz. TDP and xylene-isomerisation, when first order kinetics are assumed. The contribution of the internal reaction and the associated deactivation complicate the separation of the external contribution from the overall activity.

The semi-logarithmic plot of k/k_o versus the amount of deposited silica, n, shows the linear decrease with the slope $-\beta$:

$$\frac{d\ (ln\frac{k}{k_o})}{d\ n} = -\beta = \ (slope\ of\ plot) \tag{4.1}$$

where n denotes the amount of deposited silica on the external surface in Si/nm^2 and k_o is the reaction rate constant of the unmodified sample.

Equation (4.1) may be integrated to yield:

$$\frac{k}{k_o} = \alpha^n, \qquad 0 < \alpha < 1, \quad -\beta = ln\ \alpha \tag{4.2}$$

This equation may be interpreted as representing an incremental decrease (α) of surface activity with each layer of deposition, where n might be viewed as the number of cycles when *constant amounts of silica are deposited with each cycle.*

In this case, n represents the amount of deposited silica and thus, changes in the relative reaction rate constants are purely related to the degree of modification. In this case, large values of α show poor deposition while low values show good deposition, i.e. a high coverage shows the efficient use of the deposited silica.

Determination of α from 1,3,5-TiPB-cracking

The deactivation of the external surface is most accurately reflected by the inhibition of 1,3,5-TiPB-cracking. The fitting with linear regression via least square error minimisation is shown in Figure 4.6 and the results are summarised in Table 4.1. Hibino et al. (1991) and Röger et al. (1998a) monitored the CVD of alkoxysilanes with 1,3,5-TiPB-cracking and TDP and their published reaction data was also evaluated.

All deactivation constants for CVD treatments up to 300°C are within the range of expected error and describe the activity data satisfactorily. Since α relates activity of the surface and silica loading, the ineffective deposition at elevated CVD temperatures becomes apparent by an increase in α; it serves as a measure for the uniformity and quality of the silica deposition.

The α-value determined for the data by Hibino et al. (1991) is higher than the one which is found for the 400°C-powder series. CVD at 400°C showed least uniform deposition and the severest deactivation of the catalyst. It appears that CVD at 320°C in the static system leads to non-uniform deposition of silica on the catalyst. Rapid deposition and regeneration on the top layer of the catalyst batch could have prevent TMOS from reaching the remaining active surface in the packing. Thus, a surface barrier of silica could have formed on top of the catalyst packing which introduces diffusional constraints on bulky and slow diffusing molecules, such as TMOS and o-xylene. This would have resulted in slow uptake rates during sorption experiments while equilibrium amounts would not have been affected (Hibino et al., 1991).

It becomes apparent that the effects of CVD, performed in different modification systems, viz. static and flow, do not allow easy comparison (Weber et al., 2000; Weber, 1998).

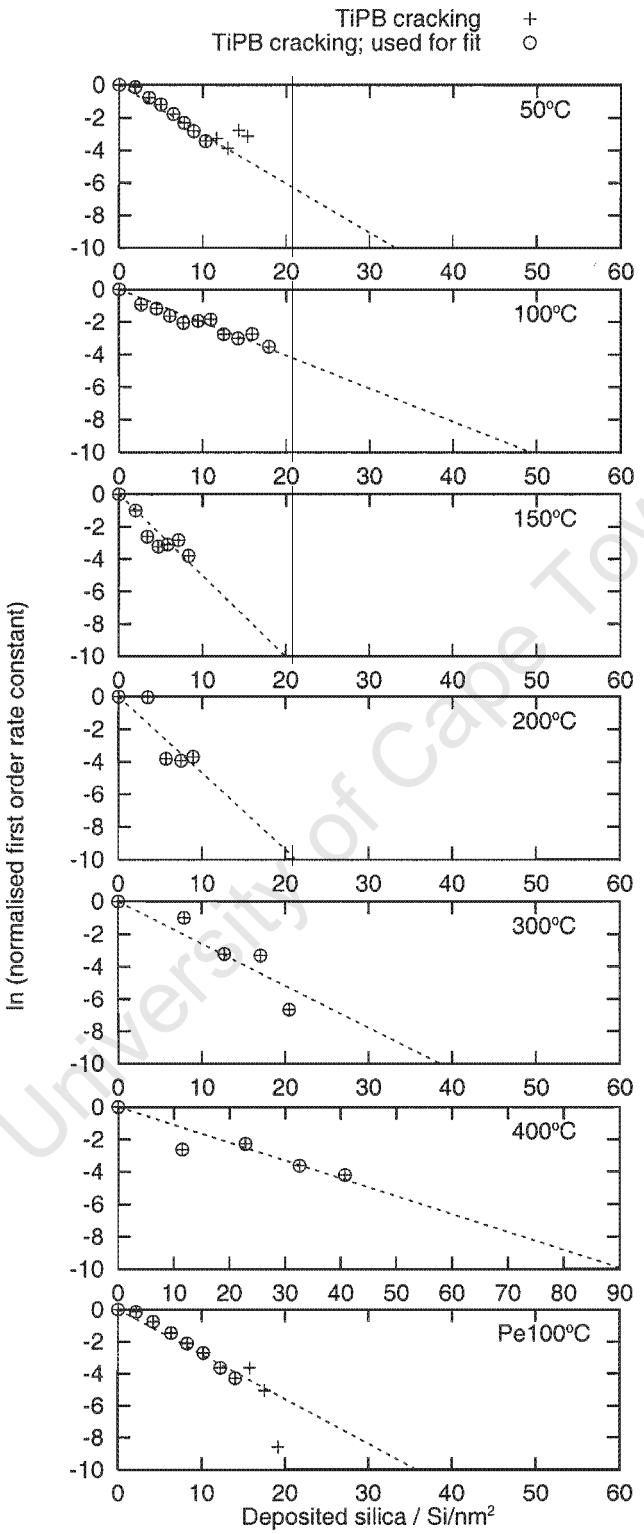

Figure 4.6: Fitting of ln(first order rate constants) for the cracking of 1,3,5-TiPB.

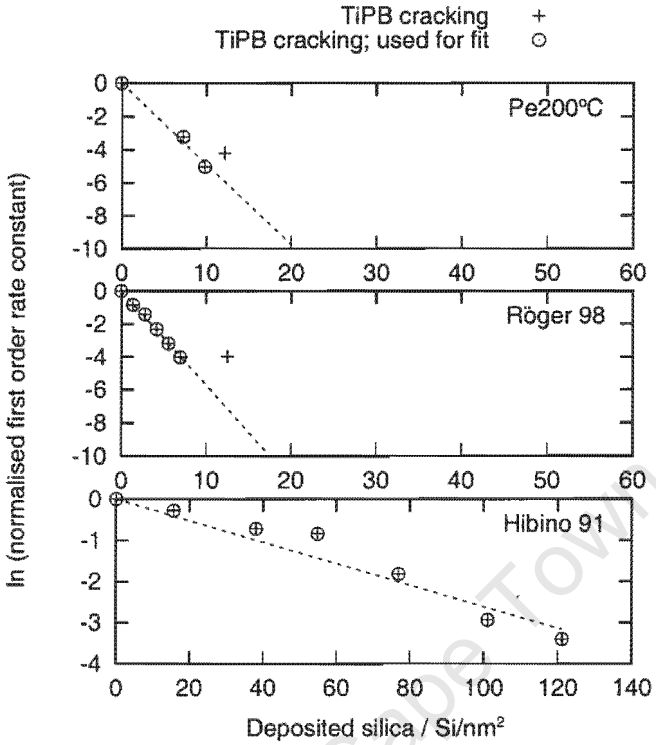

Figure 4.6: (continued) Fitting of ln(first order rate constants) for the cracking of 1,3,5-TiPB.

Table 4.1: Deactivation constants α for the respective temperature series for 1,3,5-TiPB-cracking.

CVD-series	α	R^2
50	0.75	0.95
100	0.83	0.90
150	0.61	0.79
200	0.63	0.75
300	0.77	0.90
400	0.90	0.81
Pe100°C	0.76	0.96
Pe200°C	0.61	0.99
100°C (Röger, 1998) [a]	0.57	0.99
320°C (Hibino et al., 1991) [b]	0.97	0.94

[a] TEOS in flow-through system; assuming the uniform deposition of 1.39 Si/nm^2 per CVD cycle at 100°C).

[b] TMOS modification in static vacuum system.

4.3.2 Deactivation of effective internal crystal activity

The effect of pore blocking on a crystal structure was investigated by Theodorou and Wei (1983)(see section 1.3.5). They developed a correlation between extent of pore blockage and dimensionless effective diffusivities of reactants. Theodorou and Wei make use of the relative diffusivity decrease:

$$\frac{D}{D_\circ} = F(\frac{D_i}{D_\circ} - 1) + 1 = 1 - F(x_b) \tag{4.3}$$

with

$$F(x_b) = 0.00160 - 0.1280x_b + 2.079x_b^2 - 3.078x_b^3 + 2.116x_b^4 \tag{4.4}$$

and where x_b represents the extent of blockage between 0 and 1, $D_\circ = D \cdot \tau/l^2$ is the dimensionless effective diffusivity from random walk experiments without blockage (index $\circ$) and at full blockage (index i; $D_i = 0$).

The effectiveness factor, η, of a first order reaction in a spherical particle is given by:

$$\eta = \frac{3}{\Phi}\left[\frac{1}{\tanh\Phi} - \frac{1}{\Phi}\right] \tag{4.5}$$

where $\Phi = L(k_{ISO}/D)^{1/2}$. By substituting equation 4.3 into equation 4.5 and assuming that blocking is proportional to the amount of deposited silica, i.e. $x_b = \frac{Si_{deposited}}{Si_{needed\ for\ complete\ blockage}}$, the variation of the effectiveness factor with silica deposition can be obtained.

A mathematical model which aims to describe the experimental results and serves to validate the above discussion of the two deactivation processes, will be presented in section 4.6.

4.4 Shape selectivity during TDP

4.4.1 Improvement of para-selectivity on a benzene free basis

The distribution of the xylene isomers during TDP illustrates that CVD at all temperatures gradually improves the shape selective performance of the catalyst, even at low conversion. The unmodified catalyst produces an equilibrium distribution at all levels of conversion. Figures 4.7 and 4.8 show that between 2 and 5 cycles were required before the xylene isomer distribution shifted away from equilibrium. Two criteria have to be met to enhance the para selectivity during TDP (Chen et al., 1994); (i) Sustaining the formation of the para-xylene formed in the crystals and (ii) to reduce the secondary isomerisation of para-xylene via 1,2-methyl-shift.

4.4.2 The sequence of the xylene selectivity variation with CVD

Ortho- and p-xylene were the first isomers to respond to the influence of the CVD cycles. The concentration of o-xylene decreased while p-xylene increased. At this stage the m-xylene concentration remained unaffected. A few more CVD cycles were necessary to cause the meta-selectivity to decrease. This observation does not follow the order of the measured diffusivities, $D_{px} \gg D_{ox} > D_{mx}$ (Chen et al., 1994). From the order of the diffusivities it would be expected that the m-xylene should be the first isomer to be affected by CVD, and thus should be the first isomer to decrease. This suggests that either the reported diffusivities are wrong or the formation of the o- and m-xylene come from a non-shape-selective reaction. Assuming that the reported diffusivities are correct, the only way in which m-xylene concentration can exceed o-xylene will be if the reaction proceeds in the sequence p-X $\rightleftharpoons$ m-X $\rightleftharpoons$ o-X. It may now be postulated that the intra-crystalline pore space produces a p-xylene rich product which is unaffected by the CVD modifications. The p-xylene then undergoes rapid isomerisation on the external surface to produce the equilibrium distribution (see 1,2 shift for TMB (Röger et al., 1998a)). As the external surface is deactivated by CVD, the isomerisation reaction slows down. As this is a sequential reaction, the o-xylene fraction will decrease followed by m-xylene, as observed. This provides the only plausible explanation of the results observed.

4.4.3 Pore blocking and reduced isomerisation

It becomes apparent that both reduced secondary isomerisation rates on the external surface and pore blocking could be responsible for the enhanced para-selectivity. Separation of the two simultaneously occurring effects is only possible at low CVD temperatures, viz. 50-150°C. The maximum para-selectivity is always observed after the external surface has been deactivated and before the catalyst shows signs of severe deactivation (see 4.2.2 "activity plateau").

The same effects of deactivation, as were seen for the 1,3,5,-TiPB-cracking and the external TDP,

apply for the isomerisation reaction of the external surface. Despite the inertisation of the external surface appearing complete, the xylene isomer composition is only affected marginally. This suggests that the preferential formation of a particular xylene isomer, i.e. p-xylene, inside the ZSM-5 crystal is unlikely, as implied in the previous section.

However, the xylene isomers have different intrinsic diffusivities in the unmodified catalyst, $D_\circ$ and thus also "intrinsic Thiele modulus", $\Phi_\circ$: Introduction of diffusional constraints affects the diffusivities for all molecules to the same extent (Wei, 1982). Because of the difference in $\Phi_\circ$, the effectiveness factor, η, for each reaction will vary differently, causing shape selectivity in the crystal due to pore blockage.

Pore blocking

The pore blocking model after Theodorou and Wei (1983) (see Section 1.3.5) provides insight into the changes in effective diffusivity and hence effectiveness factor for the catalytic system, as the degree of modification progresses.

The decrease in diffusivity with increasing silica loading is displayed in Figure 4.9. The degree of pore blockage is given as the ratio of deposited silica to the amount of silica which causes the total deactivation of the catalyst.

In comparison to function 4.3 an approximation of

$$\frac{D}{D_\circ} = 1 - F(x_b) \approx 1 - x_b^2 \tag{4.6}$$

is plotted in Figure 4.9a and it provides a reasonable simplification of the polynomial expression.

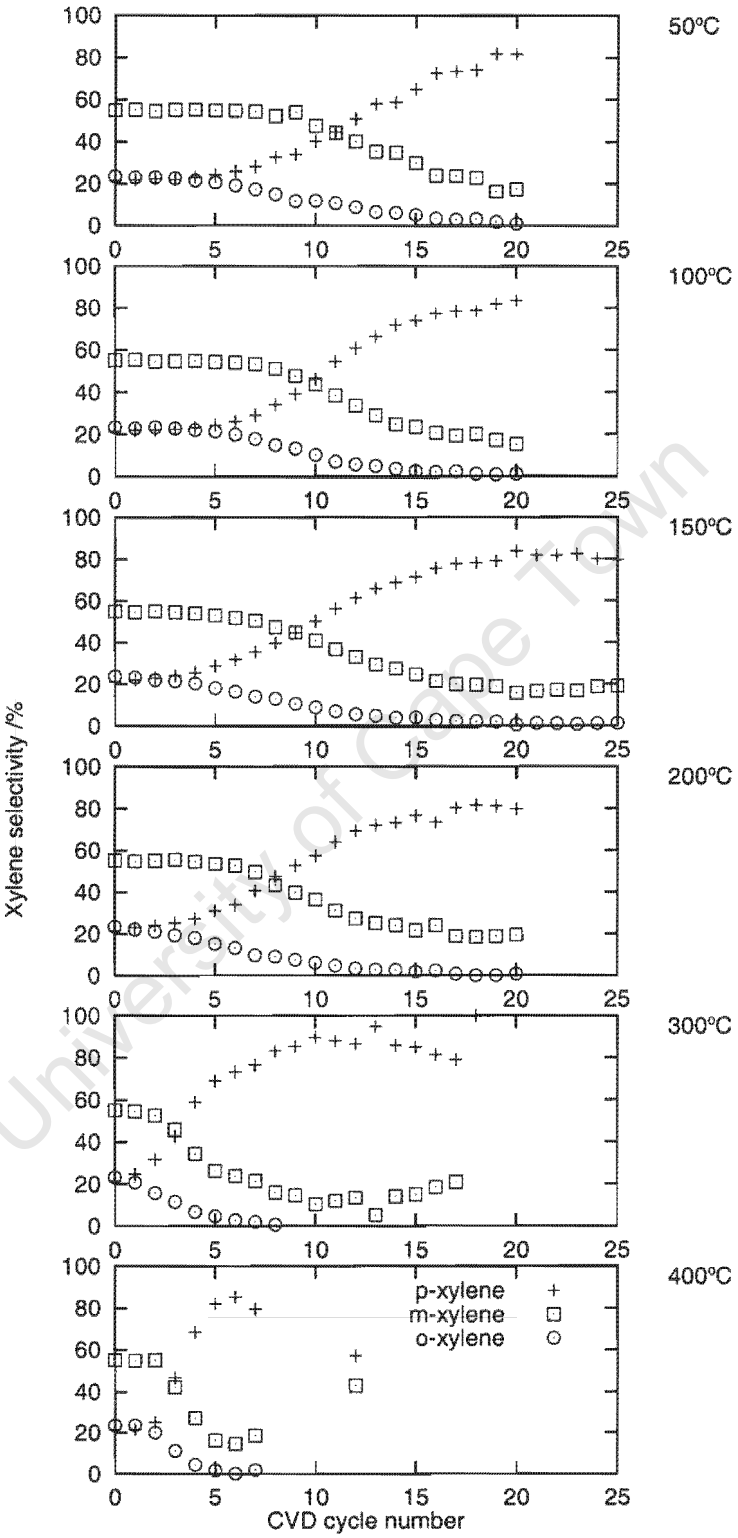

Figure 4.7: Changes in xylene-selectivities with increasing number of CVD treatments for powder samples.

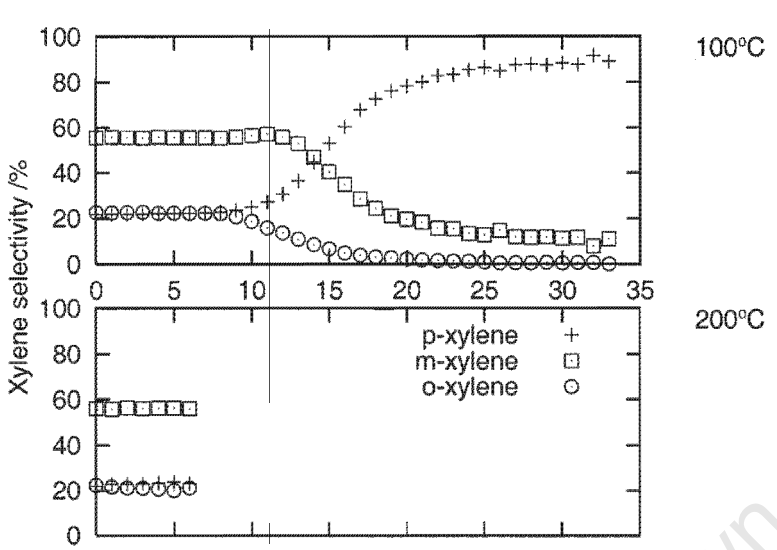

Figure 4.8: Changes in xylene-selectivities with increasing number of CVD treatments for pelletised samples.

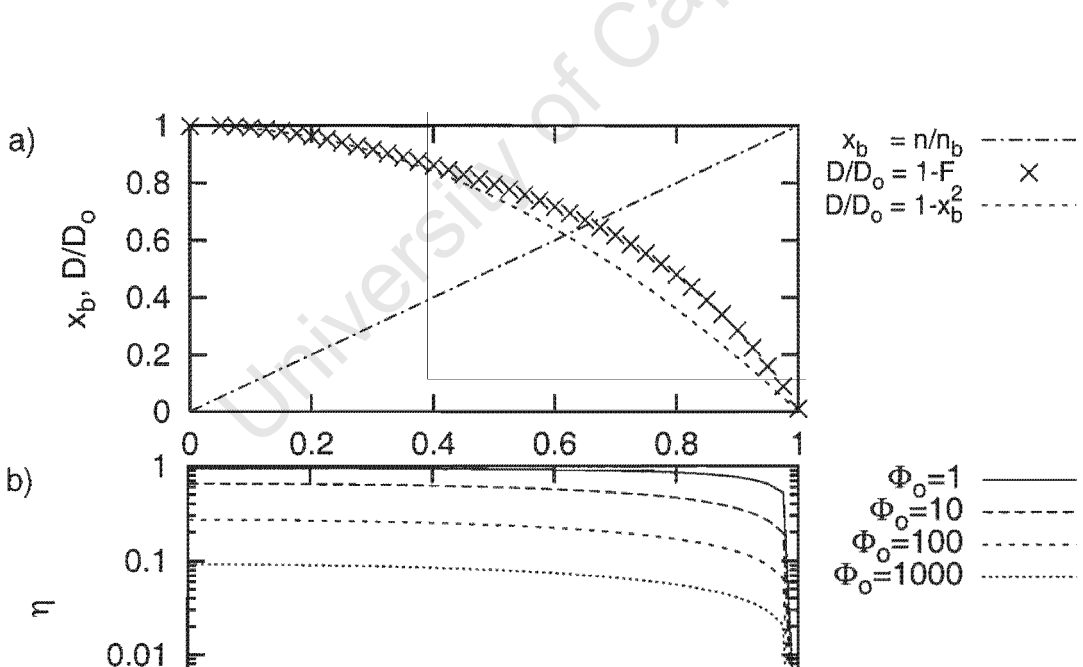

Figure 4.9: Effect of the linear increase of pore blockage with silica loading on relative diffusivity and effectiveness factor.

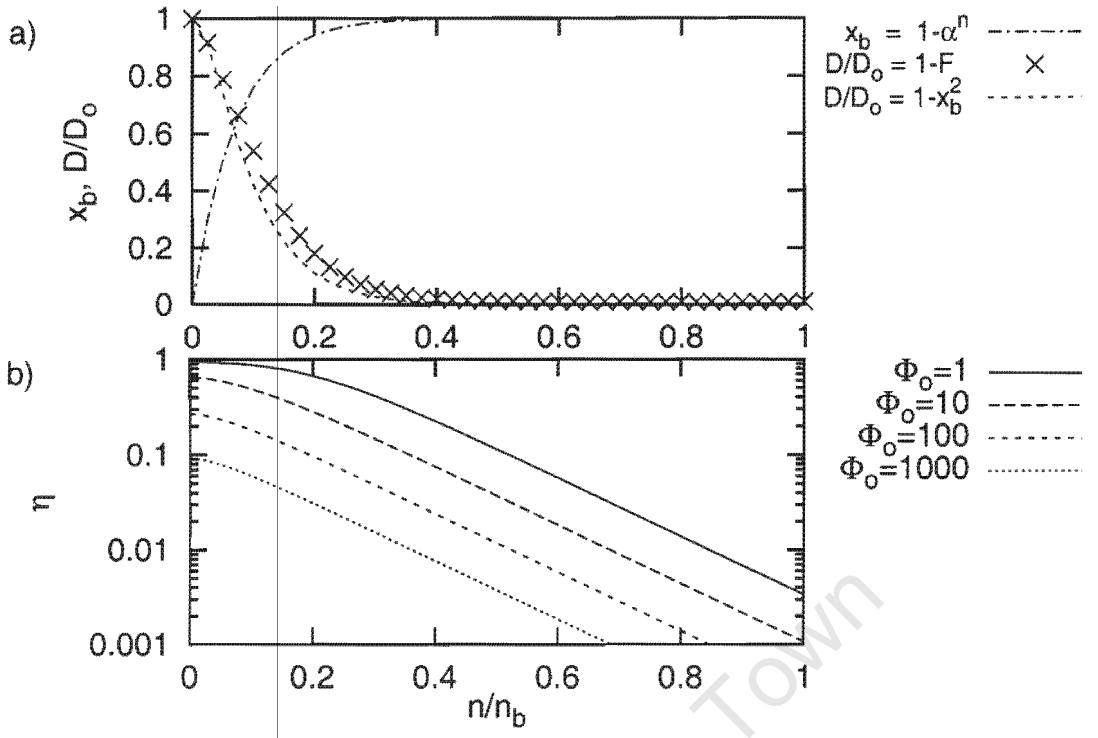

Figure 4.10: Effect of the exponential increase of pore blockage with silica loading on relative diffusivity and effectiveness factor.

For the xylene isomers the effective diffusivities and hence Φ_o vary over three orders of magnitude, causing the effectiveness factors, η, for each isomer to vary differently, as the extent of pore blockage increases. This effect is shown in Figure 4.9b. Regardless of the intrinsic value of Φ_o, pronounced changes in effectiveness factor only occur when a large fraction of the pores are blocked, i.e. $x_b > 80\%$. The effectiveness factors are affected in a way, that separation of the xylene isomers appears unlikely in the region where the experimental data show dramatic changes in xylene selectivity. Thus, it becomes evident, that the extent of pore blocking cannot be correctly represented by the linear dependence of deposited silica, as the experimental data show that significant pore blocking must already occur at lower silica loadings (Section 4.2.2).

The effectiveness of the catalytic system depends on the surface area that is available for the diffusive flux into and out of the micro-pores. Assuming that the access into the crystal decreases in the same fashion as it was found for the catalytic activity of the external surface, the extent of pore blockage can be described with $x_b = 1 - \alpha^n$ (see Section 4.3.1). The resulting changes in diffusivity and effectiveness factors are displayed in Figures 4.10a and 4.10b.

In this case, due to the exponential increase, pore blockage occurs at a much higher rate and high extents of pore blockage are achieved already after low amounts of silica are deposited on the external surface. With increasing extent of pore blockage, dramatic changes in effectiveness factors, η, for the different compounds become apparent. The effectiveness factor for compounds which are intrinsically not diffusion limited ($\Phi_o < 1$), become affected at comparatively low silica loadings, viz. approximately 20 to 40 %, and the decrease of η occurs over the entire range of pore blockage.

The effectiveness factor of initially diffusion limited compounds ($\Phi_o = 1000$) is reduced similarly, however, η assumes minimal values that a contribution of these compounds to the overall diffusive flux can be excluded. From Figure 4.10 it can be seen, that separation of compounds of different intrinsic diffusivities can be explained, when the extent of pore blockage increases exponentially. This hypothesis will be tested in Section 4.6.

Reduced secondary isomerisation on external surface

As laid out above, the fast secondary isomerisation on the external surface of ZSM-5 leads to the thermodynamic equilibrium mixture of xylenes in the product over unmodified catalyst.

The reaction conditions for TDP were kept constant throughout the modification series and the decay of the rate of secondary isomerisation must originate from a reduced reaction rate constant. The same effects of deactivation, as were seen for the 1,3,5-TiPB-cracking and the external TDP, apply to the isomerisation reaction on the external surface.

(i) unmodified, viz. n=0

The ratio of rate constants for xylene-isomerisation and TDP, viz. k_{ISO}/k_{TDP}, over ZSM-5, is reported to be in the range of 100 (Young et al., 1982) to 7000 (Olson and Haag, 1984). Xylene-isomers leaving the crystal, undergo fast isomerisation. Thus, a thermodynamic equilibrium mixture of xylenes is obtained over unmodified ZSM-5, even at low conversion levels (Olson and Haag, 1984). The powder and pellet series (Figures 3.20 and 3.21) confirm that para-selectivity over the unmodified samples did not change at conversions larger than 3 %. A marginally higher para-selectivity can be seen over the powder sample at conversion below 3% which is the expected trend at higher reaction temperature (Young et al., 1982) due to mass transport limitations (Olson and Haag, 1984).

(ii) inertisation of external surface area

When a complete silica layer was deposited on the external surface, the o-xylene fraction was marginally reduced while more p-xylene was found in the xylene mixture. At this stage, the external surface reactions were eliminated and it might be argued that this observed composition is the intrinsic xylene composition as it is formed inside the ZSM-5 crystals. However, as laid out in the previous Section, diffusional limitations of the "slowest" compound cannot be excluded, thus accounting for a decreased o-xylene fraction.

From this point on, the secondary isomerisation on the external surface does not affect the xylene composition and changes are attributed to diffusional limitations due to pore blockage only.

4.4.4 Effect of WHSV on para-selectivity

When observing TDP on shape selective zeolite crystals in an integral packed bed reactor, two time constants of the system have to be considered: (i) the apparent residence time $\tau = V/F$ in the reactor and (ii) the time constant for diffusion in the crystal, viz. D/R^2.

The two time constants can be regarded as resistances in series and, depending on their magnitude, influence the xylene composition. In general, three cases can be distinguished:

(i) $D/R^2 < \tau$

When the residence time in the reactor is high, diffusional limitations in the crystal have negligible effect on the product composition in the reactor effluent. In other words, when the diffusional limitations for all xylenes are insignificant, thermodynamic equilibrium composition is observed when the residence time, viz. WHSV, is varied. Only at very low residence times and hence, low toluene conversions, shape selective effects are observed over unmodified ZSM-5.

(ii) $D/R^2 \approx \tau$

When the two resistances are of similar order, variation of the WHSV should show a pronounced effect on the product composition. Unfortunately, in this study the WHSV was only varied in cases where high para-selectivity was already obtained, i.e. after diffusional limitations showed severe impact on the xylene composition.

(iii) $D/R^2 > \tau$

When the introduction of diffusional limitations leads to the maximal differences in effectiveness factors, maximal shape-selective effects can be observed. Variation of the WHSV alters the rate with which xylene isomers can reenter the crystal and isomerise inside the micro-pores. Since the reentry is also severely diffusion limited, changes of the WHSV would affect the product composition only to a low extent.

Figures 3.20 and 3.21 show that para-selectivity is improved with decreasing conversion. However, the separation of xylene isomers proved to be increasingly inaccurate when low concentrations were analysed, introducing large scatter in the high para-selectivities at low toluene conversions. Das et al. (1994) studied TDP over CVD modified (16 wt% silica) ZSM-5. They showed that reducing the conversion from 23 to 9% at 500°C only marginally improved the para-selectivity from 89 to 93%. Unfortunately, neither crystal size, nor external surface area are disclosed. Also, no catalytic reaction data that could be clearly attributed to the external surface are given, allowing the determination

of α. However, judging from the high para-selectivity at high conversion, their findings appear to support the hypothesis as discussed above.

4.4.5 Diffusional constraints

The knowledge of diffusional properties is indispensable for the interpretation of reactions in catalytic systems.

Introduction of diffusional constraints can be deduced from (usually unreliable) sorption uptake rate measurements. Additionally, knowledge of the deactivation constant α allows interpretation of the uniformity of the modification. However, few studies supply both diffusion and reaction data.

Hibino et al. (1991) reported suppressed adsorption rates of o-xylene as well as 99% selectivity to p-xylene during o-xylene isomerisation at 1% conversion. The ZSM-5 catalyst was modified with TMOS in a static vacuum system at 320°C. The data for the 1,3,5-TiPB-cracking indicated non-homogeneous deposition across the catalyst bed (see section 4.3.1). It appears that non-uniform deposition was the reason for severe pore blocking and thus for increased diffusional constraints in the above mentioned case. Röger et al. (1998a) modified ZSM-5 in-situ in a fixed bed reactor and reported 98% para-selectivity for TDP with no significant loss of conversion. Furthermore, investigating the effect of CVD at 100°C on the adsorption rate of p-, o-xylene and 1,2,4-TMB using a microbalance, the sorption of o-xylene and 1,2,4-TMB was drastically reduced while p-xylene was seen to be unaffected.

However, diffusion measurements are usually performed at temperatures which are far below the relevant reaction temperatures. Furthermore, diffusion of molecules in a micro-pore system is an activated process with greatly varying activation energies for the involved compounds (Chen et al., 1994). Thus, it proves to be difficult to apply results from diffusion measurements and coefficients from the published literature

The modification of ZSM-5 with TEOS at low temperatures allows separation of the contributions of external and internal reactions as well as monitoring the effect of changing diffusional properties and their impact on the product composition. Thus, by applying a suitable model that describes the experimental results, it should be possible to support the reported ratio of the diffusion coefficients of the xylene isomers under reaction conditions for TDP, viz. at 450°C. This model will be elaborated on in Section 4.6.

4.5 Catalyst performance: P-xylene Yield

4.5.1 Para-xylene yield versus toluene conversion plot

Cyclic CVD leads to improved para-selectivity while simultaneously deactivating the catalyst. In order to compare the effects of the different CVD temperatures on the catalytic performance, the decreasing conversion for TDP has to be accounted for. Plotting the p-xylene yield versus the observed conversion of toluene (pY-X-plot) allows comparison of the different samples, independent of the degree of deactivation (Ko and Wojciechowski, 1983).

The performance of the catalyst for TDP is limited by two extremes. (i) Thermodynamic equilibrium limits the p-xylene fraction giving the minimum yield, regardless of the toluene conversion. (ii) 100% selective catalysts produce only p-xylene and benzene. If CVD resulted in nonselective deactivation, viz. reduced effective catalyst mass, the same p-xylene yield to toluene conversion relation should be observed in the pY-X-plot (Wojciechowski, 1974). Due to constant TDP reaction conditions, the differences in the selectivity patterns are attributed to the CVD at different temperature.

Powder

The powder samples, modified at low CVD temperature, showed no improvement in p-xylene yield as observed over the unmodified catalyst (Figure 4.11). This is a surprising result, considering the high para-selectivities of 80-90% at 50-60% activity loss. From the benzene/xylene-ratios in Figures 3.16 and 3.17 it can be deduced that "dealkylation" of xylenes accounted for an increased concentration of benzene after extensive modification. This will be discussed below in Section 4.5.2. Bearing the costly downstream separation of the xylene-isomers in mind (Tsai et al., 1999), the p-xylene enriched product stream characterises an improved catalyst, despite the increased benzene fraction.

CVD at 200°C lead to blocking of pores and the decrease of activity outweighed the improvements in para-selectivity. Higher modification temperatures enhance the overall deactivating effect of CVD and result in poor activity.

Pellets

The 100°C-pellet series displayed outstanding catalytic performance when the 2.5-fold p-xylene yield of the parent sample was obtained. Para-selectivity was improved while a high conversion level of better than 11% was maintained.

As already found for the powder series, CVD at 200°C lead to the severe deactivation of the pellets. Despite the apparent uniformity of the deposition, pore openings are blocked already in the early stages of the modification and renders the catalyst useless.

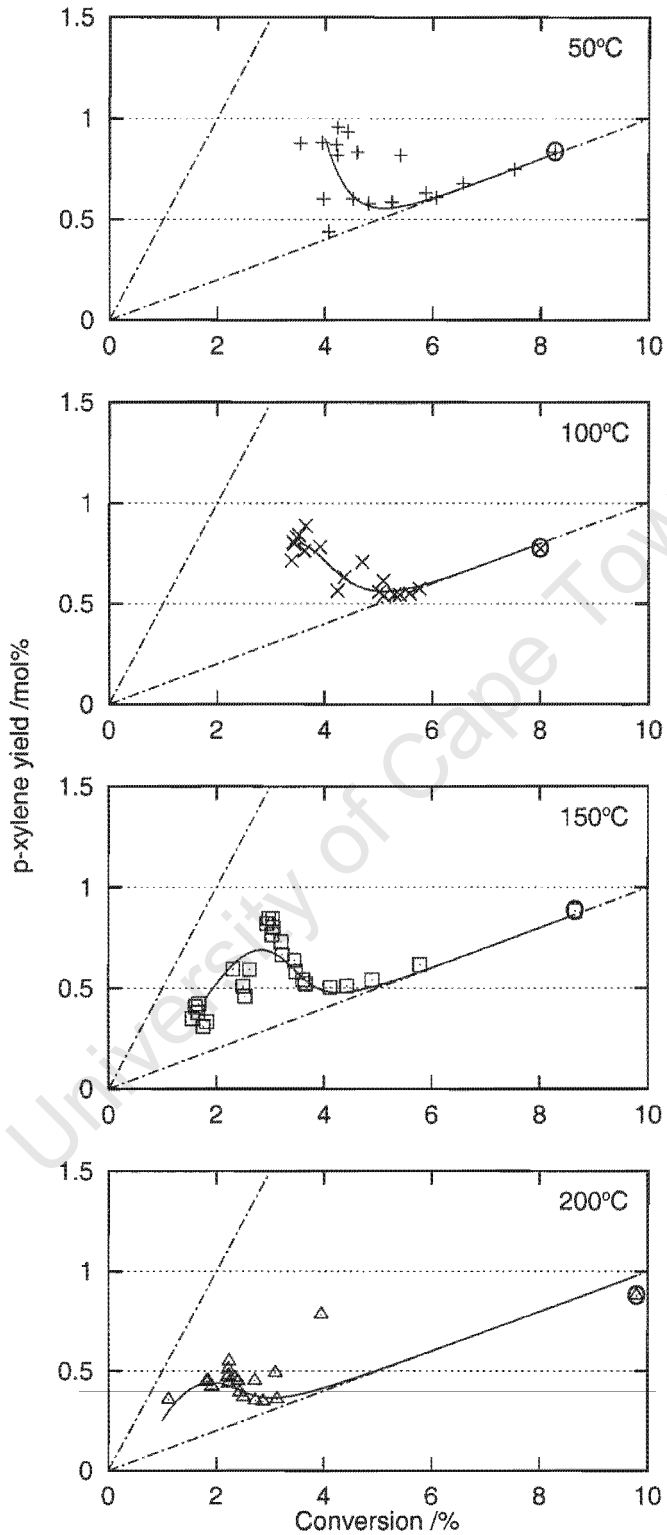

Figure 4.11: Selectivity plots for TDP over CVD modified powder and pellet samples. Data obtained over the unmodified samples are encircled.

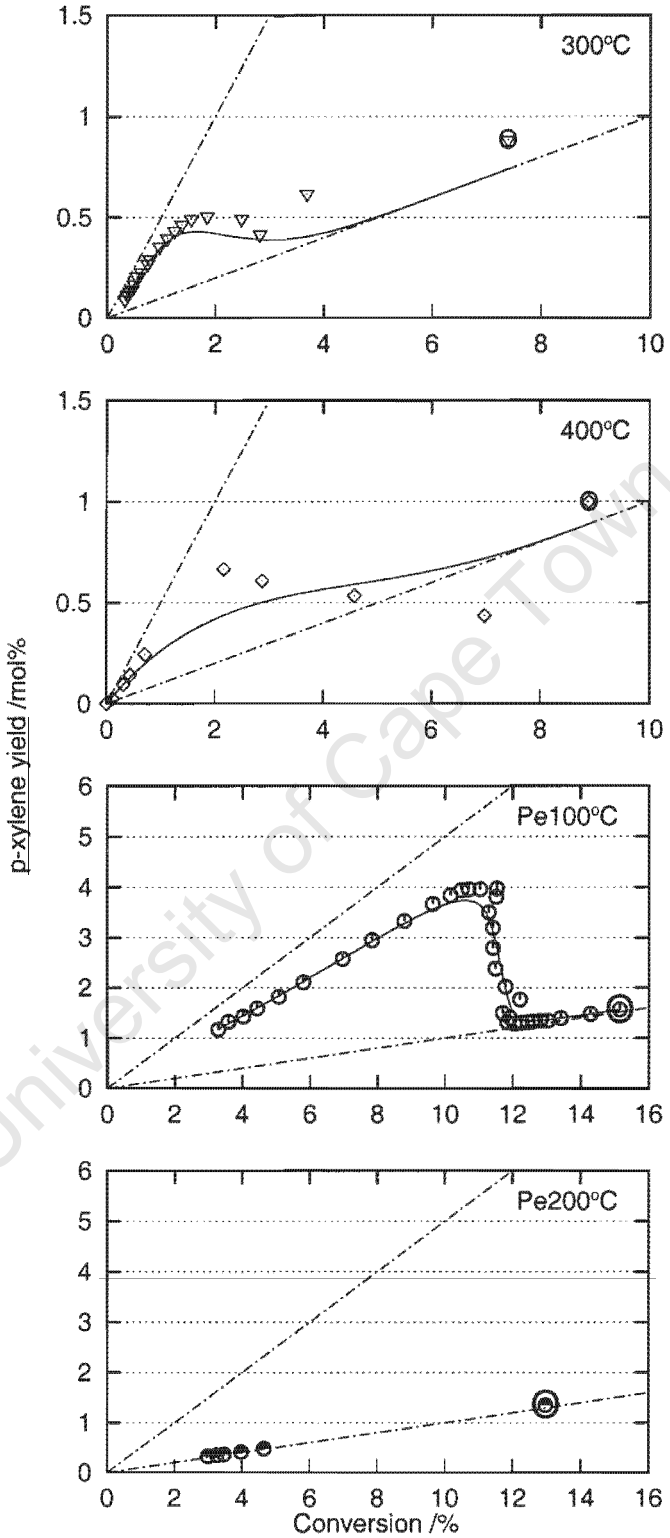

Figure 4.11: (continued) Selectivity plots for TDP over CVD modified powder and pellet samples. Data obtained over the unmodified samples are encircled.

4.5.2 Loss of xylenes

Figures 3.16 and 3.17 display the molar benzene/xylene ratios during TDP over the modified samples. The deviation from the theoretical value of unity becomes apparent. Slightly higher benzene/xylene ratios are expected at the higher reaction temperature for TDP over unmodified powder (550°C) as compared to pellets (450°C) (Kaeding et al., 1981b). The "apparent" dealkylation of xylenes is attributed to secondary reactions occurring at high temperatures. Large diffusional constraints promote the final product in series type reactions; secondary reactions which occur produce higher methylated rings via disproportionation. These can be converted to benzene and light hydrocarbons via a paring mechanism (Röger et al., 2000).

The benzene/xylene ratios over powder which was modified at 50-200°C conspicuously increases when ca. 15-20 Si/nm^2 were deposited. This effect does not occur when CVD was carried out at 300 and 400°C. The paring reaction only occurs inside the micro-pores of the crystals. Thus diffusion limitations that are introduced into the reaction system would increase the benzene/xylene ratio. This is the case at the low deposition temperatures, where progressing modification leads to the continuous blocking of pores. At high deposition temperatures, non-uniform deposition of silica leads to the complete blockage of pore openings and entire catalyst particles become inaccessible for the reactants. As consequence, the effective catalyst volume is reduced, leading to reduced conversions as well as to reduced probability for the formation of poly-alkylated aromatics and their dealkylation via the paring mechanism.

The benzene/xylene ratios over the pellet samples do not exceed values of 1.6. This must be related to the significantly lower reaction temperature of 450°C for TDP over pellets in contrast to 550°C over the powder samples. As a result of the lower temperature, diffusion is less limiting, thus reducing the probability for the xylene consuming side reactions to proceed.

4.6 Modelling effects of CVD on TDP

4.6.1 Reaction pathway

In order to develop a model for TDP over ZSM-5, the following reaction pathway was assumed.

The disproportionation of toluene (T) inside the crystal yields the kinetically favored isomers, p-xylene (pX) and o-xylene (oX), and benzene (Bz). It is assumed that the reaction is of first order in respect to the toluene concentration, irreversible and o- and p-directing. The respective rate constants, k_i, for each reaction step are given above the reaction arrows.

$$2\,T \xrightarrow{1/3\ k_1} pX + Bz \tag{4.7}$$

$$2\,T \xrightarrow{2/3\ k_1} oX + Bz \tag{4.8}$$

The isomerisation of the p- and m-xylene (mX) occurs strictly consecutively and thus allows the formation of o-xylene. The isomerisation reactions obey first order kinetics and are reversible. k_2 denotes the forward rate constant, equal for both reactions, and K_{e1} and K_{e2} are the equilibrium constants for each reaction:

$$pX \overset{k_2}{\rightleftharpoons} mX, \qquad K_{e1} = \frac{mX}{pX} \tag{4.9}$$

$$mX \overset{k_2}{\rightleftharpoons} oX, \qquad K_{e2} = \frac{oX}{mX} \tag{4.10}$$

"Xylene dealkylation" and the formation of excess benzene occurs via a paring mechanism inside the zeolite crystal (Röger et al., 1998b). The first step is the disproportionation of two xylenes to trimethylbenzene (TMB) and toluene, viz.:

$$2T \rightleftharpoons TMB + T \tag{4.11}$$

The second step is the paring of light hydrocarbons (HC's) from the polyalkylated aromatic:

$$TMB \rightarrow Bz + HC's \tag{4.12}$$

The two steps can be combined when assuming that the second step proceeds rapidly. Hence, the following reaction mechanism for each xylene isomer is obtained:

$$2\ pX \xrightarrow{k_3} T + Bz + Hc's \tag{4.13}$$

$$2\ mX \xrightarrow{k_3} T + Bz + Hc's \tag{4.14}$$

$$2\ oX \xrightarrow{k_3} T + Bz + Hc's \tag{4.15}$$

Each of these reactions are assumed to be of first order and irreversible.

The assumption of the second reaction step in the paring mechanism proceeding rapidly can be reasoned by considering strong diffusional limitations of TMB within the crystal. This leads to increased concentrations inside the micro-pores. High TMB concentrations, combined with high reaction temperature, leads to fast paring "dealkylation".

All reaction steps described above, with exception of the paring reaction, also occur on the external surface of the ZSM-5 crystal. The reaction rates on the external surface are assumed to change differently compared to the reactions occurring in the crystal interior, which leads to two more rate constants, viz. k_4 and k_5:

$$2\ T \xrightarrow{1/3\ k_4} pX + Bz \tag{4.16}$$

$$2\ T \xrightarrow{2/3\ k_4} oX + Bz \tag{4.17}$$

$$pX \overset{k_5}{\rightleftharpoons} mX, \qquad k_5 = K_{e1} = \frac{mX}{pX} \tag{4.18}$$

$$mX \overset{k_5}{\rightleftharpoons} oX, \qquad k_5 = K_{e2} = \frac{oX}{mX} \tag{4.19}$$

This assumed reaction pathway is illustrated in Figure 4.12.

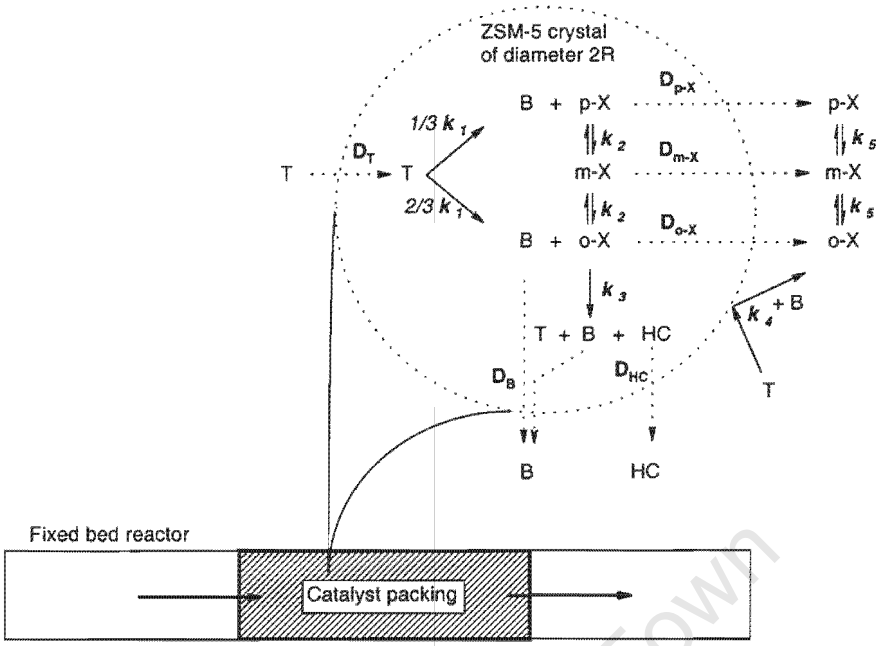

Figure 4.12: Model of TDP over ZSM-5 in a fixed bed reactor.

4.6.2 Assumed rate expressions

All involved reaction steps are assumed to obey first order reaction kinetics. The thermodynamic equilibrium conversion of toluene to form the xylene isomers and benzene at 450°C is limited to approximately 57 %. At conversion levels below 15 % effects of the reverse reaction can be neglected, and this reaction can be treated as irreversible.

The rate expressions for the reactions in the crystal interior become thus:

$$r_T^{int} = -2\ k_1\ C_T^{int} + \frac{1}{2}\ k_3\ (C_{pX}^{int} + C_{mX}^{int} + C_{oX}^{int}) \tag{4.20}$$

$$r_{pX}^{int} = \frac{1}{3}\ k_1\ C_T^{int} - k_2\left(C_{pX}^{int} - \frac{C_{mX}^{int}}{K_{e1}}\right) - k_3\ C_{pX}^{int} \tag{4.21}$$

$$r_{mX}^{int} = k_2\left[\left(C_{pX}^{int} - \frac{C_{mx}^{int}}{K_{e1}}\right) - \left(C_{mX}^{int} - \frac{C_{oX}^{int}}{K_{e2}}\right)\right] - k_3\ C_{mX}^{int} \tag{4.22}$$

$$r_{oX}^{int} = \frac{2}{3}\ k_1\ C_T^{int} - k_2\left(C_{mX}^{int} - \frac{C_{oX}^{int}}{K_{e1}}\right) - k_3\ C_{oX}^{int} \tag{4.23}$$

$$r_{Bz}^{int} = k_1\ C_T^{int} + \frac{1}{2}\ k_3\ (C_{pX}^{int} + C_{mX}^{int} + C_{oX}^{int}) \tag{4.24}$$

where C_i denotes the concentration of the species i.

The rate expressions for the reactions that occur on the external surface are:

$$r_T^{ext} = -2\ k_1\ C_T^{ext} \tag{4.25}$$

$$r_{pX}^{ext} = \frac{1}{3}\, k_1\, C_T^{ext} - k_2\left(C_{pX}^{ext} - \frac{C_{mX}^{ext}}{K_{e1}}\right) \tag{4.26}$$

$$r_{mX}^{ext} = k_2\left[\left(C_{pX}^{ext} - \frac{C_{mx}^{ext}}{K_{e1}}\right) - \left(C_{mX}^{ext} - \frac{C_{oX}^{ext}}{K_{e2}}\right)\right] \tag{4.27}$$

$$R_{oX}^{ext} = \frac{2}{3}\, k_1\, C_T^{ext} - k_2\left(C_{mX}^{ext} - \frac{C_{oX}^{ext}}{K_{e1}}\right) \tag{4.28}$$

$$r_{Bz}^{ext} = k_1\, C_T^{ext} \tag{4.29}$$

As mentioned above, the paring reaction only occurs in the spatially confined channels and does not proceed on the external surface. The formation of hydrocarbons is not required to solve this problem, as the system is dilute and the flowrates are assumed to be constant.

Furthermore, at these high temperatures (450°C) adsorption onto the surface has been assumed to be linear. The adsorption equilibrium constants are incorporated into the first order rate constant as the model is linear.

4.6.3 The effect of CVD on the reaction rate of external reactions

From the 1,3,5-TiPB-cracking and external TDP data it could be seen that the activity of the external surface decreased exponentially (see Section 4.3.1). The decrease in first order rate constant on the external surface may then be represented by:

$$k = k_\circ \alpha^n \tag{4.30}$$

where $k_\circ$ is the first order rate constant of the unmodified catalyst, n is the amount of deposited silica, k is the first order rate constant at n amount of deposited silica and α is the fractional decrease in rate constant with increasing silica deposition.

This concept is then extended to all first order reaction rate constants on the external surface, and thus the TDP and isomerisation rate constant will also decrease according to the "α^n" law.

The internal reaction rates are not affected by the CVD process as the TEOS molecule deposits exclusively on the external surface. Thus, all first order rate constants in the catalyst interior remain unchanged with increasing the amount of deposited silica.

4.6.4 The effect of CVD on diffusion properties

It is assumed that the CVD using TEOS does not alter the internal properties of the zeolite and thus, the internal diffusion coefficient remains unchanged (see Section 4.4). However, statistical simulations by Theodorou and Wei (1983) have shown that a reduction in relative effective diffusion coefficient

(D/D_o) due to pore blockage can be approximated by a polynomial function $F(x_b)$ which depends on the extent of the pore blockage, x_b (see Section 4.4.3).

It is thus possible to represent pore blockage effects by an effective diffusion coefficient which is assumed to apply throughout the whole pellet.

The variation of x_b using the silica loading can be viewed in two ways, (i) x_b increases linearly with the amount of deposited silica , i.e. $x_b = n/n_o$, and (ii) x_b varies with the α law, i.e. $x_b = 1 - \alpha^n$. These approaches have already been outlined in Section 4.4.3.

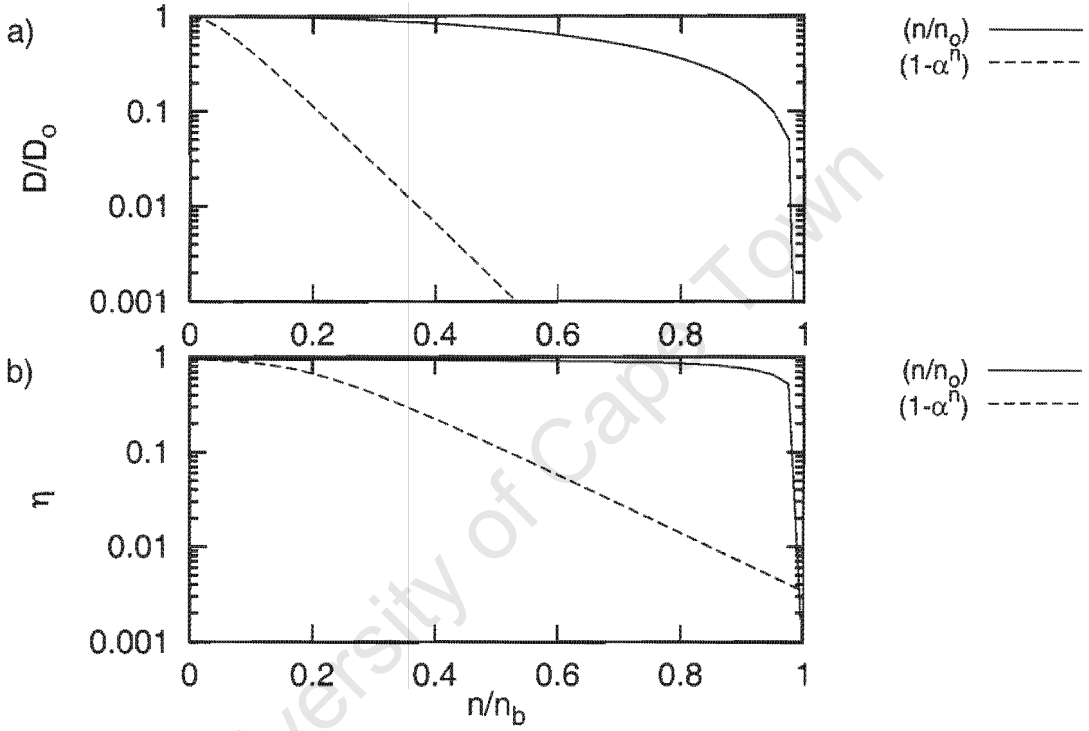

Figure 4.13: Comparison of the effect of linear and exponential increase of pore blocking $(\alpha=0.7,\ n_b=40)$.

Figure 4.13 compares the two approaches. The diffusion coefficient decreases more rapidly when using the α model after the same amount of silica is deposited. The effectiveness factor variation with the silica loading shows that when pore blockage is assumed to be linear with deposition, very high amounts of silica have to be deposited before the effectiveness factor becomes low enough for significant changes in selectivity to be observed, based on typical values of α and n_b.

Assuming the α model, (i) low effectiveness factors are reached at low silica loadings and (ii) the effectiveness factor decreases exponentially rather than quadratically. This indicates that exponential decay of the α model dominates over the quadratic decrease in diffusion and effectiveness factor. The changes according to the α model are supported by the experimental data. This also indicates that the increase in pore blockage, due to silica deposition, follows an exponential trend. The effect of CVD on diffusion, and consequently on reaction and selectivity, is then given by the following expressions:

$$x_b = 1 - \alpha^n \tag{4.31}$$

$$\frac{D}{D_\circ} = 1 - x_b^2 \tag{4.32}$$

4.6.5 Reactor and catalyst mass balance

The mass balances are based on the assumption of ideal plug flow and steady state conditions. The catalyst pellets are uniform spheres and homogeneously distributed in the reactor bed. Fickian diffusion takes place inside the catalyst particle. The adsorption of all species is assumed to be in the Henry region and thus can be incorporated into the rate constant. All diffusion coefficients are constant and independent of concentration, i.e. there is no interaction between different species. The reactor is assumed to operate isothermally and concentrations are low enough to assume constant flowrate.

For each species i within the catalyst crystal, the following mass balance applies at any given point:

$$\frac{1}{y^2}\frac{\partial}{\partial y}\left(y^2\frac{\partial C_i^{int}}{\partial y}\right) + \frac{r_i^{int} R^2}{D_i} = 0 \tag{4.33}$$

where r_i^{int} is the internal reaction rate of the species i, $y = r/R$ is the dimensionless spacial coordinate, C_i^{int} is the concentration of the species i in the catalyst, R is the radius of the catalyst particle and D_i is the diffusion coefficient of the species i. It has to be mentioned that the concentration C_i^{int} is a function of the spacial coordinates y and z. The residence time in the reactor, τ, is obtained from the crosssectional area, A, and the length, z, of the reactor and the volumetric flow rate, F, i.e. $\tau = Az/F$. Thus, τ incorporates the reactor dimension z and $C_i^{int} = C_i^{int}(y, \tau)$.

For each species i in the reactor bed the following mass balance applies:

$$\frac{\partial C_i^{ext}}{\partial \tau} = -\frac{3(1-\epsilon)}{\epsilon}\frac{D_i}{R^2}\frac{\partial C_i^{ext}}{\partial y}\bigg|_{y=1} + r_i^{ext}\frac{1-\epsilon}{\epsilon} \tag{4.34}$$

where C_i^{ext} is the concentration of the species i within the reactor bed, ϵ denotes the bed voidage and r_i^{ext} is the external reaction rate for the species i.

The concentration C_i^{ext} thus is a function of the residence time τ only, i.e. $C_i^{ext}(\tau)$.

4.6.6 Boundary conditions

The symmetry of the spherical particle is defined in the following boundary condition:

$$\left.\frac{\partial C_i^{int}}{\partial y}\right|_{y=0} = 0 \tag{4.35}$$

The concentration boundary condition relates the surface concentration of the catalyst to the gas phase concentration in the reactor, neglecting film resistance:

$$C_i^{int}(y=1,\tau) = C_i^{ext}(\tau) \tag{4.36}$$

The boundary conditions defining the concentrations of reactants and products at the reactor inlet are:

(i) for reactants:

$$C_i^{ext}(y=1,\tau=0) = 1, \qquad C_i^{int}(y,\tau=0) = 0 \tag{4.37}$$

(ii) and for products:

$$C_i^{ext}(y=1,\tau=0) = 0, \qquad C_i^{int}(y,\tau=0) = 0 \tag{4.38}$$

4.6.7 Application of collocation

Equation 4.36 allows the combining of the reactor and catalyst mass balances to yield an differential-algebraic system of equations (DAE) when collocation is applied to the catalyst equations. Writing the catalyst equation in collocation form,

$$\sum_{j=1}^{nx} B_{i,j} Y_{mj} + r_{k,i}^{int} \frac{R^2}{D_k} = 0, \qquad i = 1 \ldots n_c \tag{4.39}$$

yields nc equations for each species k,

where:

k = number of species
i = internal collocation point counter
j = internal collocation point counter
mj = $nx(k-1)+j$, offset counter for linear arrays, offset for k
nx = $nc+1$, number of collocation points including the boundary at $y=1$
nc = number of internal collocation points
$B_{i,j}$ = collocation matrix of constants
Y_{mj} = concentration in the pellet at position mj [Y(i) = $C_i^{int}/C_i^{int}(y=1,\tau=0)$]
$r_{k,i}^{int}$ = internal reaction rate of species k at position i in the catalyst

The equation for the reactor bed, incorporating the boundary condition in Equation 4.36, yields:

$$\frac{dY_{mi}}{d\tau} = \frac{3(1-\epsilon)}{\epsilon}\frac{D_k}{R^2}\sum_{j=1}^{nx} A_{nx,j}\, Y_{mj} + \frac{(1-\epsilon)}{\epsilon}\, r_{k,i}^{ext} \tag{4.40}$$

with $i =$ nx (condition at the catalyst boundary $y = 1$)
$mj =$ $nx(k-1)+i$
$A_{nx,j} =$ collocation matrix of constants
$r_{k,i}^{ext} =$ reaction rate on the external surface at position k, i

There are nc algebraic equations (4.39) and one differential equation (4.40) for each species k. There are 5 species in this reaction system and hence, this gives $5 \times nx$ equations for the complete system. These equations , a total of 155, are solved using the DDASAC DAE integrator (Stewart and Associates Engineering Software, Inc.; Software for Modeling and Parameter Estimation) using 30 internal collocation points (nc=30) which adequately represents the concentration profiles of all species, even at small effectiveness factor within the crystal.

The simulation and fitting procedure are outlined in Figure 4.14.

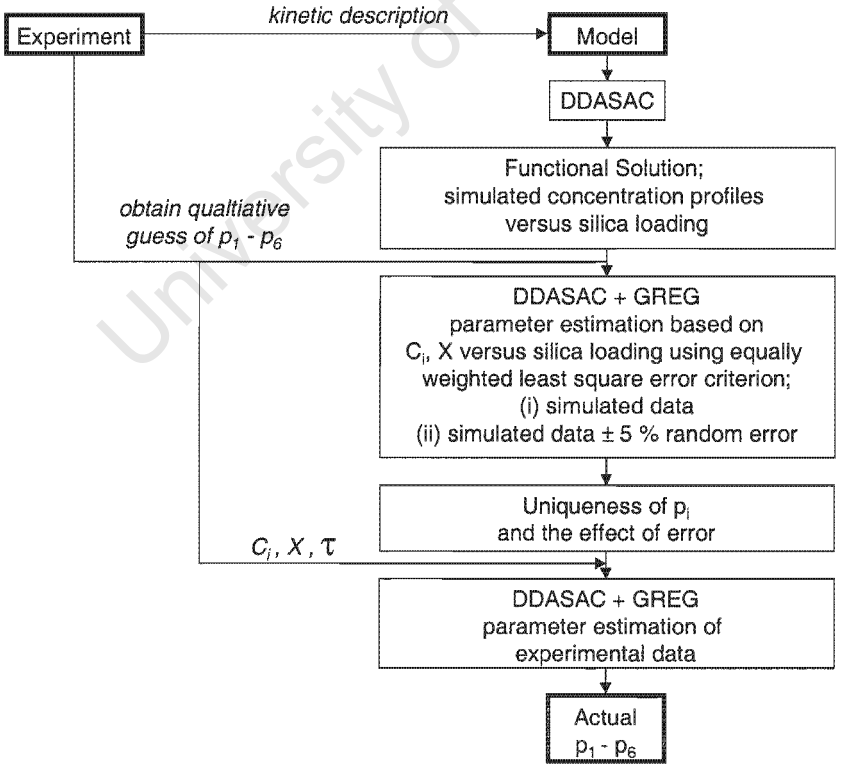

Figure 4.14: Flow chart of simulation and fitting procedure to obtain simulation parameters p_1 - p_6.

4.6.8 Typical simulation results

As mentioned in Section 4.4 the analysis of reaction data suffers from the pitfall that diffusion coefficients at high temperatures, i.e. above 250°C are not available. The relative ratio of diffusivities for the xylene isomers is believed to be in the range of D_{pX}/D_{mX}=1000, D_{oX}/D_{mX}=10 and D_{pX}=D_{Tol}=D_{Bz} (Chen et al., 1994). The activation energy for diffusion has been reported to be approximately 30 kJ/mol but can be as high as 60 kJ/mol for aromatic compounds (Chen et al., 1994). Niessen and Karge (1993) reported the diffusivity coefficient of p-xylene at 140°C to be approximately 1×10^{-9} cm^2/s. Using the above mentioned activation energies, diffusivity coefficients of 4×10^{-8} to 1.6×10^{-6} cm^2/s, respectively, can be extrapolated for p-xylene at 450°C.

Assuming a uniform diameter for spherical crystals of 0.2 μm, the diffusion time constant for p-xylene, D/R^2, is calculated as 100 s^{-1} and 4000 s^{-1}, using the activation energy of 30 and 60 kJ/mol, respectively. This is the basis of an order of magnitude estimate of the diffusion coefficients.

Furthermore, it must be expected that the activation energy for the isomers is different, hence the ratio of the diffusivities given above will not necessarily be true at the reaction temperature. For the purpose of the calculations and the fitting of the reaction data, these ratios of the diffusion time constants will be assumed for D_{oX}:D_{mX}:D_{pX}=1:1:1000.

Benzene/xylene ratio

As discussed in Section 4.5.2, xylene "dealkylation" via the paring mechanism is observed with increasing CVD modification and low toluene conversions. The increased benzene/xylene ratio could also be explained with impurities in the toluene feed. Assuming a contamination of 0.5 % in the toluene feed and additional benzene originating only from TDP, then the benzene/xylene ratio would increase with decreasing toluene conversion. The benzene/xylene ratio of 1.5 corresponds to a toluene conversion of 2 %. Such low conversions would have only been observed after considerable diffusional constraints had occurred due to CVD. The analytical grade feed had a purity of more than 99.8 % toluene and a benzene content of less than 0.1 %. Thus, an affected benzene/xylene ratio because of trace contamination appears unlikely, and the contribution of the paring reaction inside the crystal requires extended consideration.

Results

For the simulation of the effects of silica on TDP and the fitting of the experimental results, two cases were distinguished:(i) paring reaction in the crystal interior can be neglected and hence the benzene/xylene ratio is 1. (ii) The paring reaction takes place and produces benzene and light hydrocarbons and thus the benzene/xylene ratio is >1.

Table 4.2: Base and estimation parameters.

base parameters				
τ	s	10.0		residence time in reactor
k_1	s^{-1}	4.3×10^{-3}		internal: rate constant for TDP
k_2	s^{-1}	4.3		internal: rate constant for xylene isomerisation
k_3	s^{-1}	4.3×10^{-4}		internal: rate constant for paring reaction
k_4	s^{-1}	4.3×10^{-3}		external: rate constant for TDP
k_5	s^{-1}	4.3		external: rate constant for xylene isomerisation
K_{e1}		2.538		equilibrium constant pX⇌mX
K_{e2}		0.393		equilibrium constant mX⇌oX
α		0.70		inertisation constant
$(D/R^2)_{Tol}$	s^{-1}	100		diffusion time constant for toluene
$(D/R^2)_{pX}$	s^{-1}	100		diffusion time constant for p-xylene
$(D/R^2)_{mX}$	s^{-1}	0.1		diffusion time constant for m-xylene
$(D/R^2)_{oX}$	s^{-1}	0.1		diffusion time constant for o-xylene
$(D/R^2)_{Bz}$	s^{-1}	100		diffusion time constant for benzene
ϵ		0.4		reactor bed voidage
(Si_b)	(Si/nm^2)	(40)		(amount of silica for total blockage; as reference)
parameters for estimation				
p_1			$= k_1$	(rate constant for TDP)
p_2			$= k_2/k_1$	(ratio of the rate constant for xylene isomerisation to rate constant for TDP)
p_3			$= \alpha$	(inertisation coefficient)
p_4			$= D/R^2$	(diffusion time constant of toluene)
p_5			$= k_{ext}/k_{int}$ $= k_4/k_1$ $= k_5/k_2$	(ratio of the rate constants for external/internal surface activity)
p_6			$= k_3/k_1$	(ratio of the rate constant for paring reaction to rate constant for TDP)

Figure 4.15 demonstrates the results of a simulation, when the paring reaction can be neglected. The selectivity of the p-xylene increases as expected due to the increased effective diffusion resistance. The o- to m-xylene ratio decreases even though the diffusivity of both isomers are equal. A constant ratio with increased diffusion resistance may only be expected for parallel reactions. This is clearly not the case here, and the observed effect is a consequence of the interaction of both the series reaction and the reaction on the external surface.

The yield of p-xylene over the modified catalyst exceeds that obtained on the unmodified catalyst by a factor of 2.6. This shows that the production rate of p-xylene can be improved dramatically by introducing diffusion limitations, contrary to what might be expected from mass transfer limited reactions.

The maximum possible ratio of the p-xylene yields would be approximately 4 when the para-selectivity could be improved to 100 % at no loss of activity. However, because of the deactivation of the catalyst, mainly due to the deactivation of the external surface (about 30 %), this ratio cannot be achieved with CVD.

The increase in yield, as compared to the unmodified catalyst, is a consequence of the o-xylene and m-xylene reactants and reactions involving these species becoming diffusion limited within the catalyst, while those reactions involving toluene, benzene and p-xylene remain unaffected. In other words, the effectiveness factor of o- and m-xylene rapidly becomes less than 1 while those of toluene, benzene and p-xylene remain at 1. Therefore, the reactions of toluene to produce benzene and p-xylene are not diffusion limited and proceed unhindered, hence the increased yield and production rate of p-xylene.

When the paring reaction is included (see Figure 4.16), the same conceptual trend is observed. However, the benzene/xylene ratio increases rapidly when CVD starts causing severe diffusion limitations on the product molecules. The paring reaction is a secondary step, in which xylenes disproportionate to form toluene and trimethylbenzenes and polymethylbenzenes. Theses highly substituted aromatics undergo paring reactions to yield benzene and light hydrocarbons (HC's). As the diffusion limitation of the xylenes increase, the concentrations of these species increase within the pore system, promoting disproportionation reactions to higher substituted aromatics. In this way there is a sharp increase in the benzene/xylene molar ratio with increased silica deposition, at the point where the xylenes experience diffusion limitations.

Theses results qualitatively describe the observed experiments.

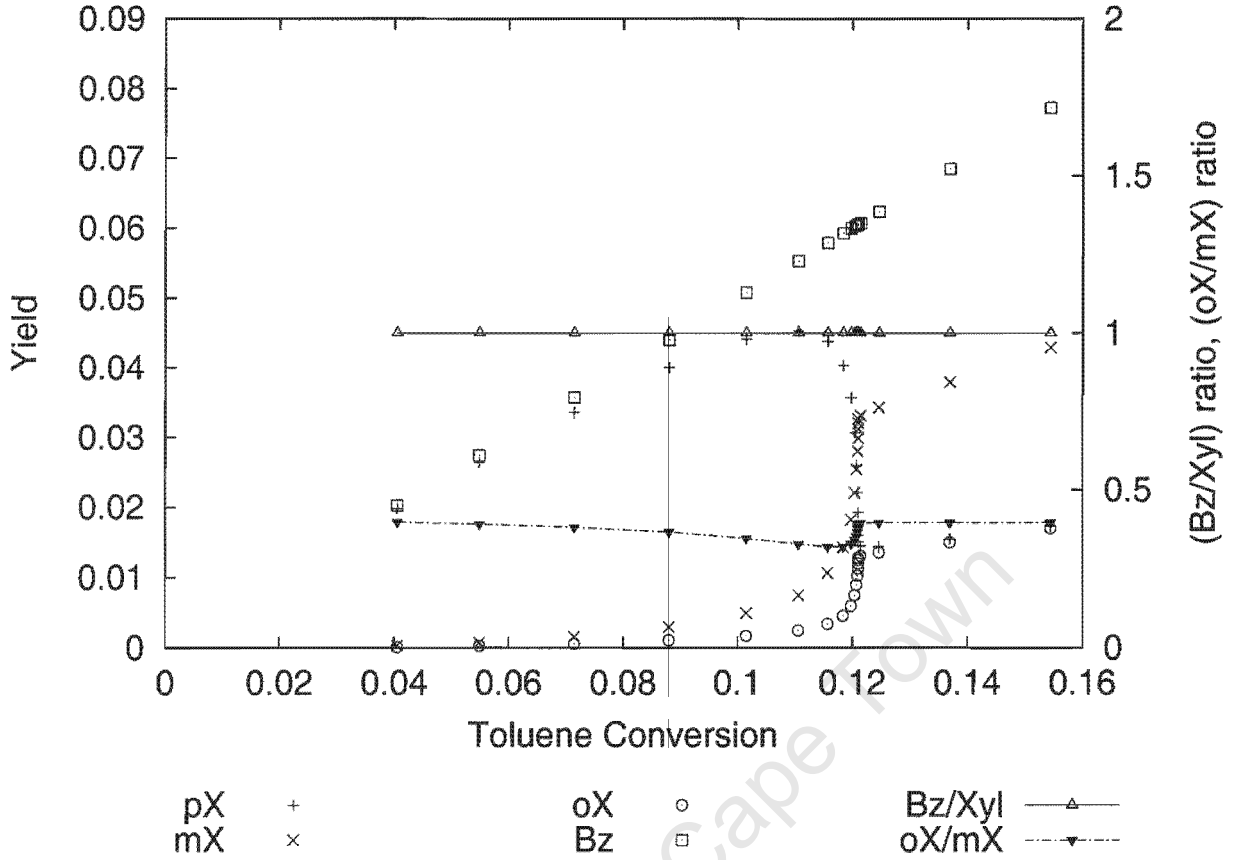

Figure 4.15: Typical simulation: selectivity versus conversion during TDP with changing amount of deposited silica without paring reaction.

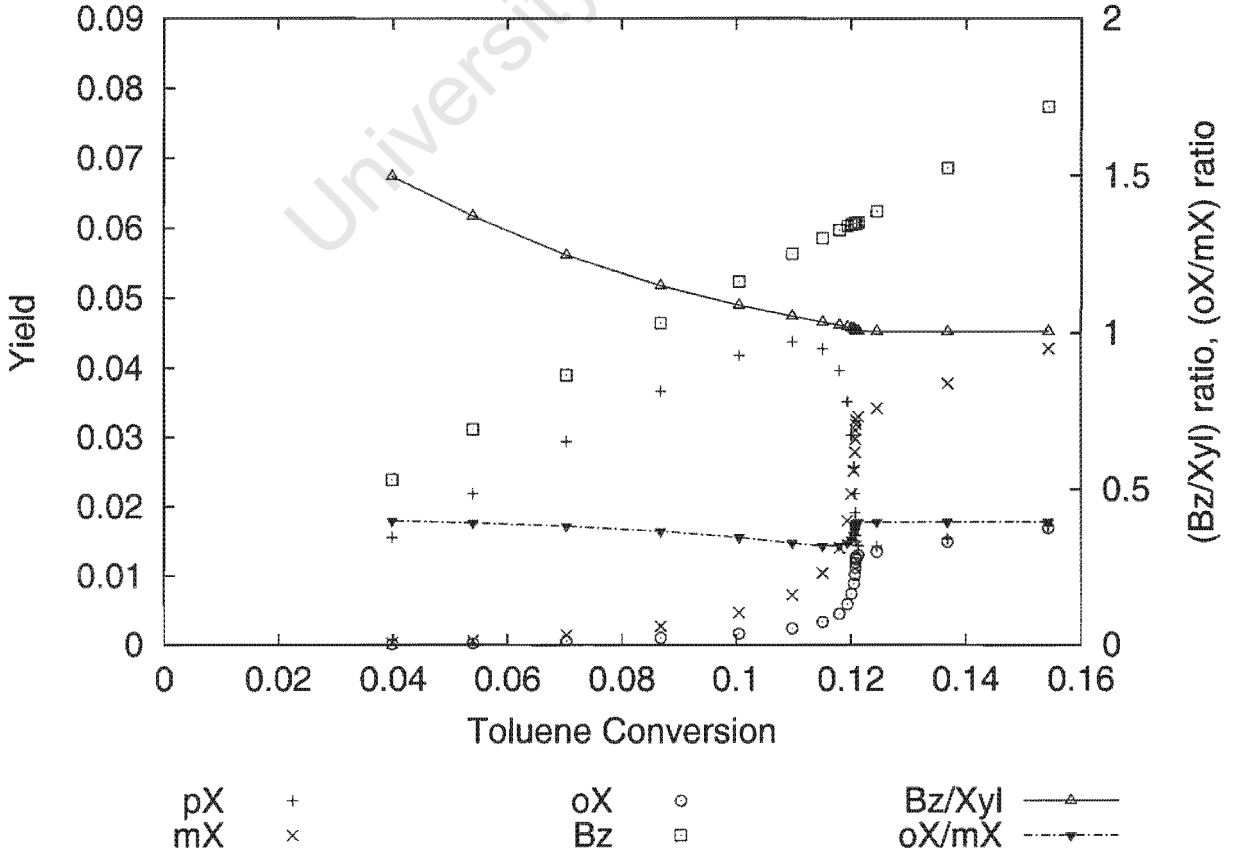

Figure 4.16: Typical simulation: selectivity versus conversion during TDP with changing amount of deposited silica including the paring reaction of xylene isomers.

4.6.9 Typical fitting of model data using GREG

The fitting procedure of simulated data

The model data $X_{toluene}$, $C_{toluene}$, C_{pX}, C_{mX}, C_{oX} and C_{Bz} is generated as a function of silica loading. This is the same form the experimental data will be analysed. The fitting procedure was carried out using the GREGPAK general regression software (Stewart and Associates Engineering Software, Inc.; Software for Modelling and Parameter Estimation). 6 responses are fitted, using a relative least square error criterion between the predicted and experimental data. All data is weighted equally. No account is taken of the fact that the lower concentration data might have a larger relative experimental error and thus have to be weighted less. The parameters (p_i) to be estimated are given by p_1 to p_6 in Table 4.2, where p_6 is only used when the paring reaction is significant. Initial model parameters obtained by qualitatively fitting the model to the experimental data, are used as starting values in each case. These values are given in Table 4.2. The parameter estimates are given with a standard deviation error, $\pm\sigma$, which is to be expected when fitting to the model.

When applying the fitting procedure to both the simulated data (i) without and (ii) with paring reaction, the model prediction was exceptionally good ($\sum error^2 \approx 1 \times 10^{-8}$). More importantly, all the model parameters are uniquely determined, as shown by all the variances (σ) being less than 0.1 % for all parameters. This means that each parameter used in the model fit is independent and has a unique measurable effect on the model response.

The resulting curves of typical model fit are shown in Figures 4.17 and 4.18, neglecting and considering the paring reaction, respectively. The determined parameters are listed in Table 4.3.

The fitting procedure of simulated data with random error

As the uniqueness of the parameter determination was confirmed, the reliability of the fitting procedure was tested when applied to noisy experimental data. ± 5 % random error was introduced to the modelled data and the fitting routine applied. Figures 4.19 and 4.20 show the match of the fitted curves to the simulated experimental data. The results are summarised in Table 4.3.

Examining the model fit, it is clear that the effect of random error has a strong influence on the position at which the p-xylene concentration curve rises. As the "experimental error" increases the accuracy and hence also the uniqueness in determining p_2, p_4 and p_6 decreases significantly, as shown by the large σ of up to 100 %. This is in part to the least square error criterion which compromises between fitting the data at constant conversion (steep rise of the p-xylene curve) with data over the other regions of regular conversion-concentration behavior. Furthermore, part of the loss of accuracy is due to the few data points which were generated, particularly in the region of the steep rise in p-xylene yield. If more model data were taken, then smaller errors would be obtained.

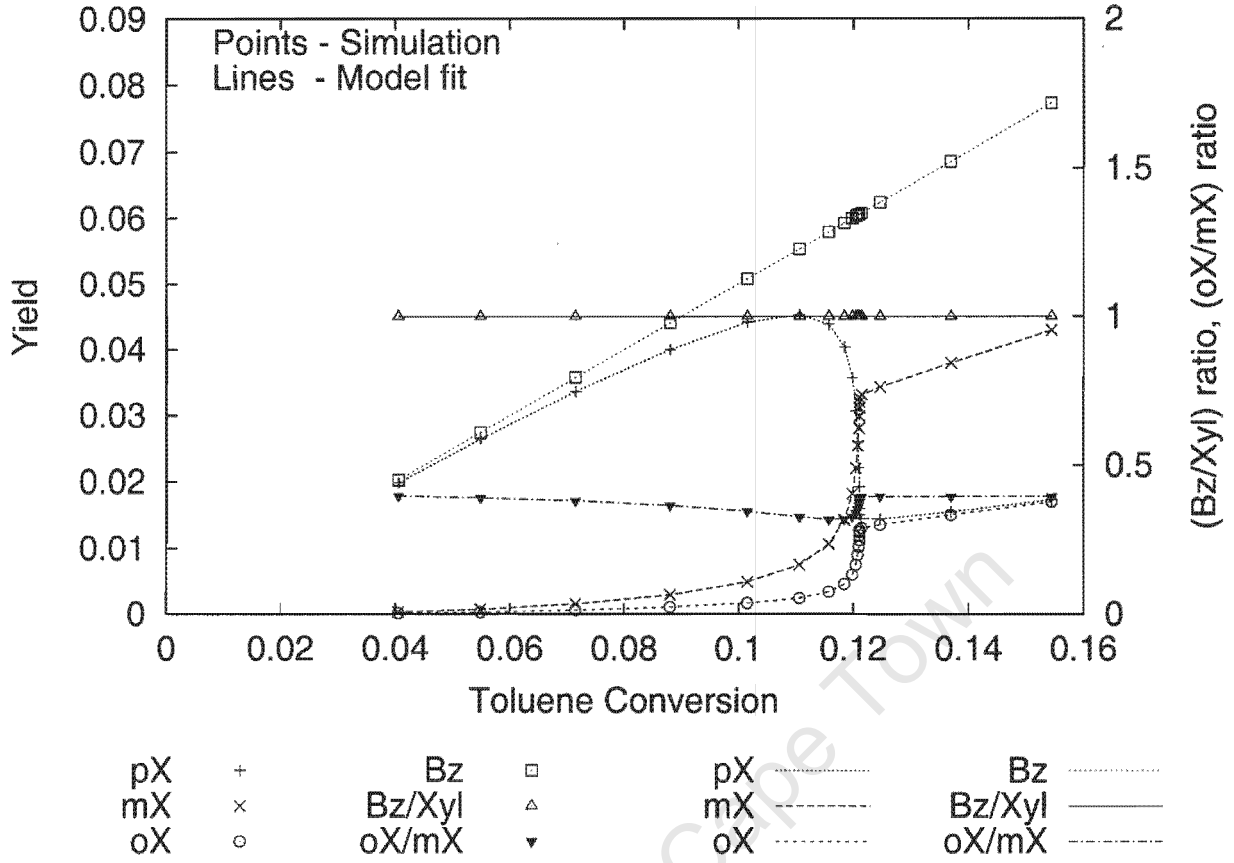

Figure 4.17: Typical fit to simulated experiments without paring reaction: uniqueness of fitted parameters.

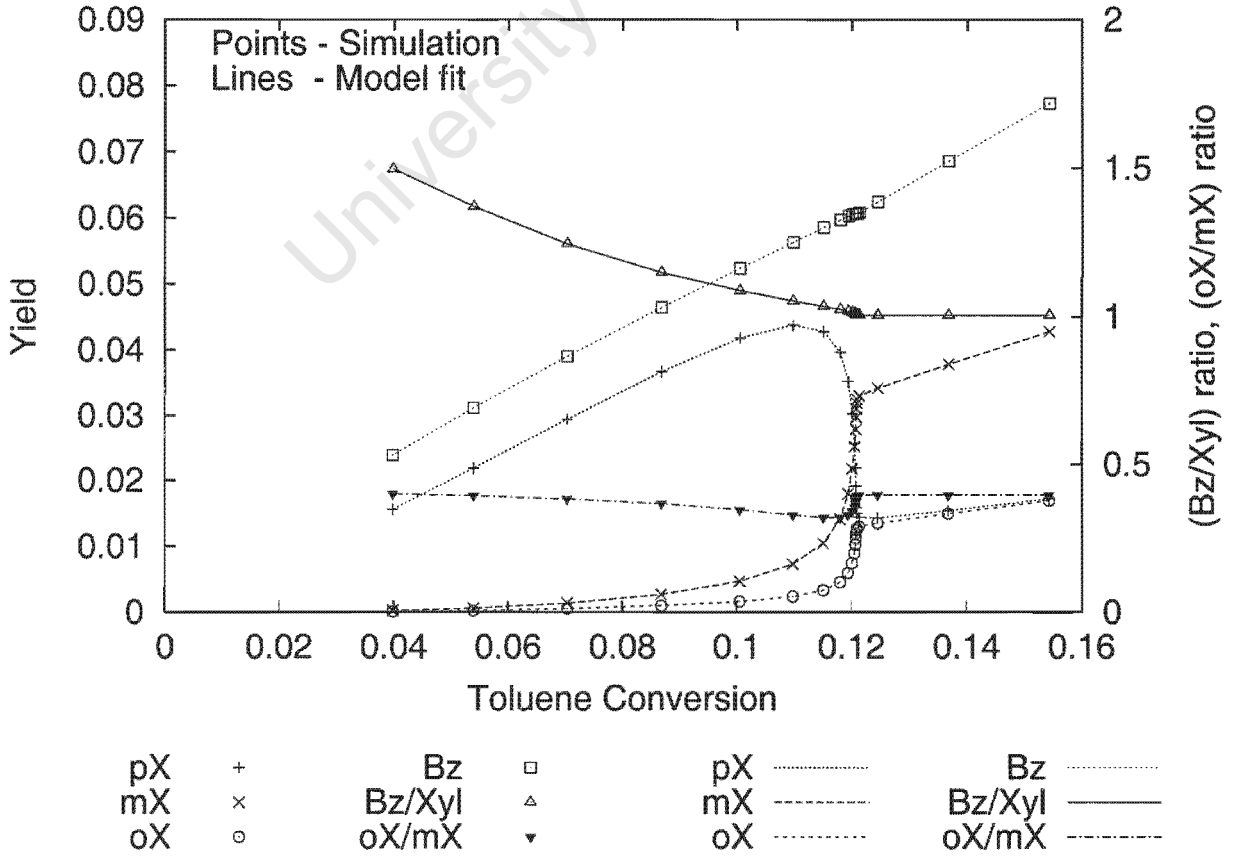

Figure 4.18: Typical fit to simulated experiments with paring reaction: uniqueness of fitted parameters.

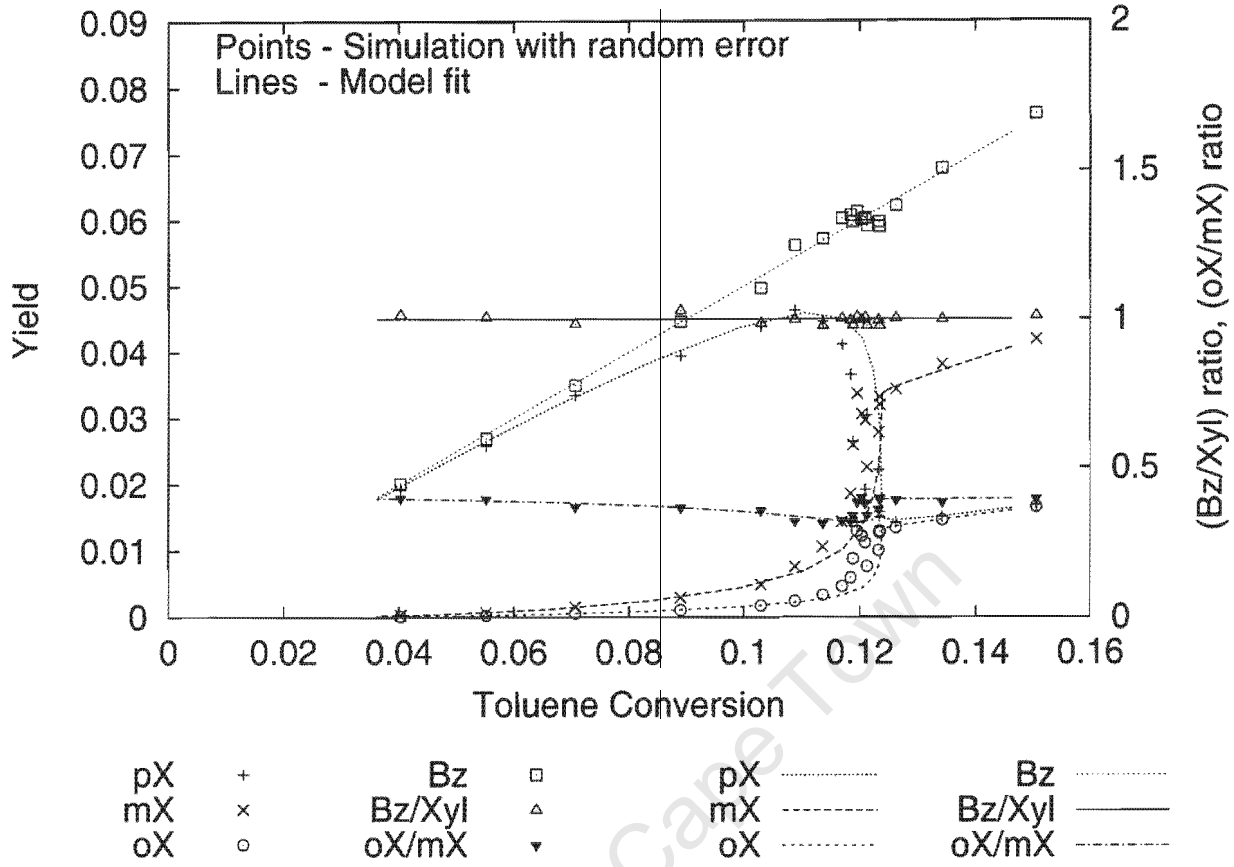

Figure 4.19: Typical fit to simulated experiments with 5 % random error without paring reaction: quality of fitting.

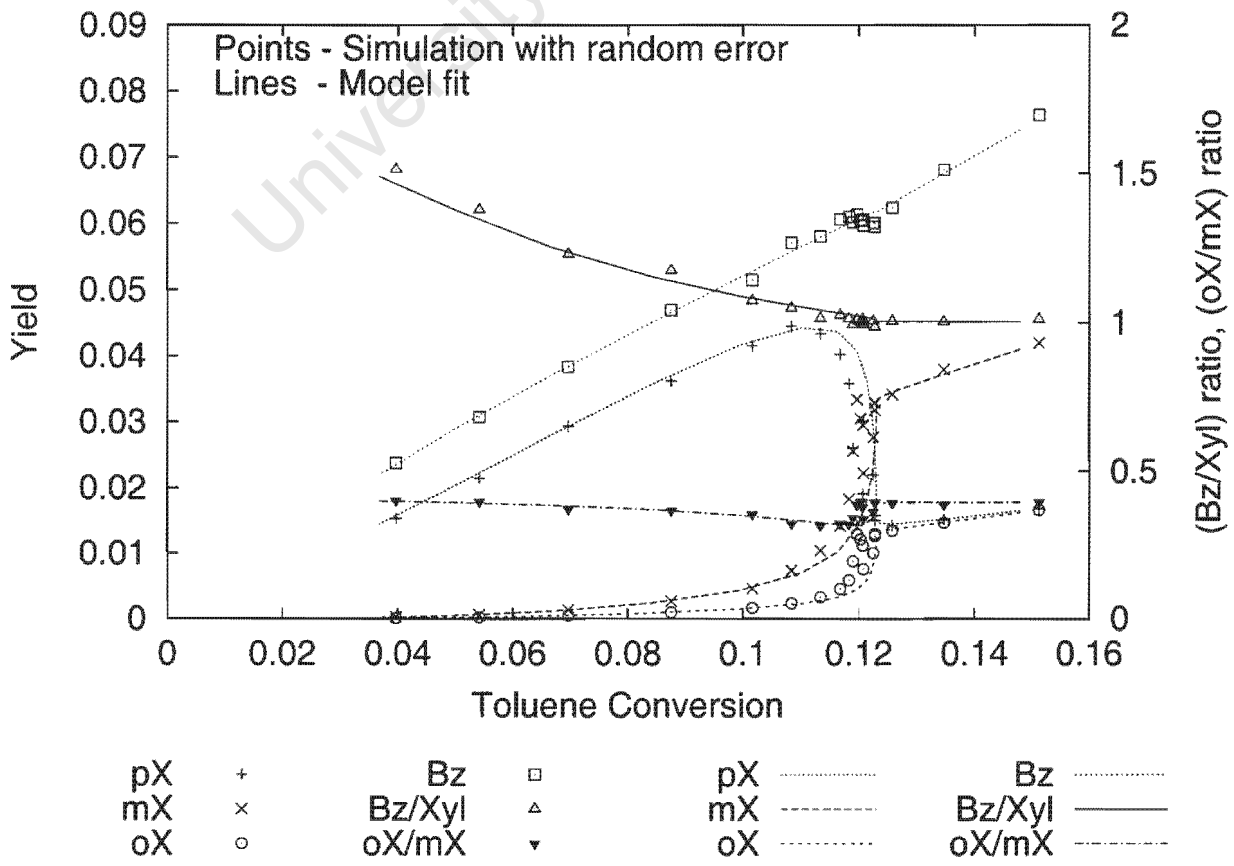

Figure 4.20: Typical fit to simulated experiments with 5 % random error with paring reaction: quality of fitting.

Table 4.3: Estimated model parameter from simulation data (values given as $p_i \pm \sigma$).

simulation type	p_1 [a] (10^{-3})	p_2 [b] (10^3)	p_3 [c]	p_4 [d]	p_5 [e]	p_6 [f]	$\sum(\text{error})^2$ (10^{-3})
τ=10, 20 pts [g], no paring reaction, all Bz/Xyl=1	4.30 ± 0.00026	1.00 ± 0.0022	0.70 ± 0.000059	99.9 ± 0.31	0.30 ± 0.00022	not used	0.000036
τ=10, 20 pts, no paring reaction, all Bz/Xyl=1, ±5% random error	4.41 ± 0.09	1.07 ± 0.93	0.696 ± 0.033	94.0 ± 157	0.196 ± 0.069	not used	4
τ=10, 20 pts, initial Bz/Xyl=1	4.30 ± 0.00024	1.00 ± 0.0017	0.70 ± 0.000013	100 ± 0.05	0.30 ± 0.00021	0.1 ± 0.00037	0.000028
τ=10, 20 pts, initial Bz/Xyl=1, ±5% random error	4.38 ± 0.072	4.55 ± 3.34	0.696 ± 0.032	102 ± 162	0.218 ± 0.056	0.089 ± 0.106	2.5

[a] k_1: reaction rate constant for internal TDP.
[b] $k_2/k1$: ratio of reaction rate constants for isomerisation to internal TDP.
[c] α: inertisation constant.
[d] $(D/R^2)_T$: diffusion time constant for toluene.
[e] k_{ext}/k_{int}: ratio of external to internal activity.
[f] k_3/k_1: ratio of reaction rate constants for paring reaction to internal TDP.
[g] Number of experimental points used for fitting procedure.

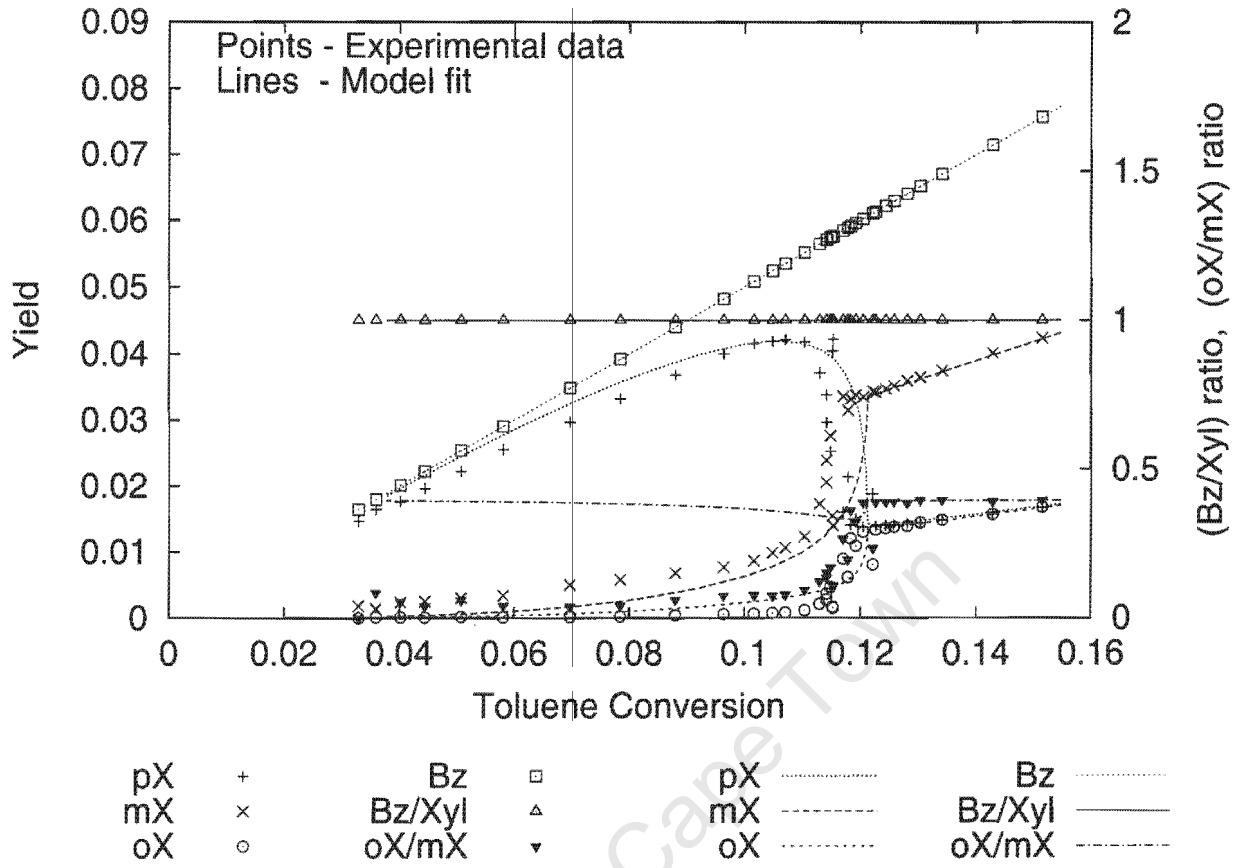

Figure 4.21: Typical fit to actual experiments without paring reaction.

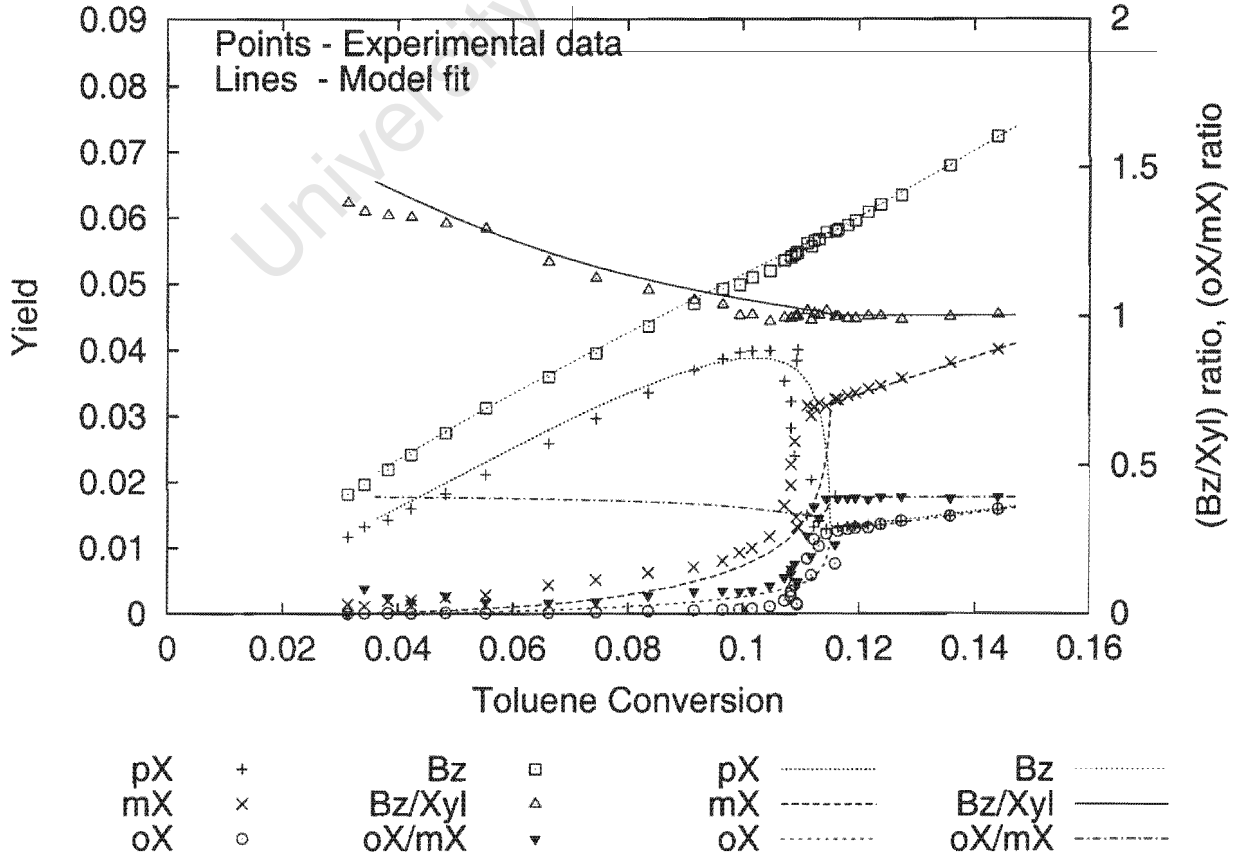

Figure 4.22: Typical fit to actual experiments with paring reaction.

Table 4.4: Estimated model parameter from experimental data (all parameters as in Table 4.3).

	p_1	p_2	p_3	p_4	p_5	p_6	$\sum(\text{error})^2$
simulation type	10^{-3}	10^3					10^{-3}
τ=10, 33 pts[a], no paring reaction, all Bz/Xyl=1	4.31 ± 0.04	2.46 ± 0.62	0.730 ± 0.003	108 ± 18	0.30 ± 0.03	not used	1.75
τ=10, 33 pts, initial Bz/Xyl=1	4.08 ± 0.03	2.51 ± 0.65	0.730 ± 0.003	107 ± 18	0.301 ± 0.034	0.085 0.047	1.59

[a]All 33 data points from the experiment were used for the fitting procedure.

The fitting procedure of actual experimental data

The above described fitting procedure was invoked to analyse the 100°C-pellet data.

Based on the experimental data, the equilibrium constants for the isomerisation of pX⇌mX, K_{e1}, and mX⇌oX, K_{e2}, were determined to be 2.538 and 0.393, respectively, assuming that the reactions over the unmodified catalyst are in thermodynamic equilibrium.

The residence time in the reactor, τ, was taken to be 10 s.

With the above stated assumptions for the diffusivities and the particle diameter, the diffusion time constants for xylene isomers are: $(D/R^2)_{Tol} = (D/R^2)_{pX} = (D/R^2)_{Bz} = 0.001\times(D/R^2)_{mX} = 0.001\times(D/R^2)_{oX}$.

With this set of given model parameters the fitting procedure was applied to the actual experimental data of the 100°C-pellet series, using 30 collocation points.

Two cases were investigated: (i) fitting to the experimental data while neglecting the paring reaction (Figure 4.21) and (ii) including the paring reaction (Figure 4.22).

In order to apply the fitting procedure to the experimental data while neglecting the paring reaction, the data has been adjusted. The combined yields of the xylene isomers were normalised to account for 50 % of the measured toluene conversion. The yield of xylenes was then assumed to be equal to the yield of benzene, hence the benzene/xylene ratio of 1 was obtained.

When paring reaction was considered and allowed to proceed inside the micro-pores, the data was adjusted such that the initial benzene/xylene ratio of 1 was obtained, to be consistent with negligible paring reaction inside the unmodified catalyst. It was not possible to simulate low benzene/xylene ratios when starting at a initial ratio of 1.1.

Quantitative comparison of the experimental data with the current model

Comparing the experimental data to the predictions by the model reveals that the general trends of toluene conversion and shape selective performance of the catalyst are well described by the

Table 4.5: Estimated reaction rate constants.

		experimental data			
		without paring reaction		with paring reaction	
k_1 (10^{-3})	s^{-1}	12.1	(1 ± 0.93 %)	11.4	(1 ± 0.81 %)
k_2	s^{-1}	29.7	(1 ± 26.1 %)	28.7	(1 ± 26.7 %)
k_3 (10^{-3})	s^{-1}	-		0.96	(1 ± 56.4 %)
k_4 (10^{-3})	s^{-1}	3.62	(1 ± 10.9 %)	3.44	(1 ± 12.1 %)
k_5	s^{-1}	8.91	(1 ± 36.1 %)	8.63	(1 ± 38.0 %)
D/R^2	s^{-1}	302	(1 ± 16.7 %)	300	(1 ± 16.8 %)
α	Si/nm^2	0.73	(1 ± 0.44 %)	0.73	(1 ± 0.44 %)

simulations. The formation of excessive benzene is well predicted, but the generation via the paring mechanism is subject of speculation. The model parameters are all uniquely determined, but the largest errors still occur by fitting the parameters p_2, p_4 and p_6 as observed previously.

Provided that the Dammköhler number, $Da = k\tau$, and Thiele modulus, $\Phi = \sqrt{R^2 k/D}$, are constant, the parameters p_1 to p_6 of the linear model can be scaled to fit the true experimental conditions, viz. $\tau_{exp} = 3.6s$. With the estimated parameters it is possible to quantify the values of the first order rate constants k_1 to k_6, D/R^2 and α which are listed in Table 4.5.

The value for the diffusion time constant for toluene and also p-xylene, $D/R^2 \approx 300s^{-1}$, is within the expected range of 100 to 4000 s^{-1}.

The ratio of the rate constants of external to internal reactions, p_5, is approximately 0.3, i.e. 30 % of the activity of the unmodified sample is located on the external surface. This value seems to be too small when considering the particle size and surface area measurements of the crystals used in this study (Section 4.2.2). Based on the fitting of random error data, this value is underestimated by approximately 30 %, so a more reasonable value would be 0.4.

The reaction rate constant of the paring reaction is approximately 10 % of the rate constant for the disproportionation of toluene inside the crystal. Over the unmodified crystals this reaction does not play a significant role due to low conversions. At high silica loadings and thus increased diffusional constraints however, xylene "dealkylation" accounts for the production of excess amounts of benzene.

The accuracy of the fit strongly depends on the number of sample points and could be improved with increased number of experimental data. Furthermore, the intrinsic error of the experimental data affects the precision of the fitting procedure. The experimental error increases with decreasing conversion levels, due to inferior separation of the compounds and integration of the peak areas during chromatographic analysis. This aggravates the fitting procedure, in particular when examining the benzene/xylene and o-xylene/m-xylene ratios which could have larger errors.

The changes of the benzene/xylene ratio in the experimental data show a good fit. In contrast, the o-xylene/m-xylene ratio cannot be satisfactorily fitted. This could either arise from wrong model assumptions or inadequately chosen diffusion coefficients for the respective xylene isomers. Furthermore, the simplifications in the assumed reaction pathways could detrimentally affect the fitting

procedure and more reaction steps should be considered. Detailed knowledge about the formation of the trimethylbenzene and other secondary reactions which might occur inside the micro-pores and the subsequent paring reaction of the polyalkylated species is required. The problem arises that these secondary steps predict the formation of TMB and poly-substituted aromatics which have not been analysed in this study and thus, cannot serve to support the parameter estimation. Experimental error, as laid out before, could account for unreliable data particularly at low conversion levels and reduced o- and m-xylene fractions.

However, the model adequately describes the experimental trends and the fitting procedure allows determination of the kinetic parameters of TDP over ZSM-5 crystals which all lie within the expected orders of magnitude.

Chapter 5

Conclusions

In this present study the cyclic chemical vapour deposition (CVD) was employed to in-situ modify the external surface of ZSM-5, using tetraethoxysilane (TEOS) as silica precursor.

- The catalytic properties of the unmodified and modified ZSM-5 were successfully studied with two test reactions: (i) cracking of 1,3,5-triisopropylbenzene (1,3,5-TiPB) to probe the external surface activity and (ii) disproportionation of toluene (TDP) to monitor internal activity and changes in the shape selective properties.
- The reaction mechanism of TEOS on ZSM-5 powder was shown to occur analogous to the mechanism of TMOS on zeolites, as proposed by (Niwa et al., 1988).
- At low temperatures, between 50 and 200°C, the dissociative chemisorption of TEOS on the surface becomes product inhibited and the deposited amount of silica is limited to the reaction of one adsorbed TEOS monolayer.
- The external activity was removed, as seen by the cracking of 1,3,5-TiPB, when approximately one silica monolayer was deposited on the external surface.
- The interference of ethanol dehydration, occurring on the accessible acid sites of the catalyst during the deposition, results in increased pore blocking.
- Pore blocking is detrimental to the catalyst's activity for TDP and the effect increases with higher deposition temperatures.
- The modification procedure of ZSM-5 powder was successfully extended to ZSM-5 pellets.
- Treatment at low temperatures, viz. 100 to 150°C, and many cycles obtained a highly shape selective catalyst of 80% para-xylene selectivity, while maintaining high activity levels of above 10% conversion during toluene disproportionation at 450°C.

- Improvement in para-selectivity is attributed to the introduction of diffusional resistances, resulting in different effectiveness factors for the xylene isomers, rather than to the elimination of the external surface activity.
- A fixed bed reactor model was developed which adequately describes the results for the disproportionation of toluene on pellets and allows quantification of the kinetic parameters.

Bibliography

R. Argauer and G. Landolt. *U.S. Patent 3.702.886*, **(1972)**.

M. Aronson, R. Dorte and W. Farneth. *J. Catal.*, **98 (1986)** 434–443.

K. Asakura, M. Aoki and Y. Iwasawa. *Catal. Lett.*, **1 (1988)** 395–404.

M. Bartram, T. Michalske and J. J.W. Rogers. *J. Phys. Chem.*, **95 (1991)** 4453–4463.

H. Bergna, M. Keane, D. Ralston, G. Sonnichsen, L. Abrams and R. Shannon. *J. Catal.*, **115 (1989)** 148–158.

S. Bessel and D. Seddon. *J. Catal.*, **1987 (1987)** 270–275.

G. Bhaskar and D. Do. *Ind. Eng. Chem. Res.*, **29 (1990)** 355–361.

Y. Bhat, J. Das and A. Halgeri. *Appl. Catal. A: General*, **115 (1994)** 257–267.

Y. Bhat, J. Das and A. Halgeri. *J. Catal.*, **155 (1995a)** 154–157.

Y. Bhat, J. Das and A. Halgeri. *Appl. Catal. A: General*, **122 (1995b)** 161–168.

Y. Bhat, J. Das and A. Halgeri. *Appl. Catal. A: General*, **130 (1995c)** L1–L4.

Y. Bhat, J. Das and A. Halgeri. *Bull. Chem. Soc. Jpn.*, **69 (1996a)** 469–472.

Y. Bhat, J. Das and A. Halgeri. *Indian J. Chem. Tech.*, **3 (1996b)** 319–323.

Y. Bhat, J. Das, K. Rao and A. Halgeri. *J. Catal.*, **159 (1996c)** 368–374.

Y. Bhat and A. Halgeri. *Appl. Catal. A: General*, **101 (1993)** 95–104.

D. Bradley. *Chem. Rev.*, **89 (1989)** 1317–1322.

K. Chandawar, S. Kulkarni and P. Ratnasamy. *Appl. Catal.*, **4 (1982)** 287–295.

C. Chang and P. Rodewald. *U.S. Patent 4.498.814*, **(1996)**.

N. Chen, W. Garwood and F. Dwyer. *Shape Selective Catalysis in Industrial Applications*. Marcel Dekker, Inc., New York, 1996.

N. Chen, J. T.F. Degnan and C. Smith. *Molecular Transport and Reaction in Zeolites*. VCH, Weinheim/New York, 1994.

K. Chihara, K. Sugizaki, N.Kato, H. Miyajima and Y. Takeuchi. In M. LeVan, ed., *Fundamentals of Adsorptions*, pp. 179–185. Kluwer Academic Publishers, Boston, Massachusetts, 1996.

A. Choplin. *J. Mol. Catal.*, **86 (1994)** 501–512.

C. Chu and K. Ng. *A. I. Ch. E. J.*, **35 (1989)(1)** 148–158.

J. Chu, J. Breslin, N. Wang and M. Lin. *Mater. Lett.*, **12 (1991)** 179–184.

Y. Chu, C. Keweshan and E. Vansant. *Stud. Surf. Sci. Catal.*, **46 (1989)** 749–758.

Y. Chun, X. Chen, A. Yan and Q. Xu. *Stud. Surf. Sci. Catal., Elsevier, Amsterdam,*, **84 (1994)** 1035–1042.

Y. Chun, Q.-H. Xu, A.-Z. Yan and X. Ye. *Stud. Surf. Sci. Catal.*, **105 (1997)** 2075–2081.

A. Corma. In E. Derouane, F. Lemos, C. Naccache and F. Ribeiro, eds., *Zeolite Microporous Solids: Synthesis, Structure and Reactivity*, pp. 373–436. Kluwer Academic Publishers, Dordrecht, 1992.

J. Crowell, L. Tedder, H.-C. Cho, F. Cascarano and M. Logan. *J. Electron Spectroscopy and Related Phenomena*, **54/55 (1990)** 1097–1104.

S. Csicsery. *Zeolite Chemistry and Catalysis*, pp. 680–713. ACS Monograph 171, 1979.

J. Das, Y. Bhat and A. Halgeri. *Ind. Eng. Chem. Res.,*, **32 (1993)** 2525–2529.

J. Das, Y. Bhat and A. Halgeri. *Ind. Eng. Chem. Res.*, **33 (1994)** 246–250.

J. Das and A. B. Halgeri. *Appl. Catal. A: General*, **194-195 (2000)** 359–363.

E. Derouane. *Stud. Surf. Sci. Catal.*, **5 (1980)** 5–18.

K. Dooley, S. Brignac and G. Price. *Ind. Eng. Chem. Res.*, **29 (1990)** 789–795.

A. Dyer. *An Introduction to Zeolite Molecular Sieves*. Wiley and Sons, 1988.

M. Farcasiu and T. Degnan. *Ind. Eng. Chem. Res.*, **27 (1988)** 45–47.

D. Fei, W. Guiru and X. W. *Chinese J. of Chem. Eng.*, **3 (1995)(4)** 208–214.

F. Fetting and U. Dingerdissen. *Chem. Ing. Tech.*, **62 (1990)(9)** 736–738.

D. Fraenkel. *Ind. Eng. Chem. Res.*, **29 (1990)** 1814–1821.

M. Guisnet, N. Gnep and S. Morin. *Microporous Mesoporous Mater.*, **35-36 (2000)** 47–59.

A. Halgeri, Y. Bhat, S. Unnikrishnan and T. P. Rao. *Symposium on Alkylation, Aromatization, Oligorimerization and Isomerization of short chain Hydrocarbons over Heterogeneous Catalysts, ACS*, **36 (1991)(4)** 792–798.

G. Handreck and T. Smith. *Zeolites*, **10 (1990)** 749–752.

G. Harvey, G. Binder and R. Prins. *Stud. Surf. Sci. Catal.*, **94 (1995)** 397–404.

J. Herzler, J. Manion and W. Tsang. *J. Phys. Chem. A*, **101 (1997)** 5500–5508.

T. Hibino, M. Niwa, A. Hattori and Y. Murakami. *Appl. Catal.*, **44 (1988)** 95–103.

T. Hibino, M. Niwa and Y. Murakami. *J. Chem. Soc., Faraday Trans. I*, **85 (1989a)(8)** 2327–2334.

T. Hibino, M. Niwa and Y. Murakami. *J. Catal.*, **128 (1991)** 551–558.

T. Hibino, M. Niwa and Y. Murakami. *Zeolites*, **13 (1993)** 518–523.

T. Hibino, M. Niwa, Y. Murakami, M. Sano, S. Komai and T. Hanaichi. *J. Phys. Chem.*, **93 (1989b)** 7847–7850.

N. Impens, P. V. der Voort and E. Vansant. *Microporous Mesoporous Mater.*, **28 (1999)** 217–232.

M. Ivanov, T. Kupryashkina, V. Kompaniets, M. Kopteva and A. Konoplev. *J. Appl. Chem.-USSR*, **58, 8 (1985)** 1691–1695.

Y. Iwasawa. In G. Ertl, H. Knözinger and J. Weitkamp, eds., *Handook of Hetrogeneous Catalysis*, pp. 853–872. VCH, Weinheim, 1997.

T. Jurgens and J. J.W. Rogers. *J. Phys. Chem.*, **99 (1995)** 731–743.

T. Jurgens-Kowal and J. Rogers. *J. Phys. Chem. B*, **102 (1998)** 2193–2206.

W. Kaeding, C. Chu, L. Young and S. Butter. *J. Catal.*, **69 (1981a)** 392–398.

W. Kaeding, C. Chu, L. Young, B. Weinstein and S. Butter. *J. Catal.*, **67 (1981b)** 159–174.

N. Katada, T. Toyama and M. Niwa. *J. Phys. Chem.*, **98 (1994)** 7647–7652.

G. T. Kerr. *U.S. Patent 3.682.996*, **(1972)**.

J.-H. Kim, Y. Ikoma and M. Niwa. *Microporous Mesoporous Mater.*, **32 (1999)** 37–44.

J.-H. Kim, A. Ishida, M. Okajima and M. Niwa. *J. Catal.*, **161 (1996)** 387–392.

J.-H. Kim, T. Kunieda and M. Niwa. *J. Catal.*, **173 (1998)** 433–439.

J.-H. Kim, M. Okajima and M. Niwa. *Stud. Surf. Sci. Catal.*, **105 (1997)** 1965–1972.

E. Klemm, J. Wang and G. Emig. *Chem. Eng. Sci.*, **52 (1997)(18)** 3173–3182.

A.-N. Ko and B. Wojciechowski. *Prog. React. Kinet.*, **12 (1983)(4)** 201–262.

G. Kokotailo, S. Lawson, D. Olson and W. Meier. *Nature*, **272 (1978)** 437–438.

G. Kühl. *Catalysis and Zeolites, Fundamentals and Applications*, chap. 3. Modification of Zeolites. Springer Verlag, Berlin, Heidelberg, 1999.

T. Kunieda, J.-H. Kim and M. Niwa. *J. Catal.*, **188 (1999)** 431–433.

L. Kva, O. Ponomareva, O. Sinitsyna, I. Moskovskaya, B. Khusid, G. Chukin, O. Parenago and E. Lunina. *Kinet. Catal.*, **30 (1989)** 1272–1278.

C. Li-Feng, T. Wacker and L. Rees. *J. Chem. Soc., Faraday Trans. I*, **85 (1989)(1)** 33.

H.-E. Lin and A.-N. Ko. *J. Chin. Chem. Soc.*, **47 (2000)** 509–518.

J. Martens, W. Souverijns, W. VanRhijn and P. Jacobs. In G. Ertl, H. Knözinger and J. Weitkamp, eds., *Handbook of Heterogeneous Catalysis*, pp. 324–365. VCH, Weinheim, 1997.

W. Meier, D. Olson and C. Baerlocher. *Atlas of Zeolite Structure Types, 4th Revised Edition*. Elsevier, London, 1996.

S. Melson and F. Schüth. *J. Catal.*, **170 (1997)** 46–53.

N. Meshram, S. Hedge, S. Kulkarni and P. Ratnasamy. *Appl. Cat.*, **8 (1983)** 359–367.

J. Moulijn, A. Tarfaoui and F. Kapteijn. *Catal. Today*, **11 (1991)** 1–12.

Y. Murakami. *Stud. Surf. Sci. Catal.*, **44 (1989)** 177–188.

S. Namba, A. Inaka and T. Yashima. *Zeolites*, **6 (1986)** 107–110.

V. Nayak and L. Riekert. *Appl. Catal.*, **23 (1986)** 403–411.

W. Niessen and H. Karge. *Microporous Materials*, **1 (1993)** 1–8.

M. Niwa, T. H. aand H. Murata, N. Katada and Y. Murakami. *J. Chem. Soc., Chem. Comm.*, **(1989)** 289–290.

M. Niwa, C. Hidalgo, T. Hattori and Y. Murakami. *Proc. 7th Int. Zeol.Conf., editors.: Y.Murakami, A. Iijima, J.W. Ward, Stud. Surf. Sci. Catal.*, **28 (1986a)** 297–304.

M. Niwa, H. Itoh, S. Kato, T. Hattori and Y. Murakami. *J. Chem. Soc., Chem. Commun.*, **15 (1982)** 819–820.

M. Niwa, N. Katada and Y. Murakami. *J. Phys. Chem.*, **94 (1990)** 6441–6445.

M. Niwa, M. Kato, T. Hattori and Y. Murakami. *J. Phys. Chem.*, **90 (1986b)** 6233–6237.

M. Niwa, S. Kato, T. Hattori and Y. Murakami. *J. Chem. Soc., Faraday Trans.*, **1 (1984a)(80)** 3135–3145.

M. Niwa, Y. Kawashima, T. Hibino and Y. Murakami. *J. Chem. Soc., Faraday Trans.*, **84 (1988)(12)** 4327–4336.

M. Niwa, Y. Kawashima and Y. Murakami. *J. Chem. Soc., Faraday Trans. I*, **81 (1985)** 2757–2761.

M. Niwa, S. Morimoto, M. Kato and T. Hattori. *Proceedings of the 8th ICC*, **4 (1984b)** 701–711.

M. Niwa and Y. Murakami. *J. Phys. Chem. Solids*, **50 (1989)(5)** 487–496.

M. Niwa, K. Yamazaki and Y. Murakami. *Ind. Eng. Chem. Res.*, **30 (1991)** 38–42.

D. Olson and W. Haag. *ACS Symp. Ser.*, **248 (1984)** 275–307.

G. Paparatto, E. Moretti, G. Leofanti and F. Gatti. *J. Catal.*, **105 (1987)** 227–232.

R. Reid, J. Prausnitz and B. Poling. *The Properties of Liquids and Gases*. McGraw-Hill, New York, 4th edn., 1987.

M. Remy and G. Poncelet. *J. Phys. Chem.*, **99 (1995)** 773–779.

H. Röger. *PhD Thesis University of Cape Town*, **(1998)**.

H. Röger, W. Böhringer, K. Möller and C. O'Connor. *Stud. Surf. Sci. Catal.*, **130 (2000)** 281–286.

H. Röger, M. Krämer, K. Möller and C.T.O'Connor. *Microporous Mesoporous Mater.*, **21 (1998a)** 607–614.

H. Röger, K. Möller and C. O'Connor. *J. Catal.*, **176 (1998b)** 68–75.

L. Rollmann. *U.S. Patent 4.203.869*, **(1980)**.

S. Sato, M. Hiratsuka, T. Sodesawa and F. Nozaki. *Bull. Chem. Soc. Jpn.*, **64 (1991a)** 2214–2219.

S. Sato, M. Toita, T. Sodesawa and F. Nozaki. *Appl. Catal.*, **62 (1990)** 73–84.

S. Sato, M. Tokumitsu, T. Sodewasa and F. Nozaki. *Bull. Chem. Soc. Jpn.*, **64 (1991b)** 1005–1007.

M. Sawa, K. Kato, K. Hirota and M. Niwa. *Appl. Catal.*, **64 (1990)** 297–308.

R. Shaikh, S. Hegde, A. Behlekar and B. Rao. *Catal. Today*, **49 (1999)** 201–209.

J. Spitzmüller, J. Braun, H. Rauscher and R. Behm. *Surf. Sci.*, **400 (1998)** 356–366.

I. Suzuki, S. Namba and T. Yashima. *J. Catal.*, **81 (1983)** 485–488.

M. Suzuki, J. Amano and M. Niwa. *Microporous Mesoporous Mater.*, **21 (1998)** 541–547.

D. Theodorou and J. Wei. *J. Catal.*, **83 (1983)** 205–224.

E. Thiele. *Ind. Eng. Chem.*, **31 (1939)** 916.

M. Trombetta, T. Armaroli, A. Alejandre, J. Solis and G. Busca. *Appl. Catal. A: General*, **192 (2000)** 125–136.

T.-C. Tsai, S.-B. Liu and I. Wang. *Appl. Catal. A: General*, **181 (1999)** 355–398.

T.-C. Tsai and I. Wang. *Appl. Catal.*, **77 (1991)** 209–222.

P. Tynjälä and T. Pakkanen. *J. Mol. Catal. A,*, **122 (1997)** 159–168.

M. Uguina, J. Sotelo and D. Serrano. *Appl. Cat.*, **76 (1991)** 183–198.

M. Uguina, J. Sotelo and D. Serrano. *Ind. Eng. Chem. Res.*, **32 (1993)** 49–55.

J. van den Berg, J. Wolhuizen and J. V. Hooff. *J. Catal.*, **80 (1983)** 139–144.

E. Vansant. *Stud. Surf. Sci. Catal.*, **37 (1988)** 143–153.

R. von Ballmoos and G. Kerr. *Stud. Surf. Sci. Catal.*, **24 (1985)** 307–318.

I. Wang, C.-L. Ay, B.-J. Lee and M.-H. Chen. In M. T. M.J. Phillips, ed., *Proceedings of the 9th. International Congress on Catalysis*, vol. 1, pp. 324–331. Calgary, 1988.

I. Wang, C.-L. Ay, B.-J. Lee and M.-H. Chen. *Appl. Catal.*, **54 (1989)** 257–266.

P. Webb and C. Orr. *Analytical Methods in Fine Particle Technology*. Micromeretics Instrument Corporation, 1997.

R. Weber, J. Fletcher, K. Möller and C. O'Connor. *Microporous Mesoporous Mater.*, **7 (1996)** 15–25.

R. Weber, K. Möller and C. O'Connor. *Microporous Mesoporous Mater.*, **23 (1998)** 179–187.

R. Weber, K. Möller and C. O'Connor. *Microporous Mesoporous Mater.*, **35-36 (2000)** 533–543.

R. W. Weber. *PhD-thesis, University of Cape Town*, **(1998)**.

J. Wei. *J. Catal.*, **76 (1982)** 433–439.

B. Wojciechowski. *Cat. Rev.-Sci. Eng.*, **9 (1974)(1)** 79–113.

Y. Xiong, P. Rodewald and C. Chang. *J. A. Chem. Soc.*, **117 (1995)** 9427–9431.

Y. Yan, J. Verbiest, P. D. Hulsters and E. Vansant. *J. Chem. Soc., Faraday Trans. I*, **85 (1989)(10)** 3095–3105.

J. Yoo, C. Lee, S.-E. Park and J. Ko. *Appl. Cat. A: General*, **187 (1999)** 225–232.

L. Young, S. Butter and W. Kaeding. *J. Catal.*, **76 (1982)** 418–432.

Y.-H. Yue, Y. Tang and Z. Gao. *Stud. Surf. Sci. Catal.*, **105 (1997)** 2059–2064.

Appendix A

BET, TPD and XRD analysis

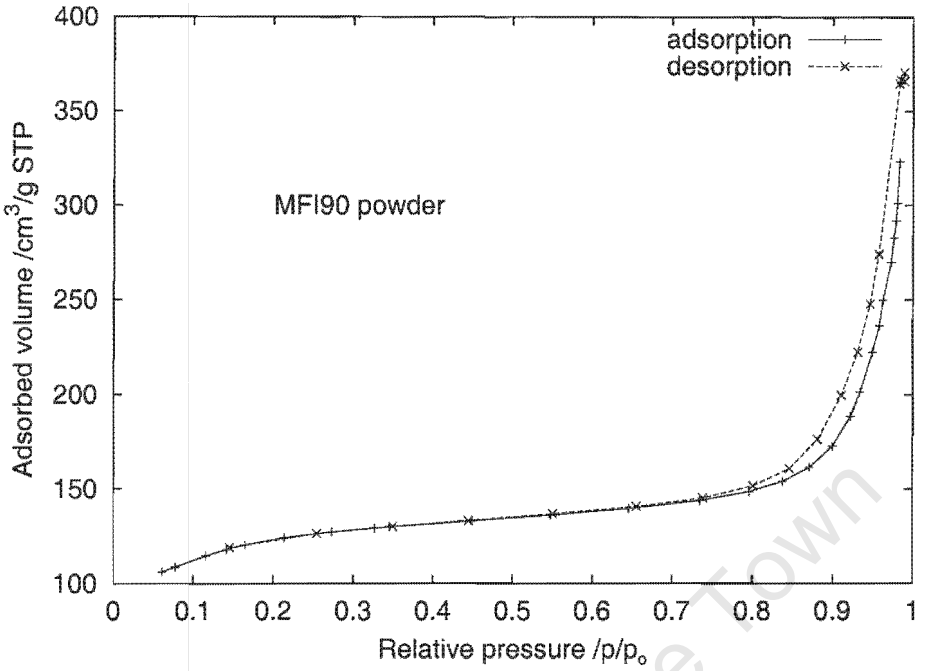

Figure A.1: Nitrogen BET isotherm of MFI-90 powder.

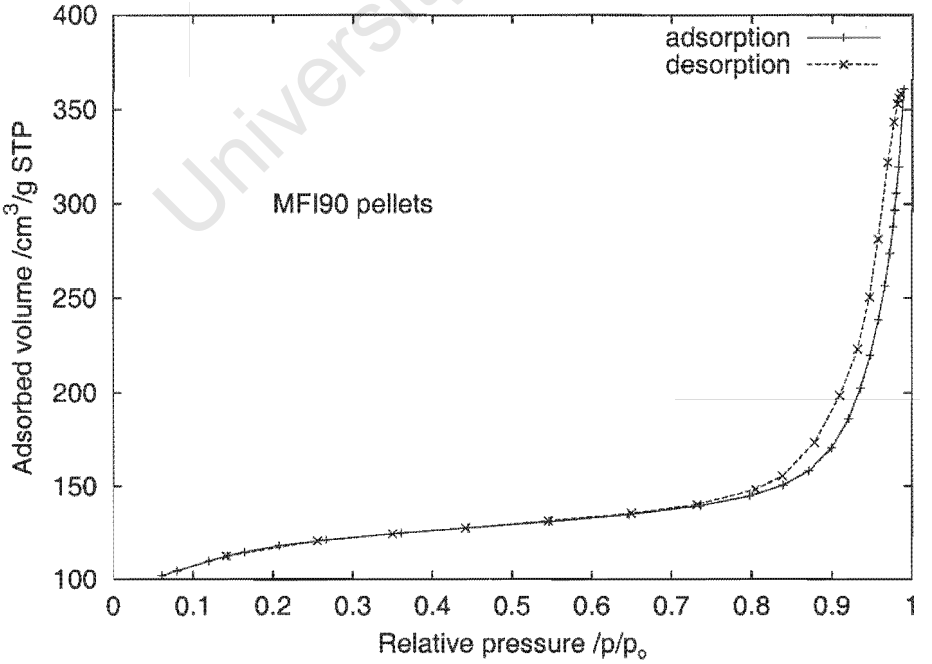

Figure A.2: Nitrogen BET isotherm of MFI-90 pellets.

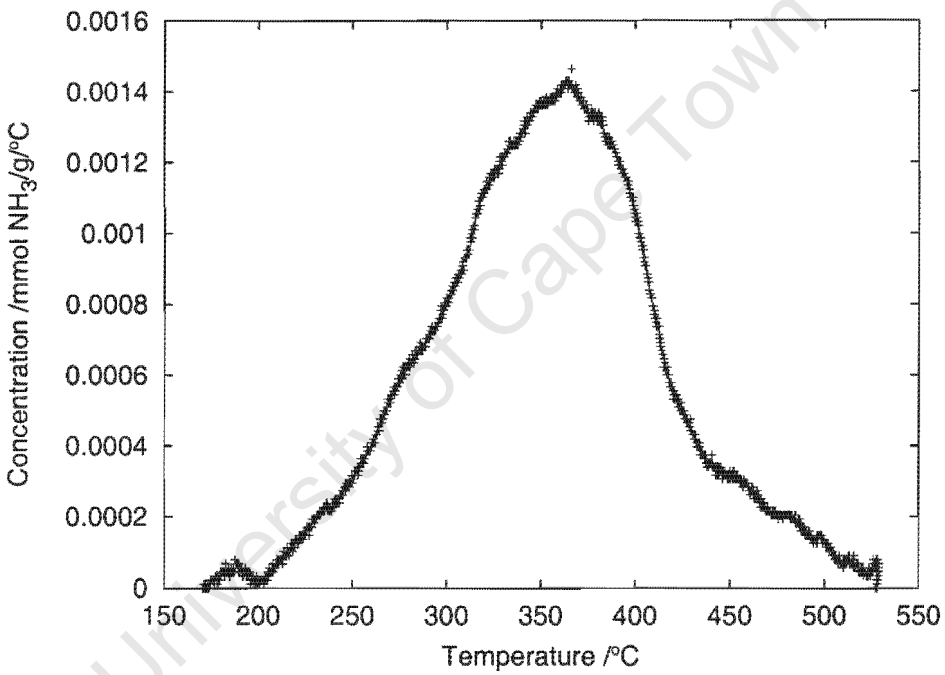

Figure A.3: NH_3-TDP-spectrum of MFI-90 powder.

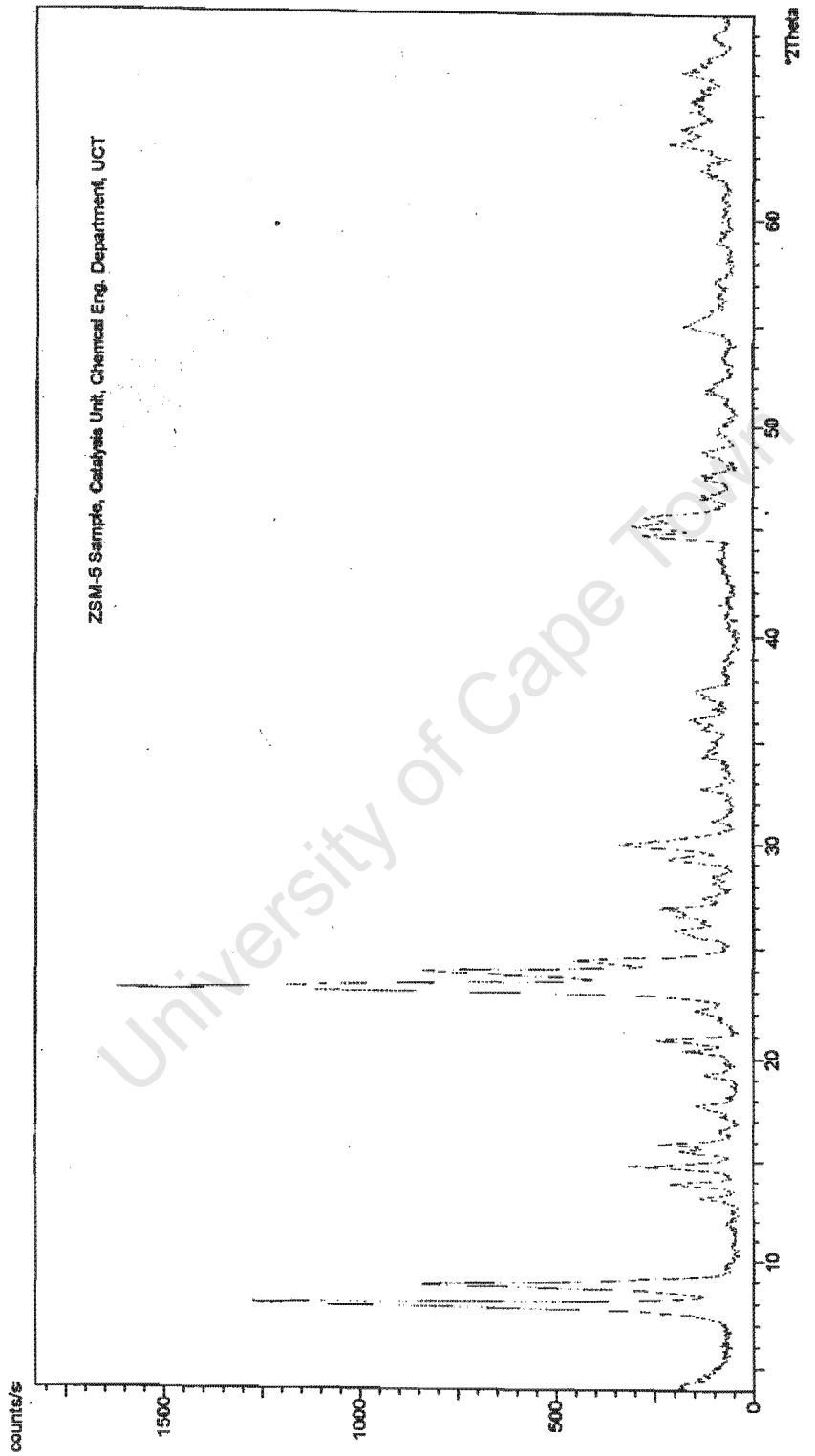

Figure A.4: XRD-spectrum of MFI-90 powder (K-α radiation source; wave length: 1.54056 Å).

Appendix B

Concentration and breakthrough curves

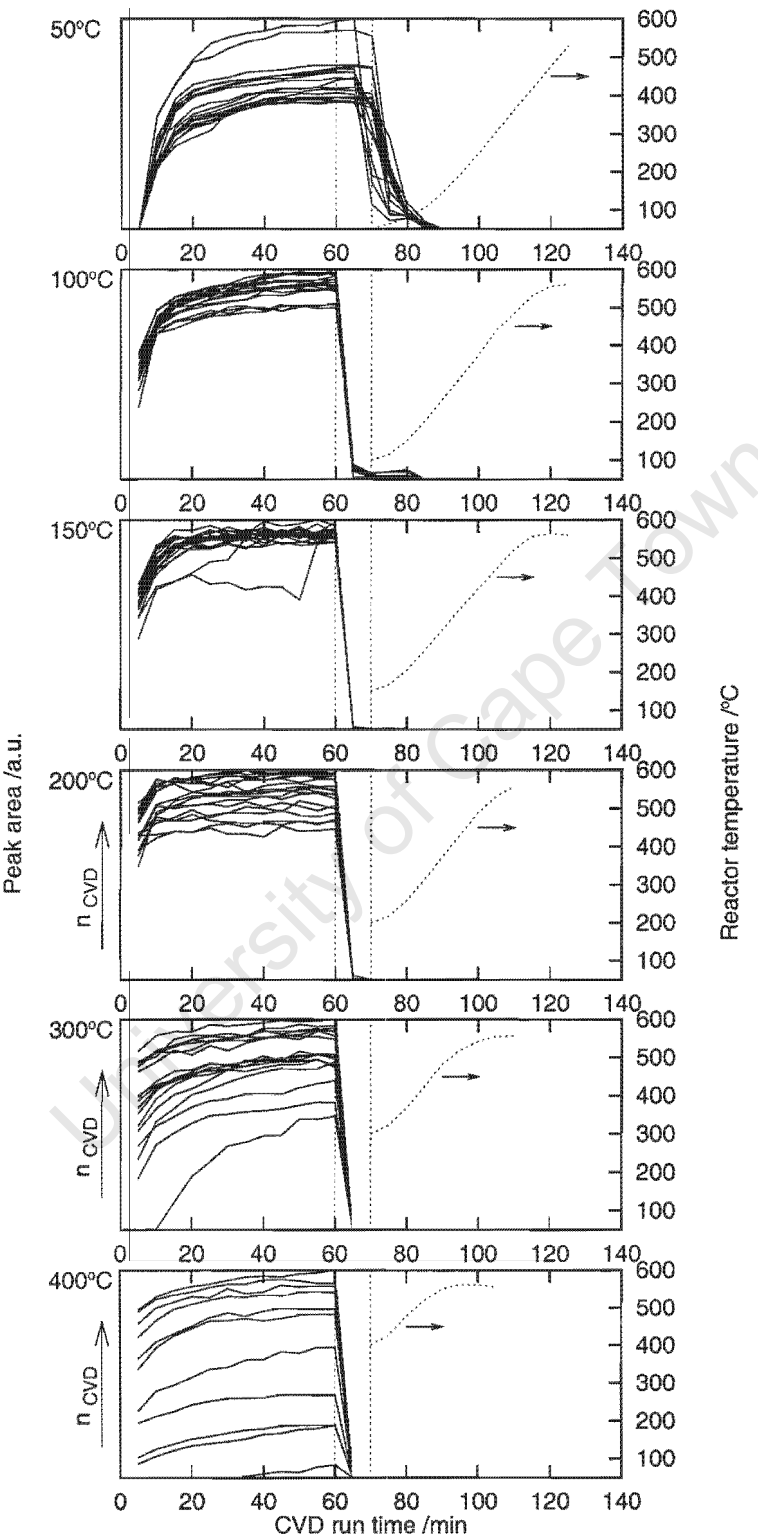

Figure B.1: TEOS concentration curves for all deposition cycles on powder at all deposition temperatures.

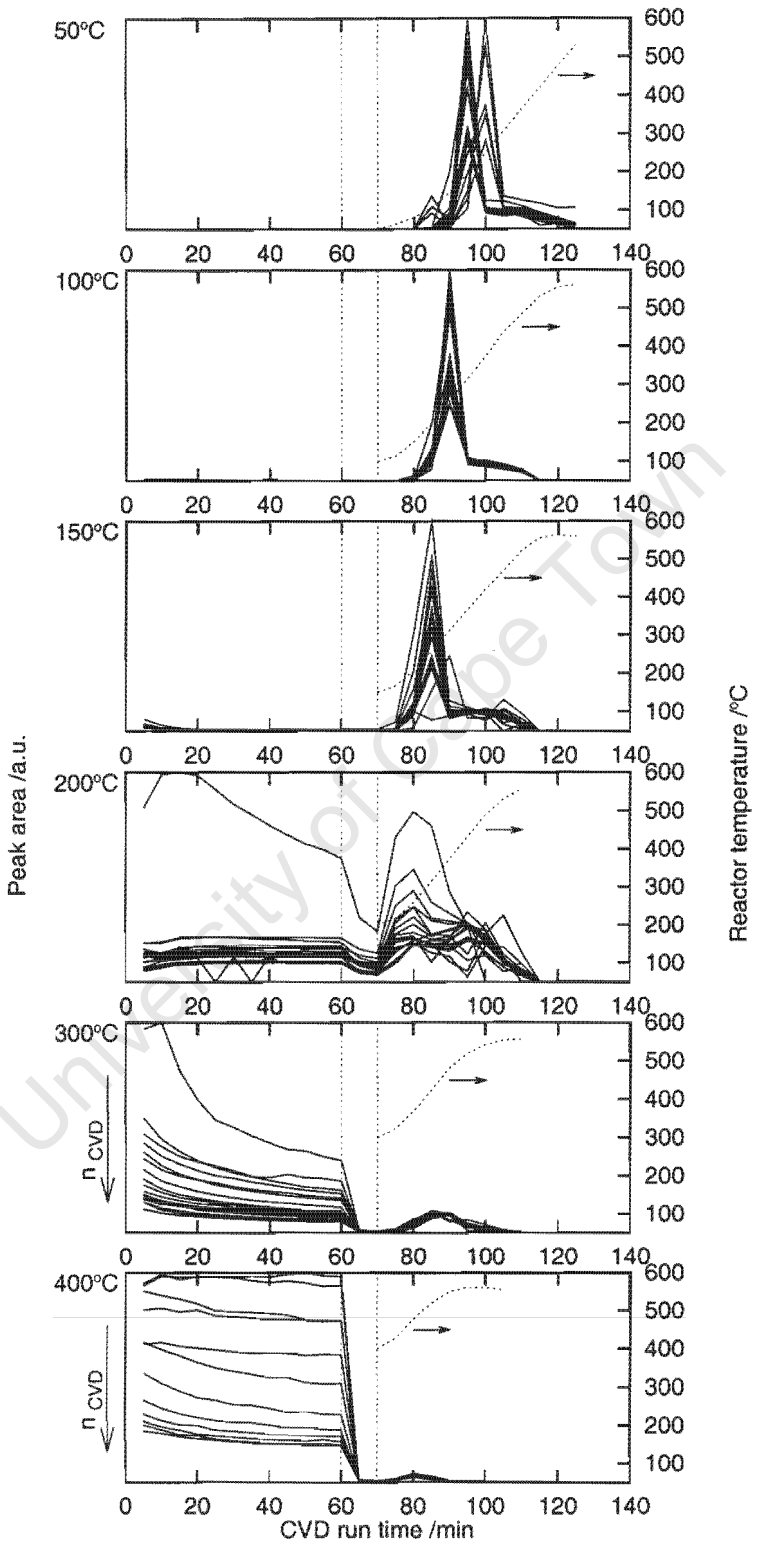

Figure B.2: Ethene concentration curves for all deposition cycles on powder at all deposition temperatures.

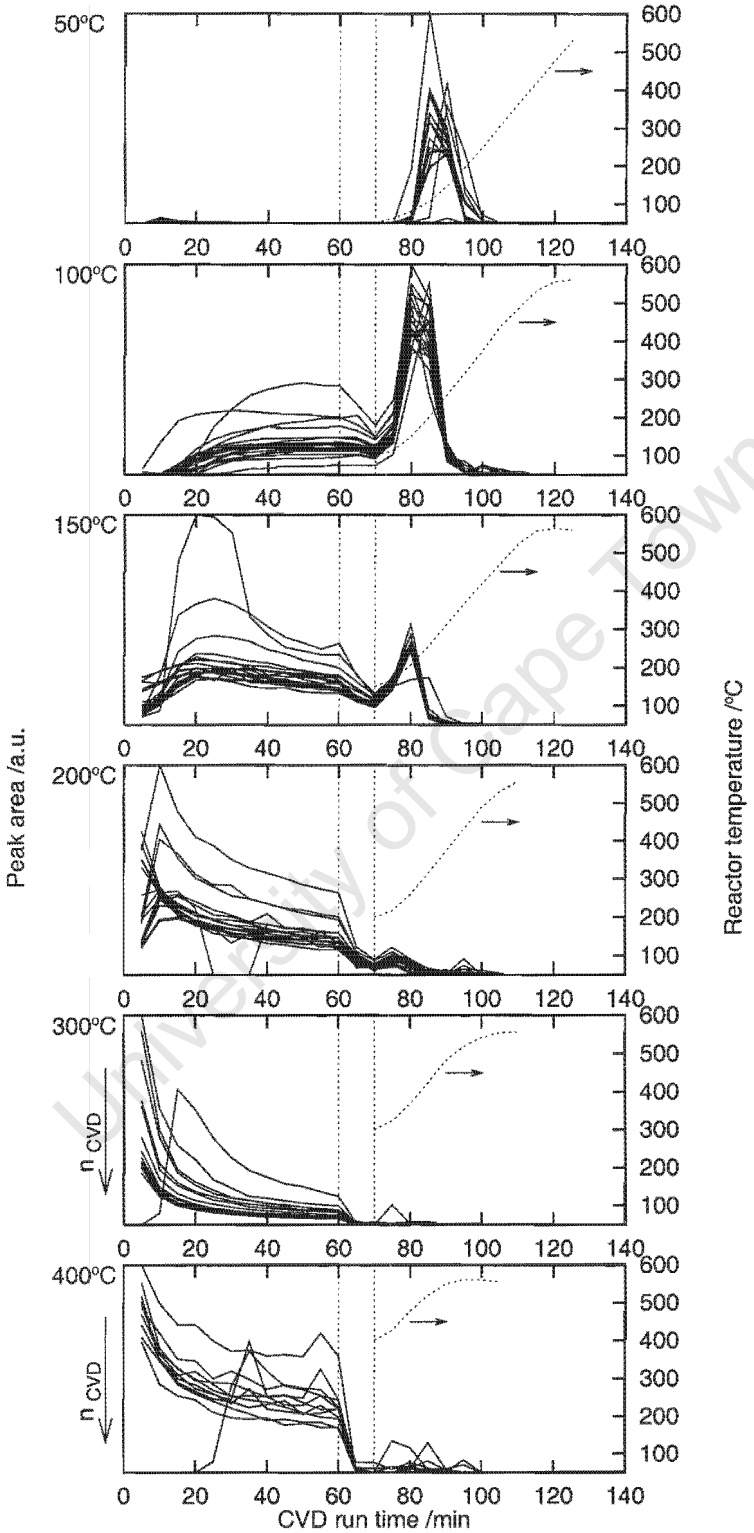

Figure B.3: Ethanol concentration curves for all deposition cycles on powder at all deposition temperatures.

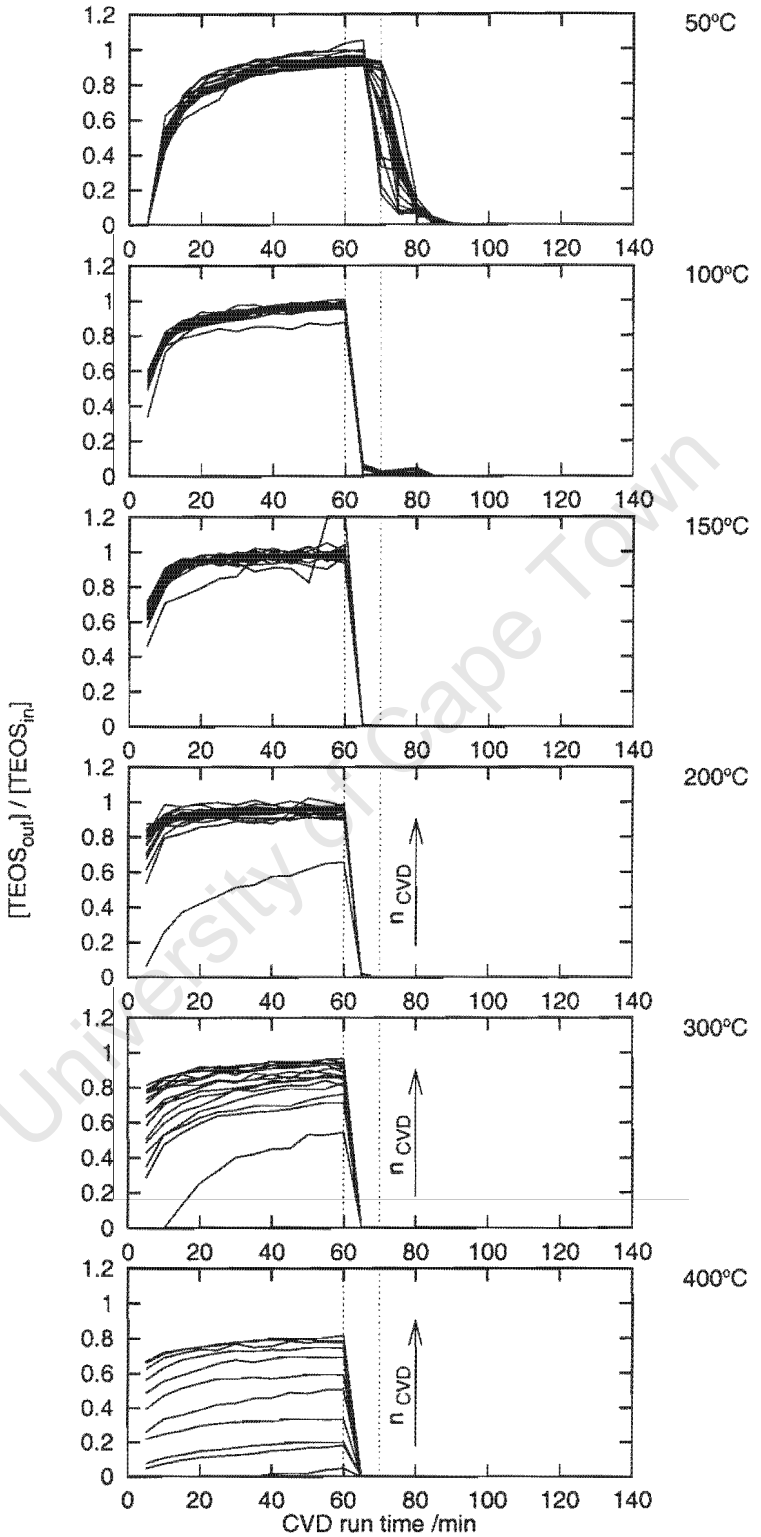

Figure B.4: Normalised TEOS breakthrough curves for powder samples at all temperatures.

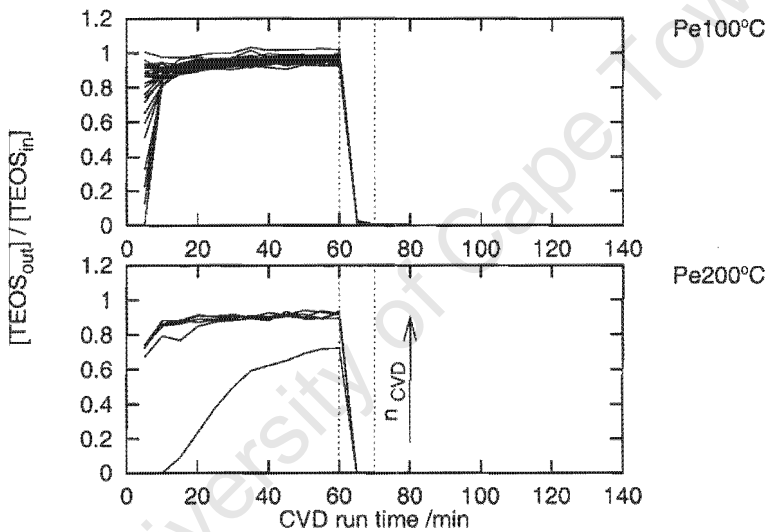

Figure B.5: Normalised TEOS breakthrough curves for pelletised samples at 100 and 200°C.

Appendix C

Sketches

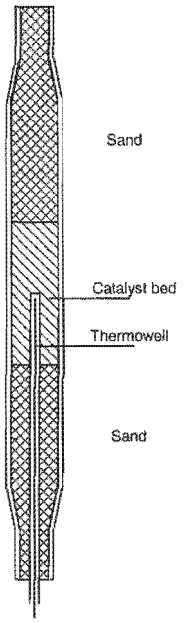

Figure C.1: Sketch of reactor.

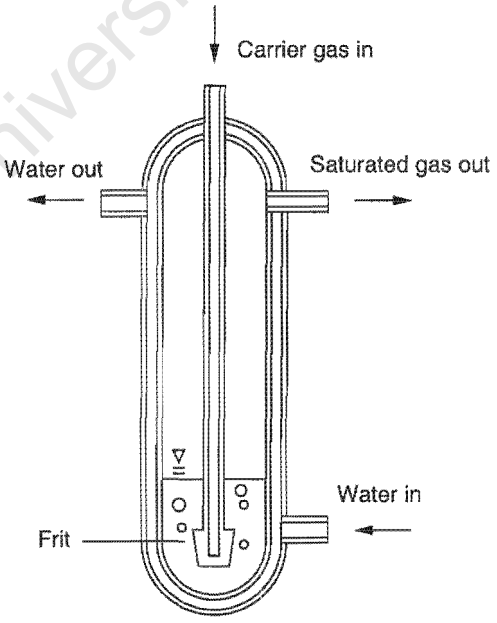

Figure C.2: Sketch of saturator.

Appendix D

Gas Chromatography

Table D.1: Specification of gas-chromatography

GC-type	Varian Series 3300
Column producer	SGE
Column specifications	25 Q C2 / BP-20-0.25; Polyehtyleneglycol (polar)
Length (m)	25
ID (mm)	0.22
film-thickness (μm)	0.25
Injector type	Split-injector
Split ratio	100:1
Carrier gas	Helium
Column head pressure (kPa)	110 (16psi)
Injector temperature (°C)	170
Detector type	FID
Detector temperature (°C)	250

Table D.2: Operation conditions for gas-chromatography

	CVD	TiPB	TDP
Column T (°C)	65	55	150
Temperature program	isothermal	isothermal	isothermal
sample intervals (min)	5	10	10

Table D.3: Specification of gas-chromatography for the analysis of the light gas fraction during CVD and TDP.

GC-type	Varian Series 3300
Column producer	Chrompack
Column specifications	CP-Sil 5CB; dimethylsilicon (non-polar)
Length (m)	50
ID (mm)	0.25
film-thickness (μm)	0.4
Injector type	Split-injector
Split ratio	100:1
Carrier gas	Hydrogen
Column head pressure (kPa)	110 (16psi)
Injector temperature (°C)	120
Detector type	FID
Detector temperature (°C)	250
Column temperature programme	Isothermal at -68, hold: 5 min, ramp to -35°C at 15 °C/min, hold: 1 min, ramp to -5°C at 10 °C/min, hold: 2.5 min, ramp to 280°C at 5 °C/min, hold: 40 min

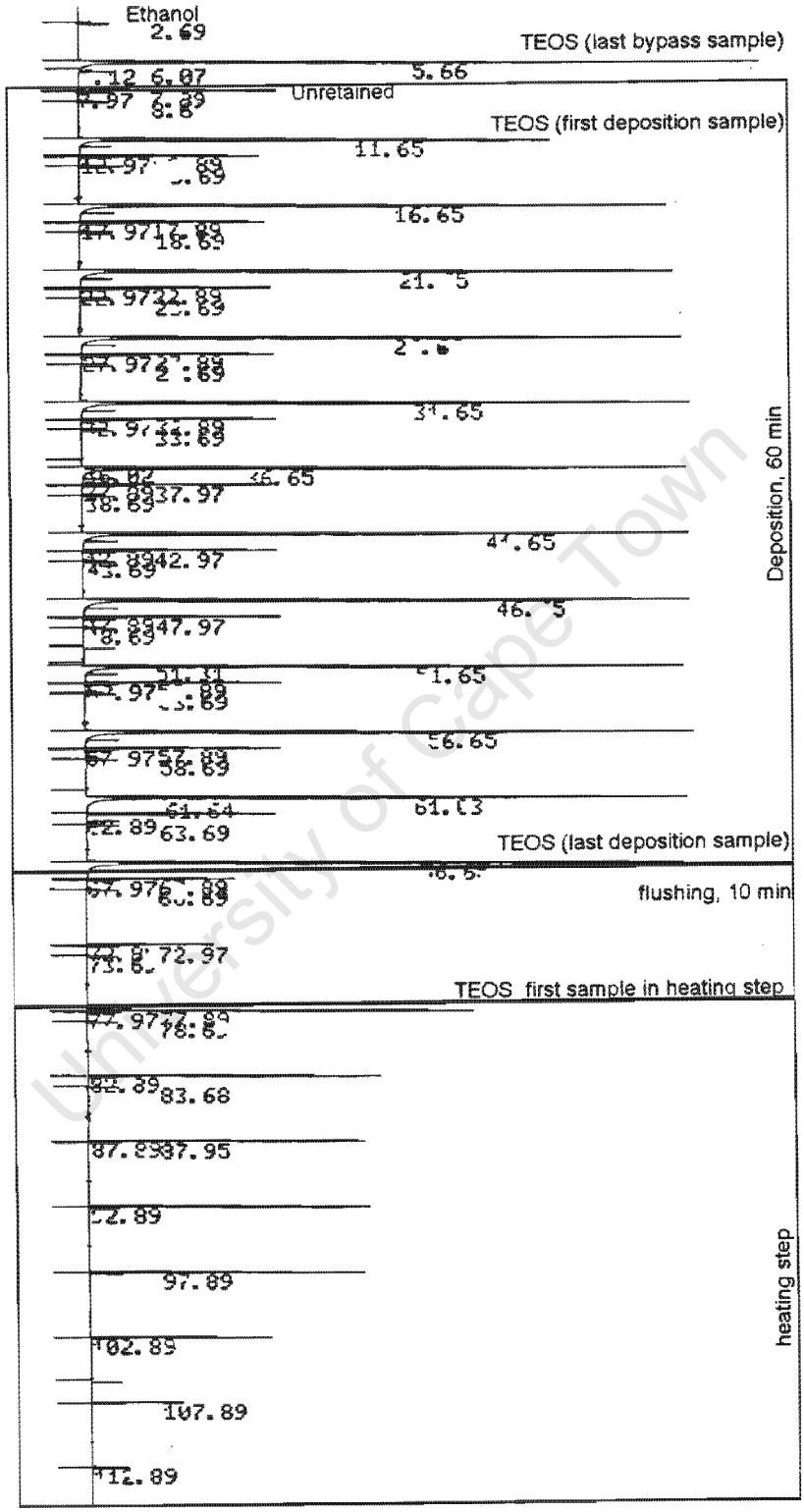

Figure D.1: GC-trace of full CVD deposition.

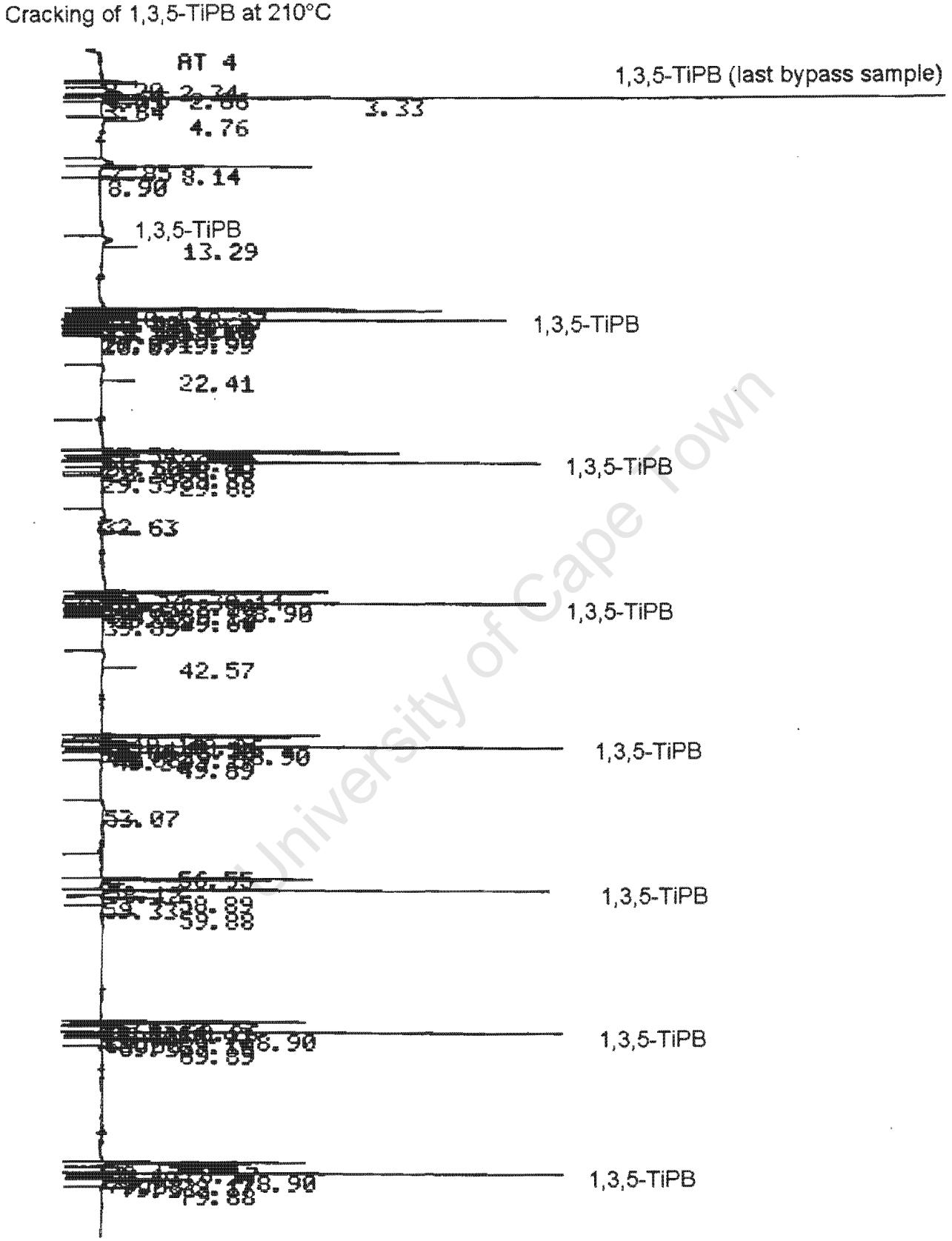

Figure D.2: GC-trace of full 1,3,5-TiPB-cracking run.

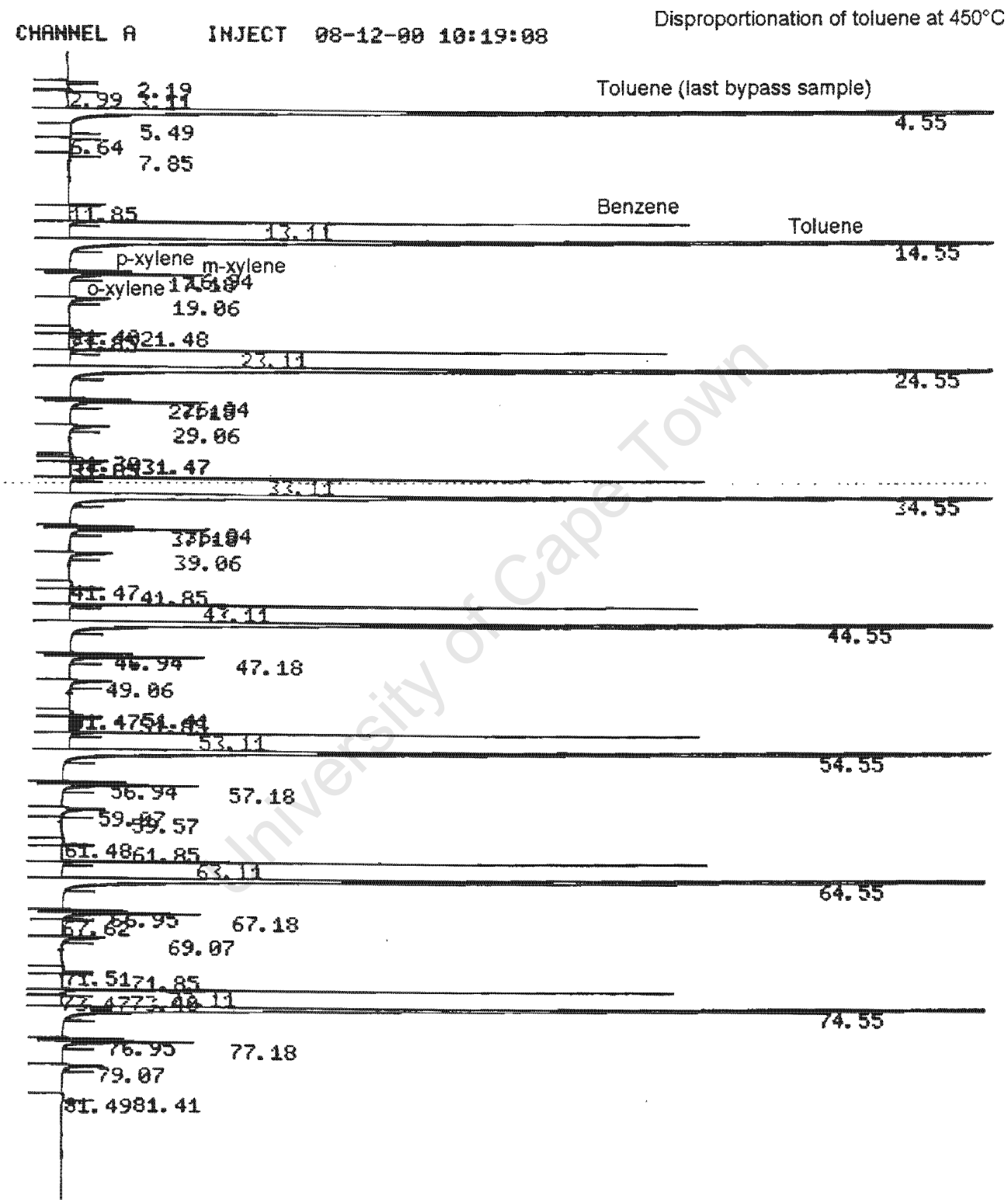

Figure D.3: GC-trace of full TDP run.

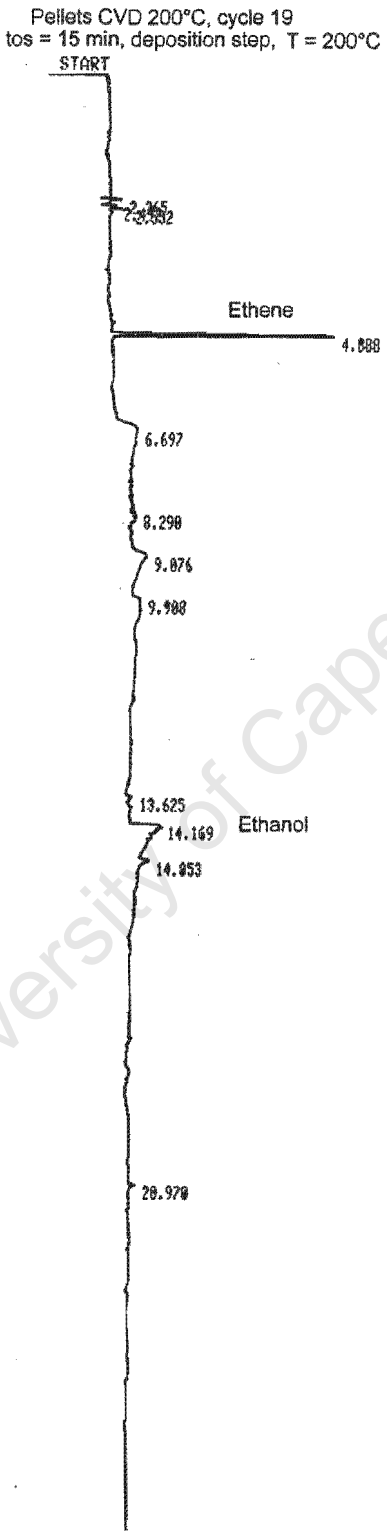

Figure D.4: GC-trace of analysis of unretained compounds during TEOS deposition at 200°C.

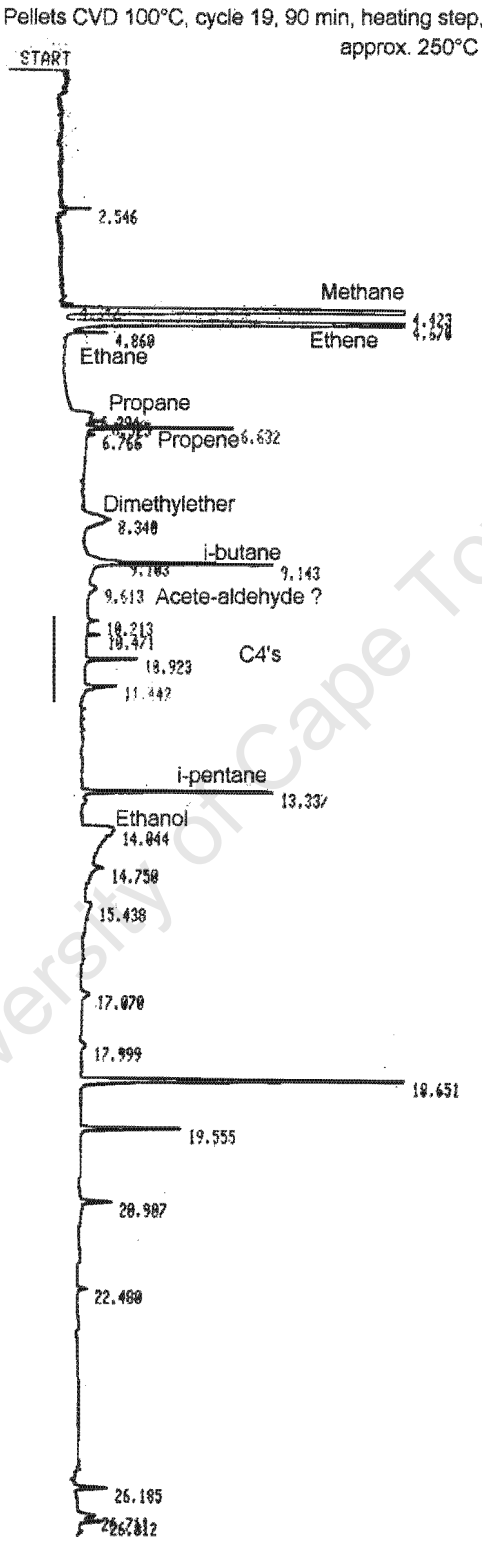

Figure D.4: (continued) GC-trace of analysis of unretained compounds during the heating step (reactor temperature approximately 250°C) of a TEOS deposition at 200°C.

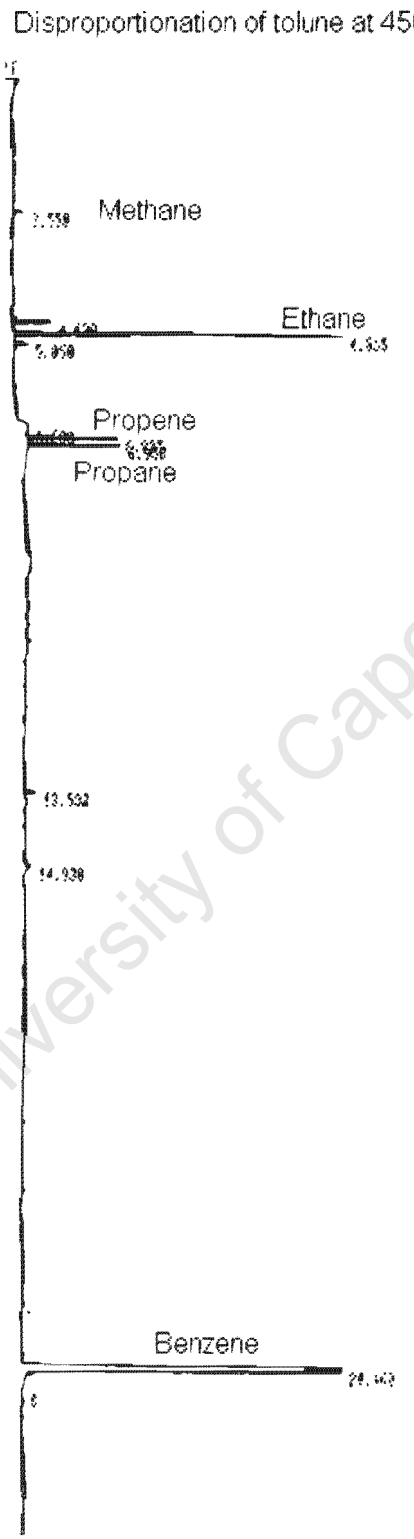

Figure D.5: GC-trace of analysis of light hydrocarbons during TDP at 550°C.

Appendix E

Additional Figures

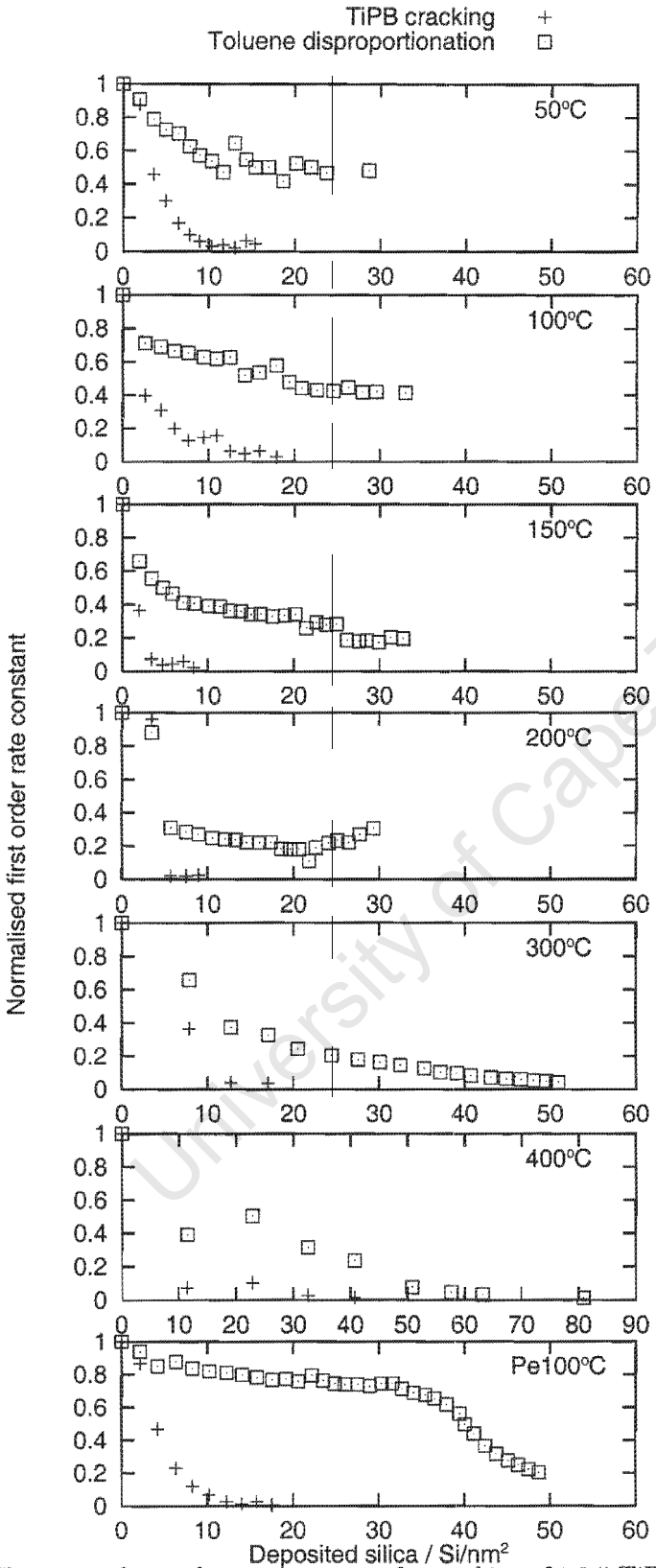

Figure E.1: Changes in first order rate constants for cracking of 1,3,5-TiPB and disproportionation of toluene with increasing Si/nm^2.

Appendix F

Methods

F.1 Reactor dead time

A Methane/Nitrogen mixture was used to determine the dead time of the reactor volume. This was done at 50 and 400°C and flow rates which were applied during CVD treatments. The minimum sampling interval was 10 s. 10 seconds after the reactor had been switched online the first sample was taken. Methane concentrations of the effluent assumed the value of the bypass sample already in the first sample. With the reactor volume of 7 cm^3 and a linear flow rate of 100 ml/min a theoretical dead time of 4.2 s was estimated. The dead time of the reactor was thus considered negligible.

F.2 Isomerisation of para-xylene

Figure F.1 shows the results for the isomerisation of p-xylene over CVD treated silica gel. The mass of the silica gel loaded into the reactor was chosen to resemble the adsorption surface area of the pelletised zeolite samples. 5 TEOS-CVD cycles at 200°C were applied to obtain a silica surface as it was deposited on the zeolite. The reaction data are given in Table G.16. A conversion of 10% was obtained when the calculation was based on the bypass samples taken prior to the reaction. Assuming 100% carbon balance for the experiment, the conversion level did not exceed 2%. The scatter in the preliminary type experiment does not allow precise determination of rate constants. It however appears that the isomerisation of p-xylene over SiO_2 at 450°C can be neglected in the overall reaction scheme for TDP over CVD modified ZSM-5.

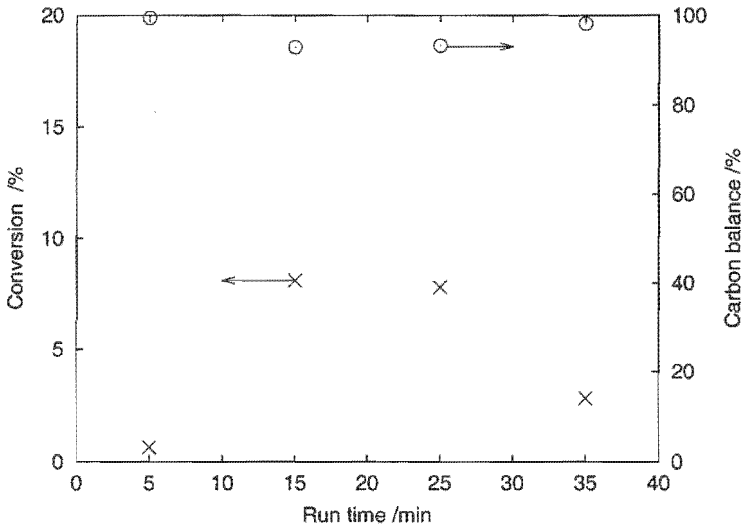

Figure F.1: Isomerisation of p-xylene over CVD treated silica gel.

F.3 Correction for internal activity during TDP

From Figure E.1 the formation of a steady conversion plateau for TDP became apparent. In order to separate the external contribution from the total activity, following "stable" activity levels (Table F.1) were assumed and considered. Thus, the corrected normalised first order rate constant was obtained:

$$k_{TDP,\ external} = \frac{k_{actual} - k_{activity\ plateau}}{k_{overall} - k_{activity\ plateau}} \tag{F.1}$$

Table F.1: Intrinsic activity plateaux

Series	activity plateau (%)
50°C	50
100°C	50
150°C	30
200°C	20
300°C	10
400°C	0
Pe100°C	80

F.4 CVD on sand

The zeolite catalyst which was modified in this study was diluted with sand. Since TEOS also reacts with silica, higher deposition amounts will be determined. In order to estimate to which extent this might affect the accuracy of the mass balances during TEOS breakthrough, CVD was carried out over a pure sand packing. 11 g sand were loaded into the reactor and 3 subsequent CVD cycles were monitored at 400°C and 2 cycles at 50°C. The results are displayed in Figure 3.26 and Table F.2.

Between 95 and 97% of the fed carbon were retrieved while ca. 7.5 and 4% of TEOS were converted at 400 and 50°C, respectively. Assuming spherical sand and catalyst particles of 200 μ and 250 nm, respectively, the mixture of a 9 g sand + 0.5 g catalyst mixture gives an adsorption area ratio of $\text{area}_{sand} : \text{area}_{catalyst} = 0.2 : 99.8$. Variation thereof is attributed to the size distribution of both sand and catalyst particles which could have varied with each new reactor packing. It was thus decided to relinquish a correction of the deposited amounts on sand for the determination of the deposited amounts on the diluted zeolite samples.

Table F.2: CVD on sand

Temperature and cycles	XTEOS (%) (%)	integral C-bal. (%) (%)	σ
50°C, 1.	4.37	97	
50°C, 2.	4.06	97	0.21
400°C, 1.	8.19	94	
400°C, 2.	7.77	94	0.60
400°C, 3.	7.01	95	

F.5 Sample calculation for silica loading

At a TEOS partial pressure of 0.88 kPa, a absolute saturator pressure of 160 kPa and the total flow rate of 92 ml/min, the TEOS loading of the gas stream can be calculated:

$$\dot{n}_{TEOS} = \frac{p_i \dot{v}_{total} p_o}{p_{saturator} R T_o}$$

which yields 0.001225 mol TEOS/h.

The average adsorption/desorption surface area of the catalyst powder was 128.37 m^2/g. The surface area of 0.5 g catalyst is thus 64.185 m^2. The silica loading at 100 % TEOS conversion per hour of deposition over 0.5 g catalyst powder thus yields:

$$\frac{0.001225 \times 6 \times 10^{23}\ parts_{TEOS}}{64.185\ nm^{18}} = 11.49 parts_{TEOS}/nm^2$$

With the assumption that each converted TEOS molecule is converted to a silica building unit the silicon loading upon 100 % conversion equals 11.5 Si/nm^2. This conversion factor allows conversion of TEOS conversion to silica-loading.

Appendix G

Tables

Table G.1: Reactor temperature in $°C$ during heating ramp.

runtime (min)	Series T(°C)					
	50	100	150	200	300	400
70	51	100	151	200	300	401
75	63	114	167	217	323	427
80	81	151	206	259	368	478
85	106	201	256	314	424	520
90	147	259	312	373	482	550
95	196	316	367	432	520	562
100	250	375	420	489	542	561
105	308	420	471	531	555	555
110	365	485	523	557	557	
115	420	532	557			
120	477	555	564			
125	530	561	560			

Table G.2: Reaction conditions: Powder modified at 50°C.

cycle number	X_{TEOS}(%)	integral carbon balance (%)	silica loading (Si/nm^2)	X_{TiPB}	σ	carbon balance (%)	σ	$X_{toluene}$	σ	p-xylene in product (%)	σ	[benzene]/[xylenes]	pS (%)	σ	mS (%)	σ	oS (%)	σ	carbon balance (%)	σ
-	-	-	-	70.43	1.79	98.06	0.79	8.26	0.36	10.11	0.34	1.13	21.53	0.31	54.98	0.24	23.5	0.48	100.71	2.59
1	16.64	97.66	1.91	65.46	2.04	102.65	2.65	7.52	0.2	9.97	0.08	1.18	21.78	0.18	55.18	0.12	23.03	0.16	97.43	0.68
2	14.41	100.9	3.57	42.84	1.16	99.43	0.44	6.56	0.11	10.36	0.53	1.15	22.27	0.18	54.61	0.18	23.11	0.2	101.67	3.82
3	12.23	102.5	4.97	30.83	1	99.49	0.68	6.07	0.18	10.04	0.1	1.18	22.1	0.11	55.24	0.14	22.65	0.22	98.81	1.21
4	12.96	98.39	6.46	18.44	1.74	94.5	4.26	5.87	0.23	10.75	0.54	1.16	23.13	0.23	55.31	0.53	21.56	0.73	101.41	3.86
5	11.23	103.66	7.75	11.21	1.58	99.54	1.59	5.24	0.13	11.14	0.11	1.19	24.37	0.19	55	0.25	20.63	0.28	99.38	1.9
6	10.18	102.61	8.92	6.96	1.43	97.81	1.13	4.81	0.14	12.04	0.49	1.16	25.91	0.31	54.9	0.39	19.19	0.62	100.73	2.72
7	12.17	102.37	10.32	3.83	1.89	101.96	1.95	4.52	0.15	13.31	0.49	1.12	28.23	0.22	54.47	0.15	17.3	0.36	101.88	2.9
8	11.61	99.42	11.65	4.48	1.3	98.39	1.25	3.97	0.08	15.13	0.58	1.17	32.8	0.22	52.24	0.11	14.96	0.3	99.97	1.99
9	11.67	102.52	13	2.51	1.31	106.57	1.62	5.4	0.19	15.13	0.54	1.25	34.13	2.44	54.18	3.23	11.7	5.64	90.08	1.08
10	11.58	100.55	14.33	7.35	1.01	95.51	1.28	4.6	0.1	18.12	0.26	1.22	40.25	0.24	47.79	0.3	11.97	0.36	100.12	0.53
11	9.22	104.48	15.39	5.18	1.08	98.88	1.26	4.21	0.09	20.67	0.95	1.16	44.77	0.28	44.39	0.47	10.84	0.64	100.41	3.15
12	13.59	96.62	16.95					4.24	0.55	19.34	4.13	1.74	50.98	0.43	40.25	0.25	8.78	0.33	91.49	8.09
13	14.86	99.3	18.66					3.55	0.12	24.76	1.17	1.35	58.03	0.56	35.44	0.58	6.53	0.08	96.77	3.43
14	12.99	95.55	20.15					4.42	0.6	21.13	2.98	1.82	58.9	3.42	34.98	2.94	6.12	0.78	86.26	2.87
15	15.05	96.47	21.88					4.24	0.2	22.6	1.81	1.89	64.96	0.78	29.88	0.79	5.16	0.33	95.21	4.68
16	15.57	94.34	23.67					3.95	0.21	22.29	1.76	2.28	72.66	0.59	23.96	0.53	3.38	0.17	85.96	3.23
17	11.55	97.04	24.99					(4.75)	0.5	17.86	3.17	3.22	73.47	0.68	23.64	0.49	2.89	0.48	81.03	5.54
18	9.98	98.62	26.14					(6.76)	1.76	11.22	4.7	6.62	74.08	0.71	22.8	0.81	3.12	0.32	71.39	9.38
19	10.88	97.85	27.39					(5.66)	1.95	11	7.77	5.69	81.84	10.19	16.34	9.17	1.82	1.07	84.16	16.68
20	10.98	96.57	28.65	16.51	4.11	91.22	3.71	4.07	2.01	10.76	3.2	7.22	81.64	2.15	17.47	1.52	0.9	1.04	0	0

Table G.3: Reaction conditions: Powder modified at 100°C.

cycle number	X_{TEOS}(%)	integral carbon balance (%)	silica loading (Si/nm^2)	X_{TiPB}	σ	carbon balance (%)	σ	$X_{toluene}$	σ	p-xylene in product (%)	σ	[benzene]/[xylenes]	pS (%)	σ	mS (%)	σ	oS (%)	σ	carbon balance (%)	σ
-	-	-	-	66.23	1.7	92.91	1.64	8	0.04	9.69	0.17	1.21	21.41	0.08	55.25	0.41	23.34	0.45	94.32	1.67
1	22.85	94.14	2.63	35.04	4.19	100.97	4.35	5.76	0.02	10	0.14	1.19	21.9	0.13	55.26	0.34	22.84	0.46	95.83	1.75
2	16.04	99.23	4.47	28.37	1.35	96.95	3.77	5.58	0.05	9.87	0.27	1.24	22.09	0.04	54.57	0.38	23.35	0.38	93.81	1.15
3	13.6	105.77	6.03	19.29	2.37	99.08	4.63	5.4	0.04	10.07	0.38	1.22	22.41	0.31	54.76	0.23	22.83	0.31	94.04	1.76
4	14.25	99.33	7.67	12.86	1.09	96.67	0.7	5.29	0.06	10.31	0.27	1.25	23.15	0.17	54.79	0.49	22.06	0.5	92.44	2.09
5	15.33	98.1	9.43	14.43	1.62	93.4	2.09	5.1	0.1	10.57	0.49	1.31	24.4	0.3	54.24	0.43	21.36	0.51	90.91	3.06
6	13.12	100.19	10.93	15.53	1.02	88.07	1.87	5.01	0.13	11.12	0.48	1.35	26.09	0.34	54	0.69	19.91	0.8	88.46	17.31
7	13.58	98.88	12.5	6.61	1.14	97.17	3.85	5.09	0.16	12.06	0.63	1.41	29.04	0.26	53.18	0.41	17.77	0.33	91.09	3.48
8	14.95	97.8	14.21	5.15	1.72	97.06	3.6	4.24	0.19	13.31	0.81	1.56	33.97	0.49	51.06	0.33	14.97	0.67	89.27	3.42
9	14.77	99.26	15.91	6.72	0.97	97.13	4.5	4.37	0.2	14.48	0.9	1.71	39.11	0.56	47.66	1	13.23	1.47	85.94	3.23
10	17.48	97.55	17.92	3.16	1.75	98.78	3.17	4.7	0.48	15.09	1.84	2.1	46.06	0.72	43.75	0.79	10.19	0.48	81.04	6.75
11	12.76	98.17	19.38					3.91	0.08	19.98	0.78	1.73	54.54	0.96	38.46	0.4	7	1.05	90.22	1.3
12	12.95	97.84	20.87					3.62	0.2	21.04	1.57	1.9	60.76	0.55	33.51	0.44	5.73	0.77	87.15	2.11
13	15.15	96.55	22.61					3.52	0.16	23.92	1.24	1.77	66.22	0.87	28.88	0.87	4.9	0.16	87.79	2.85
14	16.87	93.66	24.55					3.48	0.14	23.83	1.26	2.02	71.7	0.61	24.69	0.39	3.61	0.66	84.72	2.49
15	14.89	95.92	26.26					3.64	0.29	24.37	1.55	2.04	73.93	2.24	23.62	2.14	2.45	0.29	79.75	2.61
16	14.75	98.08	27.96					3.42	0.15	23.58	1.28	2.29	77.32	0.65	20.6	0.67	2.08	0.12	104.5	3.05
17	13.99	97.3	29.57					3.44	0.19	23.2	1.5	2.39	78.31	0.98	19.36	0.71	2.34	0.33	74.76	2.12
18	14.67	96.46	31.25					(7.32)	5.6	12.63	6.58	9.24	78.64	3.34	20.15	3.87	1.2	1.04	49.93	11.18
19	14.92	95.24	32.97					3.39	0.51	21.13	3.73	2.97	81.8	0.77	17.27	0.82	0.93	0.93	70.98	2.93
20	12.3	98.87	34.38					(6.93)	4.72	11.03	6.1	10.52	83.44	3.36	15.36	4.09	1.2	1.94	58.11	11.79

Table G.4: Reaction conditions: Powder modified at 100°C (aborted series).

cycle number	X_{TEOS}(%)	integral carbon balance (%)	silica loading (Si/nm^2)	X_{TiPB}	σ	carbon balance (%)	σ	$X_{toluene}$	σ	p-xylene in product (%)	σ	[benzene]/[xylenes]	pS (%)	σ	mS (%)	σ	oS (%)	σ	carbon balance (%)	σ
-	-	-	-	73.88	2.74	99.18	4.36	8.69	0.07	10.14	0.02	1.11	21.37	0.08	54.99	0.24	23.64	0.18	97.78	1.41
1	17.74	96.8	2.04	72.47	3.49	100.36	2.9	7.7	0.06	10.2	0.07	1.12	21.64	0.08	54.88	0.36	23.47	0.43	96.5	1.51
2	20.64	79.67	4.41	34.59	5.62	98.72	6.88	7	0.04	10.02	0.18	1.15	21.58	0.14	55.36	0.4	23.06	0.43	92.47	1.77
3	18.72	93.51	6.56	22.06	6.14	98.03	8.2	6.29	0.12	10.15	0.39	1.21	22.41	0.13	54.9	0.38	22.68	0.28	93.21	2.98
4	18.96	92.14	8.74	15.85	7.13	98.43	10.7	6.19	0.25	9.74	0.74	1.4	23.31	0.16	55.02	0.35	21.67	0.43	86.98	4.27
5	18.57	92.78	10.87	12.06	7.03	97.13	5.21	5.98	0.57	10.73	1.36	1.32	24.66	0.12	55.57	0.3	19.77	0.28	87.34	5.66
6	16.8	94.38	(12.8)	(12.65)	(18.19)	(92.48)	(2.75)	(6.68)	(0.59)	(9.78)	(1.19)	(1.79)	(26.99)	(0.96)	(54.85)	(0.99)	(18.15)	(0.75)	(78.68)	(6.9)
6a				(-0.88)	(-259.07)	(103.7)	(2.24)	(6.95)	(1.5)	(9.43)	(3.75)	(2.34)	(29.36)	(6.37)	(52.48)	(7.13)	(18.16)	(0.87)	(78.17)	(12.24)
6b				(8.59)	(24.09)	(93.95)	(2.24)													
6c				(-22.89)	(-16.22)	(97.71)	(3.67)													

Table G.5: Reaction conditions: Powder modified at150°C.

cycle number	X_{TEOS}(%)	integral carbon balance (%)	silica loading (Si/nm^2)	X_{TiPB}	σ	carbon balance (%)	σ	$X_{toluene}$	σ	p-xylene in product (%)	σ	[benzene]/[xylenes]	pS (%)	σ	mS (%)	σ	oS (%)	σ	carbon balance (%)	σ
-	-	-	-	77.98	3.4	101.86	9.17	8.65	0.36	10.22	0.01	1.08	21.21	0.09	54.9	0.42	23.89	0.35	101.75	2.29
1	17.15	98.62	1.97	42.43	1.29	98.29	3.21	5.78	0.06	10.68	0.11	1.07	22.15	0.23	54.57	0.23	23.28	0.29	96.89	0.49
2	12.41	98.9	3.4	10.45	0.42	95.69	2.86	4.89	0.05	11.06	0.1	1.08	22.98	0.17	54.96	0.24	22.06	0.17	94.56	2.2
3	11.44	98.3	4.71	5.81	2.27	103.16	1.79	4.43	0.02	11.54	0.05	1.08	24.02	0.18	54.5	0.4	21.48	0.46	99.84	2.91
4	9.61	102.74	5.82	6.52	0.62	98.86	1.21	4.12	0.06	12.24	0.03	1.09	25.58	0.14	53.96	0.27	20.46	0.3	101.06	0.73
5	11.48	99.64	7.13	8.52	3.31	93.63	3.53	3.65	0.28	14.31	1.31	1.02	28.81	0.61	53	1.01	18.2	1.58	97.78	1.93
6	10.54	99.94	8.35	3.32	1.55	99.5	2.93	3.6	0.03	15.01	0.24	1.12	31.77	0.48	51.79	0.69	16.44	0.53	98.95	1.93
7	14.84	93.91	10.05					3.48	0.01	16.74	0.21	1.12	35.45	0.37	50.47	0.23	14.09	0.37	98.14	1.57
8	11.48	97.66	11.37					3.44	0.02	18.51	0.28	1.14	39.68	0.54	47.29	0.83	13.02	0.69	96.79	1.6
9	10.21	98.68	12.54					3.22	0.05	20.66	0.49	1.16	44.61	0.39	44.79	0.95	10.6	1.09	95.43	3.66
10	11.02	98.02	13.81					3.2	0.03	22.75	0.65	1.21	50.16	0.64	40.92	0.63	8.93	0.37	92.89	2.01
11	10.11	99.23	14.97					3.03	0.04	25.26	0.88	1.23	56.26	0.8	36.71	0.51	7.03	0.38	92.93	2.69
12	9.9	98.28	16.11					3.05	0.07	26.29	1.08	1.34	61.36	1.39	33.05	1.02	5.6	1.06	94.94	3.52
13	11.87	96.09	17.47					2.94	0.06	27.93	1.49	1.36	65.78	0.54	29.37	0.67	4.85	0.24	91.91	2.29
14	12.29	95.79	18.88					2.97	0.08	28.46	1.21	1.42	68.79	1.17	27.34	0.46	3.87	0.81	96.13	1.27
15	10.9	98.05	20.14					3.04	0.13	27.77	2.15	1.58	71.35	0.82	24.72	0.59	3.93	0.32	90.59	4.3
16	11.07	94.53	21.41					2.31	0.13	25.77	2.33	1.95	75.57	0.69	21.53	0.56	2.9	0.7	90.48	2.91
17	10.31	97.18	22.59					2.61	0.48	22.67	3.77	2.52	77.77	0.7	19.97	0.75	2.25	0.15	83.56	5.92
18	9.78	97.78	23.72					2.49	0.84	20.43	6.24	3.3	78.14	0.36	19.71	0.46	2.16	0.31	84.19	7.75
19	10.85	97.08	24.96					2.53	0.34	18.19	3.45	3.46	79.11	1.56	18.94	1.16	1.95	0.66	79.59	9.16
20	10.52	94.4	26.17					1.67	0.13	25.33	2.25	2.32	83.68	1.69	15.79	1.58	0.53	0.72	87.83	1.89
21	12.09	95.8	27.56					1.61	0.14	25.3	2.01	2.25	81.96	1.08	16.69	1.07	1.36	1.05	90.1	0.71
22	8.39	98.84	28.52					1.65	0.13	22.96	1.94	2.56	81.68	1.95	17.22	1.8	1.1	0.72	89.4	1.87
23	12.09	96.02	29.91					1.55	0.12	22.49	1.75	2.66	82.35	1.03	16.87	0.9	0.78	0.75	89.24	2.47
24	12.23	96.74	31.32					1.82	0.23	18.34	2.39	3.42	80.13	0.68	18.76	0.27	1.11	0.7	84.9	2.66
25	12.61	96.45	32.77					1.75	0.16	17.68	1.63	3.51	79.67	2.42	19.07	2.58	1.26	0.81	81.6	1.15

Table G.6: Reaction conditions: Powder modified at 200°C.

cycle number	X_{TEOS}(%)	integral carbon balance (%)	silica loading (Si/nm^2)	X_{TiPB}	σ	carbon balance (%)	σ	$X_{toluene}$	σ	p-xylene in product (%)	σ	[benzene]/[xylenes]	pS (%)	σ	mS (%)	σ	oS (%)	σ	carbon balance (%)	σ
-	-	-	-	82.86	1.16	96.79	1.75	9.79	0.13	10.21	0.04	1.09	21.36	0.12	55.18	0.48	23.46	0.53	100.73	1.91
1	30.31	100.65	3.48	11.91	2.82	103.74	2.14	3.95	0.05	11.05	0.34	1.08	23.03	0.7	54.78	0.48	22.18	1	103.48	1.35
2	19.09	99.34	5.68	3.77	2.18	99.59	2.61	3.13	0.03	11.44	0.08	1.09	23.93	0.29	54.98	0.68	21.09	0.42	96.89	0.72
3	15.89	100.02	7.5	3.36	0.95	98.8	1.29	2.87	0.03	12.06	0.22	1.09	25.19	0.48	55.51	0.74	19.3	0.89	99.62	1.42
4	12.55	102.49	8.94	4.23	0.82	94.26	0.61	2.73	0.02	12.91	0.06	1.11	27.22	0.14	54.68	0.79	18.1	0.76	102.78	1.16
5	14.22	95.81	10.58					2.5	0.04	14.7	0.08	1.12	31.16	0.58	53.62	0.87	15.23	0.5	103.02	2.14
6	12.33	98.82	11.99					2.43	0.05	16.1	0.41	1.11	34.02	0.6	52.74	0.4	13.25	0.3	100.88	1.33
7	10.77	99.87	13.23					2.4	0.04	18.71	0.45	1.16	40.6	1.49	49.64	1	9.76	2.41	101.97	3.64
8	11.35	98.47	14.53					2.23	0.07	21.38	0.86	1.23	47.52	0.68	43.42	0.67	9.06	0.34	100.94	1.95
9	12.98	96.21	16.03					2.22	0.12	22.86	1.49	1.32	52.75	1.2	39.71	0.93	7.54	0.42	100.97	3.09
10	11.31	97.54	17.33					2.23	0.17	24.53	2.11	1.35	57.35	1.42	36.6	1.32	6.05	0.42	99.33	3.14
11	10.7	98.17	18.56					1.85	0.32	24.22	4.19	1.69	64	1.17	31.29	0.58	4.71	0.66	95.72	4.4
12	9.22	101.32	19.61					1.82	0.55	24.56	6.77	2.04	69.42	0.74	27.3	0.7	3.28	0.22	94.35	7.83
13	8.86	100.15	20.63					1.82	0.65	24.56	7.26	2.21	72.08	1.41	25.14	1.23	2.79	0.72	94.06	7.09
14	10.24	98.5	21.81					1.11	0.03	31.92	0.69	1.26	73.31	0.62	24.01	0.76	2.68	0.14	99.44	1.2
15	6.9	101.8	22.6					1.92	0.98	21.98	8.63	3.27	76.62	2.49	21.62	2.03	1.76	1.21	91.1	10.23
16	12.85	95.52	24.08					2.2	1.68	21.17	10.41	4.05	73.59	0.94	24.04	1.29	2.37	0.44	89.29	14.44
17	8.91	100.13	25.1					2.34	2.02	19.79	10.69	5.49	80.34	1.76	18.87	1.99	0.79	1.1	86.98	16.49
18	11.46	97.23	26.42					2.23	1.89	19.58	10.44	5.86	81.51	2.6	18.49	2.6	0	0	87.69	15.99
19	11.15	97.8	27.7					2.72	2.04	16.61	10.67	6.89	81.11	4.14	18.89	4.14	0	0	79.71	15.68
20	14.35	94.26	29.35					3.1	2.31	15.82	9.87	6.14	79.72	5.41	19.51	5.03	0.77	1.71	79.07	17.18

Table G.7: Reaction conditions: Powder modified at 300°C.

cycle number	X_{TEOS}(%)	integral carbon balance (%)	silica loading (Si/nm^2)	X_{TiPB}	σ	carbon balance (%)	σ	$X_{toluene}$	σ	p-xylene in product (%)	σ	[benzene]/[xylenes]	pS (%)	σ	mS (%)	σ	oS (%)	σ	carbon balance (%)	σ
-	-	-	-	73.05	1.83	97.63	2.78	7.4	0.1	10.22	0.05	1.12	21.65	0.22	55	0.48	23.35	0.61	101.14	1.37
1	68.59	92.27	7.88	13.79	2.24	97.17	3.34	3.69	0.06	11.57	0.06	1.13	24.68	0.22	54.52	0.79	20.81	0.58	101.1	1.75
2	42.01	99.18	12.71	5.08	1.66	99.86	1.26	2.82	0.05	14.76	0.17	1.15	31.74	0.35	52.46	1.14	15.8	1.4	99.84	1.5
3	37.9	90.54	17.06	4.63	2.03	98.47	1.94	2.48	0.04	19.9	0.28	1.14	42.48	0.19	45.88	0.29	11.64	0.21	100.4	1.39
4	29.8	100.81	20.49	-0.17	0.99	101.97	3.6	1.85	0.04	27.26	0.23	1.15	58.81	0.38	34.37	0.58	6.82	0.47	101.07	0.58
5	34.26	100.53	24.42					1.56	0.08	31.54	0.94	1.18	68.95	1.39	26.32	1.24	4.73	1.5	111.49	1.86
6	26.91	98.72	27.51					1.38	0.04	33.74	0.76	1.15	73.32	0.76	23.83	0.68	2.85	0.15	98.36	1.13
7	22.39	99.46	30.09					1.24	0.03	34.9	0.66	1.16	76.58	0.64	21.41	0.58	2.01	0.72	101.75	1.51
8	20.9	98.02	32.49					1.11	0.02	35.84	0.64	1.31	83.3	0.82	16	1.2	0.7	0.69	99.57	0.91
9	24.36	92.41	35.29					0.97	0.04	36.72	1.66	1.31	85.38	1.62	14.62	1.62	0	0	100.49	0.71
10	16.46	99.89	37.18					0.79	0.02	37.36	1.79	1.37	89.6	3.78	10.4	3.78	0	0	98.81	1
11	16.52	98.01	39.08					0.75	0.02	36.11	1.74	1.41	88	0.19	12	0.19	0	0	98.09	1.09
12	14.48	98.3	40.74					0.63	0.01	36.01	0.63	1.34	86.6	1.76	13.4	1.76	0	0	99.76	1.24
13	20.39	91.11	43.08					0.54	0.01	38.25	3	1.41	94.81	6.3	5.19	6.3	0	0	100.4	1.12
14	15.51	96.13	44.86					0.49	0.02	34.44	0.63	1.41	85.92	0.87	14.08	0.87	0	0	101.18	0.9
15	14.87	96.59	46.57					0.46	0.03	31.13	2.3	1.62	84.92	1.38	15.08	1.38	0	0	99.77	2.12
16	12.86	97.18	48.05					0.42	0.01	31.47	1.3	1.47	81.46	0.5	18.54	0.5	0	0	99.45	0.55
17	12.84	96.49	49.53					0.38	0.01	30.81	1.26	1.39	79.1	1.01	20.9	1.01	0	0	100.16	0.54
18	12.57	95.89	50.97					0.33	0.02	27.68	2.23	2.54	100	0	0	0	0	0	99.66	1.24

Table G.8: Reaction conditions: Powder modified at 400°C.

cycle number	X_{TEOS}(%)	integral carbon balance (%)	silica loading (Si/nm^2)	X_{TPB}	σ	carbon balance (%)	σ	$X_{toluene}$	σ	p-xylene in product (%)	σ	[benzene]/[xylenes]	pS (%)	σ	mS (%)	σ	oS (%)	σ	carbon balance (%)	σ
-	-	-	-	84.43	1.98	101.81	3.69	8.89	0.13	10.32	0.08	1.09	21.54	0.12	55	0.26	23.45	0.32	99.14	0.62
1	100	101.99	11.49	47.33	1.19	93.98	1.02	6.97	0.32	10.32	0.04	1.09	21.58	0.07	54.81	0.42	23.61	0.46	98.68	3.66
2	98.96	105.1	22.86	17.47	1.31	94.84	1.09	4.58	0.24	11.69	0.26	1.13	24.93	0.32	55.08	0.42	19.99	0.51	100.46	4.5
3	84.54	103.61	32.57	4.84	1.24	96.01	1.15	2.88	0.06	21.17	0.34	1.2	46.65	0.47	42.13	0.44	11.22	0.72	98.92	1.46
4	71.12	102.84	40.75	2.74	0.51	98.33	0.71	2.17	0.02	30.75	0.06	1.22	68.51	0.3	27.07	0.5	4.42	0.45	106.42	17.29
5	87.9	96.43	50.85					0.71	0.02	34.44	0.51	1.35	82.06	1.59	16.22	0.45	1.72	1.28	99.32	1.68
6	59.64	98.35	57.7					0.44	0.02	32.67	0.78	1.54	85.35	3.8	14.57	3.68	0.08	0.19	100.6	1.24
7	47.6	93.86	63.17					0.31	0.01	30.25	0.9	1.46	79.52	2.66	18.59	1.41	1.9	2.6	99.45	1.6
8	38.58	97.37	67.6																	
9	32.63	97.7	71.35																	
10	29.11	98.4	74.7																	
11	26.83	97.6	77.78																	
12	26.83	97.48	80.86					0.11	0.04	21.69	5.58	1.1	57.12	0.91	42.88	0.91	0	0	99.86	2.82

Table G.9: Reaction conditions: Pellets modified at 100°C.

cycle number	X_{TEOS}(%)	integral carbon balance (%)	silica loading (Si/nm^2)	X_{TiPB}	σ	carbon balance (%)	σ	$X_{toluene}$	σ	p-xylene in product (%)	σ	[benzene]/[xylenes]	pS (%)	σ	mS (%)	σ	oS (%)	σ	carbon balance (%)	σ
-	-	-	-	97.51	0.79	80.02	1.31	15.15	1.5	10.31	0.04	1.13	21.97	0.39	55.9	0.36	22.12	0.7	102.36	1.8
1	17.62	95.26	2.14	95.91	0.7	82.26	3.2	14.29	0.73	10.36	0.08	1.12	21.99	0.7	56.08	0.5	21.93	1.19	103.68	1.9
2	16.95	94.78	4.2	82.18	2.5	88.64	3.11	13.03	1.08	10.34	0.06	1.12	21.99	0.61	55.91	0.48	22.1	1.45	238.34	22.89
3	17.52	93.69	6.33	57.45	5.84	98.03	3.2	13.41	0.68	10.44	0.04	1.11	22.05	0.15	55.83	0.34	22.12	0.89	102.81	2.89
4	15.83	95.43	8.26	35.8	9.08	96.63	0.66	12.81	0.8	10.48	0.06	1.12	22.26	1.17	56.1	1.44	21.64	4.72	102.41	2.91
5	16	94.6	10.2	21.85	8.67	97.93	1.08	12.58	2.37	10.54	0.05	1.12	22.3	1.02	55.86	0.67	21.84	2	103.01	3.87
6	16.83	93.72	12.25	9.35	9.52	101.41	1.75	12.44	1.09	10.6	0.03	1.12	22.42	0.4	55.8	0.51	21.78	1.56	102.67	3.19
7	14.74	95.1	14.04	5.02	3.46	101.38	2.51	12.26	0.8	10.63	0.01	1.12	22.55	0.44	55.74	0.17	21.71	0.84	105.43	1.93
8	14	95.91	15.74	9.4	2.27	94.75	2.17	12.05	1.48	10.66	0.04	1.14	22.82	0.68	55.58	0.4	21.6	1.07	103.63	1.58
9	14.71	95.04	17.53	2.36	3.39	101.27	3.6	11.83	0.76	11.11	0.09	1.13	23.71	1.31	56.03	2.09	20.26	7.13	102.79	2.49
10	13.41	96.08	19.16	-0.07	1.94	102.23	1.65	11.92	1.01	11.8	0.07	1.13	25.1	0.65	56.63	0.35	18.27	1.02	107.03	8.34
11	11.51	97.73	20.56					11.7	1.84	12.78	0.13	1.14	27.38	2.72	57.37	0.39	15.26	4.17	211.85	34.81
12	13.22	96.1	22.17					12.21	0.68	14.46	0.17	1.12	30.67	0.96	56.17	0.59	13.16	2.82	105.22	2.82
13	10.88	98.08	23.5					11.79	1.2	17.14	0.12	1.11	36.18	0.57	53.41	0.6	10.41	1.65	106.11	3.35
14	11.05	97.41	24.84					11.49	1.11	20.72	0.23	1.12	43.93	0.48	47.97	0.78	8.1	2.91	103.17	3.51
15	9.63	98.76	26.01					11.42	1.26	24.48	0.34	1.12	51.84	1.09	41.8	1.51	6.36	3.49	100.35	2.92
16	12.56	94.67	27.54					11.42	1.24	27.97	0.28	1.12	59.23	0.95	35.93	1.54	4.84	6.56	104.32	2.57
17	11.58	96.47	28.95					11.3	1.85	31.02	0.4	1.12	65.7	0.93	30.56	1.45	3.74	5.07	103.36	3.12
18	11.13	96.41	30.3					11.52	2.34	33.07	0.49	1.12	70.18	1.4	26.89	3.31	2.94	4.48	111.36	16.03
19	10.61	96.87	31.59					11.53	2.01	34.47	0.18	1.12	73.25	0.7	24.2	1.95	2.55	8.53	102.65	3.69
20	9.18	98.78	32.71					11.04	0.88	35.91	0.39	1.11	75.64	0.95	22.27	3	2.1	9.65	103.3	2.81
21	11.02	95.94	34.05					10.71	2.1	36.94	0.49	1.13	78.66	1.08	19.78	3.66	1.56	19.13	100.82	3.67
22	11.36	96.16	35.43					10.48	2.31	37.57	0.1	1.13	79.88	0.85	18.72	3.53	1.4	12.61	100.44	3.91
23	8.98	98.57	36.52					10.17	2.58	37.78	0.41	1.16	81.72	0.92	16.97	3.12	1.3	19.4	105.18	1.71
24	11.58	96.01	37.93					9.64	2.43	38.07	0.3	1.18	82.94	0.68	15.88	3.51	1.18	11.9	97.6	2.06
25	12.33	94.19	39.43					8.8	3.29	37.85	0.4	1.21	83.68	0.79	15.39	4.11	0.93	15.79	99.92	3.27
26	5.36	107.85	40.08					7.84	3.32	37.62	0.21	1.25	84.69	0.67	14.71	4.74	0.61	68.31	100.74	2.68
27	8.61	96.55	41.13					6.97	2.35	36.94	0.5	1.31	85.16	0.97	14.29	4.32	0.55	61.79	100.61	2.92
28	10.8	94.25	42.44					5.81	4.15	36.32	0.41	1.42	87.83	0.92	11.7	7.85	0.47	124.14	109.22	6.24
29	10.51	94.33	43.72					5.08	2.85	35.88	0.11	1.44	87.45	0.55	11.82	4.44	0.73	19.84	111.45	0.86
30	11.42	93.21	45.11					4.44	1.85	35.89	0.02	1.46	88.29	0.11	11.28	2.62	0.44	86.65	101.83	1.37
31	9.82	94.07	46.3					4.02	1.55	35.48	0.05	1.46	87.56	0.43	11.77	3.78	0.67	9.77	109.31	0.47
32	9.82	94.38	47.5					3.59	0.58	36.86	2.73	1.48	91.47	6.06	7.86	77.43	0.68	98.43	102.87	3
33	9.96	94.45	48.71					3.29	2.16	35.51	0.1	1.51	89.04	1.11	10.96	9.02	0	0	100.2	2.13

Table G.10: Reaction conditions: Pellets modified at 200°C.

cycle number	X_{TEOS}(%)	integral carbon balance (%)	silica loading (Si/nm^2)	X_{TiPB}	σ	carbon balance (%)	σ	$X_{toluene}$	σ	p-xylene in product (%)	σ	[benzene]/[xylenes]	pS (%)	σ	mS (%)	σ	oS (%)	σ	carbon balance (%)	σ
-	-	-	-	94.46	2.29	78.68	3.73	14.29	0.49	10.23	0.02	1.08	21.33	0.17	55.87	0.15	22.81	0.42	101.85	2.77
1	47.52	96.19	5.78	9.82	50.41	99.9	2.55	6.03	0.47	10.44	0.04	1.09	21.87	0.35	55.68	0.36	22.45	1.21	59.84	1.66
2	20.33	97.31	8.25	6.85	45.52	94.83	3.63	5.66	1.92	10.35	0.03	1.14	22.16	0.94	55.48	1.53	22.36	2.89	109.57	3.51
3	17.23	96.9	10.35	2.26	209.05	98.57	4.63	5.19	0.77	10.34	0.06	1.13	22.02	0.84	55.75	0.6	22.24	2.07	109.57	3.51
4	17.55	94.34	12.48					4.7	0.47	10.54	0.03	1.11	22.23	0.27	55.69	0.34	22.08	0.87	109.57	3.51

Table G.11: Reaction conditions: Pellets modified at 200°C (reproducibility run).

cycle number	X_{TEOS}(%)	integral carbon balance (%)	silica loading (Si/nm^2)	X_{TiPB}	σ	carbon balance (%)	σ	$X_{toluene}$	σ	p-xylene in product (%)	σ	[benzene]/[xylenes]	pS (%)	σ	mS (%)	σ	oS (%)	σ	carbon balance (%)	σ
-	-	-	-	96.97	0.9	86.48	1.99	12.97	2.09	10.44	0.04	1.1	21.91	0.21	55.85	0.63	22.23	1.8	101.3	1.48
1	59.66	102.92	7.25	12.18	32.92	94.62	3.12	4.65	1.87	10.31	0.07	1.19	22.62	0.95	55.81	1.09	21.57	3.27	104.21	3.09
2	21.11	102.11	9.82	2.27	106.09	101.21	2.58	3.97	3.6	10.37	0.14	1.18	22.6	1.35	56.3	0.75	21.1	2.73	100.57	1.3
3	19.18	99.29	12.15	5.14	37.65	96.57	1.19	3.47	1.49	10.47	0.17	1.19	22.95	0.39	56.08	1.14	20.98	2.93	98.46	2.78
4	18.37	98.25	14.39					3.25	1.53	10.63	0.13	1.18	23.18	1.17	56.17	1.89	20.65	5.92	100.4	1.75
5	17.51	98.48	16.52					2.99	1.82	10.85	0.11	1.19	23.77	0.91	56.2	1.04	20.03	3.79	100.69	3.75
6	17.88	96.57	18.69					(6.53)	2.09	10.59	0.13	1.17	22.97	0.77	55.93	0.96	21.1	2.58	100.16	2.11

Table G.12: Reaction data of 1,3,5-TiPB-cracking over unmodified pellet samples (reaction temperature = 210°C).

runtime	X, run 1	C-bal, run 1	X, run 2	C-bal, run 2
(min)	%	%	%	%
5	100	5.83	100	16.72
10	100	30.91	100	55.72
15	100	71.43	99.23	81.2
20	98.71	85.73	98.16	86.59
25	97.49	88.69	97.46	83.67
35	96.57	89.68	96.68	87.76
45	96.14	85.04	96.69	86.39
55	95.01	86.53	95.88	87.98
65	94.8	86.36	96	87.83
75	94.24	87.37		
85	93.46	90.7		
95	92.97	92.53		
105	93.27	90.62		
115	93.47	89.88		
145	91.77	92.09		
150	92.67	91.54		
175	90.66	91.13		
180	90.33	94.65		
195	91.06	89.83		
205	90.46	91.1		
210	90.01	93.01		
235	88.59	95.27		
240	89.54	93.25		
265	89.06	93.92		
270	88.46	96.36		
275	89.52	92.7		
295	89.33	92.22		
300	87.59	96.29		
305	88.41	95.66		

Table G.13: Reaction data of kinetic studies of toluene disproportionation over powder samples (toluene partial pressure = 13.4 kPa).

T	sample number	catalyst mass	carrier gas flow	reactor pressure	saturator pressure	pS	mS	oS	$X_{toluene}$	[benzene] / [xylenes]
°C		g	ml/min	kPa	kPa	%	%	%	%	
unmodified powder sample										
450	1	0.51	49	150.2	157	22.05	56.25	21.7	1.59	1.13
	2	0.51	49	150.2	156.7	22.86	54.47	22.67	1.45	1.09
	3	0.51	49	150.3	157	22.75	55.22	22.03	1.43	1.07
	4	0.51	93	149.9	162.6	23.23	56.18	20.59	0.83	0.98
	5	0.51	93	150	162.4	23.32	56.03	20.65	0.81	0.99
	6	0.51	93	150	162.5	23.35	54.4	22.25	0.81	0.94
	7	0.51	127	149.8	169.1	23.39	54.48	22.13	0.6	0.88
	8	0.51	127	149.8	168.8	24.58	55.3	20.12	0.59	0.9
	9	0.51	127	149.7	168.9	24.35	55.99	19.67	0.6	0.9
	10	0.51	93	149.9	162.4	24.02	53.68	22.3	0.79	0.96
	11	0.51	96	150	162.5	22.97	53.74	23.29	0.8	0.99
	12	0.51	93	149.9	162.4	23.57	55.55	20.88	0.78	1
	13	0.51	49	149.9	156	22.28	54.94	22.79	1.35	1.02
	14	0.51	49	149.8	156.2	24.31	54.9	20.79	1.33	1.03
	15	0.51	49	149.8	155.8	21.76	53.72	24.52	1.34	1.02
	16	0.51	14	149.7	151	21.37	55.9	22.73	3.77	1.04
	17	0.51	14	149.7	150.8	21.04	56.32	22.63	3.78	1.03
	18	0.51	14	149.8	150.2	21.51	55.46	23.03	3.73	1.05
	19	0.51	49	149.7	155.7	21.86	54.33	23.8	1.31	1
	20	0.51	49	149.7	155.9	22.58	55.24	22.18	1.29	1.03
	21	0.51	49	149.7	156	22.22	56.23	21.55	1.33	0.99
500	1	0.51	49	150.2	157.1	21.86	55.47	22.67	3.51	1.09
	2	0.51	49	150.4	157.2	21.89	55.14	22.97	3.52	1.05
	3	0.51	49	150.5	157.3	21.44	54.18	24.37	3.49	1.05
	4	0.51	93	150.2	163.3	23.4	54.6	22	1.98	1.05
	5	0.51	93	150.1	162.9	21.88	55.03	23.09	2	1
	6	0.51	93	150.1	163	22.65	54.76	22.59	1.99	1
	7	0.51	127	150.2	169.5	22.89	53.2	23.91	1.47	1
	8	0.51	127	150.2	169.3	23.46	54.75	21.79	1.46	0.99
	9	0.51	127	150.1	169	23.29	54.55	22.16	1.51	0.95
	10	0.51	93	150.2	163.3	22.76	55.45	21.78	2.08	1.02
	11	0.51	96	150.2	163.2	22.45	55.27	22.28	2.08	1
	12	0.51	93	150.2	163.2	22.53	55.89	21.58	2.09	1.02
	13	0.51	49	150.2	157.3	21.74	56.21	22.05	3.47	1
	14	0.51	49	150.2	157.2	21.7	55.21	23.09	3.5	1.02
	15	0.51	49	150.2	156.9	21.92	55.11	22.96	3.51	1.03
	16	0.51	14	150.1	151.9	20.99	55.61	23.41	10.08	1.05

Table G.13: continued

T (°C)		mass	flow	p_r	p_sat	p-S	m-S	o-S	X-Tol	B/X
	17	0.51	14	150.2	152.1	20.7	55.72	23.58	9.92	1.05
	18	0.51	14	150.3	152	21	55.57	23.43	9.96	1.06
	19	0.51	49	150.2	157	20.41	57.14	22.45	3.74	1.04
	20	0.51	49	150.1	157.1	21.71	55.69	22.6	3.56	1.03
	21	0.51	49	150.2	157.1	21.86	55.45	22.69	3.57	1.02
550	1	0.51	49	149.8	157.7	21.2	55.11	23.68	9.67	1.12
	2	0.51	49	149.8	157.7	21.15	55.05	23.8	9.42	1.09
	3	0.51	49	149.8	157.7	21.34	54.39	24.27	9.29	1.09
	4	0.51	93	149.6	163.5	22	55.39	22.62	5.58	1.09
	5	0.51	93	149.7	163.1	21.95	54.9	23.15	5.59	1.08
	6	0.51	93	149.7	162.8	21.75	54.66	23.58	5.9	1.02
	7	0.51	127	149.7	171.1	22.59	55.35	22.05	3.61	1.08
	8	0.51	127	149.9	172	22.18	54.58	23.23	3.53	1.07
	9	0.51	127	149.9	171.9	22.71	54.1	23.19	3.47	1.07
	10	0.51	93	149.9	164.6	21.81	55.07	23.12	4.99	1.05
	11	0.51	96	149.6	164.3	21.77	55.12	23.11	5	1.06
	12	0.51	93	149.6	164.3	22.05	55.27	22.68	5.01	1.07
	13	0.51	49	149.9	158.6	21.09	55.5	23.42	8.53	1.06
	14	0.51	49	149.9	158.5	21.18	54.66	24.17	8.5	1.07
	15	0.51	49	150	158.4	21.23	54.89	23.87	8.51	1.07
	16	0.51	14	149.7	152.9	20.4	55.25	24.35	21.16	1.14
	17	0.51	14	149.8	153	20.71	55.18	24.11	21.19	1.13
	18	0.51	14	149.6	152.9	20.6	55.01	24.39	21.1	1.12
	19	0.51	49	149.8	158.6	21.22	55.07	23.71	8.44	1.07
	20	0.51	49	149.7	158.5	21.26	55.15	23.6	8.41	1.07
	21	0.51	49	149.8	158.5	21.4	55.07	23.53	8.41	1.08
reduced catalyst mass of powder sample										
550	1	0.11	49	149.9	164.6	27.43	50.86	21.72	1.12	1.93
	2	0.11	49	152.2	167.4	25.57	51.82	22.61	3.47	9.17
	3	0.11	49	151.2	165.6	27.67	50.83	21.5	2.02	5.07
	4	0.11	93	162.5	163.5	29.34	51.57	19.09	1.14	3.52
	5	0.11	93	162.7	163.6	27.47	52.76	19.77	1.02	2.87
	6	0.11	93	162.8	163.7	28.29	52.63	19.08	0.96	2.43
	7	0.11	127	146.7	147.3	27.77	53.7	18.52	1.19	2.25
	8	0.11	127	146.7	147.3	27.12	51.79	21.08	1.11	2.07
	9	0.11	127	146.9	147.5	26.04	49.25	24.71	1.09	1.98
	10	0.11	93	129	129.3	25.06	52.72	22.23	1.64	2.14
	11	0.11	96	129.2	129.4	26.03	53.01	20.96	1.63	2
	12	0.11	93	129.3	129.6	25.04	53.04	21.92	1.65	2.01
	13	0.11	49	151.1	149.9	25.16	54.04	20.8	1.91	1.99
	14	0.11	49	150.5	158.8	25.85	52.28	21.87	1.99	2.03
	15	0.11	49	150.6	159	25.23	52.87	21.9	1.95	2.01
	16	0.11	14	150.6	159.2	24.4	53.75	21.85	2	1.98
	17	0.11	14	149.6	161	27.77	53.53	18.7	1.06	1.97
	18	0.11	14	153.9	164.8	28.52	51.7	19.78	1.07	2.07

Table G.13: continued

T (°C)		mass	flow	p_r	$p_s at$	p-S	m-S	o-S	X-Tol	B/X
modified powder sample 15 cycles at 150°C										
450	1	0.51	49	148.7	160.1	77.79	19.22	2.99	0.74	1.52
	2	0.51	49	148.8	160.3	80.54	16.93	2.53	0.63	1.41
	3	0.51	49	148.8	160.2	78.46	18.45	3.09	0.59	1.31
	4	0.51	93	148.9	169.8	79.75	16.99	3.25	0.35	1.26
	5	0.51	93	148.8	169.5	84.44	15.56	0	0.32	1.32
	6	0.51	93	148.9	169.3	85.91	14.09	0	0.29	1.48
	7	0.51	127	148.8	179.5	82.09	17.91	0	0.24	1.06
	8	0.51	127	149	179	77.44	22.56	0	0.23	1.14
	9	0.51	127	149.1	179.1	78.72	21.28	0	0.22	1.18
	10	0.51	93	148.7	168.6	74.54	16.01	9.46	0.3	1.15
	11	0.51	96	148.9	168.6	81.59	18.41	0	0.29	1.23
	12	0.51	93	148.5	168.4	78.99	21.01	0	0.3	1.2
	13	0.51	49	148.9	160.2	77.67	19.24	3.09	0.47	1.2
	14	0.51	49	149	160.3	77.45	18.17	4.38	0.47	1.21
	15	0.51	49	148.9	160.2	77.21	22.79	0	0.48	1.15
	16	0.51	14	148.8	152.8	70.04	25.93	4.04	1.22	1.26
	17	0.51	14	148.7	152.9	69.22	27.08	3.7	1.24	1.21
	18	0.51	14	148.7	152.8	67.34	27.51	5.16	1.27	1.19
	19	0.51	49	148.7	160.2	78.34	19.39	2.27	0.46	1.15
	20	0.51	49	148.7	160.1	76.98	21.45	1.57	0.47	1.11
	21	0.51	49	148.7	160.2	80.55	19.45	0	0.45	1.21
500	1	0.51	49	149.6	160.8	74.63	23.28	2.09	1.59	1.33
	2	0.51	49	149.8	160.8	73.93	23.41	2.66	1.41	1.14
	3	0.51	49	149.7	160.8	75.25	22.42	2.33	1.22	1.22
	4	0.51	93	149.5	169.9	77.02	19.91	3.07	0.81	1.1
	5	0.51	93	149.4	169.9	64.43	17.78	17.78	0.85	0.9
	6	0.51	93	149.4	169.8	75.95	21.1	2.96	0.78	1.06
	7	0.51	127	149.6	179.8	52.26	11.76	35.98	0.67	0.68
	8	0.51	127	149.6	179.9	77.37	19.22	3.41	0.52	1.06
	9	0.51	127	149.7	179.9	83.37	16.63	0	0.5	1.16
	10	0.51	93	149.5	169.7	77.7	22.3	0	0.73	1.07
	11	0.51	96	149.4	169.3	77.76	22.24	0	0.73	1.1
	12	0.51	93	149.5	169.6	78.72	21.28	0	0.73	1.08
	13	0.51	49	149.6	160.3	62.49	19.87	17.64	1.34	0.94
	14	0.51	49	149.5	160.5	74.28	22.39	3.32	1.22	1.17
	15	0.51	49	149.5	160.5	73.64	24.45	1.91	1.24	1.16
	16	0.51	14	149.5	153.2	60.01	32.89	7.1	5.5	3.8
	17	0.51	14	149.5	153.1	59.05	32.71	8.24	13.14	19.07
	18	0.51	14	149.6	153.3	53.64	37.22	9.14	28.83	83.57
	19	0.51	49	149.5	160.7	74.1	22.91	3	1.29	1.28
	20	0.51	49	149.6	160.5	78.53	20.2	1.26	1.19	1.3
	21	0.51	49	149.7	160.8	75.22	20.92	3.86	1.24	1.2
550	1	0.51	49	149.3	161.1	70.69	26.34	2.97	3.11	1.27
	2	0.51	49	149.4	160.9	69.6	27.06	3.34	3.04	1.3

Table G.13: continued

T (°C)		mass	flow	p_r	$p_s at$	p-S	m-S	o-S	X-Tol	B/X
	3	0.51	49	149.7	161.1	70.85	25.95	3.2	3.99	2.94
	4	0.51	93	149.1	169.9	78.68	19.14	2.18	1.93	1.83
	5	0.51	93	149.4	170	79.3	18.45	2.25	1.78	1.56
	6	0.51	93	149.6	170.2	75.06	23.34	1.61	1.77	1.36
	7	0.51	127	152.6	182.6	80.29	18.98	0.73	1.2	1.34
	8	0.51	127	152.3	182	73.82	24.43	1.75	1.14	1.39
	9	0.51	127	152.5	182.4	78.72	18.99	2.29	1.19	1.26
	10	0.51	93	149.2	169.6	43.27	55.36	1.37	2.2	0.7
	11	0.51	96	149.4	169.5	75.14	22.02	2.85	1.66	1.18
	12	0.51	93	149.4	169.7	75.76	21.92	2.32	1.65	1.21
	13	0.51	49	149.5	160.1	70.43	26.18	3.38	2.88	1.27
	14	0.51	49	149.7	160.7	68.17	28.26	3.57	2.88	1.2
	15	0.51	49	149.6	160.5	70.81	25.85	3.34	2.82	1.25
	16	0.51	14	149.2	153.2	76.7	7.82	15.48	6.4	3.29
	17	0.51	14	149.2	153.3	54.13	38.95	6.92	8.06	1.55
	18	0.51	14	149.1	153.5	54.47	38.47	7.06	7.89	1.48
	19	0.51	49	149.2	160.9	70.36	26.04	3.6	2.75	1.22
	20	0.51	49	149.2	160.8	69.19	27.49	3.32	2.77	1.18
	21	0.51	49	149.1	160.9	69.47	27.47	3.05	2.78	1.2

Table G.14: Reaction data of toluene disproportionation over pellet samples (toluene partial pressure = 13.4 kPa, reaction temperature = 450°C).

run time	flow rate	pS (%)	mS (%)	oS (%)	$X_{toluene}$ (%)	[benzene] / [xylenes]
min	ml/min	%	%	%	%	%
unmodified pellet sample						
5	12	21.3	55.76	22.94	14.95	1.1
15		21.22	55.99	22.8	14.66	1.08
25		21.32	55.98	22.7	14.38	1.08
35		21.27	55.86	22.87	14.3	1.08
45		21.35	55.85	22.81	14.27	1.09
55		21.37	55.9	22.73	14.32	1.09
65		21.32	55.74	22.94	14.19	1.09
75		21.26	55.84	22.91	14.07	1.07
85		21.35	55.92	22.73	14.12	1.08
95		21.23	55.97	22.8	14.1	1.08
105		21.34	55.85	22.81	14.05	1.08
115		21.33	55.71	22.96	14.07	1.08
125		21.32	55.96	22.71	14.08	1.09
155		21.19	56.14	22.67	13.92	1.07
165		21.12	56.29	22.59	13.73	1.07
175		21.31	55.84	22.85	13.73	1.07
185		21.24	55.81	22.95	13.84	1.07
195	24.8	21.51	55.8	22.69	7.47	1.06
205		21.51	55.91	22.58	7.42	1.07
215		21.59	55.87	22.53	7.43	1.08
225		21.49	55.92	22.59	7.43	1.06
235	48.5	21.59	55.74	22.68	4.23	1.07
245		21.54	55.81	22.65	4.26	1.07
255		21.56	55.75	22.69	3.7	0.78
265		21.61	55.7	22.69	4.24	1.06
unmodified pellet sample; repeat						
5	12	21.18	55.7	23.12	15.95	1.33
15		21.28	55.93	22.79	15.52	1.3
25		21.26	56.12	22.61	15.52	1.21
35		21.27	55.76	22.97	14.98	1.25
45		20.92	56.56	22.52	14.83	1.25
55		21.36	55.74	22.9	14.57	1.23
65		21.37	55.8	22.82	14.44	1.21
75		21.32	55.94	22.74	14.29	1.19
85	24.8	21.32	56.02	22.66	7.8	1.18
95		21	56.58	22.43	7.7	1.14

Table G.14: continued

min	ml/min	%	%	%	%	%
105		21.53	55.76	22.71	7.61	1.14
115		21.43	55.92	22.65	7.56	1.13
125	48.5	21.67	55.58	22.75	4.34	1.14
135		21.5	55.95	22.55	4.26	1.12
145		21.44	55.96	22.6	4.33	1.1
155		21.58	55.77	22.65	4.31	1.11
modified sample, 20 CVD cycles at 100°C						
5	12	75.49	22.48	2.03	11.36	1.09
15		75.27	22.69	2.04	11.33	1.08
25		74.76	22.84	2.4	11.19	1.08
35		75.18	22.98	1.84	11.05	1.12
45		75.52	22.34	2.14	11.03	1.12
55		76.42	21.52	2.06	10.97	1.12
65		76.31	21.65	2.04	10.95	1.1
75		91.52	5.97	2.51	9.6	1.57
85		76.49	21.45	2.06	10.85	1.09
95		76.82	21.24	1.93	10.84	1.09
105		76.13	21.66	2.21	10.84	1.08
115		75.96	21.76	2.28	10.75	1.09
125		76.52	21.63	1.85	10.78	1.08
135		76.37	21.68	1.95	10.75	1.11
145		76.55	21.24	2.21	10.69	1.1
150		77.36	21.51	1.13	10.52	1.07
155		77.39	20.51	2.1	10.67	1.1
165		77.34	20.77	1.89	10.71	1.09
175		76.68	21.41	1.91	10.73	1.09
185		77.81	20.13	2.06	10.56	1.09
196	24.8	86.4	12.98	0.62	5.59	1.08
205		86.44	12.96	0.6	5.65	1.09
215		86.27	13.73	0	5.6	1.06
225		85.91	14.09	0	5.68	1.06
236	48.5	100	0	0	2.96	1.28
245		91.3	8.7	0	3.28	1.09
255		95.99	4.01	0	3.29	1.1
265		96.19	3.81	0	3.26	1.09

Table G.15: Linear velocities for empty reactor at reaction temperature

	flow rate carrier gas ml/min	saturator pressure kPa	reactor temperature °C	reactor pressure kPa	linear velocity cm/s
CVD: powder	92	160	50	150	1.57
	92	160	100	150	1.81
	92	160	150	150	2.06
	92	160	200	150	2.3
	92	160	300	150	2.78
	92	160	400	150	3.27
CVD: pellets	100	160	100	150	1.97
	300	170	200	160	7.02
TiPB-cracking: powder	92	160	270	150	2.63
TiPB-cracking: pellets	100	160	210	150	2.54
TDP: unmodified powder	50	160	550	150	2.34
TDP: unmodified pellets	10	120	450	102	0.62
Kinetic study TDP:	15	151	450	150	0.62
Unmodified powder	49	160	450	150	2.02
	93	160	450	150	3.83
	127	170	450	150	5.2
	15	151	500	150	0.66
	49	160	500	150	2.16
	93	160	500	150	4.09
	127	170	500	150	5.56
	15	151	550	150	0.71
	49	160	550	150	2.29
	93	160	550	150	4.35
	127	170	550	150	5.92
Kinetic study TDP:	15	151	550	150	0.71
Unmodified powder	49	160	550	150	2.29
(0.1 g catalyst)	93	165	550	150	4.34
	127	165	550	162	5.49
Kinetic study TDP:	15	153	450	150	0.62
Modified powder	49	160	450	150	2.02
	93	170	450	150	3.81
	127	180	450	150	5.18
	15	153	500	150	0.66
	49	160	500	150	2.16
	93	170	500	150	4.07
	127	180	500	150	5.53
	15	153	550	150	0.71
	49	160	550	150	2.29
	93	170	550	150	4.33
	127	180	550	150	5.89
Kinetic study TDP:	10	120	450	103	0.62
Modified pellets	21	120	450	105	1.27
	40	120	450	110	2.31
Calcination: powder	100	100	550	170	3.55
Calcination: pellets	300	100	550	180	10.81

Table G.16: Analysis of p-xylene isomerisation over CVD modified silica gel (mass of silica gel: 0.9020 g; surface area: 675 m^2/g; 35-70 mesh; pore diameter:40 Å: CVD: 5 cycles (1h) at 200°C; reaction temperature: 550°C; partial pressure of p-xylene 2.7 kPa; saturator pressure: 120 kPa; reactor head pressure: 110 kPa; carrier gas: nitrogen; flow rate: 15 ml/min).

	bypass	bypass	bypass	bypass	550	550	550	550
runtime	-35	-25	-15	-5	5	15	25	35
B	111	111	132	285	429	1437	1324	1095
T		57				289	175	323
EB	348	239	100	429		10	28	200
pX	287764	278675	284867	283998	282045	260829	261728	275862
mX					9			
oX	67	8			122	1443	1644	1626
Csum	288290	279090	285099	284712	282605	264008	264899	279106
avgCsum	284297.75	avgPX	283826					
C-bal (%)	101.4	98.17	100.28	100.15	99.4	92.86	93.18	98.17
XpX [a] (%)	-1.39	1.81	-0.37	-0.06	0.63	8.1	7.79	2.81
X100pX [b] (%)	0.2	0.16	0.1	0.28	0.25	1.4	1.37	1.31
X100Iso [c] (%)					0.05	0.55	0.62	0.59

[a]Based on bypass samples.
[b]Assuming 100% carbon balance.
[c]Based on xylenes in product.

Table G.17: Repeatability of catalytic reaction work on powder and pellets.

	X %	σ	$C-bal$ %	σ	X %	σ	Benz/Xyl	p-Sel %	σ	m-Sel %	σ	o-Sel %	σ	p-S prod mol%	σ	o-sel prod mol%	σ	$C-bal$ %	σ
	Powder series																		
	TiPB											TDP							
ø	75.55	2.09	98.32	3.46	8.52	0.17	1.12	21.44	0.15	55.04	0.36	23.52	0.42	10.13	0.1	11.12	0.29	99.37	1.7
σ	6.59	0.74	3.1	2.81	0.75	0.13	0.04	0.15	0.08	0.12	0.11	0.19	0.14	0.21	0.12	0.29	0.22	2.6	0.65
rel. error %	8.72	35.64	3.15	81.21	8.81	78.78	3.99	0.68	57.87	0.22	30.62	0.81	34.36	2.04	118.18	2.62	77.27	2.61	38.36
	Pellet series																		
	TiPB											TDP							
ø	96.32	1.33	81.73	2.34	14.14	1.36	1.1	21.74	0.26	55.87	0.38	22.39	0.97	10.33	0.03	10.64	0.12	101.84	2.01
σ	1.63	0.84	4.17	1.25	1.1	0.81	0.02	0.36	0.12	0.03	0.24	0.37	0.73	0.11	0.01	0.28	0.08	0.53	0.67
rel. error %	1.69	63.21	5.1	53.22	7.75	59.26	2.12	1.65	45.01	0.05	63.13	1.64	75.08	1.03	38.51	2.63	64.93	0.52	33.33

Appendix H

Literature Overview

Table H.1: Glossary for Tables H.2 and H.3

1,2,4-TMB	1,2,4-trimethylbenzene
1,3,5-TiPB	1,3,5-triisopropylbenzene
2Me2MOS	dimethyldimethoxysilane
3HeptMOS	triheptylmethoxysilane
3PropMOS	tripropylmethoxysilane
4MeSi	tetramethylsilane
A	zeolite A
BaldNH3	benzaldehydeamonia
BEA	zeolite beta
BuOH	butylalcohol
c-	cyclo-
C6	hexane
C7	heptane
C8	octane
ck	cracking
deal	dealuminated
dealk	dealkylation
dehy	dehydration
DiPB	diisopropyl-benzene
DEB	diethylbenzene
DP	disproportionation
EB	ethylbenzene
ESCA	electron spectroscopy chemical analysis
ETHC	ethanol to hydrocarbon
EtOH	ethanol
hydrog	hydrogenation
iso	isomerisation
isopropOH	isopropylalcohol
MAS	nagic angle spinning
Me3MOS	methyltrimethoxysilane
MeOH	methanol
mod.Wang88	modified method after Wang 1988
MOR	zeolite mordenite
MQ	4-methylquinoline
MTHC	methanol to hydrocarbon
MTO	methanol to olefin
m-X	meta-xylene
n-	normal-
Niwa84	method after Niwa 1984
NMR	nuclear magnetic resonance
o-X	ortho-xylene
PhOH	phenol
p-X	para-xylene
Py	pyridine
s-	sec-
t-	tert-
TBOS	tetrabutoxysilane
TEM	transmission electron microscopy
TEOS	tetraethoxysilane
TEOGe	tetraethoxygermanium
TMOS	tetramethoxysilane
TMOGe	tetramethoxygermanium
Tol	toluene
transalk	transalkylation
Wang88	method after Wang 1988
X	zeolite X
XPS	X-Ray photoelectron spectroscopy
XRD	X-Ray diffraction
Y	zeolite Y
ZK5	zeolite ZK5
ZSM-5	zeolite ZSM-5

Table H.2: Overview of literature related to CVD of alkoxy-precursors on zeolitic and similar material.

Material	Modifier	Deposition temperature [K]	System and method	Reference
H-MOR, Alumina, Silica, Alumina-Silica-mix	TMOS	593	vacuum system, static	(Niwa et al., 1984a) (Method: Niwa84)
H-ZSM-5, Silica-Alumina, Alumina, Kieselguhr	TEOS+ TOL/MeOH, TMOS, TBOS	453-503	flow system, in-situ	(Wang et al., 1988) (Method: Wang88)
Alumina	TEOS	473-613	flow system	(Sato et al., 1990)
Alumina	TEOS	513-573	flow system	(Sato et al., 1991b)
Ga-ZSM-5	TEOS	503	Wang88	(Halgeri et al., 1991)
Ga-ZSM-5	TEOS	513	(mod. Wang88)	(Bhat et al., 1996a)
H-BEA	TEOS	413/423	Wang88	(Tsai and Wang, 1991)
H-BEA	TEOS	294-523	static	(Chun et al., 1994)
H-ZSM-5	TEOS	593	vacuum system, static	(Kva et al., 1989)
H-ZSM-5	TEOS	473	Wang88	(Wang et al., 1989)
H-ZSM-5	TEOS	503	Wang88	(Bhat and Halgeri, 1993)
H-ZSM-5	TEOS	503	Wang88	(Das et al., 1993)
H-ZSM-5	TEOS	503	Wang88	(Das et al., 1993)
H-ZSM-5	TEOS	503	(mod. Wang88)	(Bhat et al., 1994)
H-ZSM-5	TEOS	503	(mod. Wang88)	(Das et al., 1994)
H-ZSM-5	TEOS	503	(mod. Wang88)	(Bhat et al., 1995b)
H-ZSM-5	TEOS	503	(mod. Wang88)	(Bhat et al., 1995a)
H-ZSM-5	TEOS	353-673	flow	(Fei et al., 1995)
H-ZSM-5	TEOS	503	(mod. Wang88)	(Bhat et al., 1995c)
H-ZSM-5	TEOS	503	(mod. Wang88)	(Bhat et al., 1996c)
H-ZSM-5	TEOS	513	(mod. Wang88)	(Bhat et al., 1996b)
H-ZSM-5	TEOS	593/673	vacuum system, static	(Weber et al., 1996)
H-ZSM-5	TEOS	373	flow-system, cycles	(Röger et al., 1998a)
H-ZSM-5	TEOS	373	flow-system, cycles	(Röger, 1998)
H-ZSM-5	TEOS	323-673	static, flow, liquid	(Weber, 1998)
H-ZSM-5	TEOS	473	static	(Yoo et al., 1999)

Table H.2: continued

Material	Modifier	Deposition temperature [K]	System and method	Reference
H-ZSM-5	TEOS	373	flow-system, cycles	(Röger et al., 2000)
H-ZSM-5	TEOS	503	(mod. Wang88)	(Das and Halgeri, 2000)
H-ZSM-5, H-MOR, H-BEA	TEOS	298/673	static, flow, liquid	(Weber et al., 2000)
Silica-Alumina	TEOS	443	flow system	(Sato et al., 1991a)
H-ZSM-5	TEOS+ TOL/MeOH	473-483	flow system	(Shaikh et al., 1999)
Na-Y, K-X	TEOS, Me3MOS	298	static	(Chun et al., 1997)
H-ZSM-5	TEOS, (TEOGe)	388	flow-system, hydrolysis, cycles	(Tynjälä and Pakkanen, 1997)
(ZSM-5	TEOZr	473	static	(Asakura et al., 1988))
(H-MOR	TMOGe	333	(mod. Niwa84)	(Niwa et al., 1986a))
(H-MOR	TMOGe	333	(mod. Niwa84)	(Hibino et al., 1989a))
(H-MOR	TMOGe	333	(mod. Niwa84)	(Hibino et al., 1989b))
Alumina	TMOS	593	water admission (mod. Niwa84)	(Niwa et al., 1989)
Alumina	TMOS	593	Niwa84	(Niwa et al., 1990)
Alumina	TMOS	373-673	vacuum system, static	(Katada et al., 1994)
H-MOR	TMOS	593	vacuum system, static	(Niwa et al., 1982)
H-MOR	TMOS	593	vacuum system, static	(Niwa et al., 1984b)
H-MOR, deal-MOR, Ba-MOR	TMOS	593	Niwa84	(Sawa et al., 1990)
H-ZSM-5	TMOS	593	Niwa84	(Niwa et al., 1986b)
H-ZSM-5	TMOS	593	flow	(Handreck and Smith, 1990)
H-ZSM-5	TMOS	593	cycles, Niwa84	(Hibino et al., 1991)
H-ZSM-5, H-MOR, deal-H-MOR	TMOS	593	cycles, water admission (mod. Niwa84)	(Hibino et al., 1993)

Table H.2: continued

Material	Modifier	Deposition temperature [K]	System and method	Reference
Na-A	TMOS	673	cycles, water admission (mod. Niwa84)	(Niwa et al., 1991)
Na-A	TMOS	573-673	fluidised bed	(Chihara et al., 1996)
Na-MOR, Na-H-MOR	TMOS	593	water admission (mod. Niwa84)	(Hibino et al., 1988)
Pt-H-MOR	TMOS	593	Niwa84	(Niwa et al., 1985)
Pt-H-MOR	TMOS	593	Niwa84	(Suzuki et al., 1998)
ZK5	TMOS	623	static	(Fetting and Dingerdissen, 1990)
H-MOR-NaMOR, Silica, Alumina	TMOS, Me3MOS, 4MeSi	291-373	(mod. Niwa84)	(Niwa et al., 1988)
H-ZSM-5	TMOS, Me3MOS, 2Me2MOS, Me3MOS, 3HeMOS	593	Niwa84	(Kim et al., 1996)
H-Y	TMOS, 2Me2MOS	373-673	(mod. Niwa84)	(Kim et al., 1999)

Table H.3: Overview of catalytic studies on ZSM-5 employing CVD of alkoxysilanes (TEOS and TMOS).

Material	Modifier	Catalytic Reactions	Sorption	Other	Reference
Alumina	TEOS	BuOH-dehy, m-X-iso, n-C7-ck, cumene-ck		NH_3-TPD, P-MAS-NMR	(Sato et al., 1990)
Alumina	TEOS	1-butene-iso		Py-TPD	(Sato et al., 1991b)
Ga-ZSM-5	TEOS	EB+EtOH, TOL+EtOH, TOL+MeOH			(Halgeri et al., 1991)
Ga-ZSM-5	TEOS	TOL+MeOH		NH_3-TPD	(Bhat et al., 1996a)
H-BEA	TEOS	cumene-DP		XRD, Si-MAS-NMR	(Tsai and Wang, 1991)
H-BEA	TEOS	isopropOH-ck, 1,3,5-TiPB-ck	n-C6	NH_3-TPD IR	(Chun et al., 1994)
H-ZSM-5	TEOS	MTHC, ETHC			(Kva et al., 1989)
H-ZSM-5	TEOS	TOL+ethylene			(Wang et al., 1989)
H-ZSM-5	TEOS	EB+EtOH, EB-iso, m-X-iso			(Bhat and Halgeri, 1993)
H-ZSM-5	TEOS	EB+TOL			(Das et al., 1993)
H-ZSM-5	TEOS	EB-dealk		Al-MAS-NMR	(Das et al., 1993)
H-ZSM-5	TEOS	EB+EtOH+ (various)			(Bhat et al., 1994)
H-ZSM-5	TEOS	TDP			(Das et al., 1994)
H-ZSM-5	TEOS	EB+EtOH		NH_3-TPD	(Bhat et al., 1995b)
H-ZSM-5	TEOS	EB+EtOH		NH_3-TPD	(Bhat et al., 1995a)
H-ZSM-5	TEOS	EB+EtOH, 1,3,5-TiPB-ck	c-C6	XRD, NH_3-TPD	(Fei et al., 1995)
H-ZSM-5	TEOS	n-pentene to aromatics			(Bhat et al., 1995c)

Table H.3: continued

Material	Modifier	Catalytic Reactions	Sorption	Other	Reference
H-ZSM-5	TEOS	TOL+EtOH		SEM	(Bhat et al., 1996c)
H-ZSM-5	TEOS	TOL+EtOH		NH_3-TPD	(Bhat et al., 1996b)
H-ZSM-5	TEOS			NH_3-TPD, Py-TPD, MQ-TPD	(Weber et al., 1996)
H-ZSM-5	TEOS	1,2,4-TMB-conv	o-X, p-X, 1,2,4-TMB		(Röger et al., 1998a)
H-ZSM-5	TEOS	n-C6-ck, TDP, 1,2,4-TMB-transalk, 1,3,5-TiPB-ck	o-X, p-X, 1,2,4-TMB		(Röger, 1998)
H-ZSM-5	TEOS		n-C6, o-X, p-X, 1,2,4-TMB	NH_3-TPD, Py-TPD, MQ-TPD	(Weber, 1998)
H-ZSM-5	TEOS	catechol + t-butylOH		IR	(Yoo et al., 1999)
H-ZSM-5	TEOS	1,2,4-TMB-conv			(Röger et al., 2000)
H-ZSM-5	TEOS	PhOH+EtOH		NH_3-TPD	(Das and Halgeri, 2000)
H-ZSM-5, H-MOR, H-BEA	TEOS	1,3,5,-TiPB-ck	n-C6, p-X, o-X	NH_3-TPD, Py-TPD, MQ-TPD	(Weber et al., 2000)
Silica-Alumina	TEOS	cumene-ck, 1-butene-iso			(Sato et al., 1991a)
H-ZSM-5	TEOS	EB-DP		IR, Si/Al-MAS-NMR, NH_3-TPD, SEM	(Shaikh et al., 1999)
H-ZSM-5, Silica-Alumina, Alumina, Kieselguhr	TEOS	TDP, TOL+MeOH, TOL+EtOH			(Wang et al., 1988)
Na-Y, K-X	TEOS, Me3MOS		n-C6	NH_3-TPD	(Chun et al., 1997)
H-ZSM-5	TEOS, TEOGe	n-C6-ck, MTHC, 1,3-DiPB-ck		IR, H/Si/Al-MAS-NMR	(Tynjälä and Pakkanen, 1997)

Table H.3: continued

Material	Modifier	Catalytic Reactions	Sorption	Other	Reference
ZSM-5	TEOZr	MeOH to isopentane		EXAFS	(Asakura et al., 1988)
H-MOR	TMOGe	C8-ck	C6, p-X	NH_3-TPD, ESCA	(Niwa et al., 1986a)
H-MOR	TMOGe	C8-ck		EXAFS, XPS	(Hibino et al., 1989a)
H-MOR	TMOGe	C8-ck		EXAFS, XPS, TEM	(Hibino et al., 1989b)
Alumina	TMOS	cumene-ck		BaldNH_3-titration	(Niwa et al., 1989)
Alumina	TMOS	cumene-ck, s-/t-BuOH-dehydr, iso		BaldNH_3-titration, IR	(Niwa et al., 1990)
Alumina	TMOS	butene-iso			(Katada et al., 1994)
H-MOR	TMOS	TDP	H_2O, o-X	NH_3-TPD	(Niwa et al., 1982)
H-MOR	TMOS	C8-ck	C6		(Niwa et al., 1984b)
H-MOR, Alumina, Silica, Alumina-Silica-mix	TMOS		H_2O, p-X, o-X	NH_3-TPD, IR, XPS	(Niwa et al., 1984a)
H-MOR, deal-MOR, Ba-MOR	TMOS	MTO		NH_3-TPD, TGA	(Sawa et al., 1990)
H-ZSM-5	TMOS	MTHC	H_2O, N_2	NH_3-TPD, IR	(Niwa et al., 1986b)
H-ZSM-5	TMOS	n-C6			(Handreck and Smith, 1990)
H-ZSM-5	TMOS	Tol+MeOH, o-X-iso, TDP, 1,3,5-TiPB-ck	o-X, p-X		(Hibino et al., 1991)
H-ZSM-5, H-MOR, deal-H-MOR	TMOS	1,3,5-TiPB-ck	1,3,5-TiPB	SEM, XRD, Al-MAS-NMR	(Hibino et al., 1993)

Table H.3: continued

Material	Modifier	Catalytic Reactions	Sorption	Other	Reference
Na-A	TMOS		N_2, O_2, Kr, Ar	ESCA	(Niwa et al., 1991)
Na-A	TMOS		O_2, N_2, CO_2, CH_4		(Chihara et al., 1996)
Na-MOR, Na-H-MOR	TMOS	C8-ck			(Hibino et al., 1988)
Pt-H-MOR	TMOS	C8-ck, c-C6-hydrog	CO, H_2		(Niwa et al., 1985)
Pt-H-MOR	TMOS		H_2O		(Suzuki et al., 1998)
ZK5	TMOS			IR, SIMS	(Fetting and Dingerdissen, 1990)
H-MOR-NaMOR, Silica, Alumina	TMOS, Me3MOS, 4MeSi			IR (reaction mechanism)	(Niwa et al., 1988)
H-ZSM-5	TMOS, Me3MOS, 2Me2MOS, Me3MOS, 3HeptMOS	1,3,5-TiPB-ck, Tol+MeOH	o-X, p-X	NH_3-TPD, IR	(Kim et al., 1996)
H-ZSM-5, H-Y	TMOS, 3PropMOS	1,3,5-TiPB-ck	o-X, p-X	IR	(Kim et al., 1997)
H-Y	TMOS, 2Me2MOS		1,3,5-TiPB, N_2		(Kim et al., 1999)